INVESTIGATING ADI-PEG20 METABOLIC THERAPY TO TARGET IMPROVED ANTI-CANCER IMMUNE RESPONSES AND OUTCOMES FROM CHIMERIC ANTIGEN RECEPTOR T-CELL THERAPY

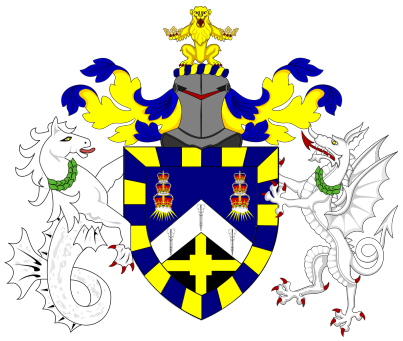

Michael James Austin

Submitted in partial fulfillment of the requirements

of the Degree of Doctor of Philosophy

School of Medicine and Dentistry

Queen Mary University of London

September 2023

This work was funded by Cancer Research UK City of London Centre

Statement of originality

I, Michael James Austin, confirm that the research included within this thesis is my own work or that where it has been carried out in collaboration with, or supported by others, that this is duly acknowledged below and my contribution indicated. Previously published material is also acknowledged below.

I attest that I have exercised reasonable care to ensure that the work is original, and does not to the best of my knowledge break any UK law, infringe any third party's copyright or other Intellectual Property Right, or contain any confidential material.

I accept that the College has the right to use plagiarism detection software to check the electronic version of the thesis.

I confirm that this thesis has not been previously submitted for the award of a degree by this or any other university.

Signature:

Date: 01/09/2023

Details of collaboration and publications:

Collaborations

Shruti Patel performed mouse tibial bone marrow aspirations on my behalf for the experiment

in figures 6.4.1a and 6.4.1b from week 7 and onwards, after I had returned to work full-time in clinical medicine. I had trained Shruti in the technique. Shruti performed the practical bone marrow aspiration, staining and flow cytometry acquisition, then the resultant data was processed and analysed by myself.

Publications

Austin, M. J., Halim, L., Miraki-Moud, F., Taussig, D., Bomalaski, J., Maher, J., Gribben, J., Szlosarek, P., & Wrench, B. (2021). Priming Death Receptor Mediated Apoptosis with Arginine Starvation Sensitises Arginine Auxotrophic B-ALL to CAR-T. Blood, 138(Supplement 1), 2787–2787. https://doi.org/10.1182/BLOOD-2021-151734

Approximate word count: 55000

Abstract

Amino acid starvation with the asparagine degrading enzyme asparaginase has been a key component of therapy for Acute Lymphoblastic Leukaemia (ALL) since its introduction in the 1960s and 70s, and has contributed to the radical improvement of treatment outcomes during this time, especially in children. However, it is a high toxicity agent and is therefore reduced or omitted from treatment protocols used for some adults, where outcomes lag behind those of paediatric counterparts. Recently, an alternative amino acid starvation approach with arginine degradation has gained attention in solid cancer for tumours lacking the arginine synthesising enzyme Argininosuccinate synthetase 1 (ASS1), with a survival benefit demonstrated as part of multi-agent treatment of mesothelioma, along with a favourable safety profile. We therefore aimed to characterise the scope, functionality and potential of arginine starvation as a low-toxicity addition to ALL therapy, particularly for those patients or phases of treatment where asparaginase is not suitable.

Through analysis of large scale transcriptome data we show that large portions of both adult and paediatric B-ALL express non-random, low-levels of *ASS1* and this is associated with consistent alterations in a wider network of metabolism related genes. This finding theoretically supports the usage of arginine starvation as therapy for B-ALL, since deficient expression of *ASS1* predicts impaired capacity for arginine synthesis and therefore vulnerability to its degradation.

Using *in vitro* cell line models as well as mouse models of primary human B-ALL we then show that pegylated arginine deiminase (ADI-PEG20), the clinical grade arginine degrading enzyme that has reached phase 3 trials in solid tumour oncology, leads to cell cycle arrest, DNA damage and apoptosis with caspase cleavage in those tumours where baseline ASS1 expression is lowest. Furthermore, we show that the effect of ADI-PEG20

can be potentiated when combined with BH3 mimetic agents, along with an additive effect when combined with the standard of care drug dexamethasone.

Finally, based on a hypothesised interaction between arginine starvation and the death receptor apoptosis pathway, which is known to be a key mediator of Chimeric Antigen Receptor (CAR)-T cell cytotoxicity, we show the results of an investigation into the potential of ADI-PEG20 to be used as a tumour-priming therapy prior to CAR-T. Using *in vitro* models, we delineate an exciting effect whereby pre-treatment of ALL blasts with ADI-PEG20 leads to improvement in CAR-T "cytokine efficiency", that we propose to have the potential to generate clinically significant benefits in terms of both treatment efficacy and toxicity management.

Collectively, these data strongly support the further development of ADI-PEG20 for ASS1-low ALL, both as a component of pharmacological and immunotherapy treatment paradigms.

Acknowledgements

A heartfelt thank you to my *viva* panel, Dr Sarah Martin and Dr Paul Maciocia, for accepting to examine my thesis. Likewise, a very big thank you to my thesis committee, Dr Jeff Davies, Dr John Maher and Dr John Riches, for the thought-provoking discussions we shared that have brought my thesis to a significant improvement.

This work was made possible by the continued encouragement, patience and inspiration from my primary supervisor Dr Bela Wrench, as well as my secondary supervisor Professor Peter Szlosarek. It has been a privilege to work in the supportive, nurturing environment that they provided along with all of the other researchers and technicians in the Centre for Haemato-Oncology and wider Barts Cancer Institute.

A special thanks has to go to my lab team-mates Ionela Pislariu and Shruti Patel who provided great support as well as assisting me on occasions when I had to ask for help, usually when my children's nursery called me to go and pick them up early. The entire lab community was invaluable to my learning and progress but I have to also at least mention by name (in no particular order) Raul Sanchez, Vilma Dembitz, Keith Woodley, Quentin Heydt, Chrysi Xintaropoulou, Rebecca Gresham, Marta Crespi, Ronas Kesmez, Iuliia Pavlyk, Joana Campos and Katarina Kluckova for being all-round fantastic colleagues.

Finally, I must acknowledge the support and immense patience that has been given to me by my wife throughout my thesis and especially during writing up. The same goes to my fantastic daughters who were both born between starting and finishing my thesis and continually provided motivation and distraction in equal measures, but always spurred me on to make the absolute most of my time in the lab.

Dedication

I dedicate this work to my sister Anna, who lost her fight with glioblastoma multiforme just before my 9-month thesis panel review. She was a brilliant researcher, economist and statistician, as well as mum, daughter and sister, who inspired me in everything but particularly in trying to become a scientist. Me and mum are so proud of you and I hope you'd approve of my thesis.

And to all of the people and families that I have met along the way in the haematology clinic, especially those with acute leukaemias, who have provided not small amounts of inspiration to get this project done, let's hope that one day there are better treatments.

Contents

List of Figures

List of Tables

Acronyms

AARE Amino Acid Response Elements

ADI-PEG20 pegylated arginine deiminase

ADT Arginine Deprivation Therapy

AKT Protein Kinase B

ALL Acute Lymphoblastic Leukaemia

AML Acute Myeloid Leukaemia

ANOVA Analysis of Variance

AO-PI Acridine orange and Propidium iodide

ASNS Asparagine Synthetase

ASS1 Argininosuccinate synthetase 1

ATF4 Activating Transcription Factor 4

ATP Adenosine triphosphate

AZA 5-azacytidine

BCT-100 Pegylated arginase

BSA Bovine serum albumin

CAR Chimeric Antigen Receptor

CASTOR Cellular Arginine Sensor for mTORC1

CCLE Cancer Cell Line Encyclopedia

CHOP C/EBP Homology Protein

CI combination index

CLL Chronic Lymphocytic Leukaemia

CPI Check Point Inhibition

CRS Cytokine Release Syndrome

CyTOF Cytometry by time-of-flight

D10 DMEM media supplemented with 10% FBS and 1% P-S

DAPI 4',6-diamidino-2-phenylindole

DDIT3 DNA Damage Inducible Transcript 3

DEGs differentially expressed genes

DLBCL Diffuse Large B-cell Lymphoma

DMEM Dulbecco's Modified Eagle Medium

DR Death Receptor

DTT Dithiothreitol

E:T Effector:Target

EC_{max} Maximal effective concentration

eIF2 Eukaryotic Initiation Factor 2

ELISA Enzyme-linked Immunosorbent Assay

ER Endoplasmic Reticulum

FACS Fluorescence activated cell sorting

FBS Foetal Bovine Serum

FC Fold Change

FDR False Discovery Rate

FMO Flow Minus One

GALV Gibbon Ape Leukaemia Virus

GCN2 General Control Nonderepressable 2

GFP Green Fluorescent Protein

GRCh38 Genome Research Consortium human build 38

GSEA Gene Set Enrichment Analysis

HCC Hepatocellular Carcinoma

HeH High Hyperdiploid

HLH Haemophagocytic lymphohistiocytosis

HPC High Performance Computing

HSA Highest Single Agent

ICANS Immune effector cell-associated neurotoxicity syndrome

IFN-γ Interferon-γ

IQR Inter-quartile range

IU International Units

KMT2Ar KMT2A rearrangement

k-NN k-Nearest Neighbour

LC-MS/MS Liquid Chromatography with tandem Mass Spectrometry

log_2FC log_2 Fold Change

MCSB Maxpar Cell Staining Buffer

MDS Multidimensional Scaling

MOI Multiplicity of Infection

MPM Malignant Pleural Mesothelioma

MRD measurable residual disease

mTORC1 Mechanistic Target of Rapamycin Complex 1

mTORC2 Mechanistic Target of Rapamycin Complex 2

NO Nitric Oxide

NSG NOD.Cg-Prkdc^{scid}IL2rg^{tm1Wjl}/SzJ

NT Non-transduced

OTC Ornithine transcarbamylase

PBMC peripheral blood mononuclear cell

PBS Phosphate Buffered Saline

PCA Principal Component Analysis

PCR polymerase chain reaction

PDAC Pancreatic Duct Adenocarcinoma

Ph+ Philadelphia chromosome positive

PHA Phytohaemagglutinin

P-S Penicillin-Streptomycin

PDX Patient Derived Xenograft

Ph-L Philadelphia-like

qPCR Reverse transcription-quantitative polymerase chain reaction

R20 RPMI media supplemented with 20% FBS and 1% P-S

R5 RPMI media supplemented with 5% human serum

RNA-seq RNA-sequencing

RPMI Roswell Park Memorial Institute

SCLC Small Cell Lung Cancer

SOM Self Organising Maps

STRING Search tool for recurring instances of neighbouring genes

T_m melting temperature

TBS Tris-buffered saline

TKI Tyrosine Kinase Inhibitor

TME Tumour microenvironment

t-SNE t-distributed stochastic neighbor embedding

TRAIL TNF-related apoptosis-inducing ligand

TSS Transcription Start Site

UMAP Uniform Manifold Approximation and Projection

Chapter 1

Introduction

1.1 Acute lymphoblastic leukaemia

ALL is an aggressive haematological malignancy that arises from precursor cells of the lymphoid lineage that transform at an early stage of development. The disease is characterised by rapid bone marrow replacement by malignant lymphoblasts that results in anaemia, leukopenia and thrombocytopenia and leads to clinical features such as fatigue, breathlessness, immune-compromise and bleeding or bruising.

Epidemiology and aetiology

The incidence of ALL depends on age and is most common in the 0-4 year age group with an annual incidence of around 6 per 100000 [1]. This incidence then drops off with increasing age to its lowest point between 30-40 years and then slowly increases to a 2nd, albeit smaller, peak in incidence in adults aged 75-79 years old [1]. This means that, depending somewhat on where the divide is drawn, about half of ALL cases are in children and half in adolescents and adults [2]. Age is a major discriminant in prognosis; with 5 year survival approximately 90% for children, 65% for adolescents and young adults and around 25% for adults aged over 40 [3, 4]. The main caveat to this range in survival is for infant patients, defined as those diagnosed before the age of 1 year, where survival is particularly poor due to a higher incidence of an aggressive form of ALL that is driven by rearrangements of the *KMT2A* gene [5].

The aetiology of ALL in children has been widely studied and is most likely to involve a multi-step process combining genetic pre-disposition and environmental exposure [6]. This model proposes, for example, the *in utero* acquisition of a cytogenetic aberration that generates a leukaemia predisposition, which is then followed by a leukaemia initiating event, such as an abnormal immune response to infection in early childhood. In adults, the aetiology of ALL is less well understood and while the disease is still characterised by recurrent cytogenetic aberrations, those seen commonly in adults are less frequent in children, suggesting that leukemogenesis may have distinct mechanisms.

Classification

While recurrent cytogenetic aberrations are one of the key features of ALL, the primary categorisation of the disease is made according to the lymphoid lineage involved, with B-cell ALL making up around 75% of cases and T-cell ALL around 25%, although some variations occur according to age, with T-ALL being slightly less common in paediatric patients. After this categorisation, each lineage of ALL is further subdivided into groups according to common cytogenetic or genetic features. The majority of B-ALL cases can be subdivided by cytogenetic aberrations including ploidy changes and chromosomal rearrangements and the latest World Health Organisation definition includes 13 subgroups [7]. Fewer subdivisions exist within T-ALL since clinico-biological behaviour of the disease is not as strongly associated with cytogenetic alterations as in B-ALL [7]. However, the majority of T-ALL cases are associated with aberrant behaviour of *NOTCH1* and *CDKN2A* genes as well as translocations involving oncogenic transcription factors and T-cell receptor genes [2, 8].

Subdividing the disease is important for clinical management since subgroup is an important predictor of prognosis as well as for academic understanding of disease biology. The risk attributed by subgroup is thus used to guide treatment intensity, and in the case of BCR::ABL1 translocated ALL, also known as Philadelphia chromosome positive (Ph+) ALL, to guide the addition of targeted therapy with a Tyrosine Kinase Inhibitor (TKI). In this latter case, the ability to identify patients with the BCR::ABL1 oncogene and administer targeted therapy has transformed what was once a high risk subgroup of ALL to one where

outcomes may now be more favourable, especially for older patients where more intensive chemotherapy may not be appropriate [9].

Management

The current favourable prognosis expected for paediatric patients belies the dismal prognosis associated with the disease in the mid-20th century and is a result of collaborative efforts between numerous international trial groups. The initial step in modern treatment of ALL was with the introduction of the anti-metabolite agent aminopterin by Sidney Farber in the late 1940s [10], with the next revelation being the introduction of the "total therapy" concept by the St Jude Research Hospital in Memphis, USA in the 1960s [11, 12]. The total therapy concept employs the use of sequential, multi-agent induction, consolidation and then maintenance chemotherapy and remains the basis of modern treatment to this day, with the now favourable prognosis of paediatric ALL being a result of incremental optimisations through serial trials run by the St Jude team along with other international trial groups [11].

Geographical variations exist but most protocols follow a similar overall design. In the UK, standard induction therapy consists of a 5 week cycle combining dexamethasone, vincristine, asparaginase and daunorubicin, with oral mercaptopurine introduced in the final week. Consolidation then follows with a 5 week cycle consisting of continued daily mercaptopurine and repeated blocks of cyclophosphamide and cytarabine. Less intensive maintenance then begins with oral mercaptopurine and methotrexate, with intermittent pulses of dexamethasone and vincristine and lasts for 9 weeks. A final intense block consists of a condensed repeat of both induction and consolidation components in a combined 6 week cycle. This is followed by a 2 year maintenance period, again with oral mercaptopurine and methotrexate, punctuated by intermittent pulses of dexamethasone and vincristine. Every cycle of treatment also contains prophylaxis against relapse of ALL in the central nervous system using intrathecally administered methotrexate. There are also targeted interventions that may be added to the standard backbone of treatment, such as the already discussed addition of a TKI for treatment of Ph+ ALL and the addition of rituximab for CD20 positive ALL, the latter based on a significant event free survival benefit in the phase 3 GRAALL-2005R study [13].

One of the most important components of modern ALL management is the monitoring of so-called measurable residual disease (MRD), since low level persistent disease is the strongest predictor of relapse in those obtaining remission [14]. MRD is defined as post-therapy disease that is detectable in patients in a morphological remission by the use of more sensitive methods than traditional morphological/immunohistochemical assessment. The routine methods employed for MRD assessment include Fluorescence activated cell sorting (FACS) and Reverse transcription-quantitative polymerase chain reaction (qPCR), with the latter being considered the gold-standard test in the UK. qPCR based MRD assessment utilises a patient and leukaemia cell specific target that is first sequenced from the clonally rearranged junctional region of the immunoglobulin or T-cell receptor genes, isolated from diagnostic DNA samples. This sequence target is then analysed in post-therapy bone marrow biopsies and allows the detection of residual leukaemia at a sensitivity of down to 1 cell in 100000. This degree of sensitivity then allows for accurate predictions of those who are at higher relapse risk, to allow for intensification of treatment or changes in treatment approach. Other techniques are possible, including FACS based MRD analysis, which is generally less sensitive then qPCR, or more recently with next generation sequencing technology, that promises greater levels of sensitivity and the potential for treatment monitoring using blood rather than bone marrow [15].

Beyond conventional chemotherapy based induction and maintenance, allogeneic stem cell transplant is an important consideration in management of ALL. In the paediatric population it is generally not recommended for any patients in first remission but traditionally has been used in subsequent remissions for those patients who either relapse or have primary treatment failure, or for those with persistent levels of MRD above agreed thresholds. For adult patients, and especially those over 40 years of age, there is a clear rationale for stem cell transplantation given the overall worse prognosis, and transplant has been standard of care in first remission for patients deemed to be at high risk of treatment failure (*e.g.* according to cytogenetic subgroup) based on the outcome of a number of trials (for review, see [16]). However, trends are changing and evidence is emerging that for adults treated with intensive, "paediatric-inspired" protocols, stem cell transplant does not benefit those who can achieve deep eradication of MRD [17], such that clinicians are increasingly

using MRD response to guide transplant decisions.

Salvage therapy

Another major influence on changing trends in ALL management has been the emergence of pharmacological and cellular immunotherapies. These novel additions to the treatment arsenal have changed the approach to both the upfront and relapse management of the disease, which in the latter case traditionally consisted of intensified cytotoxic chemotherapy followed by transplantation.

Blinatumomab is a bispecific T-cell engager, that is, a synthetic molecule with parallel CD3 and CD19 binding sites, which therefore brings host $CD3^{pos}$ T-cells into proximity with $CD19^{pos}$ B-ALL blasts and leads to cell mediated tumour clearance. The phase 3 TOWER study compared blinatumomab to conventional chemotherapy salvage in relapsed patients, finding that 44% of blinatumomab treated patients obtained a complete remission (compared to 25% for chemotherapy) and a significant, albeit modest, improvement in median overall survival from 4 months for chemotherapy to 7.7 months for blinatumomab [18]. Arguably more impressive were the results of the phase 2 BLAST study, which investigated the use of blinatumomab for patients in remission after induction therapy but with positive MRD, finding that for 78% of patients blinatumomab could achieve complete MRD eradication [19] and after prolonged follow up that where MRD is eradicated, patients can be considered cured with (and in some cases without) consolidation by stem cell transplant [20]. Other practice changing findings from blinatumomab trials include a remarkable survival benefit for infant ALL patients where blinatumomab is added to upfront treatment [21] and likewise for adult patients in remission (including MRD-negative) where blinatumomab is added to the maintenance phase of initial treatment [22].

Another drug which has significantly altered the treatment landscape of relapsed B-ALL is inotuzumab-ozogamicin (more frequently referred to simply as inotuzumab), an antibody-drug conjugate that combines ozogamicin, a potent antitumour antibiotic, with an anti-CD22 antibody, such that the cytotoxic payload is preferentially delivered to $CD22^{pos}$ ALL blasts. Inotuzumab was trialled in the phase 3 INO-VATE study, which compared the outcome of Inotuzumab against standard of care chemotherapy in patients with relapsed

B-ALL and showed an improvement in overall survival that was linked to an improved rate of successfully bridging patients to stem cell transplantation [23, 24]. An important note is the average duration of response in the INO-VATE trial was less than 6 months [23] meaning that despite its improvement over traditional salvage chemotherapy, stem cell transplant is still required to consolidate the response.

Less progress has been made for relapsed T-ALL. Nelarabine, a purine nucleoside analogue, is licensed in this context following pivotal phase 2 monotherapy trials in both children and adults 2 decades ago [25, 26]. More recently the drug is combined with other cytotoxics (usually with etoposide and cyclophosphamide, the so-called NECTAR protocol) and real world evidence has shown that nelarabine based combinations are effective at re-inducing remission in 55% of patients as well as improving overall survival independently of ability to transplant [27]. The 2 year survival for nelarabine based combination salvage and transplant in this retrospective data set was 55%, which is favourable when compared to nelarabine monotherapy or conventional chemotherapy salvage but comes at a cost of potentially severe neurological toxicity.

The anti-CD38 monoclonal antibody daratumumab has also recently garnered interest after the phase 2 DELPHINUS study showed that, when combined with chemotherapy, a 40-60% complete remission rate could be achieved in relapsed T-ALL depending on patient age [28]. Another recent development that is being adopted in the clinic is the combination of the Bcl-2 and Bcl-x_L inhibitors venetoclax and navitoclax with chemotherapy, which was shown in a phase 1 study to generate complete remissions in 60% of combined T- and B-ALL patients.

These emerging options have undoubtedly offered a new degree of hope to patients with relapsed ALL, but in almost all cases are either bridges to transplantation or, in some cases, bridges to the CAR-T cellular immunotherapy modality, that was first approved for B-ALL in 2017.

Chimeric antigen receptor T-cell therapy in B-ALL

CAR-T cell therapy, which has gained traction in relapsed B-cell malignancies as well as myeloma, is an adoptive cellular immunotherapy that is based on the *ex vivo* manipulation of

host T-cells to generate tumour cell reactivity. To achieve this, patient T-cells are apheresis harvested and synthetically activated *ex vivo* followed by viral transgene insertion to generate expression of a chimeric receptor that is able to activate T-cell cytotoxic functions upon ligation with tumour cell antigens. In the case of B-cell malignancies, the CAR is usually directed against the pan-B cell CD19 antigen, such that when CAR-T cells are re-infused into the patient and subsequently meet tumour cells expressing CD19, a potent anti-tumour response is generated by activation of the CAR. This technology was first tested clinically in 2012 to treat the then 6-year-old Emily Whitehead, who was suffering a relapse of B-ALL that had progressed so rapidly that no remaining effective treatment options were believed to exist. As of 2023, Emily remains alive, cured of ALL and her journey through treatment, as well as her own patient advocacy, has inspired a new paradigm in ALL immunotherapy that has revolutionised treatment of relapsed or refractory disease [29], with 2 currently licensed commercial CAR-T products available for patients in this setting.

Perhaps the most important feature of this technology is the synthetic structure of the CAR protein. This is composed of numerous individual elements of native T-cell activation that are brought together to form the functional CAR unit. The chimeric protein consists of a leader peptide taken from a surface expressed molecule (such as CD8a), an antigen recognition domain in the form of linked heavy and light single chain variable fragments of an appropriate antibody, an extracellular and transmembrane domain that are fused to an endodomain containing modules that instigate downstream T-cell activation signalling upon extracellular ligation of the target antigen (for a review of CAR design, see [30]). The antigen recognition domain for B-cell malignancies is usually derived from the mouse anti-human FMC63 monoclonal antibody but variations exist, with particular interest in using non-CD19 antigens to combat tumour cell downregulation of the CD19 antigen (*e.g.* see [31]) or in using humanised, as opposed to mouse antibody components, to reduce immunogenicity (*e.g.* see [32]).

The design of the endodomain also has key importance. First generation CAR-T cells contained a single activation module in the endodomain derived from CD3ζ but, despite pre-clinical success, had either no or limited clinical activity and a failure to persist [33]. The advent of 2nd generation CAR-T cells, with a dual endodomain combining CD3ζ with

either of the co-stimulatory molecules CD28 or 4-1BB (also known as CD137), allowed for enhanced activation, cytokine production and persistence *in vivo*, that ultimately led the way to clinical translation and this design remains the basis of all currently approved CAR-T constructs [33]. Differences in the co-stimulatory component of the endodomain can lead to different clinical characteristics with the CD28 molecule generally leading to a more rapid initial activation but shorter persistence, and *vice versa* for 4-1BB containing constructs [34]. However, for treatment of B-ALL, the currently approved, commercial products consist of the 4-1BB containing tisagenlecleucel (tisa-cel), and CD28 containing brexucabtagene autoleucel (brexu-cel), suggesting that there is no clear overall advantage to one over the other for this disease.

Tisa-cel was first licensed for B-ALL based on the pivotal, phase 2 ELIANA trial, that enrolled 92 children and young adults with relapsed B-ALL and treated 75 with CAR-T, resulting in an 81% rate of complete remission, all with negative MRD amongst treated patients [35] (compare to 44% complete remission for blinatumomab in the TOWER trial [18]). Even more compelling is data from longer term follow up of the ELIANA study that has reported an overall survival of 63% of all infused patients at 3 years, and around one third of responding patients will survive long-term with no additional therapy, suggesting that with careful patient selection CAR-T alone can be considered curative [36]. Brexu-cel is licensed in adult patients with relapsed B-ALL and was tested in the phase 2 ZUMA-3 study, which enrolled 71 patients and successfully treated 55, with 71% of infused patients achieving complete remission, of which 38/39 were MRD negative [37]. Longer term follow up of the ZUMA-3 cohort has shown that survival at just over 25 months is 50%, which is less promising than the long term follow up of ELIANA (although it should be acknowledged that these trials treated different cohorts of patients with inherent differences in patient fitness and disease biology) but better than a matched historical cohort of patients treated with standard of care therapies, including blinatumomab and inotuzumab, where 50% of patients had died within 6 months of enrollment [38]. Even allowing for the pitfalls of comparing phase 2 trial data to historical controls this data remains compelling, and combined with data for tisa-cel it is clear that CAR-T offers hope for patients where historically there were few effective options.

However, challenges persist and one of the clear weaknesses is that data discussed above relates only to infused patients, who account for 82% of patients from the initial ELIANA analysis and 77% of patients from the initial ZUMA-3 analysis. The majority of patients who were not infused in either trial were affected by either disease progression or toxicity [35, 37] and this points to a major issue, that is, in controlling progressive disease while waiting for *ex vivo* manufacture of CAR-T cells or controlling the adverse events related to treating patients with interim, also known as "bridging" chemotherapy. Furthermore, CAR-T related toxicity can be severe and does preclude some patients from treatment, although it is also true to say that since the approval of the therapy, collaborative efforts to develop management protocols have made most of these toxicities manageable [39–43]. Finally, another clear issue with CAR-T cell therapy is the stark disparity in access, with the product currently limited to higher income economies

For those patients who are infused not all patients stay in remission and it remains controversial as to whether allogeneic stem cell transplant consolidation should be routinely included for some patients. Failure of CAR-T therapy in B-ALL can be broadly divided into that related to primary resistance (or failure of initial remission), which occurred in 19% and 29% of infused patients in ELIANA and ZUMA-3, respectively, as well as relapse from remission. Relapse from remission can be further subdivided into that related to loss of CD19 expression in residual tumour cells or that driven by re-emergence of CD19-positive leukaemia, the former leading to inherently resistant tumour cells that can proliferate despite a maintained pool of CAR-T cells and the latter attributed to a loss of ongoing CAR-T tumour surveillance of some form.

CD19 loss has been reported in 9-25% of patients in clinical trials of anti-CD19 CAR-T (reviewed in [44]) and numerous mechanisms have been proposed for this phenomena. In a detailed study of the clinical course of patient with CD19-negative relapse, Rabilloud *et al.* used single cell RNA-sequencing to identify an alternative CD19 isoform that crucially was present in a subclonal population at the pre-infusion analysis, suggesting that this CD19-negative relapse was driven by subclonal outgrowth under immune pressure [45]. Further evidence for this phenomena has been reported in a series of both paediatric and adult patients where loss of CD19 exon 2, which corresponds to the FMC63 binding epitope,

was found in pre-treatment samples [46]. Furthermore, in a larger series of 237 B-ALL patients, 72% of diagnostic samples were found to harbour CD19-negative blasts and when the response of these patients to CAR-T was assessed it was shown that this subclone expanded with treatment, with a trend to increased relapse risk in those patients with higher frequencies of pre-treatment CD19-negative B-ALL cells [47]. The main mitigation strategy currently being explored for CD19 loss is the use of alternative target antigen directed therapy, and in the case of B-ALL this is usually CD22. Approaches to this include the utilisation of an alternative CAR-T product that specifically targets CD22 [48], to employ a dual infusion of both anti-CD19 and anti-CD22 CAR-T cells [49] or to incorporate parallel targeting of both antigens in a single CAR construct [50]. As of yet, none of these strategies have made it to approval stage and treatment with conventional therapy is difficult, given most patients will have exhausted other standard avenues of treatment prior to CAR-T therapy.

CD19-positive relapse is generally considered to be linked to loss of ongoing tumour surveillance due to either a loss of functionality of persistent CAR-T cells or a failure of CAR-T cells to persist. However, CD19 positive relapse is also strongly linked to patients who achieve remission without MRD clearance [51], raising the question as to whether CD19-positive relapse is actually a manifestation of suboptimal initial function of CAR-T, with the speed of relapse being inversely proportional to the depth of initial disease clearance. Furthermore, long-term remissions have been reported for CD28 co-stimulatory CAR-T cells [37], which are not traditionally believed to persist long-term after infusion, suggesting that the requirement for persistence may be context specific, that is, required for 4-1BB co-stimulated CAR-T cells but not necessarily for CD28 co-stimulation. Another intriguing facet of CD19-positive relapse is that it is generally unresponsive to repeat anti-CD19 CAR-T infusion [52], suggesting that inherent tumour cell characteristics beyond CD19-loss can be involved in relapse. Supporting this concept, it has been shown with pre-clinical models of B-ALL with engineered dysfunction in apoptotic pathways to simulate primary CAR-T resistance, that incomplete initial blast clearance can lead to long-term CAR-T dysfunction due to chronic exposure to target antigen [53]. Other proposed mechanisms for CAR-T dysfunction or loss that allows for CD19-positive relapse include suboptimal

T-cell phenotypes in pre-manufacture apheresis or pre-infusion products [54, 55], CAR-T cell exhaustion driven by tonic CAR signalling [56] or loss of CAR-T cells due to immune reactivity against mouse or viral components of the synthetic CAR molecule [57].

Strategies to mitigate potential causes of CD19-positive relapse have, similarly to attempts to counter CD19-negative relapse, focused mainly on CAR design and manufacturing. Promising approaches in this area include obecabtagene autoleucel (obe-cel) which has an engineered "fast off-rate" CAR, designed for improved antigen recognition dynamics and increased persistence [58, 59]. Other developments have included the refinement of manufacturing conditions to generate favourable pre-infusion CAR-T products [60] and the humanisation of CAR components to reduce immunogenicity [32].

CAR-T has thus become a key treatment option for patients with unfavourable responses to conventional therapy of B-ALL. Further refinements and incremental improvements aimed at increasing the proportion of responding patients as well as prolonging the duration of responses should eventually be the outcome of intense research in this field and may result in a broadened scope for CAR-T cell therapy of B-ALL.

1.2 Amino acid starvation therapy in ALL

Amino acid starvation, with the asparagine degrading enzyme asparaginase is a crucial component of ALL therapy. Evidence for the benefit of asparaginase is particularly clear for paediatric ALL where intensive dosing is incorporated into multi-drug regimens [61]. For adults, cumulative evidence points to the benefit of asparaginase [62, 63], and modern practice is increasingly incorporating asparaginase-intensive, "paediatric-inspired" protocols for adolescents and adults who are deemed fit enough to tolerate the potential toxicities [64]. Toxicity of asparaginase is a major limiting factor and where treatment is curtailed due to adverse effects, disease free survival is generally inferior [65, 66]. Importantly, for some subgroups of patients, namely those with Ph+ ALL and those in older age groups, the toxicity of asparaginase is severe enough to mandate reduction or omission from the outset of therapy [67].

The development of asparaginase began in the 1950s with the seminal work by John

G. Kidd [68] where xenografted lymphomas were noted to regress in the presence of guinea pig serum, which was later discovered to be due to asparaginase content [69]. Asparaginase's anti-cancer effect against ALL blasts is the result of a recurring phenotype within the disease known as asparagine auxotrophy, in which cells cannot endogenously synthesise asparagine due to epigenetic silencing of the gene encoding the asparagine synthesising enzyme Asparagine Synthetase (ASNS) [70]. Upon asparagine starvation, ALL blasts undergo G1 cell cycle arrest and apoptosis with cleavage of caspase 3 [71, 72]. It should also be noted that part of the effect of asparaginase comes from its secondary glutamine degrading activity, and this ancillary effect allows activity against ALL cells where *ASNS* expression is intact [73].

As stated, toxicity is a major limiting factor for asparaginase usage with its principle adverse effects being pancreatitis, hepatitis, thrombosis and allergic/anaphylactoid reactions. The latter adverse effect is important since it poses a serious threat to patient safety and is also associated with the formation of anti-asparaginase antibodies that reduce the pharmacological effectiveness of the drug, although this is known to happen in both overt and silent immunological reactions and the impact on clinical efficacy is not clear [74, 75]. It has been demonstrated that resistance to asparaginase treatment may be mediated by microenvironmental cell shunting of asparagine and/or glutamine to leukaemic blasts to preserve amino acid homeostasis [76–78]. Another notable mechanism of resistance is via a leukaemia cell transcriptional response to asparagine starvation, which involves an upregulation of survival pathways that are orchestrated by the action of Activating Transcription Factor 4 (ATF4) [79].

Asparaginase is therefore an irreplaceable drug in the treatment of a large proportion of patients with ALL. However, it is less effective where toxicity precludes or curtails its use, such as in elderly or Ph+ patients [67], or where there is intrinsic or acquired resistance that is likely to be a feature for patients who either relapse after or do not respond to conventional multi-drug therapy. Much effort has been applied to the possibility of reducing or managing asparaginase toxicity (*e.g.* see [80, 81]), but little attention has so far been paid to the possibility of using alternative forms of amino acid starvation where asparaginase is not suitable.

1.3 Emergence of arginine starvation as cancer therapy

Arginine degradation is analogous to asparagine degradation and has emerged as a novel amino acid starvation strategy for solid tumour oncology. In this treatment paradigm, tumours that are arginine auxotrophic, that is, those that cannot endogenously synthesise arginine can be targeted by arginine degrading enzymes that remove arginine from extra-cellular fluid and starve tumour cells of the proteinogenic amino acid, thus causing tumour cell death. This approach has been developed over recent decades and results of the recent phase 3 ATOMIC-MESO trial for Malignant Pleural Mesothelioma (MPM) have suggested a promising role for arginine starvation [82].

Arginine is a semi-essential amino acid used in protein synthesis and as an intermediary in other processes such as the hepatic urea cycle, generation of Nitric Oxide (NO), synthesis of molecules such as polyamines and creatine [83] as well as being a regulator of immune functions including T-cell receptor expression [84]. Routine bioavailability in the adult human comes from dietary intake as well as protein catabolism and renal synthesis of arginine from intestinally released citrulline [85, 86]. The availability of arginine regulates cell growth via binding to the sensor molecule CASTOR (Cellular Arginine Sensor for mTORC1) and when not sufficient cell growth is inhibited [87]. However, if arginine demand outstrips supply, healthy cells can increase local biosynthesis by upregulating expression of ASS1, which synthesises argininosuccinate from citrulline and aspartate, and then argininosuccinate is converted to arginine by argininosuccinate lyase [88]. For a detailed review of arginine physiology and its relevance to cancer see the work by Grzywa *et al.* [83].

The silencing of ASS1 is a recurrent feature in cancer cells and has been linked to a proliferation advantage by allowing diversion of aspartate from arginine synthesis toward pyrimidine formation [89]. However, this proliferation advantage relies on freely available arginine and therefore generates a vulnerability that can be exploited by arginine degradation. The most clinically advanced arginine degrading enzyme is pegylated arginine deiminase, known as ADI-PEG20. This mycobacterial derived enzyme converts arginine to citrulline and ammonia, with the pegylation process serving to reduce immunogenicity and increase the *in vivo* half-life of the drug [90]. Analogous to the targeting of deficient *ASNS* expression

by asparaginase, ADI-PEG20 targets arginine auxotrophic tumour cells that lack the ability to endogenously synthesise arginine through silencing of *ASS1*. In addition to ADI-PEG20, other researchers have investigated the use recombinant forms of arginase, a human enzyme that converts arginine to ornithine and urea, although there has been less progress with this approach than with that of ADI-PEG20 [91].

The existence of arginine auxotrophy across cancer types has been studied in pre-clinical models of arginine deprivation that have demonstrated evidence of an arginine auxotrophic phenotype in a range of malignancies including Hepatocellular Carcinoma (HCC), ovarian, melanoma, breast, MPM, glioblastoma multiforme, lymphoma, Small Cell Lung Cancer (SCLC), prostate, sarcoma, bladder, Acute Myeloid Leukaemia (AML) and pancreas (reviewed in [92]). In these studies there is consensus evidence that where there is low expression of ASS1, tumour cells will be sensitive to arginine degradation with varying effects including DNA damage, autophagy, growth inhibition and apoptosis [92]. However, fewer studies have included tumour-group wide studies of ASS1 expression to make predictions about the potential applicability of arginine degradation in larger clinical cohorts of patients. Where this data has been generated, there is evidence to suggest that suppressed expression of ASS1 generally exists at subgroup level rather than as a pan tumour-type characteristic [93, 94] and may be linked to genetic or transcriptional characteristics of individual tumour subgroups [95–97].

Following on from pre-clinical development of arginine degradation in cancer therapy there have now been numerous clinical trials of ADI-PEG20 as well as a smaller number of trials of the arginase derived product BCT-100. In the phase 3 ATOMIC-MESO trial, ADI-PEG20 in combination with pemetrexed and cisplatin was compared against chemotherapy alone in 249 patients with non-epithelioid subtypes of MPM and showed a significant increase in median overall survival [82]. Importantly, this trial recruited patients with non-epithelioid subtypes of MPM, where pre-clinical evidence has shown that loss of *ASS1* is most likely [93]. In the only other completed phase 3 study, there was no observed benefit of ADI-PEG20 in HCC when compared to placebo in a total cohort of 635 patients [98]. Contrasting the ATOMIC-MESO study, the recruitment in this trial did not target a specific cohort of HCC with a predicted arginine auxotrophic phenotype and, furthermore, it was

noted that there was a high frequency of previous treatment with sorafenib, which has been shown to increase expression of *ASS1* and therefore likely reduce sensitivity to ADI-PEG20. A phase 3 trial of BCT-100 has also been completed in AML, comparing the combination of BCT-100 with low-dose cytarabine against chemotherapy alone, finding no significant difference between the treatment arms in a trial where recruitment was not targeted at low *ASS1* expressing subgroups [91].

Numerous earlier phase trials of ADI-PEG20 have also been completed with mixed results. Limited activity was seen for ADI-PEG20 monotherapy trials including in melanoma [99] and SCLC [100] but some encouraging potential activity was found, especially as part of combination therapy, including trials in prostate [101], pancreas [102] and high grade glioma [103]. After subgroup analysis of earlier melanoma trials there was increased interest in the use of ADI-PEG20 for uveal melanoma [99] and further trials showed the potential for stabilisation of the disease where few treatment options are otherwise available [104]. Of note from this trial, post treatment tumour biopsies revealed an increase in ASS1 expression, which potentially would have led to acquired resistance to ADI-PEG20.

ADI-PEG20 has also been trialled in AML, both as monotherapy and in combination with chemotherapy. In a phase 2 monotherapy trial for poor risk AML, just 2 out of 21 evaluable patients responded to ADI-PEG20 but remissions were in both cases longer than 7 months, which is longer than expected survival in this subgroup of patients [105]. In a follow-up phase 1 trial, ADI-PEG20 was combined with low-dose cytarabine in both previously untreated as well as relapsed patients and found rates of complete remission of 57.1% and 27.3%, respectively [106]. There was also an increase in response rate to 44.4% for those in the poor risk subgroup (including relapsed patients) when compared to the previous ADI-PEG20 monotherapy trial in poor risk AML, suggesting a potentially effective combination with low-dose cytarabine for this difficult to treat subgroup.

As with asparaginase, there are potential modes of resistance to ADI-PEG20 that have been delineated using pre-clinical models and also from clinical trial observations. Anti-ADI-PEG20 antibodies have been shown to be generated in clinical trial cohorts and their rising titre is inversely proportional to the degree of ongoing arginine suppression [107]. *ASS1* upregulation may also hamper treatment effect and this can be driven by

tumour cell adaptation to arginine stress or be influenced by prior or concomitant therapy [98, 104]. In either of these cases, *ASS1* plasticity may be the result of epigenetic factors including DNA methylation [107, 108] or modulation of transcriptional networks involving c-Myc [105]. Another notable resistance mechanism that was discovered from clinical trial biopsy specimens is the influx of macrophages into the arginine deprived tumour bed and subsequent *in vitro* modelling has shown their ability to transfer argininosuccinate to tumour cells, allowing arginine biosynthesis to bypass ASS1 dysfunction and hence restore arginine homeostasis [109]. Investigation of these resistance mechanisms and how they may be countered is therefore a crucial factor in the ongoing development of ADI-PEG20 cancer therapy.

Given the emergence of promising results with ADI-PEG20 in combination with pharmaceutical agents for MPM therapy it is rational to investigate its utility in other cancer types, and none more so than ALL, which is already proven to be highly sensitive to amino acid starvation. However, a key tenet of the potential of ADI-PEG20 for any specific cancer type is the existence of arginine auxotrophy due to *ASS1* deficiency and some data, albeit sparse, has implicated this as a recurrent phenotype within ALL.

1.4 Rationale for investigation of arginine starvation in ALL

Some published reports have suggested that within ALL a cohort of tumours have deficient arginine synthesis capacity and are therefore sensitive to arginine starvation. For example, De Santo *et al.* demonstrated a sensitivity to arginine starvation with BCT-100 amongst more than half of a small cohort of primary B-ALL samples [110] while Hernandez *et al.* have shown a similar effect in T-ALL [111]. The use of ADI-PEG20 has not been tested in ALL but non-pegylated arginine deiminase has been shown to potently induce cell cycle arrest and cell death in some ALL cell lines, with parallels between the functional effects of arginine starvation and the effects of asparaginase being drawn [112]. These reports therefore support a rationale for investigating the use of arginine starvation with ADI-PEG20 for ALL. However, what has not been characterised in this disease is the frequency of arginine auxotrophy, predicted by deficient *ASS1* expression, at a broader population level and this

knowledge is a crucial component for estimating the likely clinical impact of ADI-PEG20 amongst ALL patients.

Another important consideration for the potential of any new approach is how the drug or intervention might be scheduled with existing treatments. As discussed, asparaginase is highly effective in the current management of ALL, especially for children, and so there is little rationale to explore alternative amino acid starvation for the majority of patients in the front line setting. However, the highest clinical need in ALL lies in the adult setting and is especially acute for relapsed disease of either lineage but particularly for T-ALL [113]. The treatment of elderly patients also remains a challenge and, since asparaginase is general considered too toxic in this setting [9], alternative amino acid starvation, if safe and effective, could have a significant impact as part of low intensity induction regimens. Interest in lower toxicity approaches is also increasing in the management of Ph+ ALL, where the use of targeted kinase inhibition allows for good outcomes in the absence of chemotherapy [114]. Here the opportunities are twofold: targeting incremental gains by the incorporation of additional low toxicity agents into existing "chemo-free" regimens, or to attempt to mirror the achievements of targeted therapy in Ph+ disease if arginine auxotrophism were found to be a targetable feature of an ALL subgroup with poor conventional treatment response and no existing targeted therapy, such as Philadelphia-like (Ph-L) or KMT2A rearrangement (KMT2Ar) ALL. Therefore, important considerations for the development of ADI-PEG20 therapy for ALL include how it may fit in with either conventional or modern, non-chemotherapy agents as well as whether it would be employed in a cross-disease setting (as for asparaginase) or rather as a targeted intervention, if arginine auxotrophism was limited to certain subgroups of ALL.

One specific and highly challenging area of ALL management where new treatments are urgently needed is in so-called "bridging" treatment for CAR-T therapy. CAR-T has revolutionised the management of relapsed B-ALL since its first clinical use in 2012 and subsequent approvals by regulatory agencies from 2017 onwards. In this therapy, patients' healthy T-cells are harvested and genetically modified to specifically target tumour cell surface proteins prior to re-infusion and remission rates for relapsed patients who are successfully infused are unprecedented [35, 37]. However, during the CAR-T manufacture

period most patients require treatment (referred to as "bridging") to maintain some form of disease control and since, by definition, these patients are refractory to conventional therapies, preventing disease progression is highly challenging [115, 116].

A basic advantage of any novel treatment in this area is the increased chance of response to an agent that has not been used in prior lines therapy [117]. However, for arginine starvation there is an intriguing rationale for its use as bridging therapy to CAR-T. In pre-clinical models based on clinical trial observations it has been shown that the anti-cancer effect of CAR-T relies in part on the activation of tumour cell Death Receptor (DR) mediated apoptosis via the expression/secretion of corresponding death ligands by CAR-T cells [53]. It has also been reported in pre-clinical models that the efficacy of CAR-T can be enhanced by upregulating tumour cell surface expression of death receptors using radiotherapy [118] or pharmacological intervention [119]. The potential relevance of ADI-PEG20 here comes from its reported sensitising effect on tumour cells to the death ligand TNF-related apoptosis-inducing ligand (TRAIL) [120], with TRAIL being a principle component in the interaction between CAR-T and the tumour cell DR apoptosis pathway [53]. Therefore, if these effects extended to B-ALL, ADI-PEG20 might offer both tumour control and a tumour sensitisation effect in the bridging period prior to CAR-T.

An important consideration for a proposed combination of arginine starvation and CAR-T is the well understood and critical role of arginine for the activation of T-cells, due to its regulation of T-cell receptor expression [88, 121]. This represents a risk to the concept of using ADI-PEG20 as a bridging and priming therapy prior to CAR-T and, in fact, some studies have argued that one of the barriers to CAR-T success in solid tumours is arginine depletion in the Tumour microenvironment (TME) [122]. An extension to this rationale, and somewhat opposed to combining ADI-PEG20 with CAR-T, is the demonstration by Fultang *et al.* that arming CAR-T cells with ectopic arginine producing enzymes can enhance their functionality in an arginine deplete TME [123]. However, the characteristically arginine deplete TME seen in some cancer types is generated by locally expressed arginase [122, 124], which converts arginine to the amino acid ornithine, whereas ADI-PEG20 generates supraphysiological levels of citrulline that can be utilised by activated T-cells for arginine synthesis via upregulation of ASS1, allowing preservation of activation dynamics in arginine

deplete conditions [88]. Whether or not ADI-PEG20 as a pre-treatment to CAR-T would generate a similar immunosuppressive effect as TME arginase is unknown and testing this needs to be built into experimental plans but conceptually the risk is low given the proposal for sequential, rather than concomitant treatment, as well as the above discussed capacity for activated T-cells to meet arginine requirements by metabolism of citrulline.

In summary, based on pre-clinical data demonstrating the efficacy of arginine starvation in ALL and the emerging evidence of clinical safety and effect in other tumour types, we have chosen to perform an in-depth analysis of the potential of ADI-PEG20 in ALL, focusing specifically on B-ALL, given a potentially exciting interaction with CAR-T cell therapy.

Chapter 2

Aims and objectives

2.1 Project rationale

As discussed in the previous chapter, new agents for ALL are needed, particularly in adults in the setting of refractory disease, where the re-use of front line agents is rarely successful. Added to this, an even more challenging clinical scenario is in the bridging of refractory patients to CAR-T, and again, new agents are very clearly needed in this arena.

We are proposing to investigate a novel amino acid starvation approach with the arginine degrading enzyme ADI-PEG20, which could potentially have a role in ALL as an alternative to conventional amino acid starvation with asparaginase where its toxicity precludes use or where patients do not respond. Furthermore, based on a reported interaction of ADI-PEG20 with DR-mediated apoptosis, which is known to be an effector mechanism of CAR-T therapy for B-ALL, we propose to investigate its use as a pre-treatment, tumour cell "priming" therapy prior to CAR-T.

As discussed in the previous chapter, the efficacy of ADI-PEG20 relies on loss of tumour cell *ASS1*, and baseline expression of this gene has not been described at a population level in ALL. Furthermore, while some pre-clinical data does exist for the use of arginine starvation with other agents in ALL, the use of ADI-PEG20 is so far untested in any context. We have therefore crystallised some key research questions which should be answered by this investigation.

Focusing on B-ALL, what is the distribution of ASS1 expression and can this be

used to predict responsiveness to ADI-PEG20?

What are the basic functional effects of ADI-PEG20 on B-ALL?

What is the potential to incorporate ADI-PEG20 into either conventional or newer treatment approaches for ALL, and specifically can ADI-PEG20 increase effectiveness of CAR-T?

2.2 Project aims

1. Understand the scope of arginine starvation therapy within B-ALL.
2. Describe the functional effects of ADI-PEG20 on B-ALL cells.
3. Define where arginine starvation therapy with ADI-PEG20 may fit into treatment.
4. Ask how tumour cell arginine starvation interacts with CAR-T therapy, including effects on both B-ALL and CAR-T cells.

Chapter 3

Materials and methods

3.1 Gene expression dataset re-analysis

Exploratory analysis of "*PAX5*" dataset

The gene expression dataset originally published by Gu *et al.* [125], hereafter referred to as the "*PAX5*" dataset, was identified by a search of PubMed using the term "lymphoblastic transcriptome analysis" and selected based on the large dataset (n=1988) comprising both paediatric and adult patients and with detailed subgroup metadata.

The dataset was downloaded as HTseq [126] count data and processed using R version 4.2.2 [127]. The count data was converted to a deseq2 object using the *deseq2* package [128]. The deseq2 dataset was then filtered to remove lowly expressed genes, such that only genes with at least 10 counts in at least 100 of the individual patient samples were kept

Basic *ASS1* analysis

ASS1 expression per subgroup was compared using the *vst* transformed counts via the *deseq2* package and compared using Analysis of Variance (ANOVA) with the null hypothesis of a random distribution of expression across subgroups. *Post hoc* testing was then performed with Dunnett's test, using the "Other" subgroup, as originally defined by the *PAX5* dataset's authors [125], as the control group, assuming that this group of patients, with no unifying transcriptional feature, would not have a common, programmed level of *ASS1* expression. An initial *ASS1*-low cohort was defined as being the combination of all patients

from subgroups found to have significantly lower *ASS1* expression than the control group while the opposite, *ASS1*-high cohort was defined as the combined group of patients from those subgroups with significantly higher *ASS1* expression than the control group.

ASS1 centred sub-network analysis

A list of Differentially expressed genes (DEGs) between the *ASS1*-high and *ASS1*-low cohorts was generated using the non-parametric Wilcoxon test. Since the sizes of each cohort's constituent subgroups varied and hence DEGs would be dominated by gene expression characteristic of the largest subgroups, we first down-sampled to 10 patients per subgroup such that both *ASS1*-high and *ASS1*-low cohorts consisted of 40 patients. Down-sampling was performed following the method of the original publication [125] by choosing the top 10 patients per subgroup when ranked by sequencing coverage, estimated by the sum of all counts in each patient's sequencing data. Batch effects arising from the different sequencing technologies used in the original project were then modelled and adjusted using the *removeBatchEffect* command from the *limma* package [129]. The Wilcoxon test was then used to generate DEGs. The computational methodology for this was described in [130] and our implementation can be found in the Wrench Lab Group github repository https://github.com/BCI-WrenchLab.

The list of DEGs was filtered using the Search tool for recurring instances of neighbouring genes (STRING) app [131] to generate a sub-list of genes that encode proteins that are known or predicted to directly interact with ASS1. Expression of these genes amongst the full cohort of patients from the *PAX5* dataset was analysed using dimensional reduction with Uniform Manifold Approximation and Projection (UMAP) and clustering in UMAP space with the R package *dbscan*.

Marker gene analysis of *ASS1*-low patient clusters

Marker genes were identified by comparing per cluster expression of each ASS1-interacting gene with that of *ASS1* using the pairwise Wilcoxon test using the *findMarkers* function from the R package *scran* [132]. Genes where the test statistic indicated either consistently down- or up-regulated expression were kept as potential marker genes.

Validation with ECOG2993 microarray data

Validation of findings from the *PAX5* dataset was performed with gene expression data from the ECOG2993 trial [133]. Ph-L patients, not identified in the original publication, were annotated by comparing gene expression of otherwise un-assigned patient samples (originally defined as "Negative" in the ECOG2993 data) to the sub-cohort of Ph+ patients using 13 genes from a panel set out by Harvey *et al.* [134] (originally consisting of 15 genes but not all represented in the ECOG2993 data). Samples were partitioned into 2 groups by k-means clustering and those samples that were originally defined as "Negative" but clustered together with Ph+ samples were assigned as Ph-L. Cross-validation was performed using a k-Nearest Neighbour (k-NN) classifier trained on $z-$transformed gene expression data from known Ph-L samples from the PAX5 dataset and then tested on the ECOG2993 data. The marker gene signature for proposed arginine auxotrophy was then tested by means of a K-NN classifier, trained on the cluster membership from the *PAX5* data and tested on samples from the *ECOG2993* data.

3.2 Cell lines and culture

B-ALL cell lines Reh and RS4;11 were obtained from ATCC (American Type Culture Collection). MUTZ-5 and TOM-1 were obtained from DSMZ (German Collection of Microorganisms and Cell Cultures). All cells were maintained in Roswell Park Memorial Institute (RPMI) media supplemented with 20% Foetal Bovine Serum (FBS) and 1% Penicillin-Streptomycin (P-S) (referred to henceforth as R20) in a standard incubator. Cells were routinely passaged by centrifugation at 300 $\times g$ for 5 minutes then re-suspended in fresh media. Passaging was performed with cells growing in log-phase and cells were used for experiments at low passage numbers. For drug or CAR-T treatment experiments, cells were plated 24-hours in advance of the treatment at a density to allow for log-phase growth to continue from the time of drug treatment administration to end-point.

For use with retroviral transduction experiments, the retroviral producing cell line 293Vec was given as a gift by Manuel Caruso (BioVec-Pharma, Canada). These cells are based on the HEK293 cell line and stably produce retroviral packaging and envelope proteins,

pseudotyped to the Gibbon Ape Leukaemia Virus (GALV). A daughter cell line, transduced to stably produce retroviral particles containing the RNA sequence encoding the FMC63-28ζ CAR (described later) was given as a gift by Leena Halim and John Maher (Maher lab group, King's College London). For lentiviral transductions, Lenti-X 293T (TaKaRa) were used, a commercial HEK293 based cell line, optimised for lentiviral particle production. All HEK293 derived cells were maintained in adherent culture in Dulbecco's Modified Eagle Medium (DMEM) supplemented with 10% FBS and 1% P-S (referred to henceforth as D10) in a standard incubator. Cells were passaged when approximately 80% confluent with gentle washing, with ratios of 1:2 to 1:6 depending on the application.

All cell lines were routinely checked for mycoplasma contamination with the MycoAlert kit (Lonza). B-ALL cell lines were cultured for a maximum of 20 passages from receipt and were discarded if routine viability measurements fell below 90% (85% for MUTZ-5 and TOM-1). HEK293 based cell lines were cultured for a maximum of 8 passages.

3.3 Reverse transcription-quantitative polymerase chain reaction

Cell pellets for RNA extraction were prepared after experimental conditions as described in respective results sections. Total RNA was extracted using QIAGEN RNeasy columns following the manufacturer's instructions. Eluted RNA was then quantified and assessed for impurities by spectrophotometry using the NanoDrop system (ThermoFisher Scientific). To generate cDNA, 100ng of RNA was diluted into 10µl of nuclease free water (Ambion, Invitrogen) and mixed at a 1:1 volume ratio with reverse transcriptase master mix prepared using the Applied Biosystems High Capacity Reverse Transcription kit. The reverse transcriptase reaction was then performed at 37° for 120 minutes and then quenched at 85° for 5 minutes before resultant cDNA was retrieved, diluted 1:25 in nuclease free water and either used immediately or frozen at -20°.

qPCR primers were designed using published sequences for intended targets and assessed with Primer-BLAST [135], with the goal of primer pairs with melting temperature (T_m) between 50-65°, GC content of 50-60%, avoidance of off-target amplification (especially

Gene		Sequence 5' — 3'
ASS1	F	GCGAATGACCTGATGGAG
	R	TTCGTGTAGAGACCTGGAG
BID	F	CTTAGCCAGAAATGGGATG
	R	AGTCACAGCTATCTTCCAG
CASP10	F	ATGCAGGTAGTAATGAGATCC
	R	AGAGTAGACAGCTCCAAATC
CASP3	F	AAAGCACTGGAATGACATC
	R	CGCATCAATTCCACAATTTC
CASP7	F	AAGCCATGGAGAAGAAAATG
	R	CCTGAATGAAGAAGAGTTTGG
CASP8	F	CTACAGGGTCATGCTCTATC
	R	ATTTGGAGATTTCCTCTTGC
CEBPB	F	AACTCTCTGCTTCTCCCTCTG
	R	AAGCCCGTAGGAACATCTTT
FADD	F	CTAGACCTCTTCTCCATGC
	R	TGCACACAGGTCTTCTTC
FAF1	F	AGAACAAATCACCGATGTTC
	R	CAAATACTTCTCCATCATCCAC
FAS	F	CTGTCCTCCAGGTGAAAG
	R	TGTACTCCTTCCCTTCTTG
GAPDH	F	CTCTCTGCTCCTCCTGTTC
	R	GGTGTCTGAGCGATGTGG
RIPK1	F	TGATAATACCACTAGTCTGACG
	R	ACAGTTTTTCCAGTGCTTTC
RIPK3	F	AACTTTCAGAAACCAGATGC
	R	GTTGTATATGTTAACGAGCGG
TNFRSF10A	F	CCACTGAGACTCTGATGC
	R	CAGTTTTGTTGACCCATTTC
TNFRSF10B	F	CACTGAGACTCTGAGACAG
	R	GCTTTAGCCACCTTTATCTC
TNFRSF1A	F	CCCCTGGTCATTTTCTTTG
	R	ATTTCCCACAAACAATGGAG
TNFRSF1B	F	ACCAGGTGGAAACTCAAG
	R	TTTCAGTTCCTGGTCTGG
TNFRSF25	F	AGCAGTTCACCCTTCTAC
	R	CAGTATCTCTGCGGGAAC
TNFRSF9	F	ACAACCATTTATGAGACCAG
	R	ACATCCTCCTTCTTCTTCTTC
TRADD	F	TCAGCCTGTAGTGAATCG
	R	CCTTGCGCCATTTGAG

Table 3.1: qPCR primers. F: forward, R: Reverse.

if undesired amplicon size close to target amplicon size) and if possible amplification across an exon-exon junction (to avoid amplification of contaminating genomic DNA). Primers were synthesised by Sigma-Aldrich and then working stocks were prepared at 100µM by adding 10µl of nuclease free water per nanomole of lypholised oligo-nucleotide. A list of qPCR primer sequences can be found in table 3.1.

qPCR was performed by preparing a 10µl reaction volume using 5µl of 2X SYBR green mastermix (BioRad) and 5µl of cDNA with 2µM each of forward and reverse primers. For each gene and cDNA sample, reactions were performed in triplicate in 384 well format. Data acquisition was performed with either a BioRad C1000 or QuantStudio 7 (Thermo Fisher) qPCR machine programmed to start with a 95° hold for 2 minutes followed by 40 cycles of 5s at 95° then 30s at 60° and finally a melt curve generated using the inbuilt melt-curve protocol from the respective hardware used.

Data were analysed using the $\Delta\Delta C_T$ method [136]. Cycle thresholds for genes of interest were referenced to the per sample cycle threshold for *GAPDH* amplification and then normalised to either a positive, negative or baseline control value, individually specified in figure legends. Where possible, robust baseline control values averaged over a number of biologically distinct samples were preferred.

3.4 Western blotting

Whole cell protein lysates were prepared after experimental stimulation as described in respective results sections. Cells were counted and washed twice in ice cold Phosphate Buffered Saline (PBS) and then lysed in SDS buffer (Cell Signalling) supplemented with Halt Protease and Phosphatase Inhibitor Cocktail (Thermo Scientific) at a concentration of 10^6 live cells per 40µl of lysis buffer. Lysed cell pellets were incubated on ice for 10 minutes and then DNA sheared via multiple passages through a 21ga needle, followed by a further 10 minute incubation on ice. Lysates were then centrifuged at $13000 \times g$ for 10 minutes at 4° and the supernatants retrieved by careful pipetting. Protein concentration was measured using the Pierce BCA assay kit (Thermo Scientific) following the included microplate protocol. Lysates were then prepared for electrophoresis by first equalising

Protein	Manufacturer	Clone	Cat. No.
ASS1	Cell Signaling	D404B	70720
ATF4	Cell Signaling	D4B8	11815
Bcl-2	Cell Signaling	124	15071
Bcl-x_L	Cell Signaling	54H6	2764
Caspase 3	Cell Signaling	D3R6Y	14220
C/EBPβ	Santa Cruz	H-7	sc-7962
CHOP	Cell Signaling	L63F7	2895
Cleaved-caspase 3	Cell Signaling	D3R6Y	14220
Cofilin	Cell Signaling	D3F9	5175
DR4	Cell Signaling	D9S1R	42533
DR5	Cell Signaling	D4E9	8074
Fas	Cell Signaling	C18C12	4233
p21	Cell Signaling	12D1	2947
TNFR1	Cell Signaling	C25C1	3736
Vinculin	Cell Signaling	E1E9V	13901

Table 3.2: Western blotting antibodies, listed in order of appearance.

protein concentrations with lysis buffer then mixing to make a 1X solution with 3X blue protein loading buffer (Cell Signalling) and 30X DTT (Cell Signalling). Prepared lysates were then denatured by heating to 70° for ten minutes and subsequently stored at -20°.

Protein separation was performed with gel electrophoresis using pre-cast NuPAGE 4-12% Bis-Tris gels (Invitrogen) with 10-15μg or protein loaded per lane. Electrophoresis was performed using either NuPAGE MES or MOPS running buffer (Invitrogen, the latter for increased resolution on higher molecular weight proteins) and ran at 170V until the protein front had migrated across the entire gel. Proteins were then transferred to methanol pre-wetted PVDF membranes (Thermo Scientific) using a wet transfer tank with gel-membrane sandwiches submerged in NuPAGE transfer buffer (Invitrogen) supplemented with 20% methanol and ran at 100V for approximately 1 hour (longer times if higher molecular weight proteins were of interest) at 4°.

After completion of protein transfer, membranes were rehydrated in Tris-buffered saline (TBS) then blocked with either 5% Bovine serum albumin (BSA) (Merck) or 5% nonfat milk (Cell Signaling) in TBS with 0.1% tween at room temperature on a rocking platform for 1 hour. Primary antibodies were applied at a concentration of 1:500-1:2000 according to manufacturer's recommendations and/or titration experiments in TBS with 5% BSA and 0.1% tween (unless alternative buffer recommended by antibody manufacturer) and incubated on

a rocking platform at 4° overnight. A list of primary antibodies can be found in table 3.2.

After primary antibody incubation the membranes were washed 3 times in TBS with 0.1% tween and then secondary antibodies were applied at 1:2000 concentration in TBS with 5% milk and 0.1% tween at room temperature on a rocking platform for 2 hours. Membranes were washed again in TBS with 0.1% tween then finally in deionised water. Protein signal acquisition was performed by briefly blotting membranes dry then performing a 30 second incubation with either SuperSignal West Pico PLUS Chemiluminescent Substrate or SuperSignal West Femto Maximum Sensitivity Substrate (both Thermo Scientific, latter for low expression targets), followed by luminescence acquisition using an Amersham Imager 600 (GE Healthcare) with membranes sandwiched between clear plastic film.

Resultant .tiff images were imported into Adobe Photoshop and an identical colour/tone adjustment was applied to all. Images were then cropped using Abode Illustrator and corresponding protein of interest and loading control images were placed in annotated montages, again using Adobe Illustrator. Displayed results are representative examples from repeated western blots using protein lysates extracted from at least 2 independent experiments.

3.5 ADI-PEG20

Frozen clinical trial grade stocks of ADI-PEG20 were given as a gift by Peter Szlosarek (Barts Cancer Institute, Queen Mary University of London). Clinical trial grade ADI-PEG20 comes in a sterile solution at a concentration of 11.5mg/ml (approximately 100 International Units (IU)/ml). For *in vitro* experiments the drug was diluted in complete media and administered in a 2-step dilution, which we felt increased precision amongst technical replicates. For *in vivo* experiments the drug was diluted in sterile PBS at a concentration of 5 IU/200μl and administered via intraperitoneal injection using 29ga insulin syringes.

3.6 ATP based luminescent cell counting

Measurement of cell viability/cell counts in 96-well plate format was performed using CellTiter-Glo (Promega), a luminescent ATP sensing assay that generates a proxy for

viable cell count according to total ATP content. Measurements were performed according to the manufacturer's protocol. Briefly, cells were suspended in opaque white 96-well plates in 100µl total volume per well and incubated with experimental treatments for specified times. At the end of the incubation, plates were removed from incubators and equilibrated with room temperature then mixed with reconstituted CellTiter-Glo reagent in a 3:5 ratio (a locally validated adaptation from 1:1 ratio advised by manufacturer) before briefly shaking to homogenise and lyse cells, followed by a ten minute incubation at room temperature. Luminescent signal was then acquired using an Optima Fluostar plate reader (BMG Labtech) in luminescence mode. Initial titration experiments were used to ensure signals at typical cell densities were being detected within the linear range of detector.

3.7 Arginine and citrulline detection

Cell culture media was treated with ADI-PEG20 or control (in absence of cells) and then at specified time points harvested and centrifuged at 16000 $\times g$ for 5 minutes at 4°. Next, 50µL of supernatant was added to 750µL extraction buffer consisting of 50% Liquid Chromatography with tandem Mass Spectrometry (LC-MS/MS) grade Methanol, 30% Acetonitrile, 20% Ultrapure water (all Optima brand, Fisher Chemical) with 100ng/ml HEPES (Gibco), vortexed then incubated at 4° for 15 minutes on a mixing platform followed by 1 hour at -20°. The solution was then centrifuged twice at 16000 $\times g$ with the supernatant extracted each time by careful pipetting. After the final centrifugation samples were transferred to autosampler vials (Thermo Scientific) and stored at -80°. LC-MS/MS was then performed by Dr Valle Morales in the Mass Spectrometry core facility at Barts Cancer Institute. Resultant arginine and citrulline values were normalised to those from untreated media.

3.8 Proliferation and viability assay

Cells were passaged by centrifugation on day -1 and suspended in triplicate at optimal growth concentration in a series of 48-well plates then incubated under standard conditions. ADI-PEG20 or control media were added to corresponding wells on day 0. On each day of the experiment, the cell suspension from a single plate was homogenised by gentle

Panel	Protein	Fluorophore	Manufacturer	Clone	Cat. No.
Apoptosis	ZombieViolet		BioLegend		423114
	Annexin-V	APC	BioLegend		640941
Cell cycle	ZombieNIR		BioLegend		423106
	DNA	DAPI			
	Ki-67	APC	BioLegend		350514
In vivo B-ALL	ZombieViolet		BioLegend		423114
engraftment	mouse CD45	FITC	BD	30-F11	553080
	human CD45	APC	BD	HI30	561864
	CD19	PE-Cy5.5	eBioscience	SJ25C1	35-0198-42
In vivo ASS1	ZombieNIR		BioLegend		423106
expression	ASS1	None	Abcam	R *poly*	ab191165
	R IgG	BV421	BioLegend	D *poly*	406410
	CD19	PE-Cy5.5	eBioscience	SJ25C1	35-0198-42
In vitro ASS1	ZombieNIR		BioLegend		423106
expression	ASS1	None	Abcam	R *poly*	ab191165
	R IgG	BV421	BioLegend	D *poly*	406410
	GFP				
CAR-T	ZombieViolet		BioLegend		423114
co-culture	CD3	BV711	BioLegend	OKT3	317328
	c-Myc	AF647	Abcam	9E10	ab223895
	CD19	PE	BD	4G7	345777
	CD20	FITC	BD	2H7	560962

Table 3.3: FACS antibodies. APC: Allophycocyanin, DAPI: 4',6-diamidino-2-phenylindole, FITC: Fluorescein isothiocyanate, PE: Phycoerythrin, Cy: Cyanine, R: Rabbit, BV: Brilliant Violet, D: Donkey, *poly*: polyclonal, GFP: Green fluorescent protein, AF: Alexa Fluor.

pipetting then an aliquot of cells from each replicate well was stained with Acridine orange and Propidium iodide (AO-PI) then counted with a Luna II automated fluorescence cell counter (Logos Biosystems), giving a readout of live cell number and overall viability.

3.9 Fluorescence activated cell sorting

After treatment or control conditions, an aliquot of cells was counted with AO-PI staining using a Luna II automated fluorescent cell counter (Logos Biosystems) and then analysed by FACS. In general, entire experimental wells were harvested by pipette transfer to 5ml polypropylene tubes but for some applications fixed cell numbers were used, and for both we aimed to always stain between 2.5×10^5 and 1×10^6 cells. After transfer, cells were washed with cold PBS with 2% FBS and then pelleted by centrifugation at 500 $\times g$ for 5 minutes at 4°. Supernatants were then discarded by decanting and pellets were dried by

blotting tube mouths whilst still inverted. Viability staining was performed using BioLegend's "Zombie" range of fixable viability dyes at a concentration of 1µL per 10^7 equivalent cells suspended in PBS for 15 minutes at room temperature in the dark, with individual stains depending on application. Further staining with or without fixation was performed depending on application, as described in the following subsections; a list of FACS antibodies organised by panel can be found in table 3.3. Cell data was acquired using an Attune NxT cytometer (Invitrogen) using the fixed volume acquisition setting to allow for direct comparison of cell concentrations where required. Data was analysed using FlowJo version 10 software (BD Biosciences). Basic gates were set up for all experiments to exclude low forward- and side-scatter events, deemed to be non-cellular debris, as well as doublet events based on unequal scaling of height and area from forward scatter impulse. For all applications except apoptosis analysis, dead cells were excluded by viability dye positivity. Thresholds for positivity were set using Flow Minus One (FMO) and/or internal reference standards (*e.g.* wild type cells were used as thresholds for GFP positivity in transduction experiments).

3.9.1 Analysis of apoptosis by Annexin-V expression

After viability staining with ZombieViolet, all subsequent wash and staining steps were performed with 1X Annexin-V binding buffer (Biovision). Cells were stained with anti-Annexin-V-APC (BioLegend) for 15 minutes at room temperature in the dark. Cells with both positive and negative viability dye signals were included and apoptotic cells were enumerated as ZombieViolet^{pos}Annexin-V^{pos} while residual live cell were ZombieViolet^{neg}Annexin-V^{neg}.

3.9.2 Cell cycle analysis with Ki-67 and DNA staining

For all cell cycle analyses, 2.5×10^5 cells were stained per sample. After viability staining with ZombieNIR cells were washed in ice cold PBS with 2% FBS, pelleted by centrifugation at 500 $\times g$ for 5 minutes at 4° then resuspended in 1ml ice cold PBS with 2% FBS. Cells were then fixed and permeabilised by adding 3ml freshly prepared ice cold 70% ethanol whilst held on a moderate speed vortex to prevent cell clumping. The fixed cells were then held at -20° for between 24 hours and 3 weeks prior to further staining.

After being held at -20° cells were pelleted at 500 $\times g$ for 5 minutes at 4° then after

discarding supernatants were washed twice in ice cold PBS with 2% FBS and further pelleting at 500 $\times g$ for 5 minutes at 4° each time. After the final wash, cell pellets were stained with 6µL per pellet of anti-Ki67-APC (BioLegend) and incubated for 30 minutes at room temperature in the dark. Cells were subsequently washed in PBS with 2% FBS and pelleted at 500 $\times g$ for 5 minutes at 4°. Finally washed cell pellets were resuspended in 500µL of 1:100 DAPI solution and incubated for a minimum of 30 minutes at 4° in the dark. Immediately prior to acquisition, cell suspensions were passed through a 35µm mesh to prevent cell clumping in the cytometer fluidics.

3.10 Apoptosis pathway protein immunoblotting array

Analysis of 35 human apoptosis pathway proteins was performed using the R&D Systems Human Apoptosis Proteome Profiler array kit following the manufacturer's instructions. Briefly, after 72 hours treatment or control conditions, 4×10^6 cells were lysed in kit lysis buffer then lysate collected as supernatant after centrifugation at 14000$\times g$ for 5 minutes. Protein concentration was then quantified as for western blotting lysates. Array cards were blocked and then incubated overnight with protein lysates before washing. Protein data was then acquired by chemiluminescence using the kit supplied reagents with an Amersham Imager 600 (GE Healthcare). Individual protein spot pixel densities were calculated using ImageJ software (United States National Institutes of Health) and averaged over duplicate spots before removal of average background signal. Finally, $\log_2$ transformed ratios of treatment to control signals were calculated for presentation.

3.11 RNA-seq

Next generation sequencing of messenger RNA, referred to hereafter as RNA-sequencing (RNA-seq), was performed on total RNA extracted using the same protocol as for qPCR. RNA integrity was assayed with the Agilent Tapestation system and frozen RNA was submitted to Novogene UK for poly(A) tail capture based library preparation and 150bp paired end sequencing using the Illumina NovaSeq platform. We were unable to extract high integrity RNA from FACS sorted CAR-T cells, due to cell attrition in the sorting process,

and so for this experiment library preparation was performed using the SMARTer cDNA kit (TaKaRa) by Novogene UK prior to sequencing.

Raw sequencing data was uploaded to Queen Mary University of London's Apocrita High Performance Computing (HPC) cluster and aligned to the Genome Research Consortium human build 38 (GRCh38) reference genome [137] using STAR aligner [138]. Aligned BAM files were then indexed and filtered to removed unmapped reads using samtools [139] followed by the generation of gene level count data using the Rsubread package [140] within an R instance on the HPC. Downstream processing of count level data was then performed using R version 4.2.2 [127] using the *deseq2* package [128] with visualisations and analysis of DEGs using the packages *EnhancedVolcano* [141], *ComplexHeatmap* [142], *pheatmap* [143] and *ClusterProfiler* [144, 145]. Comparison of DEGs with known transcription factor targets was performed using the TRRUST database [146] utilising the web based analysis platform enrichr [147].

The implementation of the above can be found in the Wrench Lab Group github repository https://github.com/BCI-WrenchLab.

3.12 Animal experiments

All *in vivo* experiments were done under the license PP1404533 or PP4153210 approved by the Home Office of the United Kingdom and in accordance with institutional guidelines. Immunodeficient NSG mice (NOD.Cg-Prkdc^{scid}IL2RG^{tm1Wjl}/SzJ) were obtained from Charles Rivers Laboratories. We used balanced male:female ratios except for experiments where limited xenograft starting material was available, in which case we used female mice only as we experienced more robust engraftment per cell dose in this gender. All mice were housed in individually ventilated cages in the Biological Services Unit at Queen Mary University of London, Charterhouse Square. For generation of Patient Derived Xenograft (PDX) models, cryopreserved mononuclear cells from blood or bone marrow of ALL patients were thawed and resuspended in PBS with 10% FBS and injected into 4-6 week old non-irradiated mice at a minimum cell dose of 10^6 cells per mouse using weight based dosing such that mice received the same dose per gram body weight. Injections were by tail vein or direct hind-leg

intratibial bone marrow cavity injection. In the latter mode of administration mice were anaesthetised with isofluorane gas and administered peri-procedural buprenorphine by subcutaneous injection.

PDX engraftment was monitored fortnightly with intratibial bone marrow aspiration. Briefly, mice were anaesthetised using isofluorane gas with suitable depth of anaesthesia confirmed by absent paw withdrawal response. Mice were then positioned supine with the hind-knee hyperflexed to expose the tibial head. Bone marrow was aspirated using a 27ga needle inserted into the intercondylar region following the longitudinal axis of the tibia until the cortical bone was pierced. Approximately 20-40µL of bone marrow was aspirated and post-procedure mice received a subcutaneous dose of buprenorphine as analgesia. In some experiments, haematological spread of PDX cells was monitored by weekly tail vein bleeding which was performed by venepuncture with a 27ga needle in mice that had been heated in a 37° heatbox for 5 minutes.

Animal wellbeing and weight were regularly monitored, and mice were euthanised when signs of ill health developed, in compliance with approved severity monitoring protocols, or at leukaemia cell engraftment of >90%, as determined by intratibial sampling. At the conclusion of experiments or where humane euthanasia was required, mice were killed by manual cervical dislocation and then were dissected to retrieve hind-leg bone marrow and spleen, as well as to inspect the abdominal cavity for any signs of unexpected ill health.

Post-mortem bone marrow and spleen samples were processed by crushing in a pestle and mortar (for bone marrow) or mashing through a 70µm cell straining mesh (spleens) into a solution of PBS with 2% FBS and 2mM EDTA. Resultant cell suspensions, or liquid samples taken by bone marrow or tail vein bleed samples, were passed again through a 70µm mesh then diluted into 15ml PBS with 2% FBS before pelleting by centrifugation at 500 $\times g$. Pellets were incubated with 5ml ammonium chloride based red cell lysis buffer (RBC Lysis Buffer, BioLegend) for 5 minutes on ice then the reaction was quenched with the addition of 40ml PBS with 2% FBS and then re-pelleted by centrifugation. Pellets were then resuspended in 2ml PBS with 2% FBS and transferred to 5ml polystyrene tubes via a 35µM cell straining mesh to remove any larger particles or cell clumps and then used for downstream applications.

Primer	Sequence 5' — 3'
Forward	TTTTGTGTTTATAATTTGGG
Reverse	TCCAAAAACCTAAAATCC

Table 3.4: Bisulfite specific primer sequences for upstream promoter region at *ASS1* locus.

3.13 Bisulfite specific PCR

To assess DNA methylation status, DNA was extracted from cell lines after 72 hours of treatment with ADI-PEG20 or control using the QIAGEN DNeasy blood and tissue kit using the manufacturer's instructions. Whole DNA extracts were then bisulfite converted using the Zymo EZ DNA Methylation kit, again following the manufacturer's instructions. A 379 base pair region immediately upstream of the *ASS1* Transcription Start Site (TSS) was then PCR amplified using QIAGEN HotStarTaq DNA Polymerase and polymerase chain reaction (PCR) primers that were generated using Methyl Primer Express software (Applied Biosystems). The primer sequences can be found in table 3.4. Amplified bisulfite converted DNA was purified using AMPure XP beads (Beckman Coulter) and then submitted to Eurofins Genomics for Sanger sequencing, using the reverse PCR primer. Sanger sequencing data was analysed using the R package *ABSP* [148] using the suggested workflow with adjustments to quality criteria as detailed in the main text.

3.14 Viral transductions

Viral transductions were used for gene overexpression, shRNA gene knockdown and CAR-T cell manufacture. All viral work was performed following locally approved safety procedures. We found that cell selection with either puromycin or FACS was not possible with the cell lines MUTZ-5 and TOM-1. For puromycin selection, despite apparent *PAC* gene expression based on differential viability compared to non-transduced cells when treated with puromycin, neither cell line would successfully grow fast enough to generate a usable pool of transduced cells. For FACS we also found that after sorting neither MUTZ-5 nor TOM-1 would successfully grow. We therefore used bulk cells with unselected transduced and non-transduced cells for subsequent experimental work.

3.14.1 ASS1 overexpression in MUTZ-5 and TOM-1 cell lines

To generate ASS1-overexpressing subclones within wild-type MUTZ-5 and TOM-1 cell cultures we used pre-made, commercially available lentiviral particles (OriGene) encoding either a GFP-tagged *ASS1* cDNA clone or GFP-tagged control cDNA sequence not corresponding to any known gene. MUTZ-5 and TOM-1 cells were subcultured in non-TC treated plates that had been impregnated with 12µg/ml retronectin solution for 24 hours and then once growing in logarithmic phase lentiviral particles were added at a Multiplicity of Infection (MOI) of at least 5. Cells were then passaged with fresh media every 3 days until a minimum of 8 days had elapsed at which point transduction efficiency by GFP expression was assessed by FACS.

3.14.2 DR5 shRNA gene knockdown

Lentiviral particles encoding a GFP-tagged shRNA targeting *DR5* or a scrambled control were generated by transient transfection of Lenti-X HEK293 cells with DNA contained in Lipofectamine 3000 (Invitrogen) lipid nanoparticles. Fresh media was supplied at 24 hours then viral supernatants were harvested at 48 and 72 hours, clarified by centrifugation then snap frozen at -80°. On the day of transduction, TOM-1 cells were resuspended at twice their usual culture density in viral supernatant with 4µg/ml polybrene (Merck) and centrifuged in sealed plates for 90 minutes at 800 $\times g$ at 32°. The plates were then left undisturbed in a tissue culture incubator for 4 hours before having the media volume expanded with R20. This process was repeated the following day and the GFP transduction efficiency was tested by FACS 5 days later.

3.14.3 CAR-T cell manufacture

CAR-T cells were generated using retroviral transduction of activated T-cells from mononuclear cell preparations extracted from healthy donor peripheral blood. Retroviral particles were prepared using supernatants from 293Vec cells that were subcultured to be just sub-confluent at a low passage number on the day of viral transduction. The 293Vec cells stably produce retrovirus encoding the FMC63-28z CAR which consists of a CD8a

leader peptide, the heavy and light single chain variable fragments of the FMC63 mouse anti-CD19 antibody connected by a linker, the CD28 extracellular (containing c-Myc epitope tag), transmembrane and intracellular domains then the CD3ζ endodomain. The amino acid sequence for the CAR protein can be found in Appendix A.

Mononuclear cell prep

Mononuclear cells were isolated from human blood by density gradient centrifugation. Peripheral blood samples were obtained as leukocyte reduction cones from NHS Blood and Transplant non-clinical issue stocks under the license P294. Blood was harvested from the cone devices by repeated washing with PBS with 2% FBS. Harvested blood was then diluted up to a volume of 50ml with PBS with 2% FBS and gently mixed. The solution was then layered carefully onto density gradient medium (Lymphoprep, Abcam) and centrifuged at 500$\times g$ for 30 minutes with minimum acceleration and deceleration. Mononuclear cells at the interface of the plasma supernatant and density gradient medium were then retrieved by careful pipetting and washed by diluting into 50ml PBS with 2% FBS. Recovered and washed cells were pelleted by centrifugation at 500$\times g$ and then red cell lysis was performed by incubating the pellet with 5ml ammonium chloride based red cell lysis buffer (RBC Lysis Buffer, BioLegend) for 5 minutes on ice. The reaction was then quenched with 45ml PBS with 2% FBS and the cells were washed twice by centrifugation. Finally, cells were counted and viably cryopreserved in a mixture of FBS with 10% DMSO in aliquots of 20-50 million cells depending on the number recovered from the original starting material. A total of 8 independent donor samples were used to generate the data presented in this thesis.

Activation and retroviral transduction

Mononuclear peripheral blood cells were thawed and rested overnight in RPMI media supplemented with 5% human serum (hereafter referred to as R5 media) at a density of 10^6/ml in a standard tissue culture incubator to allow monocytic cells to adhere to plastic, leaving lymphoid cells enriched in suspension. The suspended fraction was then harvested and replated without adjusting density in fresh R5 media in 6-well plates. T-cells within this suspension were then activated by addition of the leukoagglutinating ("L-")

fraction of Phytohaemagglutinin (PHA) (eBioscience PHA-L Solution (500X), Invitrogen) at a concentration of 5µg/ml. The following day recombinant human IL-2 (BioLegend) was added at a concentration of 100U/ml. The following day, non-TC treated 6-well plates that had been pre-coated with a 12µg/ml suspension of retronectin (TaKaRa) were impregnated by 90 minute room temperature incubation with retroviral particles from 293Vec retroviral supernatants that had been clarified by centrifugation. During the incubation, activated T-cells were harvested, counted and then resuspended at a density of 10^6 cells/3ml clarified 293Vec retroviral supernatant. Control non-transduced cells were generated by using a parallel incubation in plain D10 media. The resultant cell suspensions were cultured in the impregnated or control plates with the addition of recombinant human IL-2 (BioLegend) at a concentration of 100U/ml. After 3 days the transduced cells were harvested and aggregated per donor and transduction condition into flasks and then given fresh media to maintain the starting cell density and IL-2 concentration. This was then repeated every 2-3 days until a minimum of 8 days, at which point CAR-T cells could be harvested and analysed by FACS for transduction efficiency before starting co-culture experiments.

3.15 IFN-γ assay

Interferon-γ (IFN-γ) levels from cell culture supernatants were measured using the IFN gamma Human ELISA Kit (Invitrogen) following the manufacturer's protocol. In brief, supernatants from CAR-T co-culture experiments were collected after centrifugation of harvested samples by careful pipetting and then snap-frozen in dry ice. Once all experiments had been performed samples were defrosted together and incubated in duplicate alongside prepared standards in antibody pre-coated 96-well plates with formation of a streptavidin-biotin sandwich detection Enzyme-linked Immunosorbent Assay (ELISA). IFN-γ concentrations were then read using an Optima Fluostar plate reader (BMG Labtech) in absorbance mode at 450nm. Sample concentrations were calculated using standard curves generated with standard well readouts.

3.16 CyTOF

B-ALL/CAR-T co-cultures were performed as described in relevant sections and harvested for analysis after 72 hours. Unless stated otherwise all reagents were Standard BioTools, Cytometry by time-of-flight (CyTOF) grade to reduce sources of contamination. The following protocol is based on Standard BioTools suggested workflows along with that described by Michelozzi *et al.* [149]. Metal-tagged antibody cocktails for barcoding, surface, cytoplasmic and nuclear staining were pre-prepared at titrated antibody concentrations and frozen at -80° to improve inter-run consistency.

Four hours prior to harvest brefeldin A (BioLegend) was added to cultures at 1:1000 to prevent ongoing cytokine secretion followed by the addition with 30 minutes remaining prior to harvest of Cell-ID 127 IdU (Standard BioTools) at 1:1000 to mark S-phase cell DNA. Individual experimental wells containing approximately 10^6 cells were harvested and washed, then pelleted by centrifugation at 500 $\times g$ and resuspended in 50µL Maxpar Cell Staining Buffer (MCSB) containing 1:10 TruStain FcX (BioLegend) Fc receptor blocker. Individual live cell pellets were then barcoded by incubation for 30 minutes at room temperature with pre-prepared unique combinations of metal-tagged anti-CD45 antibodies using a 6-choose-3 schema. Pellets were then washed twice with MCSB and then aggregated into a single sample. Viability staining was then performed by incubation with Cell-ID Cisplatin (Standard BioTools) in warmed serum free media for 5 minutes at room temperature before quenching using a minimum 5 times volume expansion with MCSB. Pelleted cells were then surface stained by incubation with the appropriate pre-made cocktail for 30 minutes at room temperature and after washing cells were fixed by incubation in 1.6% formaldehyde (Pierce, Thermo Scientific) for 10 minutes at room temperature. After initial fixation all centrifugation steps were performed at 1200 $\times g$ to improve cell recovery. Fixed cells were washed twice in MCSB and stored overnight in pellets at 4°.

The next day cell pellets were disrupted by gentle vortexing then permeabilised using Maxpar Perm-S buffer (Standard BioTools) for 10 minutes at room temperature. After washing, permeabilised cells were stained with the cytoplasmic antibody cocktail in Maxpar Perm-S buffer for 30 minutes at room temperature. After washing all subsequent nuclear

staining steps were performed on ice, using ice cold buffers and reagents. Nuclear permeabilisation was performed by mixing cell pellets with 50% methanol whilst agitated on a moderate vortex to prevent clumping and then incubating for 10 minutes on ice. After washing, cells were stained with the nuclear antibody cocktail for 30 minutes on ice. Cell fixation with 1.6% formaldehyde was then repeated and pellets were left overnight in Cell-ID Intercalator-Ir solution (Standard BioTools) at 4°.

Prior to acquisition the next day, cells were washed twice with MCSB and a total cell number was estimated using Trypan Blue bright field counting. CyTOF acquisition was then performed using the CyTOF XT analyser with the assistance of core staff at the University College London Cancer Institute Flow Cytometry Translational Technology Platform.

CyTOF data in .fcs format were then analysed following the suggested workflow of Nowicka *et al.* [150] using the *CATALYST* package [151, 152]. Briefly, aggregated cytometry data was imported into R version 4.2.2 [127] and signals were normalised using bead events before beads were removed. Normalised data were then debarcoded and gated to include only intact, live, single cells using custom gating functions adapted from the suggested workflow of Rybakowska *et al.* [153] to sequentially remove cells with outlying Iridium DNA intercalation signal (non-intact), outlying event length (doublets) and high Cisplatin signal (dead). Individual experimental conditions were then re-aggregated into a single cell experiment analysis object and analysed as outlined in the relevant results sections.

3.17 Statistics and reproducibility

Unless stated otherwise in individual figure legends, cell line experiment data were aggregated from 9 technical replicates performed over 3 independent experiments. Experiments with primary cells, mainly those involving CAR-T cells, were performed in technical triplicates per individual primary cell source, with a minimum of 3 primary cell donors used as "biological" replicates. In animal experiments, individual mice were considered as biological replicates and minimum group sizes of 3 were used. Group sizes were empirically determined without power calculations since no estimates of effect size were available. Statistical tests are described in individual figure legends.

Chapter 4

Predicting arginine auxotrophy in B-ALL

4.1 Across B-ALL subgroups *ASS1* expression is non-random and low expression is associated with altered metabolic gene networks

The experience to date with ADI-PEG20 has shown that clinical benefit is most likely to be derived in those tumour types with lowest *ASS1* expression. Furthermore, it has been reported that aberrant ASS1 expression and hence sensitivity to arginine starvation is a specific feature of metabolically distinct subtypes of SCLC [95] or genetically defined groups of mesothelioma and hepatocellular carcinoma [96, 97]. Within ALL, ADI-PEG20 has not been studied and no such investigation into determinants of ASS1 expression has been reported. However, altered sensitivity to asparaginase in ALL does appear to correlate with cytogenetic group [79]. We therefore hypothesised that sensitivity to ADI-PEG20, which is known to be driven by suppression of ASS1 expression in other tumour types, would be a function of cytogenetic group in B-ALL.

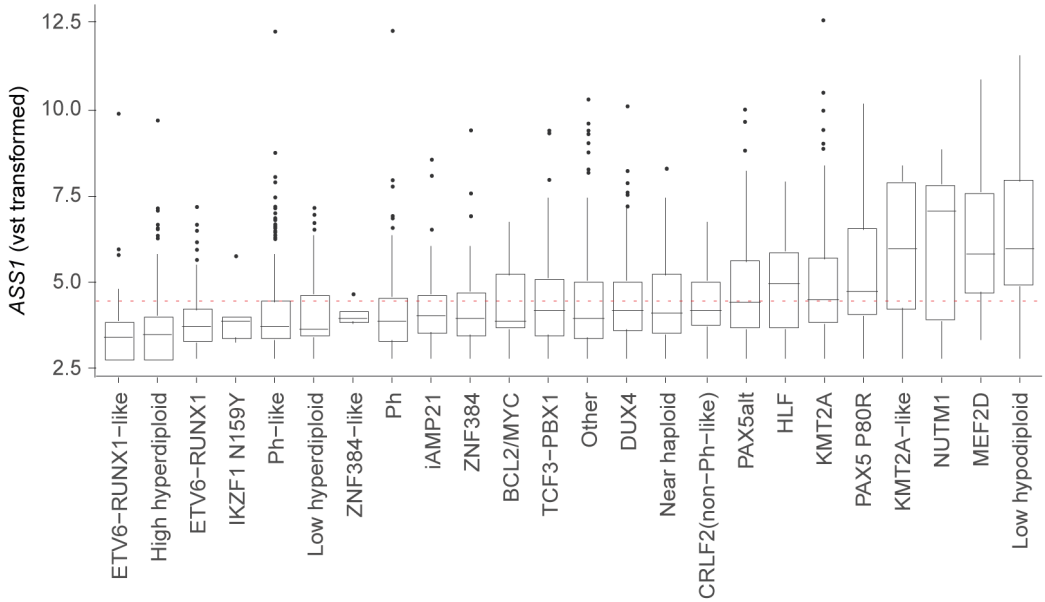

Figure 4.1.1: **Across B-ALL subgroups *ASS1* expression is non-random and low expression is associated with altered metabolic gene networks**
Boxplot of ASS1 expression across B-ALL subgroups as defined by Gu *et al.* [125]. *ASS1* expression from variance stabilised transformation of exon level count data using *deseq2* [128]. Mid-bar represents median, box limits represent inter-quartile range, whiskers represent 95% dispersion and individual points represent outliers. Red dotted line represents mean *ASS1* expression from the transcriptionally undefined "Other" subgroup. Subgroup labels as per naming convention from original paper.

ASS1 is under-expressed in specific B-ALL subgroups

To ask whether *ASS1* expression, and therefore predicted sensitivity to ADI-PEG20, would depend on B-ALL subgroup we analysed the extensive transcriptome dataset, originally published by Gu *et al.* [125], looking for patterns of *ASS1* and related gene expression.

We found a non-random distribution of *ASS1* expression across B-ALL subgroups ($p < 2 \times 10^{-16}$ from ANOVA, figure 4.1.1) and using Dunnett's *post hoc* test with the transcriptionally undefined "Other" subgroup as a control, showed that 4 subgroups had significantly lower average *ASS1* expression while in 4 others it was significantly higher (figure 4.1.2). The former "*ASS1*-low" group consists of the individual subgroups ETV6::RUNX1 ($p = 5.15 \times 10^{-4}$), ETV6::RUNX1-like ($p = 1.04 \times 10^{-2}$), High-hyperdiploid ($p = 6.12 \times 10^{-7}$) and Ph-like ($p = 2.19 \times 10^{-2}$). Its counterpart "*ASS1*-high" is made up of the subgroups Low hypodiploid ($p = 0$), MEF2D ($p = 5.67 \times 10^{-12}$), NUTM1 ($p = 9.77 \times 10^{-3}$) and PAX5

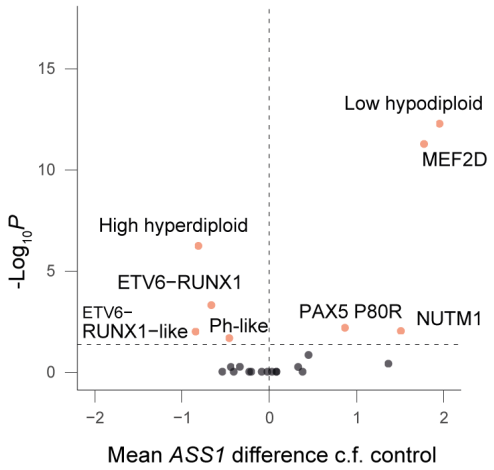

Figure 4.1.2: **Across B-ALL subgroups *ASS1* expression is non-random and low expression is associated with altered metabolic gene networks**
Volcano plot displaying results of Dunnett's *post hoc* test of differences in mean *ASS1* expression between subgroups and "Other" control. Red points represent those with $p < 0.05$

P80R ($p = 6.77 \times 10^{-3}$).

Using data from the original publication, the *ASS1*-low cohort represents 43.6% of all B-ALL while the *ASS1*-high cohort represents 8.9% (table 4.1) Overall, these data suggest that low *ASS1* expression is a feature of certain B-ALL subgroups that combined make up a large proportion of total B-ALL cases and would be predicted to be most sensitive to ADI-PEG20.

Low *ASS1* expression correlates with wider modulation of metabolism related genes

We next reasoned that if *ASS1* expression is not distributed randomly amongst B-ALL subgroups then there should be wider, coordinated transcriptional changes that associate with *ASS1* expression levels. To investigate this we sought to identify macro-level transcriptional patterns associated with *ASS1* expression by examining DEGs between the *ASS1*-low and *ASS1*-high cohort members. To minimise bias toward the overall transcriptional signature of the more populous subgroups from either *ASS1* defined cohort, and to remove samples with lowest sequencing depth, we selected the 10 patient samples with highest estimated

Subgroup	% total cases
***ASS1*-low**	**43.6**
ETV6::RUNX1	9.4
ETV6::RUNX1-like	2.1
High-hyperdiploid	14.0
Ph-L	18.1
***ASS1*-high**	**8.9**
Low-hypodiploid	3.9
MEF2D	2.2
NUTM1	0.6
PAX5 P80R	2.2

Table 4.1: **Across B-ALL subgroups *ASS1* expression is non-random and low expression is associated with altered metabolic gene networks** Proportional make-up of *ASS1* defined cohorts of B-ALL.

read coverage from each of the 8 subgroups, giving a final comparison of 40 *ASS1*-low and 40 *ASS1*-high group members. We analysed DEGs with the non-parametric Wilcoxon test after variance stabilising log transformation and batch correction for sequencing platform, following a recently suggested methodology for optimised comparison of DEGs between large groups [130].

Comparing gene expression in the *ASS1*-low group to the *ASS1*-high group and using an FDR threshold of 0.001 we found 1045 genes were downregulated while 2076 were upregulated (figure 4.1.3a). We then analysed these significant genes according to their $\log_2$ fold change values using Gene Set Enrichment Analysis (GSEA) with the Molecular Signatures Database "Hallmark" gene sets. We found a number of downregulated gene sets in the *ASS1*-low group, notably a downregulation of "Myc targets" and "Oxidative phosphorylation" as well as "MTORC1 signalling" and "E2F targets" (figure 4.1.3b). The coordinated modulation in expression within these gene sets raises the possibility of a contrasting metabolic/cell cycle phenotype between the *ASS1*-low and *ASS1*-high cohorts, and adds biological plausibility for the existence of these as recurrent *ASS1*-associated phenotypes, since arginine auxotrophy is known to be associated with altered metabolic pathways outside of simple arginine synthesis [89] and c-Myc targets were observed to be downregulated in AML patient samples from responding patients in a phase 2 trial of ADI-PEG20 [105].

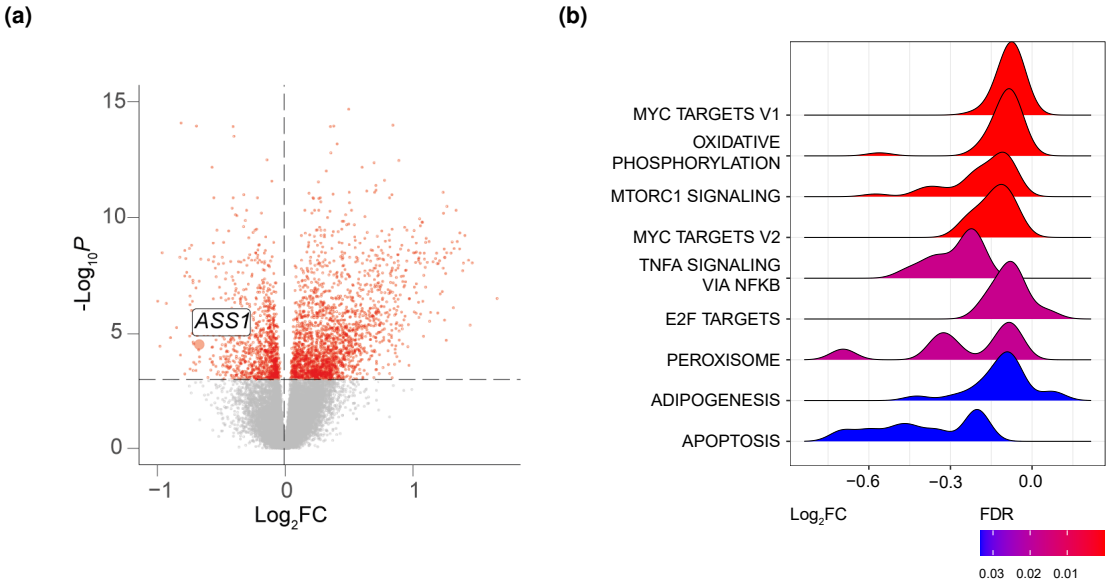

Figure 4.1.3: **Across B-ALL subgroups *ASS1* expression is non-random and low expression is associated with altered metabolic gene networks**
a) Volcano plot of $\log_2$-fold change in gene expression modulation across all genes, comparing *ASS1*-low to *ASS1*-high group samples. FDR p-values calculated from Wilcoxon test and adjusted by Benjamini-Hochberg method. Red points represent those with an FDR < 0.001.
b) Ridge plot of GSEA results using *ASS1*-low to *ASS1*-high DEGs. x-axis displays $\log_2$-fold change expression difference and density functions represent distributions of significantly modulated genes within each gene set.

ASS1 related sub-network expression suggests contrasting arginine metabolism across B-ALL subgroups

The previous analysis of gene expression raised a contrasting predicted transcriptional phenotype between *ASS1*-defined cohorts but it is important to note that this may predict altered arginine metabolism in either the *ASS1*-high or -low cohorts (or both), rather than being specific for an arginine auxotrophic phenotype. We therefore wanted to follow this with a comparison of gene expression related to arginine metabolism across all subgroups. To make our comparison more specific to *ASS1* related genes we generated an "*ASS1*-signature" by filtering the DEGs between the *ASS1*-low and -high cohorts to include only those encoding proteins either proven or predicted to have a first degree interaction with ASS1, using the STRING app [131]. This process curated a 29 member gene set, consisting largely of metabolic genes, including multiple that encode amino acid metabolising

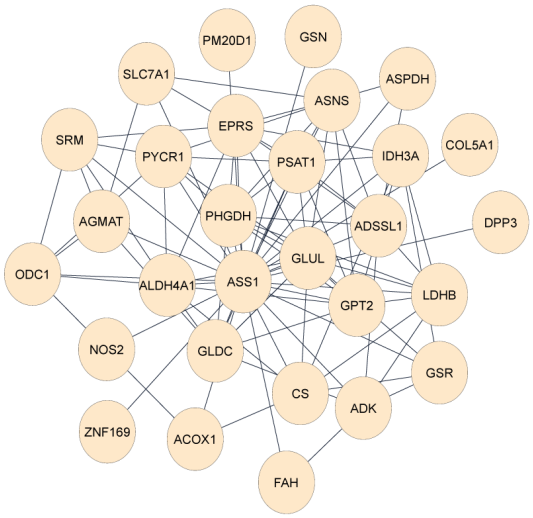

Figure 4.1.4: **Across B-ALL subgroups *ASS1* expression is non-random and low expression is associated with altered metabolic gene networks**
Network of interacting genes centred on *ASS1* extracted from DEGs using STRING.

enzymes (figure 4.1.4) and we reasoned that amongst these genes there would be coordinated expression within subgroups with programmed, aberrant *ASS1* expression, to either compensate for, or cooperate with, altered levels of arginine synthesising capacity.

To investigate expression within this network we performed UMAP dimensional reduction [154] and then segregated the samples within the UMAP space using a density based clustering approach [155], which arrived at a set of 8 stable clusters after iterating the threshold neighbour distance (ϵ) and minimum neighbour parameter (figure 4.1.5, left panel). Where the clustering algorithm could not assign a sample to a specific cluster it was designated as noise (pale blue points, cluster 0, figure 4.1.5, left panel). We then recoloured the UMAP plot by z-normalised *ASS1* expression (figure 4.1.5, right panel) and noticed that cluster 2 appeared to contain the majority of samples with low expression while clusters 3 and 7 appeared to represent the highest expressing samples. By plotting the range of *ASS1* expression per cluster (figure 4.1.6) we again identified cluster 2 as the most likely to represent an arginine auxotrophic phenotype, with clusters 3 and 7 confirmed as containing the highest *ASS1* expressing patients.

We next examined the make-up of each cluster by B-ALL subgroup (figure 4.1.7) and found, as expected, that the majority of the originally defined *ASS1*-low cohort samples

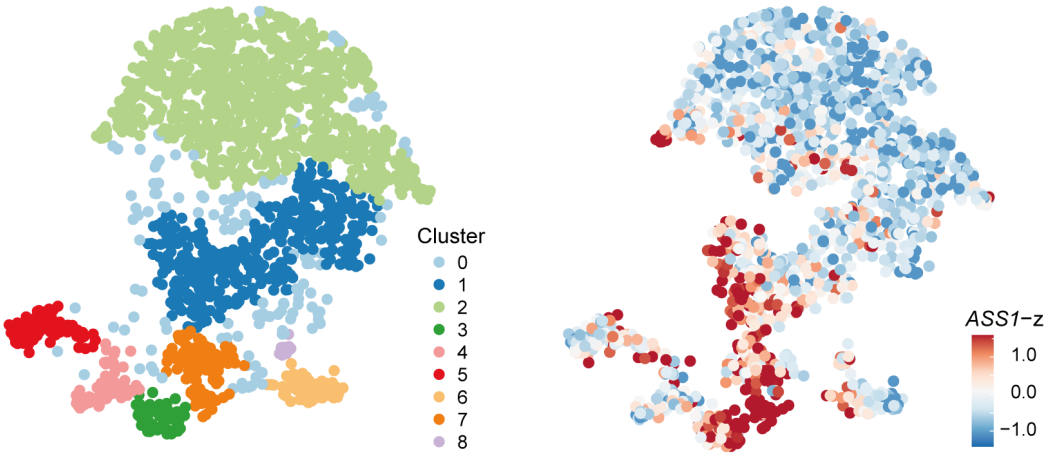

Figure 4.1.5: **Across B-ALL subgroups *ASS1* expression is non-random and low expression is associated with altered metabolic gene networks**
Left panel: UMAP representation of *ASS1*-interacting gene network expression, with each patient data point coloured by cluster assignment. Right panel: Same UMAP representation recoloured by *ASS1* expression z-score (data assigned as noise removed).

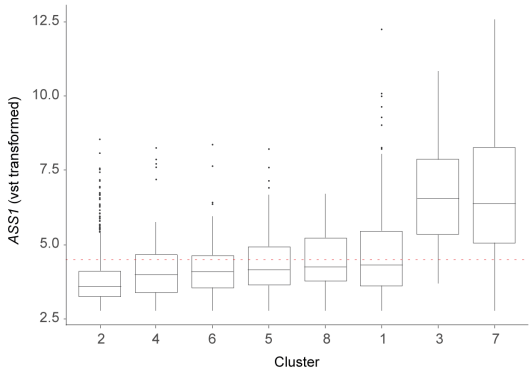

Figure 4.1.6: **Across B-ALL subgroups *ASS1* expression is non-random and low expression is associated with altered metabolic gene networks**
ASS1 expression per cluster from UMAP analysis. Mid-bar represents median, box limits represent IQR, whiskers represent 95% dispersion and points represent outliers. Red dotted line represents mean *(*ASS1) expression from the non-transcriptionally defined "Other" subgroup.

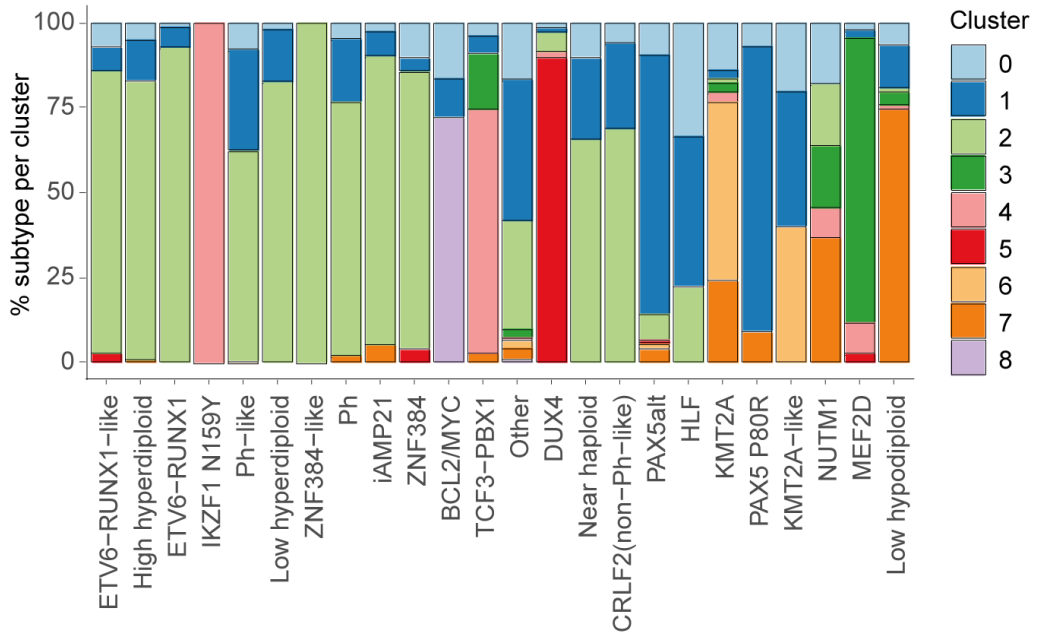

Figure 4.1.7: **Across B-ALL subgroups *ASS1* expression is non-random and low expression is associated with altered metabolic gene networks**
Proportion of individual subgroup samples assigned to each UMAP cluster. Subgroup labels as per naming convention from original paper.

(ETV6::RUNX1, ETV6::RUNX1-like, High Hyperdiploid (HeH) and Ph-L) were assigned to cluster 2. We also noted that numerous other subgroups, including the clinically significant groups Ph+, iAMP21 and low hyperdiploid, were majority assigned to cluster 2, and that this cluster accounted for 48.6% of the entire dataset, suggesting that a gene expression signature associated with *ASS1*-low status extends beyond the originally defined cohort from the Dunnett test analysis (figure 4.1.2) and raising the possibility that sensitivity to arginine starvation might be present in a large proportion of B-ALL tumours.

We also noticed that some clusters were almost exclusively populated by individual subgroups (*e.g.* cluster 5 and DUX4 samples). This proposes the fascinating possibility that as part of the transcriptional definition of these B-ALL subgroups, there are shared patterns of expression within a network of genes associated mainly with amino acid metabolism, and this may be one of the factors that discriminates these subgroups at a clinico-biological level. This might, for example, account for contrasting responses to asparaginase (and *ASNS* is one of the interacting components of this network), as has been described as a discriminating factor between ALL subgroups elsewhere [79].

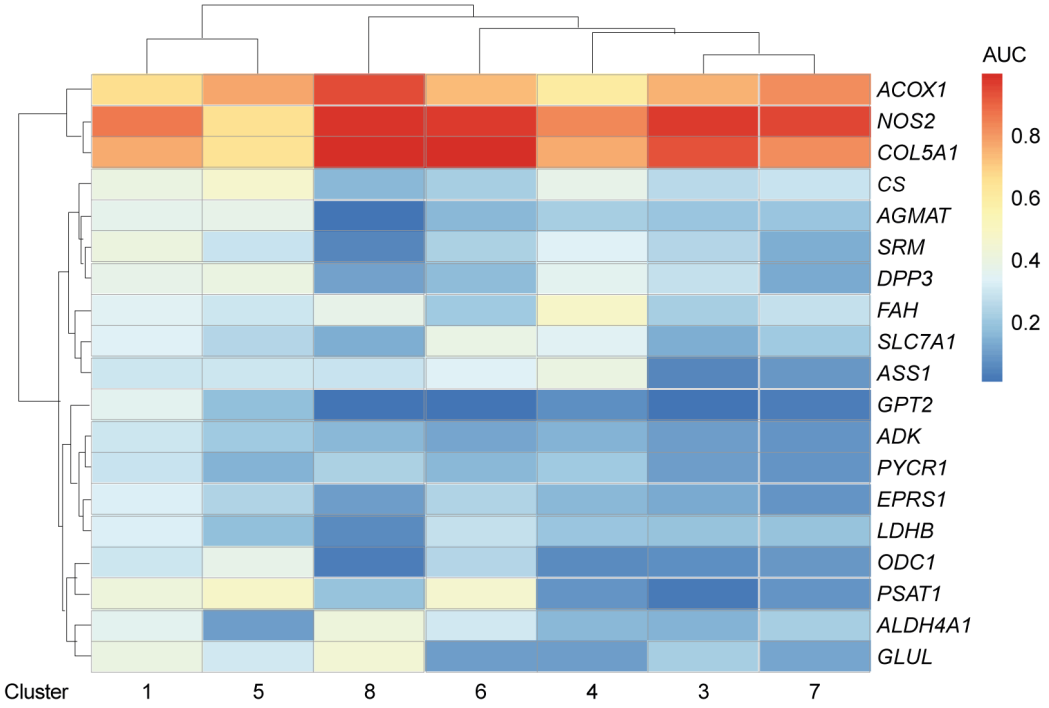

Figure 4.1.8: **Across B-ALL subgroups *ASS1* expression is non-random and low expression is associated with altered metabolic gene networks**
Heat map depicting area under curve (AUC) of Wilcoxon test for difference in marker gene expression between UMAP cluster 2 and other clusters represented by columns. AUC < 0.5 denotes a downregulation and AUC > 0.5 denotes upregulation in cluster 2 compared to annotated cluster.

The identification of this network of genes, whose expression associates with *ASS1* states as well as distinct subgroups of B-ALL, again adds support via biological rationale to the existence of distinct arginine biology across subgroups. It also infers that while singular *ASS1*-low status identifies certain individual subgroups of B-ALL as most likely to be sensitive to ADI-PEG20, there is a shared pattern of expression within this network that extends to large portions of patients within other major subgroups of B-ALL that may therefore also be predicted to have increased sensitivity to arginine starvation.

Marker gene analysis as a potential tool for refined identification of arginine auxotrophy

We next wondered if amongst this network of *ASS1*-related genes the expression of any subset of genes might act as markers for this proposed *ASS1*-low, likely ADI-PEG20

sensitive phenotype. This could be potentially clinically useful since analysis of a larger gene expression set might not be practical while a more focused set of genes could be more easily incorporated into diagnostic practice. To investigate this we compared expression within the gene network by performing pairwise Wilcoxon rank sum tests between cluster 2 and all other clusters, then taking the median adjusted $p-$value for each gene across all pairwise cluster comparisons (a workflow more commonly used for cluster marker gene identification in single cell RNA-seq datasets [156]). We then restricted the gene set to those with an adjusted $p-$value < 0.001 and concordant up- or downregulation across all inter-cluster comparisons, arriving at a final 19-member set of genes (figure 4.1.8).

Of these 19 genes, a subset of 3 genes, *ACOX1*, *NOS2* and *COL5A1*, were noted for being consistently upregulated in cluster 2 when compared to all other clusters. Whether the contrasting expression of these genes is genuinely a part of re-wired metabolism in *ASS1*-low B-ALL is of course purely speculative and would require further investigation. These marker genes could form the basis of a diagnostic test for arginine auxotrophy, for example by using high expression of a marker gene (or corresponding protein) when combined with absent or low expression of ASS1 as a refined predictor of response to ADI-PEG20, although whether this would be an improved prediction of functional arginine auxotrophy would need to be tested.

Validation of postulated arginine auxotrophic signature in adult data set

To validate the proposed existence of an *ASS1*-low, predicted arginine auxotrophic cohort of patients within B-ALL we turned to a second data set representing 191 adult patients with B-ALL originally published by Geng *et al.* [133]. This dataset was derived from microarray analysis of gene expression from a sub-cohort of 215 patients aged 15-59 that had enrolled on the ECOG2993 trial. This was itself a sub-cohort of the international UKALLXII/ECOG2993 trial that set out to assess optimal post-induction therapy and prognostic factors for adolescent and adult ALL [157].

Since the original publication of the Geng *et al.* data set did not include the identification of Ph-L patients, but these were an important group within the analysis of the Gu *et al.* data set, we first attempted to reclassify patients with unclassified cytogenetics (denoted

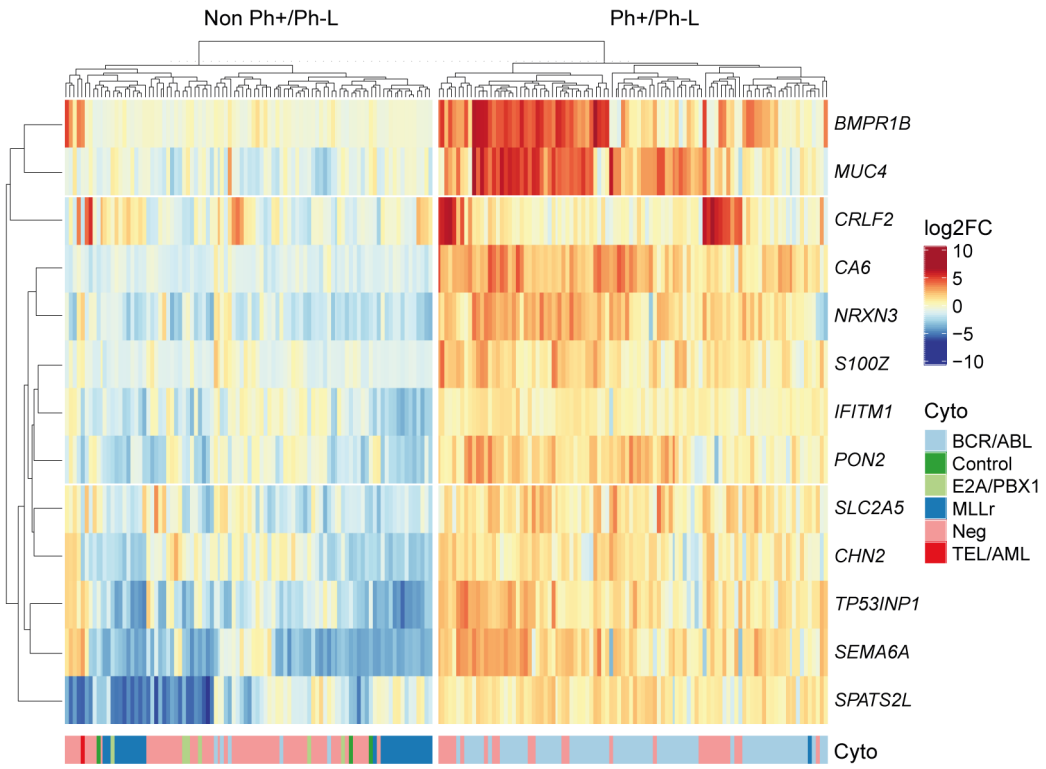

Figure 4.1.9: **Across B-ALL subgroups *ASS1* expression is non-random and low expression is associated with altered metabolic gene networks**
k-means clustering of gene expression within Ph-L gene set for reclassification of unclassified B-ALL samples from Geng *et al.* dataset [133]. Cytogenetic (Cyto) group labels as per naming convention in original paper, equivalent group annotations from Gu *et al.* dataset: BCR/ABL $\equiv$ Ph, E2A/PBX1 $\equiv$ TCF3-PBX1, MLLr $\equiv$ KMT2A, Neg $\equiv$ Other, TEL/AML $\equiv$ ETV6-RUNX1.

as "Negative" in the original publication [133]) as either Ph-L or otherwise. To estimate this we used an unsupervised learning approach with k-means clustering to partition the data into 2 categories based on the expression of a panel of 13/15 genes that was developed for the identification of Ph-L patients from gene expression data [134, 158] (2/15 genes were not represented on the microarray). Using this approach we found that 26/81 previously unclassified samples were assigned to the cluster that also contained 73/78 Ph+ patient samples and we therefore annotated these patient samples as Ph-L (a single sample from the KMT2Ar group was assigned to this cluster but by definition cannot be reclassified as Ph-L) (figure 4.1.9).

Reclassifying these samples meant that 14% (26/191) of the patients in this data set were classified as Ph-L, which compares to the estimated prevalence of 20-25% amongst

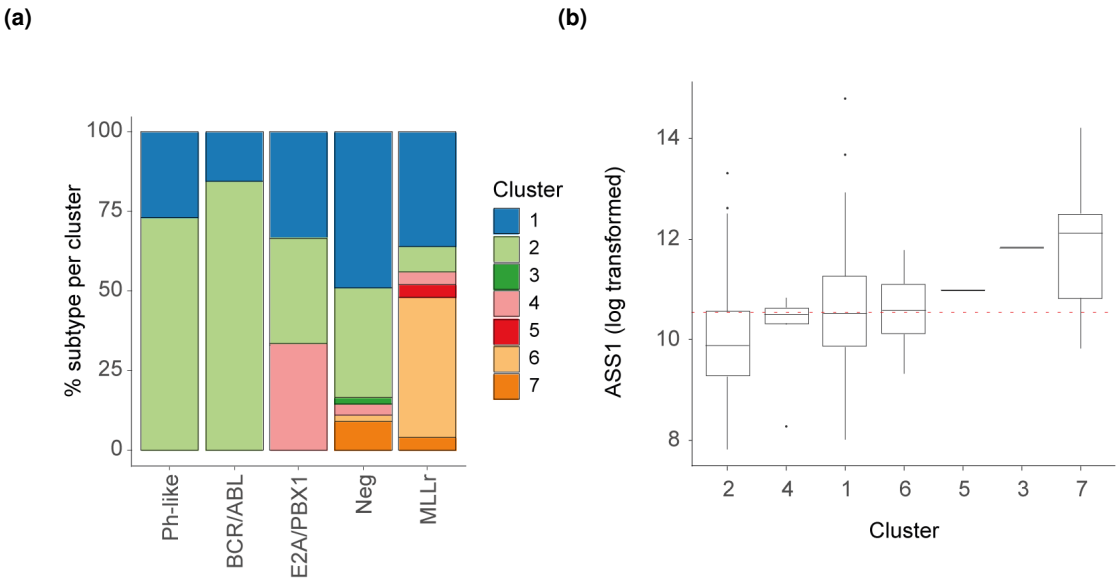

Figure 4.1.10: **Across B-ALL subgroups *ASS1* expression is non-random and low expression is associated with altered metabolic gene networks**
a) Assignment of Geng *et al.* samples to clusters from Gu *et al.* UMAP analysis by k-NN classification. Group labels as per naming convention in original paper, equivalent group annotations from Gu *et al.* dataset: BCR/ABL ≡ Ph, E2A/PBX1 ≡ TCF3-PBX1, MLLr ≡ KMT2A, Neg ≡ Other, TEL/AML ≡ ETV6-RUNX1.
b) Boxplot of *ASS1* expression per assigned cluster in Geng *et al.* dataset. Mid-bar represents median, box limits request IQR, whiskers represent 95% dispersion and points represent outliers. Red dotted line represents mean *ASS1* expression from the remaining unclassified "Negative" cytogenetic samples.

adults with B-ALL [159], suggesting an adequate level of accuracy with a likely low false positive rate. As a validation step, we performed k-NN classification, training the classifier on z-transformed expression values from the Gu *et al.* RNA-seq data, where Ph-L status was established as part of diagnostic workup, and then used the trained classifier to test likewise z-transformed microarray expression from the Geng *et al.* dataset. In this repeated analysis we found that 23/26 samples annotated as Ph-L were again classified as Ph-L (the remaining 3 were all classified as high hyperdiploid), while none of the remaining unclassified samples from the Geng *et al.* data set were assigned as Ph-L, indicating an acceptable degree of accuracy.

Next, to test whether our cluster 2 specific 19 marker gene set could robustly identify *ASS1*-low samples in the validation data, we trained another k-NN classifier to predict cluster membership based on the cluster 2 z-transformed marker gene expression from the

entire Gu *et al.* RNA-seq cohort and then tested this in the Geng *et al.* microarray data (figure 4.1.10a). In broad agreement with the initial clustering, we found that 66/78 Ph+ and 19/26 Ph-L samples were assigned to cluster 2, the cluster most likely to be arginine auxotrophic, as well as a similarly corresponding assignment of KMT2Ar samples to clusters 6 and 7 as in the original clustering of the Gu *et al.* dataset (figure 4.1.7). Comparing *ASS1* between the assigned clusters in the validation data (figure 4.1.10b) we again found a similar distribution of expression as in the original clustering analysis (figure 4.1.6), with cluster 2 the lowest and cluster 7 the highest, which is expected since *ASS1* was a training feature.

4.2 Summary

By analysis of gene expression from a combined cohort of 2179 adult and paediatric patients with B-ALL we have formed the hypothesis that around half of B-ALL patients are expected to have low expression of *ASS1* that is part of a recurrent transcriptional signature within a network of genes concerned with amino acid metabolism. These patients are predicted to be the most likely to derive clinical benefit from ADI-PEG20 but the functional effect is as-yet undefined and requires to be benchmarked for tumour cells with representative levels of *ASS1*. If ADI-PEG20 showed promising activity in B-ALL as a function of baseline *ASS1* expression, then this could be incorporated into diagnostic work-up and combined analysis of marker gene expression might refine the prediction of response to treatment by highlighting those samples with a truly re-wired *ASS1* signature.

Chapter 5

Functional models of ADI-PEG20 susceptibility in B-ALL

5.1 ASS1 expression varies across cell line models of B-ALL

In the previous chapter we established that *ASS1* expression is heterogeneous amongst B-ALL subtypes, making the prediction that there would be a range of sensitivities to arginine starvation across the disease. We therefore wanted to benchmark the functional effects of arginine starvation using ADI-PEG20 against models of B-ALL representing a range of *ASS1* expression. The clinical experience to date with ADI-PEG20 has shown that only those with the lowest *ASS1* expression benefit from this therapy [98] and so we began with the simple hypothesis that *ASS1*-low expressing B-ALL would be sensitive to arginine starvation while *ASS1*-high expressing B-ALL would be resistant.

To generate a panel of cell lines with a range of *ASS1* expression for testing we first used publicly available gene expression data [160] to stratify a large cohort of established B-ALL models by *ASS1* (figure 5.1.1). From this range we wanted to select cell lines with low *ASS1* (predicted sensitive), high *ASS1* (predicted resistant) and also were particularly interested to test cell line models of ETV6::RUNX1 translocated, HeH, Ph-L and/or Ph+ ALL, since these represent the major paediatric and adult groups that had clustered together in the dimensional reduction analysis of our core *ASS1*-related gene set from the previous chapter (figures 4.1.4, 4.1.5 and 4.1.7).

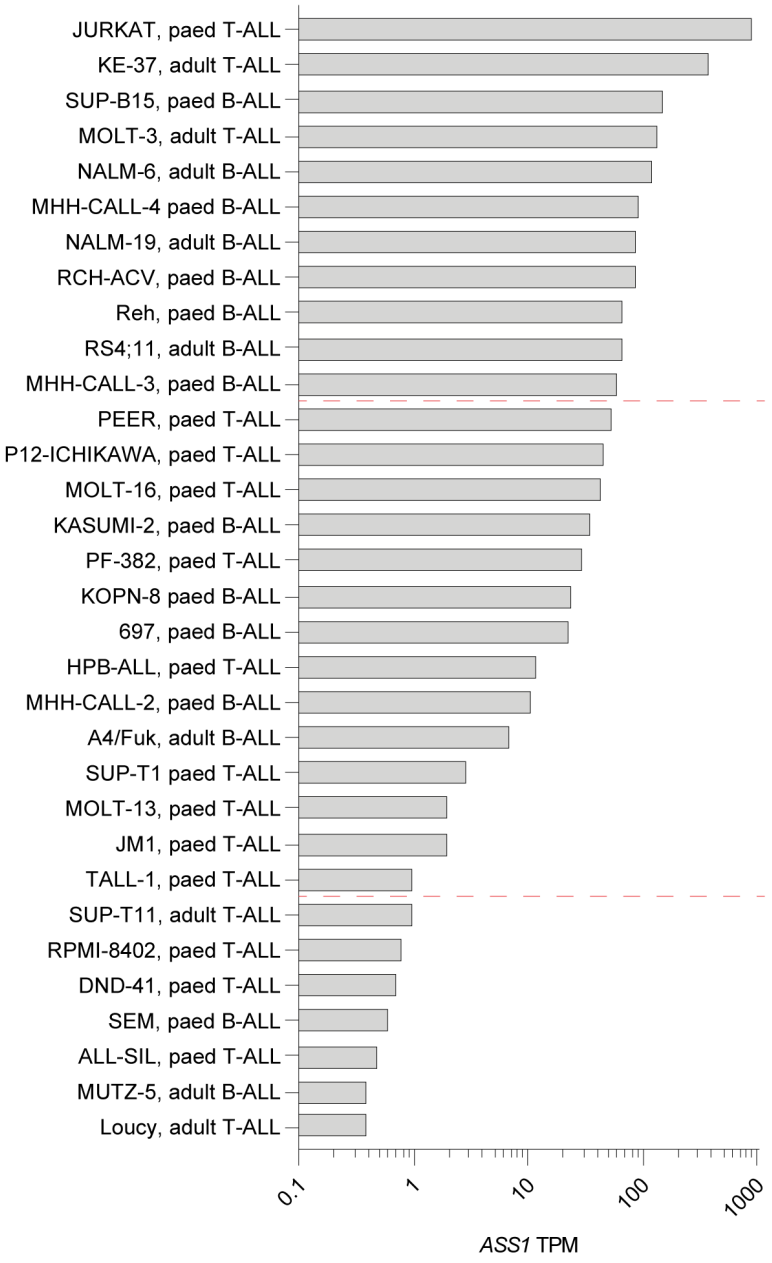

Figure 5.1.1: ***ASS1* expression varies across cell line models of B-ALL**
Cell line *ASS1* expression as transcripts per million (TPM), from Cancer Cell Line Encyclopedia [160]. Red dashed lines indicate tertiles of *ASS1* expression.

We used the lowest tertile of *ASS1* expression as the sub-cohort predicted to have highest sensitivity to ADI-PEG20 and from this we chose MUTZ-5, a cell line derived from the peripheral blood of a 26 year-old male at relapse with a CRLF2 rearranged Ph-L phenotype [161, 162], and therefore in keeping with our previous prediction that Ph-L B-ALL would have low *ASS1* expression. The alternative B-ALL model from the lowest tertile was SEM and despite being a widely cited cell line was not chosen since this resembles a mixed phenotypic leukaemia with KMT2Ar [163, 164] with demonstrated lineage switch potential [165] and therefore potentially a confounding issue in planned CAR-T experiments.

From our previous analysis it would have been a useful validation to use a low-hypodiploid cell line model as our predicted-resistant control but a cell line with this phenotype was not part of the gene expression data set. We therefore chose the cell line RS4;11 from the upper tertile, assuming that cell lines from this sub-cohort would be the least sensitive to ADI-PEG20. As with SEM, RS4;11 is a KMT2Ar B-ALL model [166, 167] with the potential to lineage switch [165] but since this was selected as a predicted-resistant control for initial functional modelling, this was less of a concern.

To include a model of ETV6::RUNX1 rearranged B-ALL we selected Reh, a widely cited cell line from this subgroup [168]. Contrary to our prediction from the previous chapter that this cytogenetic group would have low *ASS1* expression this cell line came from the top tertile of gene expression. However, there were no other ETV6::RUNX1 models included in the data set and likewise no HeH models that had also been predicted to be *ASS1*-low[1] and so Reh was included for functional testing.

Similarly, we wanted to include a Ph+ B-ALL model but found that the corresponding cell line from this data set, SUP-B15 [170], was again part of the top tertile of *ASS1* expression. However, in the case of Ph+ B-ALL another widely cited cell line is TOM-1 [171] and based on an alternative publicly available gene expression data set [172] we predicted that this would have very low *ASS1* expression and therefore fit more closely to the prediction from our previous chapter that Ph+ B-ALL would generally be *ASS1*-low. This cell line was therefore chosen as a model of Ph+ B-ALL and based on the published gene expression data was predicted to be ADI-PEG20 sensitive.

[1] MHH-CALL-2 is sometimes cited as a high hyperdiploid cell line but likely represents the near haploid cytogenetic group [169]

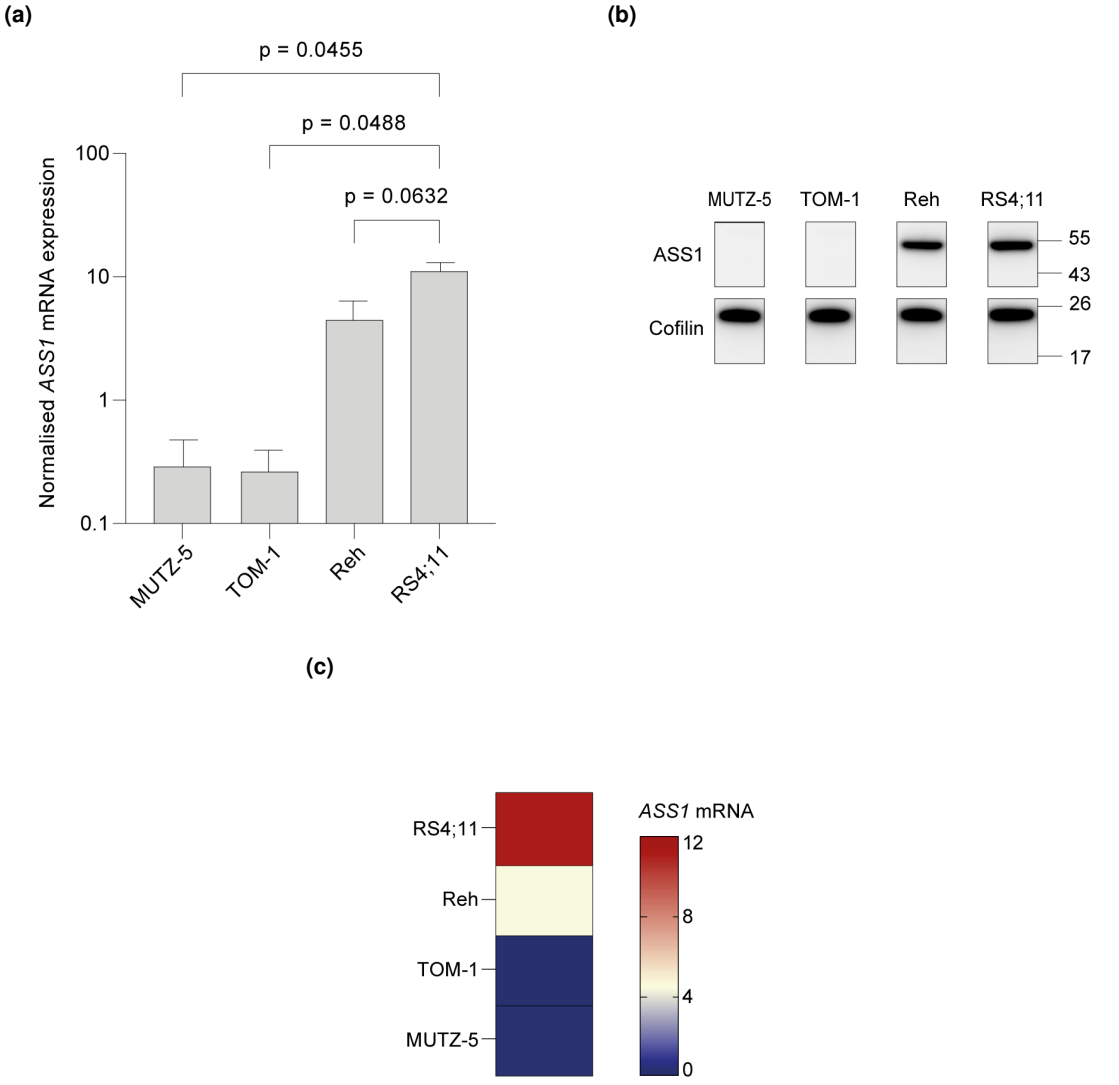

Figure 5.1.2: ***ASS1* expression varies across cell line models of B-ALL**
a) Baseline *ASS1* expression from chosen cell line panel. *ASS1* values calculated by $\Delta\Delta C_T$ method using internal *GAPDH* references and normalised to robust whole panel average. Data represent averages from 3 independent RNA-extracts, each ran in technical triplicates, p-values from ANOVA with Dunnett's multiple comparison test using RS4;11 as control.
b) Western blot analysis of baseline ASS1 protein expression across cell line panel.
c) Heatmap defining cell line colour codes based on baseline *ASS1* mRNA expression from figure 5.1.2a for quick reference in figures hereafter.

To validate the data obtained from these public sources we measured ASS1 expression by qPCR and western blotting in the panel of cell lines (figures 5.1.2a and 5.1.2b). We observed low *ASS1* mRNA levels in both MUTZ-5 and TOM-1 cell lines, with corresponding effectively undetectable protein levels. In the Reh and RS4;11 cell lines we observed an intermediate and high level of *ASS1* mRNA, respectively, with a similar level of protein expression. Finally, to allow for a convenient and rapid reference to the baseline *ASS1* expression level in figures hereafter, we used a heatmap depiction of the mRNA expression to develop corresponding colour codes for each cell line (figure 5.1.2c).

Using our in-house measurement of gene and protein expression, our fundamental hypothesis of the inverse relationship between sensitivity to ADI-PEG20 and baseline *ASS1* expression therefore predicts increased sensitivity to ADI-PEG20 amongst MUTZ-5 and TOM-1, a more resistant phenotype in RS4;11 and possibly an intermediate phenotype in Reh.

5.2 ADI-PEG20 leads to growth inhibition via cell cycle arrest and apoptosis in ASS1-low B-ALL

To make an overview assessment of the response to arginine starvation in our panel of cell lines and to titrate the optimum concentration of ADI-PEG20 for more detailed further studies, we first tested a range of doses over a 72 hour *in vitro* exposure, using ATP content as a surrogate for viability (figure 5.2.1a). The greatest reduction in viability was in the TOM-1 cell line, with residual ATP signal reduced to 10.4% of untreated control (95%CI 8.54-12.24%) at ADI-PEG20 concentrations of 1000ng/ml or higher. This concentration appeared to represent the EC_{max} for all cell lines and in keeping with our prediction, the depth of maximum response was next greatest for MUTZ-5 with residual ATP signal of 35.57% (95%CI 29.76-41.10%), then Reh with residual ATP signal of 50.96% (95%CI 42.40-57.10%) and finally RS4;11 with a residual ATP signal of 72.10% (upper 95%CI 76.45%). This indicates that in all cell lines there is a degree ADI-PEG20 effect in terms of an ATP content reduction, and the depth of response inversely correlates with baseline *ASS1* expression.

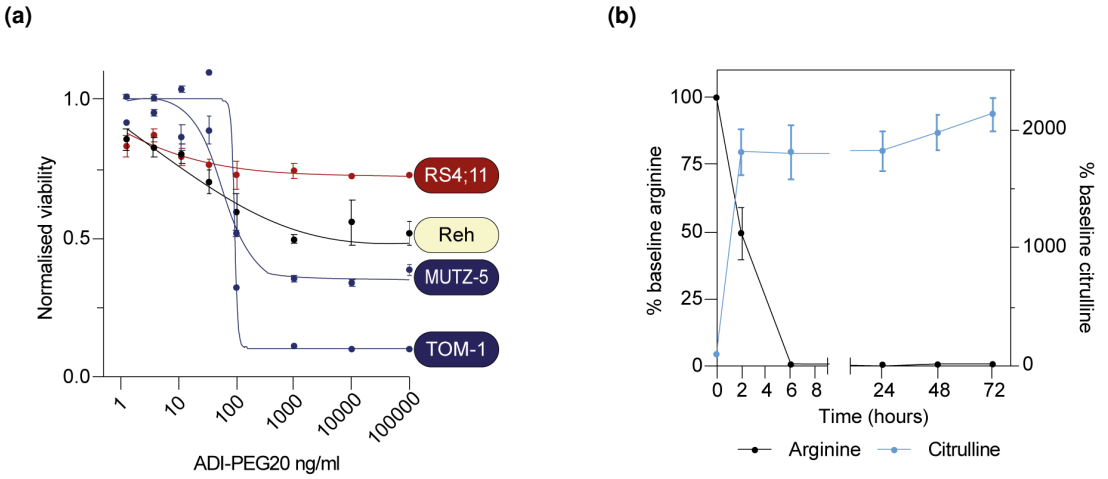

Figure 5.2.1: **ADI-PEG20 leads to growth inhibition via cell cycle arrest and apoptosis in ASS1-low B-ALL**
a) ADI-PEG20 dose titration against cell line panel using ATP based assay for viability estimate. Data represent averages of 3-6 independent experiments. Cell line labels coloured to reflect *ASS1* expression as per figure 5.1.2c.
b) Normalised arginine and citrulline concentrations in culture media incubated at 37° in presence of 1000ng/ml ADI-PEG20. Data represent averaged results from 3 independent ADI-PEG20 treatments, each analysed in duplicate.

Finding a similar estimated EC_{max} for all cell lines is rational for an enzyme base treatment and likely represents the concentration of ADI-PEG20 at which all substrate (arginine) is rapidly bound, and therefore increasing concentrations do not speed up the conversion of arginine to citrulline. Others have described a similar saturation effect for ADI-PEG20 [173] but the actual dynamics of arginine conversion have not been clearly mapped.

To assess this, we tested the arginine and citrulline concentrations in ADI-PEG20 treated media over a 72 hour time course using LC-MS/MS (figure 5.2.1b). We observed that at an ADI-PEG20 concentration of 1000ng/ml, arginine is completed converted to citrulline within 6 hours of ADI-PEG20 exposure and while arginine is rendered undetectable, citrulline increases to around 20-times the baseline concentration. The *in vivo* pharmacodynamic properties of ADI-PEG20 have been tested elsewhere and at clinical doses, arginine is depleted rapidly with levels undetectable by 24 hours [174, 175]. Allowing for timescale differences between *in vitro* culture models and clinical dosing, we therefore decided to utilise this EC_{max} concentration of ADI-PEG20 for all further studies as an approximate

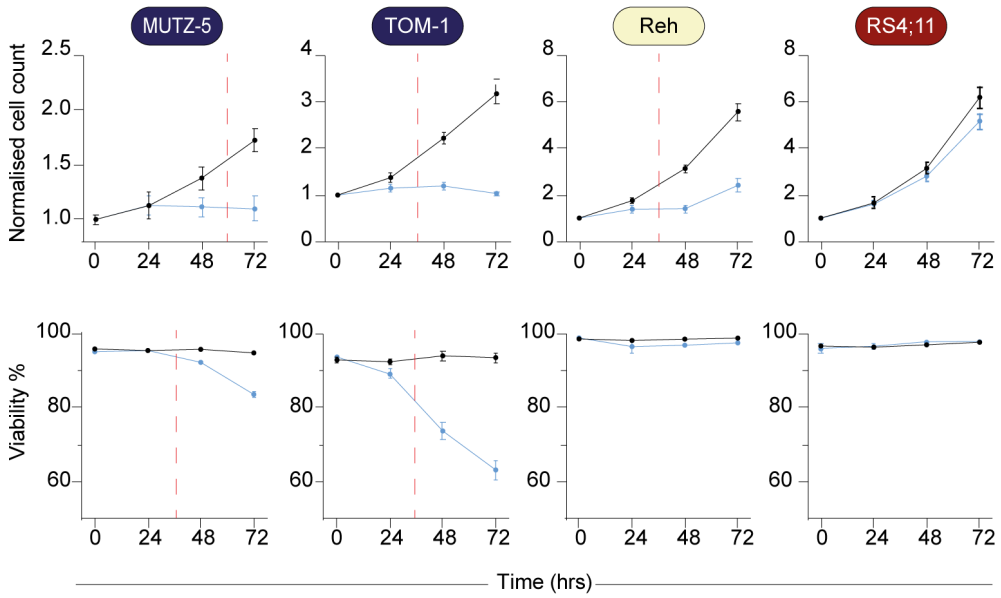

Figure 5.2.2: **ADI-PEG20 leads to growth inhibition via cell cycle arrest and apoptosis in ASS1-low B-ALL**
Cell line growth (top row) and viability (bottom row) during 72 hours of exposure to 1000ng/ml ADI-PEG20 (blue points/lines) or control (black points/lines). Data represent 9 technical replicates per plot aggregated from 3 independent experiments. Red dashed lines indicate thresholds after which differences in cell count and/or viability between consecutive time points are significant at $p \leq 0.05$ from 2-way ANOVA using treatment and time as factors with Šídák's multiple comparisons test.
Cell line labels coloured to reflect *ASS1* expression as per figure 5.1.2c.

reflection of a clinically relevant pharmacodynamic effect.

Having ascertained the basic response profile of our cell line panel as well as the EC_{max} concentration using ATP content as a surrogate for viability we next wanted to ask how ADI-PEG20 would affect cell line proliferation and viability using a more direct assay. We therefore serially enumerated cells and measured viability during the course of treatment using automated fluorescence cell counting (figure 5.2.2). In the *ASS1*-low cell lines MUTZ-5 and TOM-1, we observed cytostasis (2-way ANOVA $p = 0.0035$ for difference in cell counts at 72 hours for MUTZ-5, $p < 0.0001$ from 48 hours for TOM-1) and a significant, progressive reduction in viability from 48 hours in MUTZ-5 ($p < 0.0001$) and 24 hours in TOM-1 ($p < 0.0001$). In keeping with the ATP reduction seen in the *ASS1*-intermediate Reh cell line, we also saw an approximately equivalent reduction in cell count at 72 hours, but we did not see a reduction in viability, indicating that while ADI-PEG20 reduced growth it did not lead to cell death. We had also seen a minor reduction in ATP content in the *ASS1*-high

RS4;11, but when measuring cell count and viability directly, we saw neither reduction in growth nor viability.

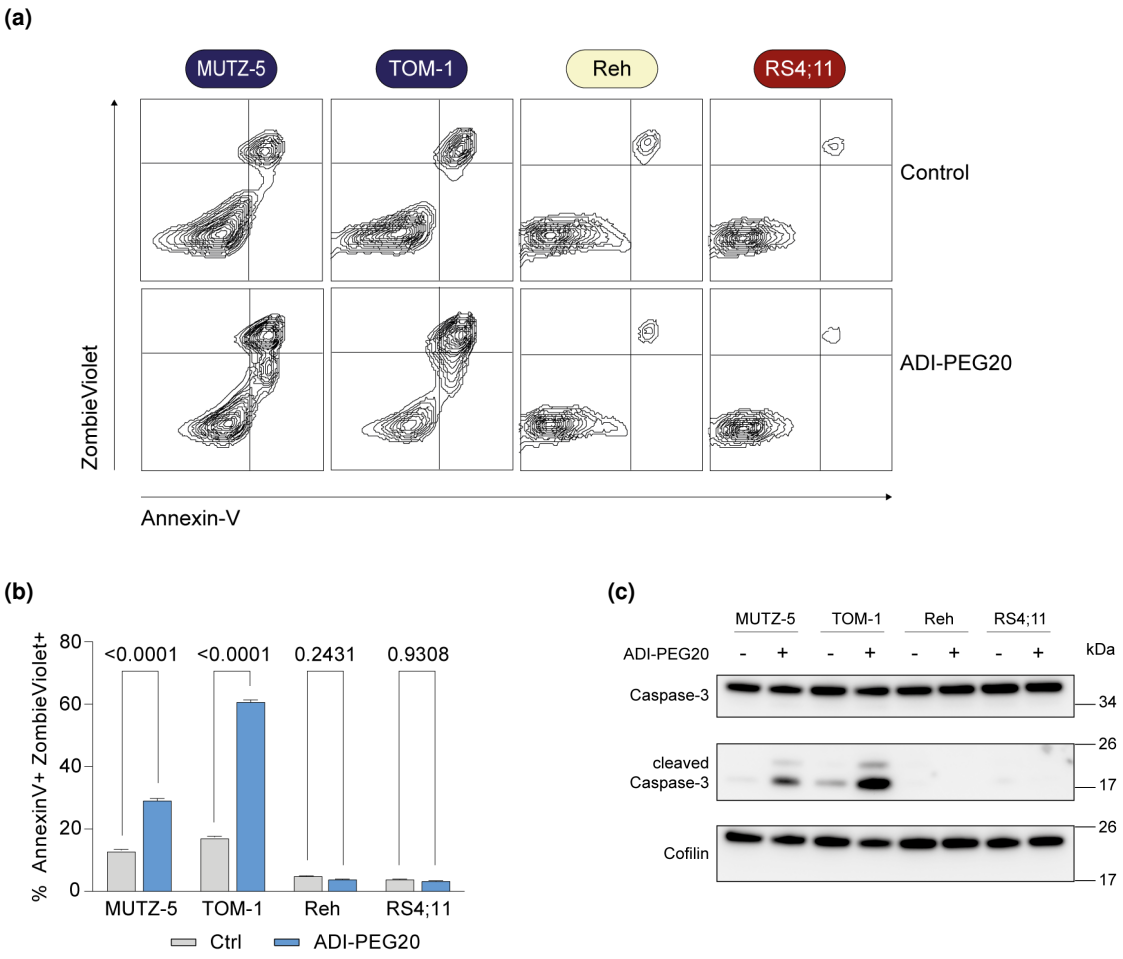

Figure 5.2.3: **ADI-PEG20 leads to growth inhibition via cell cycle arrest and apoptosis in ASS1-low B-ALL**
a) Representative contour plots representing density of cell events acquired by FACS across cell line panel with or without ADI-PEG20. Cell line labels coloured to reflect *ASS1* expression as per figure 5.1.2c.
b) Proportion apoptotic cells as calculated by FACS analysis of viability and Annexin-V expression. p-values from 2-way ANOVA using treatment and cell line as factors, with 9 technical replicates aggregated over 3 independent experiments per condition.
c) Western blotting analysis of caspase-3 cleavage after 72 hour exposure to ADI-PEG20, compared to control.

To ask whether this observed reduction in viability was through a regulated cell death process we next tested Annexin-V expression alongside staining by ZombieViolet, a fluorescent viability dye, by FACS (figures 5.2.3a and 5.2.3b). In keeping with the previous

analysis we observed that after 72 hours of ADI-PEG20 there was a significant increase in cells double positive for Annexin-V expression and viability staining (indicating apoptosis) in the *ASS1*-low cell lines MUTZ-5 ($p < 0.0001$) and TOM-1 ($p < 0.0001$), but no change in the *ASS1*-intermediate or -high Reh and RS4;11, respectively. We also noted that in the MUTZ-5 cell line there was an increase in pre-apoptotic cells, marked by Annexin-V positivity but no viability dye staining (lower right quadrants, figure 5.2.3a), suggesting that while the depth of response in MUTZ-5 is not as great as in TOM-1, this would likely progressively deepen if the 72 hour treatment period could be extended. Confirming that cell death was via regulated apoptosis, we measured activation of caspase-3, through cleavage to its p17 (17kDa) form, by western blotting (figure 5.2.3c). In keeping with the previous results, we saw a clear cleavage of caspase-3 that was confined to the *ASS1*-low cell lines MUTZ-5 and TOM-1.

Having established that ADI-PEG20 triggers apoptosis in the *ASS1*-low cell line models, we next wanted to ask what were the molecular determinants of regulated cell death. To do this we used a 35-target immuno-blotting array, consisting of a range of pro- and anti-apoptotic proteins and tested cell lysates generated from MUTZ-5 and TOM-1 after 72 hours of ADI-PEG20 (figure 5.2.4). In general, we saw an increase in protein expression across all targets, most notably from TOM-1 lysates and therefore limited our attention to those proteins whose expression at least doubled in a concordant manner across both cell lines.

Amongst the subset of protein targets with either executioner or pro-apoptotic functions we saw a concordant increase in cleaved caspase-3, in keeping with our previous measurement of the same molecule by western blotting (figure 5.2.3c). We also saw concordant increases in Bax and cytochrome-c expression, which are 2 cooperating proteins in regulated apoptosis [176], reinforcing the concept that arginine starvation with ADI-PEG20 induces programmed cell death.

Also notable was the concordant, dual upregulation of DR4 and DR5, receptors for exogenous and autocrine death ligands that initiate the extrinsic, also known as death receptor mediated, apoptosis pathway. The upregulation of these receptors is in-keeping with other reports regarding ADI-PEG20 treatment [120] and has been implicated in the sensitisation of arginine starved cells to the effects of TRAIL. This will be the focus of, and

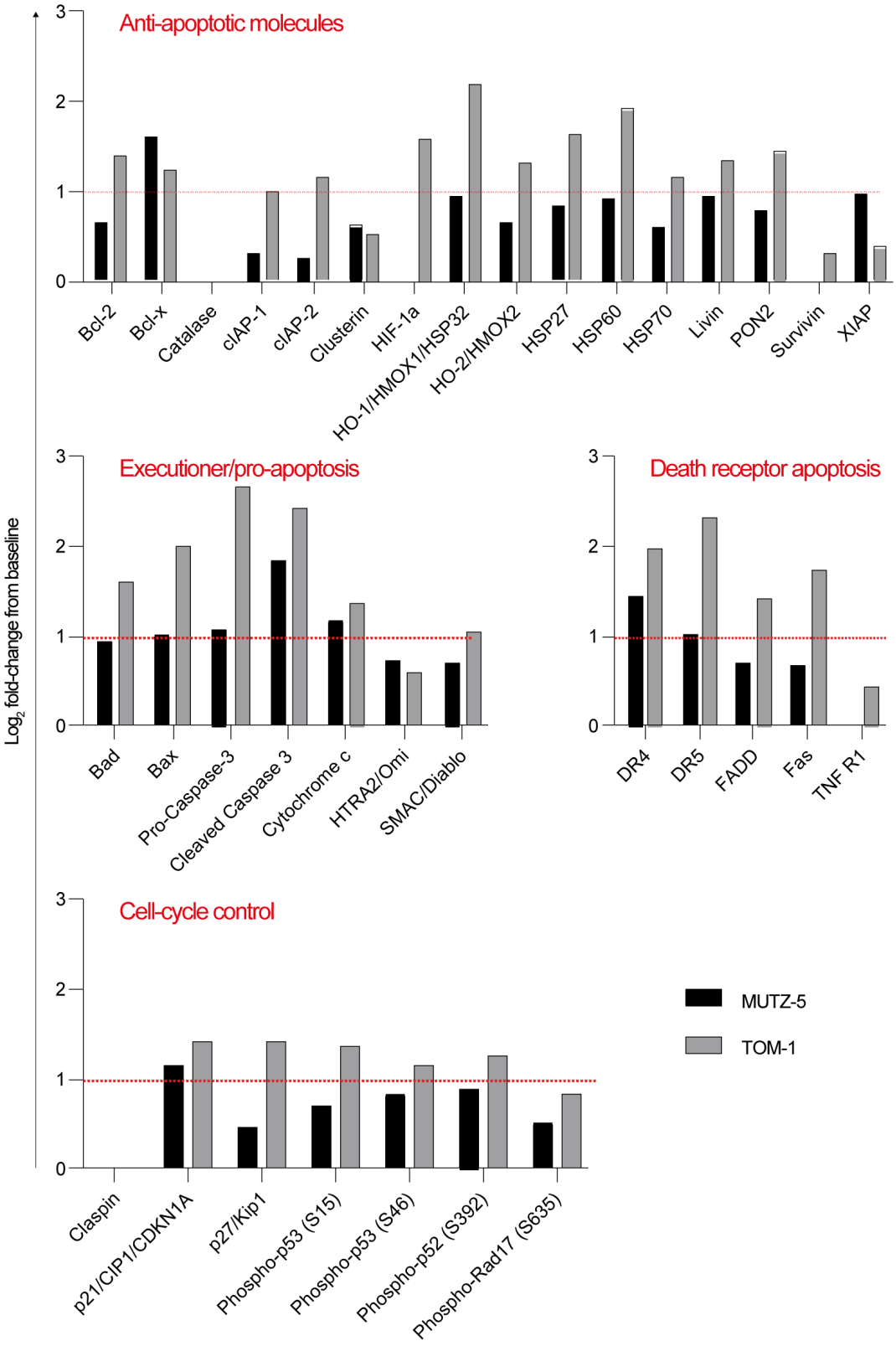

Figure 5.2.4: **ADI-PEG20 leads to growth inhibition via cell cycle arrest and apoptosis in ASS1-low B-ALL**
Protein expression results from immuno-blotting array. Array spots density was averaged over duplicate repeats and data are presented as $\log_2$ Fold Change ($\log_2$FC) treated from baseline.

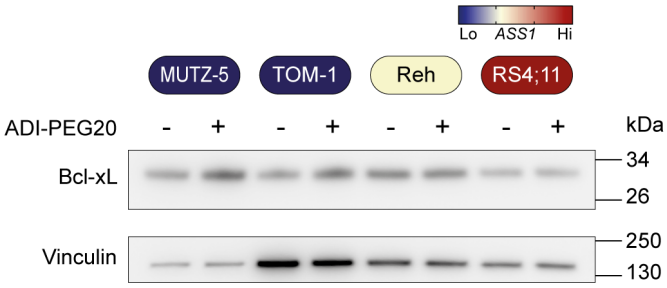

Figure 5.2.5: **ADI-PEG20 leads to growth inhibition via cell cycle arrest and apoptosis in ASS1-low B-ALL**
Western blotting analysis of Bcl-x_L expression in cell line panel with or without 72 hour treatment with ADI-PEG20. Cell line labels colour coded by baseline *ASS1* expression.

therefore discussed in greater detail in, following chapters.

We were next interested by the upregulation of Bcl-x, a member of the Bcl-2 family of proteins, subdivided into a pro-apoptotic short isoform Bcl-x_S and an anti-apoptotic long isoform Bcl-x_L. We were particularly interested in the possible increased expression of Bcl-x_L, since targeting of this anti-apoptotic molecule with the drug navitoclax has gained some traction in B-ALL [177] and if expression were to increase during ADI-PEG20 treatment then concomitant inhibition of Bcl-x_L would be a rational combination approach. To investigate this potential further we therefore analysed expression of Bcl-x_L in independent lysates extracted from our entire cell line panel after an equivalent 72 hour incubation with ADI-PEG20 (figure 5.2.5). We saw a subtle but noticeable increase in Bcl-x_L after ADI-PEG20 treatment that was present in both *ASS1*-low cell lines, MUTZ-5 and TOM-1, but not in the *ASS1*-intermediate or -high cell lines, Reh and RS4;11, respectively. Intriguingly, inhibition of Bcl-x_L has been shown in the work by Braun *et al.* to sensitise cancer cells to nutrient starvation conditions [178] and further investigations with combined ADI-PEG20 and Bcl-x_L inhibition follow in the next chapter.

As well as delineating the protective effect of Bcl-x_L, Braun *et al.* [178] also demonstrated the anti-apoptotic role of the cell cycle regulator p21 in cancer cells undergoing nutrient

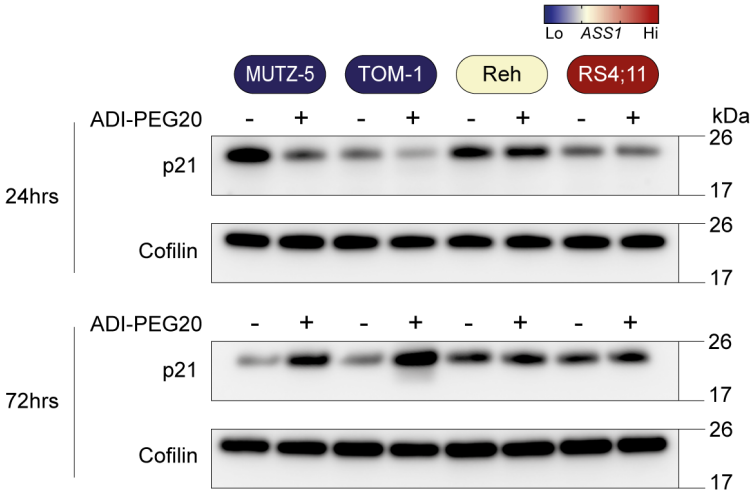

Figure 5.2.6: **ADI-PEG20 leads to growth inhibition via cell cycle arrest and apoptosis in ASS1-low B-ALL**
Western blotting analysis of cell cycle regulator p21 expression in cell line panel with or without 24 or 72 hour treatment with ADI-PEG20. Cell line labels colour coded by baseline *ASS1* expression.

starvation. In line with this, we saw a concordant upregulation of p21 in our immunoblotting array across both *ASS1*-low cell lines and when we repeated this by western blotting we found strong p21 upregulation at 72 hours in the *ASS1*-low cell lines but not in the *ASS1*-intermediate or -high controls (figure 5.2.6 lower blot).

p21 exerts its protective effect during metabolic stress via negative regulation of cell cycle progression [179] and so increased expression in lysates generated from surviving MUTZ-5 and TOM-1 cells after 72 hours of ADI-PEG20 is in keeping with the reduced growth rate of *ASS1*-low cell line models observed in our proliferation assays (figure 5.2.2). In the *ASS1*-intermediate and -high controls, Reh and RS4;11 respectively, the growth rate at 72 hours was approximately the same amongst ADI-PEG20 treated and control cells (figure 5.2.2) and corresponding with this we did not see any change in p21 expression at this time point (figure 5.2.6 lower blot). In the *ASS1*-intermediate cell line Reh we had observed an apparent initial reduction in growth rate between 24 and 48 hours of ADI-PEG20 and so we wondered if there may have been an earlier upregulation of p21. However, when we measured this by western blotting we saw no difference in 24 hour lysates between treatment and control (figure 5.2.6 upper blot). Unexpectedly, we did see a downregulation

of p21 in the *ASS1*-low cell lines at 24 hours which contrasts the pattern of expression at 72 hours. However, since there were no statistically significant differences in cell counts at this time point in these cell lines this is not necessarily contradictory to the observed effect at 72 hours. Interestingly, it has been reported that p21 expression is negatively regulated by c-Myc [180] and separately has also been reported in cancer models that c-Myc is upregulated under arginine stress [181, 182], which is therefore a potential explanation for the initial downregulation of p21 expression, although we did not test this.

Since we had seen a reduction in overall proliferation in 3 of 4 of our cell line panel with a range of degrees of apoptosis (figure 5.2.2) and combined with a clear induction of the cell cycle regulator p21 in MUTZ-5 and TOM-1 at 72 hours, we next hypothesised that the growth inhibition elicited by ADI-PEG20 was at least in part via cell cycle arrest. To test this we again used FACS to analyse the expression of Ki-67 and DNA content after gating on live cells (figures 5.2.7a and 5.2.7b). Using this analysis we saw an increase of live cells that were in the G0 and G1 cell cycle states with a corresponding reduction in both S- and G2/M-phase cells in the *ASS1*-low cell lines MUTZ-5 and TOM-1, with no difference seen in the *ASS1*-intermediate or -high Reh and RS4;11, respectively. Most notably the DNA content of the G0 state cells for both *ASS1*-low cell lines, but especially for TOM-1, smeared towards sub-diploid intensity, with the most likely explanation for this being fragmentation of DNA as part of regulated cell death. Cell cycle arrest is consistent with the previously reported effects of ADI-PEG20 in other arginine auxotrophic cancer types and of a previous report of the use of arginine deiminase (*i.e.* the non-pegylated precursor of ADI-PEG20) in both T- and B-ALL cell line models [112]. Furthermore, this is similar to the cell cycle effect of asparaginase in ALL [183]. The observation of fragmented DNA in intact membrane, G0-arrested cells suggests that apoptosis is being triggered at least in part from the cell-cycle arrested state.

Taken together, these data demonstrate that ADI-PEG20 induces cell death via regulated apoptosis with cell cycle arrest in the lowest *ASS1* expressing B-ALL models. Where *ASS1* was intermediate, as in Reh, ADI-PEG20 induced a degree of cytostasis but did not induce cell death and by 72 hours the cell cycle profile was identical to that of untreated cells. This brings the effects of ADI-PEG20 on *ASS1*-low B-ALL in-line with those in other arginine

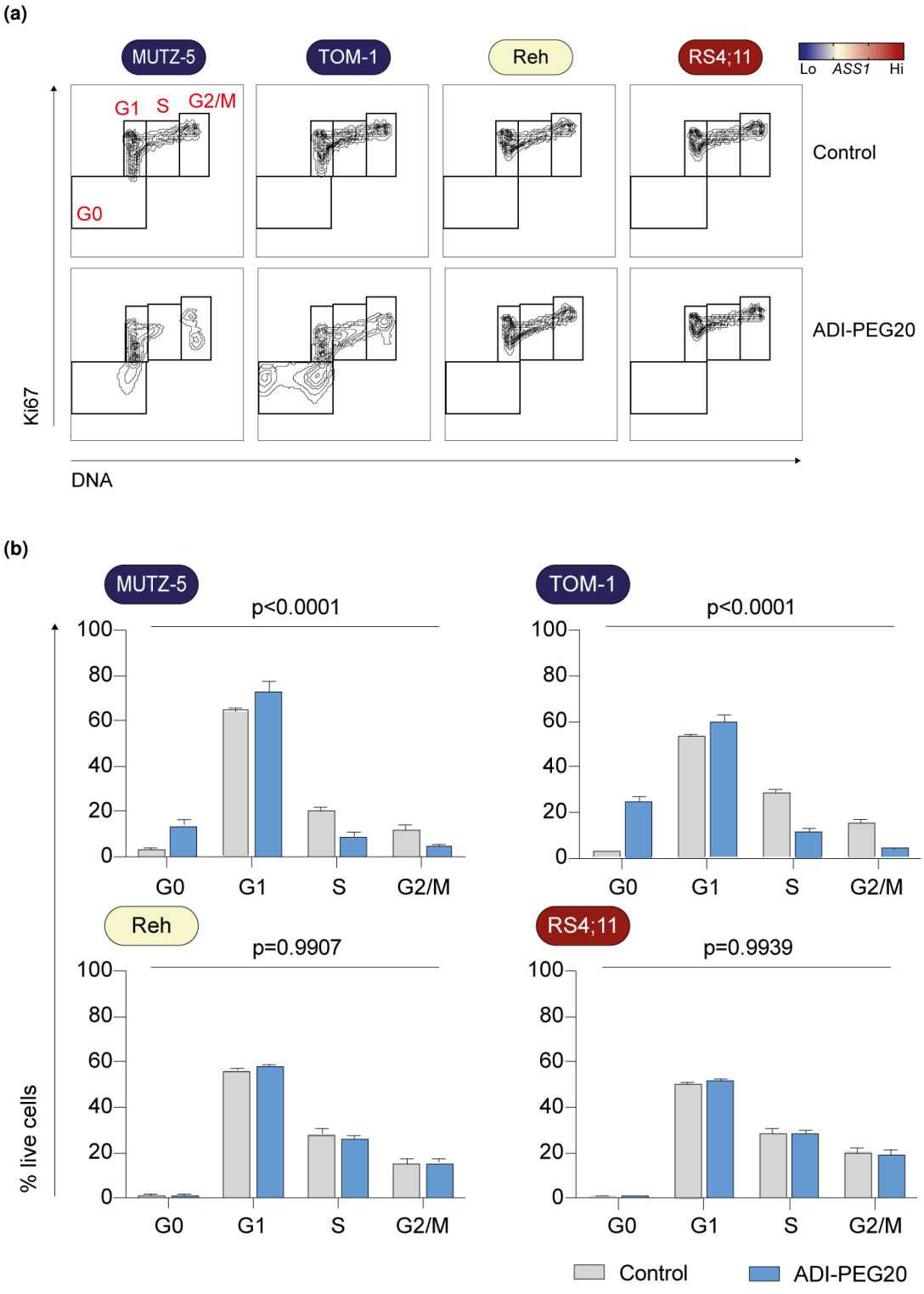

Figure 5.2.7: **ADI-PEG20 leads to growth inhibition via cell cycle arrest and apoptosis in ASS1-low B-ALL**
a) Representative contour plots depicting cell cycle after 72 hours ADI-PEG20 or control. b) Proportions of live cells per cell cycle phase. Data from 5 replicates aggregated over 2 independent experiments, p-values from χ^2 test using % cell cycle phase averaged across all replicates

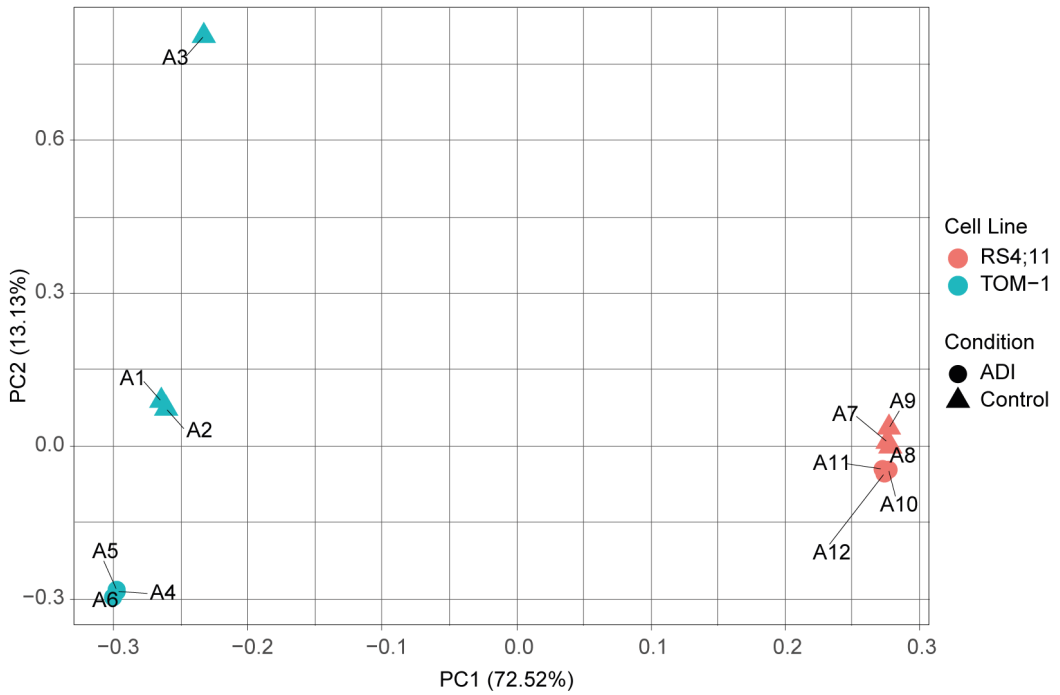

Figure 5.3.1: **ADI-PEG20 activates cell stress signalling**
PCA plot illustrating distribution of transcriptome replicates in dimensionally reduced space.

auxotrophic tumour types and draws some parallels to the effects of asparaginase in B-ALL.

5.3 ADI-PEG20 activates cell stress signalling

Having characterised the induction of cell cycle arrest and apoptosis at a functional level, we next wanted to understand more about the molecular drivers of the fate of *ASS1*-low B-ALL when starved of arginine by ADI-PEG20. To begin, we extracted RNA from *ASS1*-low TOM-1 cells and *ASS1*-high RS4;11 cells after 24 hours of treatment or control and submitted extracts for bulk RNA-sequencing.

Assessing the individual replicates from each cell line and condition in dimensionally reduced space (figure 5.3.1) we noticed, as expected, the greatest degree of transcriptional contrast was that driven by the different cytogenetic backgrounds of the cell lines. A further contrast was observed between treated and untreated TOM-1 cells along the 2nd principle component, although one replicate of treated TOM-1 cells (A3, figure 5.3.1) appeared to have a more exaggerated response than in the other TOM-1 treatment replicates.

Contrasting this spread in TOM-1, there was very little separation, if any, between

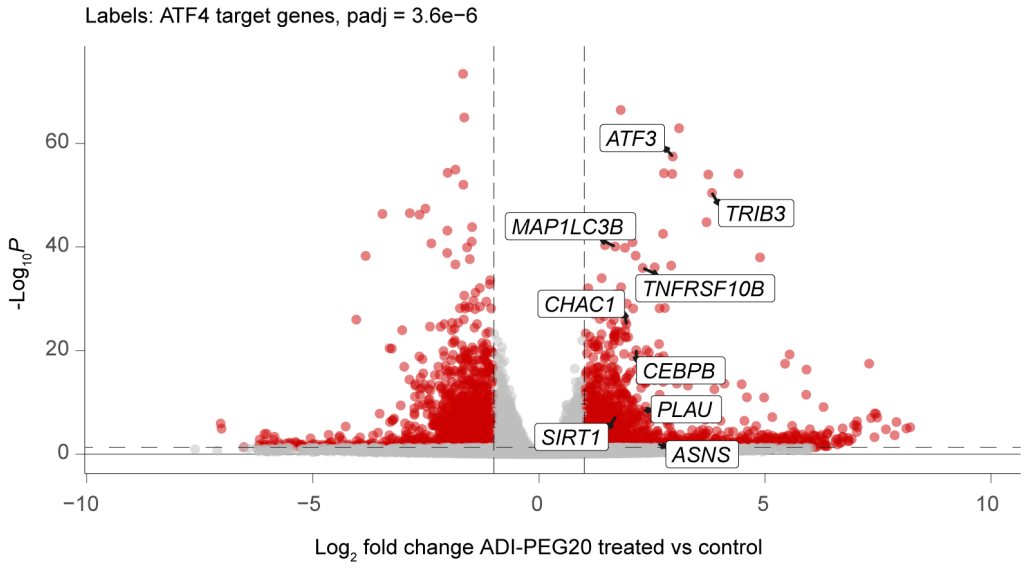

Figure 5.3.2: **ADI-PEG20 activates cell stress signalling**
Volcano plot illustrating DEGs between ADI-PEG20 treated and control TOM-1 cells. Genes labelled according to the top over-represented transcription factor target gene set from TRRUST database [146]. RNA-seq performed on triplicate extracts from independent experiments. Red points indicate genes with absolute $\log_2$FC > 1 and adjusted $p < 0.05$, grey points are those not meeting same criteria.

treatment and control replicates of RS4;11. Indeed, using the R package *deseq2* to fit a linear model to the data and compare DEGs between treatment and control in the RS4;11 cell line, we did not observe a single gene with any fold change difference between ADI-PEG20 treatment and control meeting the adjust p-value threshold of $p < 0.05$. This was somewhat surprising given the gross shifts of arginine and citrulline in the culture media triggered by ADI-PEG20, but suggests that the higher baseline expression of *ASS1* by RS4;11 endows the cell line with sufficient intrinsic capacity to metabolise citrulline so as to restore intracellular arginine flows within 24 hours and therefore normalise necessary adaptations, if any, to arginine deplete media.

Using the same linear model analysis of DEGs between treatment and control in the TOM-1 model we did see a wide ranging modulation of gene expression with 1623 genes upregulated with a $\log_2$FC > 1 and adjusted p-value of less than 0.05, and 1685 genes downregulated with $\log_2$FC < -1 and same adjusted p-value criteria (figure 5.3.2). Using this set of up- and downregulated genes we performed GSEA analysis using the "Hallmark"

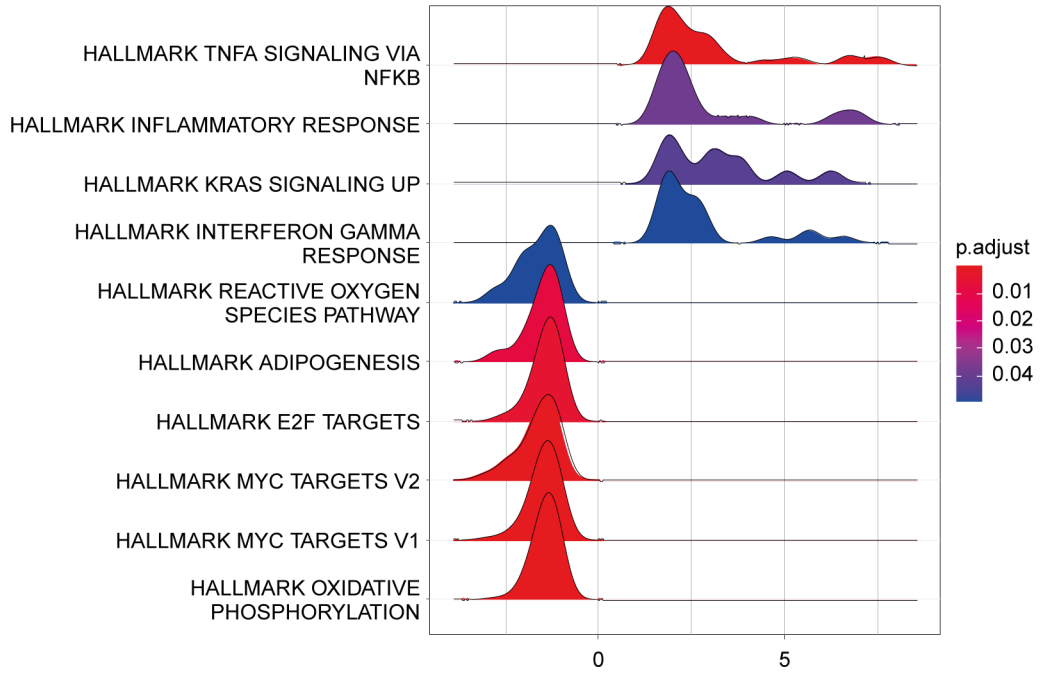

Figure 5.3.3: **ADI-PEG20 activates cell stress signalling**
Ridge plot illustrating pathway gene density according to $\log_2$FC treatment *vs* control from TOM-1 GSEA results after 24 hours treatment with ADI-PEG20 *vs* control. x-axis displays $\log_2$-fold change expression difference and density functions represent distributions of significantly modulated genes within each gene set.

gene set database and discovered an upregulation of genes belonging to inflammatory pathways and, in keeping with the previous functional analysis, a downregulation of genes associated with cell-cycle and metabolic pathways (figure 5.3.3). The downregulation of Myc targets is in keeping with that observed in responding patients from a trial of ADI-PEG20 in AML [105].

We were interested to ask if this gene expression modulation would be coordinated by the action of specific, for example, stress responsive transcription factors and so submitted our gene lists for analysis against the TRRUST database [146]. This analysis suggested that there was a significant over-representation of ATF4 target genes within the gene lists (adjusted $p = 3.6 \times 10^{-6}$, individual genes labelled in figure 5.3.2). The upregulation of gene targets of ATF4 makes sense in the context of ADI-PEG20 treatment, since this transcription factor is widely recognised as being a master orchestrator of the cellular response to amino acid stress, including arginine starvation [184, 185].

This analysis was also in agreement with the previously observed upregulation of DR5,

encoded by *TNFRSF10B*, and known to be triggered by ATF4 signalling as part of the response to prolonged Endoplasmic Reticulum (ER)-stress [186], that can be a result of, amongst other things, amino acid starvation [187]. What we did not observe however, was any modulation of *ATF4* mRNA expression itself ($\log_2$FC 0.4, adjusted $p = 0.9071$), although this does not preclude enhanced expression, since ATF4 protein expression is regulated by translational as well as transcriptional modulation [188].

To complement the GSEA analysis we also wanted to ask which were the most biologically important nodes within the set of genes modulated by ADI-PEG20 treatment in the *ASS1*-low TOM-1 cell line. To definitively answer this a set of detailed functional experiments would be required, but for the hypothesis generation stage it has been proposed that the *centrality* of a gene within a biological network is dictated by the degree of inter-connectivity of the corresponding protein with other proteins within that network [189]. To apply this concept to our data, we used the *cytoHubba* module [190] within the *Cytoscape* app, to reduce our data set to the top 20 most interconnected genes, according with predicted or known corresponding protein-protein interactions from the STRING database [131] (figure 5.3.4a). This sub-network of so-called "hub" genes contained a number of ER-stress and unfolded protein response elements (*ERN1*, *CEBPB*, *DDIT3*, *ATF3*) and other stress responsive elements (*BIRC3*, *JUN*, *HSPA1A*, *HSPA8*, *HSPB1*, *HSPE1*, *PPP1R15A*, *SOD1*). Also represented in this sub-network were genes with roles in inflammation (*CSF1R*, *ICAM1*) and other elements involved in regulation of transcription and translation (*NHP2*, *PHB*, *POLR2L*, *RPS15*).

We were particularly interested in the apparent centrality of *DNA Damage Inducible Transcript 3 (DDIT3)* amongst the ADI-PEG20 responsive genes, since its corresponding protein C/EBP Homology Protein (CHOP) is a downstream target of ATF4 and is responsible for initiation of apoptosis upon unresolved ER-stress [191]. We therefore wondered if the expression of ATF4 and CHOP might distinguish those cell line models destined to die under arginine starvation with ADI-PEG20 and those able to survive. To answer this question we performed western blotting analysis of these proteins with or without 24 hours of ADI-PEG20 treatment (figure 5.3.4b). In keeping with the prediction that ATF4 responsive genes were modulated by ADI-PEG20 (figure 5.3.4a), we observed a clear induction of ATF4 expression

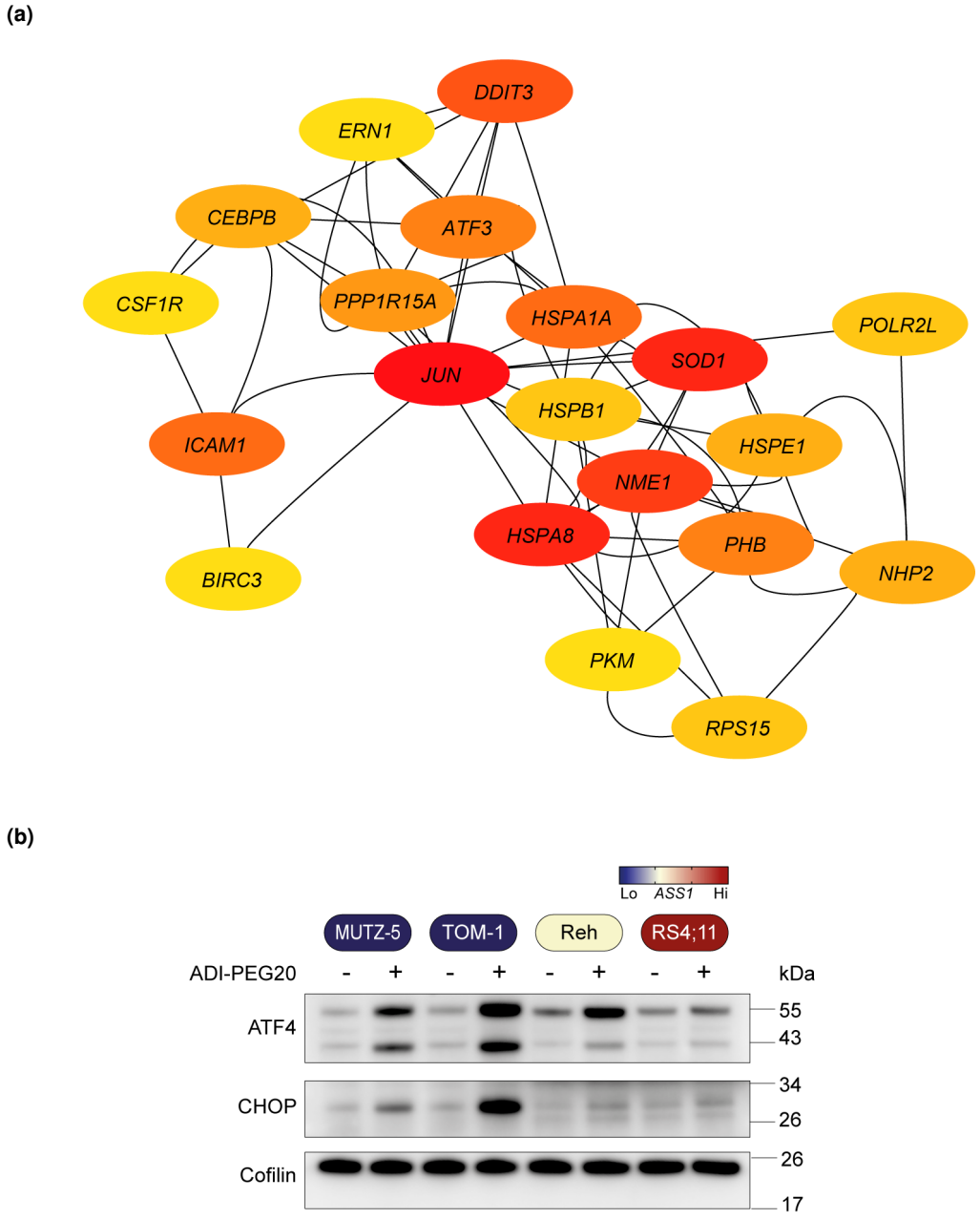

Figure 5.3.4: **ADI-PEG20 activates cell stress signalling**
a) Sub-network of "hub" genes, defined as top-20 genes according to degree of interconnectivity, from within stringently defined DEG set with absolute $\log_2$FC > 2 and adjusted $p < 0.001$. Lighter to darker colouring indicates increasing degree of interconnectivity with other members of aforementioned DEG set, connecting lines represent interactions within hub gene set.
b) Western blotting analysis of ATF4 and CHOP induction by 24 hour treatment with ADI-PEG20. Cell lines coloured by baseline *ASS1* expression.

in both *ASS1*-low cell lines and also to a lesser extent in the *ASS1*-intermediate cell line Reh. However, while the expression of CHOP was also clearly upregulated in the *ASS1*-low cell lines we observed at most a subtle change in the *ASS1*-intermediate cell line. The degree of CHOP modulation was also proportional to the degree of sensitivity to ADI-PEG20 amongst the *ASS1*-low cell lines, with the greatest effect seen in the TOM-1 cell line which displays a more rapid and higher degree of apoptosis compared to MUTZ-5 (figure 5.2.3b).

Put together, these analyses highlight cellular stress induction as a key feature of ADI-PEG20 treatment in *ASS1*-low and intermediate B-ALL cell lines. The upregulation of AT4 protein expression and a number of its transcriptional targets suggests that ER-stress is prominent in *ASS1*-low models but also appeared to be a feature of the *ASS1*-intermediate cell line. The induction of the known ATF4 responsive, pro-apoptotic molecule CHOP discriminates between the *ASS1*-low and *ASS1*-intermediate cell lines and suggests that cell fate is in line with induction of either the pro-survival or pro-apoptotic arms of the ATF4 driven response to arginine stress. The role of CHOP is reinforced by the previous demonstration of DR5 upregulation which has been identified as a downstream target of CHOP upon prolonged ER-stress [192].

5.4 ADI-PEG20 is active against *in vivo* models of primary B-ALL

We next wanted to validate the *in vitro* findings generated with cell line models by testing ADI-PEG20 in a physiological context against PDX models of B-ALL. This is a crucial step for amino acid deprivation studies, since culture media is not necessarily representative of physiological solute concentrations and cell lines by their nature adapt over time to *in vitro* culture conditions. We tested baseline *ASS1* expression amongst our existing library of PDX engraftable ALL samples (table 5.1 and figure 5.4.1), using the MUTZ-5, Reh and RS4;11 cell line gene expression as a range of functionally characterised controls. We made an assumption that PDX samples with a lower baseline *ASS1* expression than MUTZ-5 should be sensitive to ADI-PEG20, while those with higher expression than Reh would likely be resistant; with this we observed that 4/18 samples fell within the predicted-sensitive range,

ID	Lineage	Cytogenetics
ALL-01	B	Fail
ALL-02	B	t(9;22)
ALL-03	T	
ALL-04	B	t(9;22)
ALL-05	T	
ALL-06	B	
ALL-07	B	t(1;19)
ALL-08	B	Normal
ALL-09	B	t(4;11)
ALL-10	B	Hyperdiploid
ALL-11		
ALL-12		
ALL-13	T	del(6)
ALL-14	B	Normal
ALL-15		
ALL-16	B	t(4;11)
ALL-17	T	
ALL-18	T	

Table 5.1: Primary samples ordered by baseline *ASS1* expression. Where fields are blank no information is available. Horizontal dividers correspond to red dashed lines in figure 5.4.1.

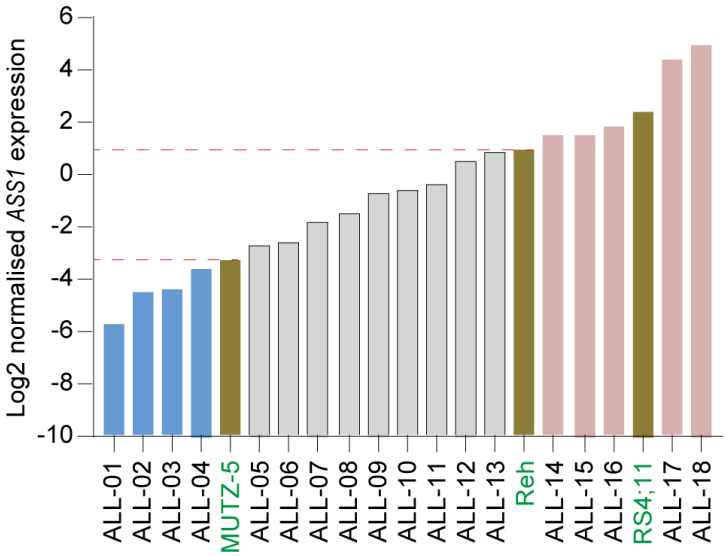

Figure 5.4.1: **ADI-PEG20 is active against *in vivo* models of primary B-ALL**
Primary sample *ASS1* expression measured by qPCR. Based on comparison to cell line expression (green labels, gold bars), blue bars represent those primary samples predicted to be sensitive to ADI-PEG20, pink resistant and grey unknown. *ASS1* values calculated by $\Delta\Delta C_T$ method using internal *GAPDH* references and normalised to robust average across cell line samples. Samples measured in triplicate.

5/18 samples within the predicted-resistant range and 9/18 in an intermediate range. In keeping with our previous predictions we saw that both Ph+ samples were in the *ASS1*-low band. With regard to the intermediate samples the gene expression covered a 4 fold range in *ASS1* expression and so it is not unreasonable to assume that at the lower end of this range the functional characteristics of these tumours would be closer to that of MUTZ-5 than Reh, and *vice versa*.

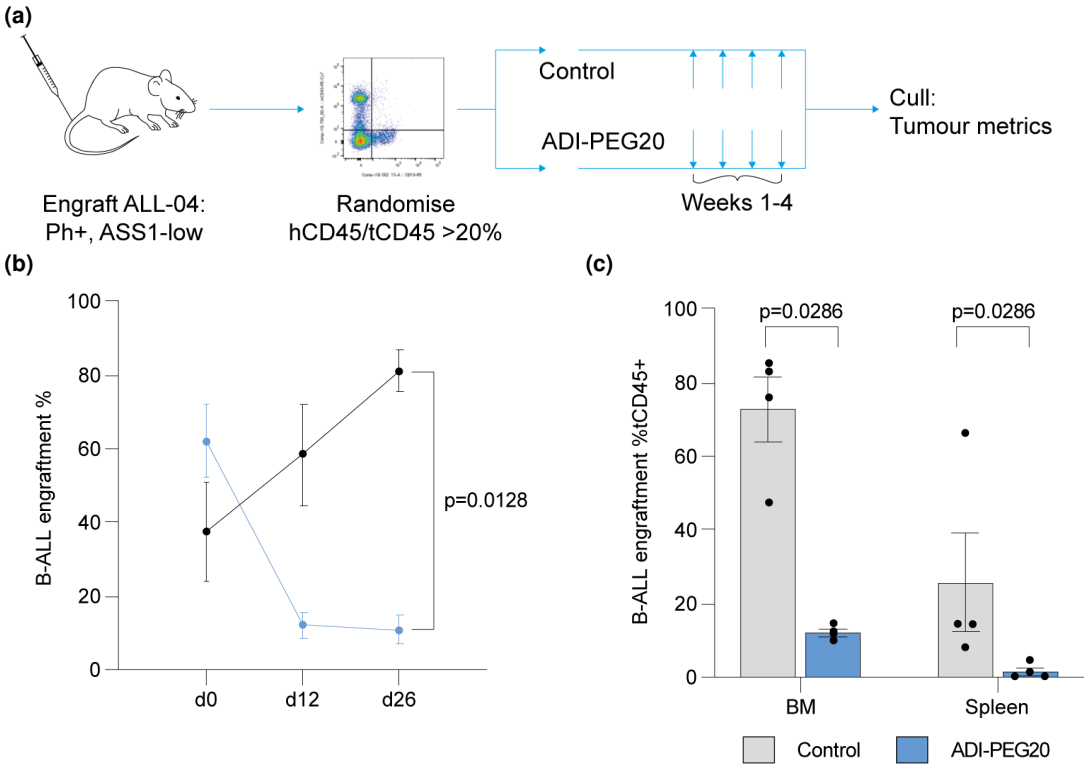

Figure 5.4.2: **ADI-PEG20 is active against *in vivo* models of primary B-ALL**
a) Treatment overview for *in vivo* assessment of ADI-PEG20 in ASS1-low PDX.
b) On-treatment tumour monitoring via intratibial bone marrow aspiration with FACS analysis of engraftment for control (black points/lines) and ADI-PEG20 treated mice (blue points/lines). Points and bars represent mean and SEM of 4 mice measured at each time point, p-value for comparison of ADI-PEG20 vs control from 2-way ANOVA with time and treatment as factors.
c) B-ALL engraftment in harvested organs after 4 weeks treatment with ADI-PEG20. Points and bars represent mean and SEM of 4 mice measured at each time point, p-value for comparisons of ADI-PEG20 vs control from Mann-Whitney test.

To extend our cell line benchmarking of ADI-PEG20 response against *ASS1* expression into our primary sample cohort, we first engrafted the *ASS1*-low, and therefore predicted

ADI-PEG20-sensitive, ALL-04 sample (figure 5.4.1), which had been cryopreserved from the bone marrow of a patient with Ph+ B-ALL. After intravenous tumour cell injection, we monitored engraftment by means of fortnightly bone marrow aspiration and started treatment with ADI-PEG20 once the proportion of human-CD45^{pos}CD19^{pos} cells was at least 20% of total combined human- and mouse-CD45^{pos} cells (figure 5.4.2a). We then treated the mice with 4 weekly intraperitoneal injections of ADI-PEG20 at a dose of 5 IU per mouse, which is known to deplete arginine for approximately 1 week [193], or PBS as control. We then continued to monitor B-ALL engraftment by bone marrow aspiration on days 12 and 26 of the treatment period and then culled the mice 2 days after the final bone marrow aspiration for bone marrow and spleen tumour burden assessment.

In a cohort of 4 treated and 4 control mice we observed a marked tumour reduction after 12 days (2 doses of ADI-PEG20) from baseline in the treated mice compared to controls, and this cytoreduction was then maintained through to the final bone marrow aspiration on day 26 ($p = 0.0128$ from 2-way ANOVA, figure 5.4.2b). After culling the mice we again tested both the harvested bone marrow and spleen for engraftment of B-ALL and found a significant reduction in the ADI-PEG20 treated mice in both organs (in both cases $p = 0.0286$ from Mann-Whitney test, figure 5.4.2c).

Since the major tumour reduction appeared to take place between the start of treatment and day 12, and thereafter the tumour burden appeared static between 10-20% of total CD45^{pos} cells, we wondered if the residual tumour cells would be cell cycle arrested, as had previously been seen in cell line models. To our surprise, when we analysed the cell cycle of CD19^{pos} harvested bone marrow cells, we found no difference in cell cycle state composition between treated and control mice (figure 5.4.3a). We therefore wanted to ask if these surviving cells had acquired resistance to ongoing arginine starvation via upregulation of *ASS1*. Analysing both protein expression by FACS and mRNA expression by qPCR, we found a concordant trend toward ASS1 upregulation but were unable to reject the null hypothesis of no difference with a maximum 5% type 1 error rate (figures 5.4.3b and 5.4.3c).

We next wanted to test the *in vivo* response of primary B-ALL with baseline *ASS1* expression in the intermediate range from figure 5.4.1. We chose 2 PDX samples with known *in vivo* engraftment potential, ALL-08 and ALL-07 (figure 5.4.1), representing patients with

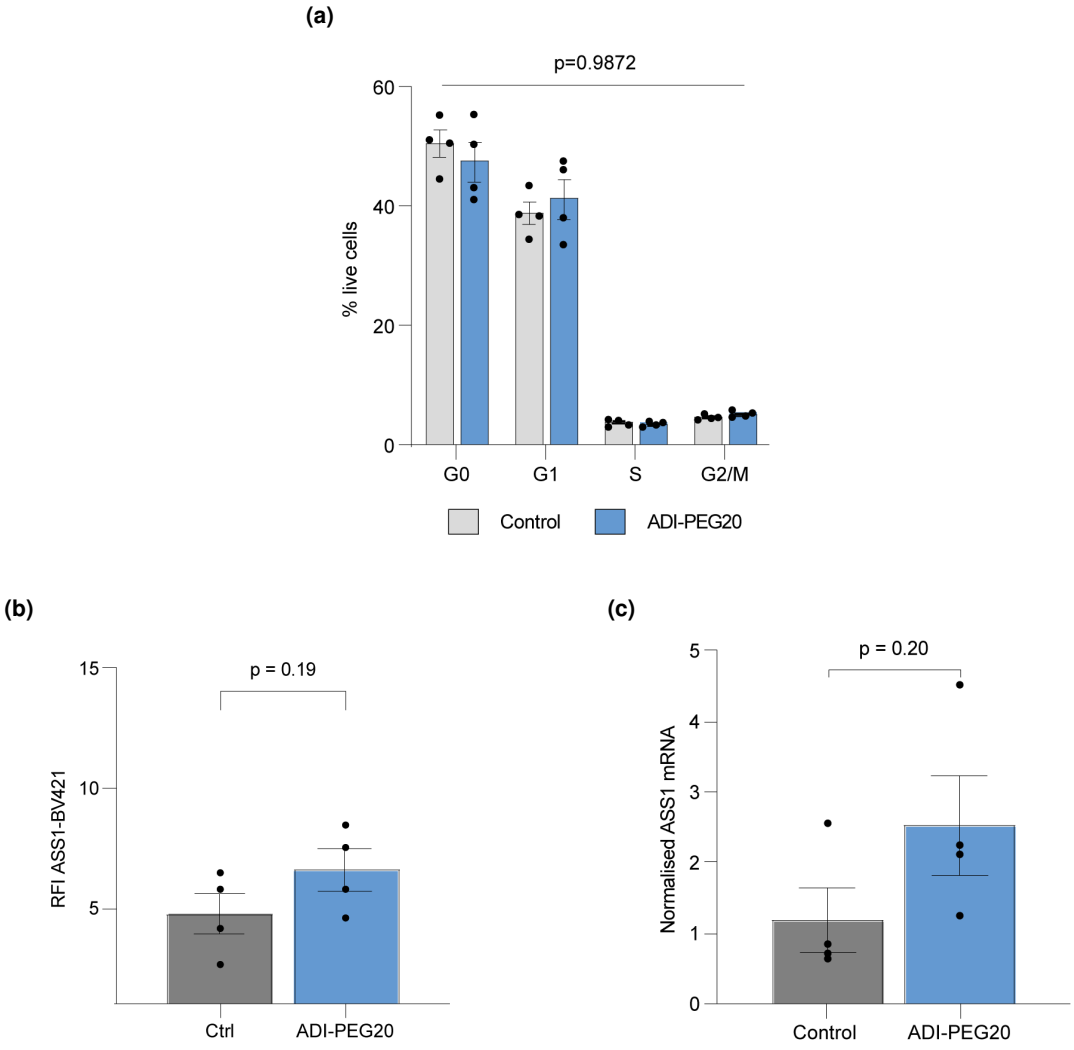

Figure 5.4.3: **ADI-PEG20 is active against *in vivo* models of primary B-ALL**
a) Proportion of live cells per cell cycle phase from harvested bone marrow cells. Analysed by FACS after gating on $CD19^{pos}$ cells. Points and bars represent mean and SEM of 4 mice measured at each time point, p-values from χ^2 test using % cell cycle phase averaged across all replicates.
b) and c) ASS1 expression as analysed by b) FACS and c) qPCR. p-values from t-test (b) and Mann-Whitney test (c).

diagnostic TCF3::PBX1 rearranged B-ALL and a relapsed patient with normal cytogenetics, respectively. In both of these samples, we used the same experimental design as the previous study, except *in vivo* engraftment was performed by direct intratibial injection of tumour cells. This technique gives the advantage of reducing the required number of starting cells but also means that fortnightly bone marrow aspiration monitoring is impossible, since engraftment is not symmetrical between legs, and mice do not tolerate 14 day serial

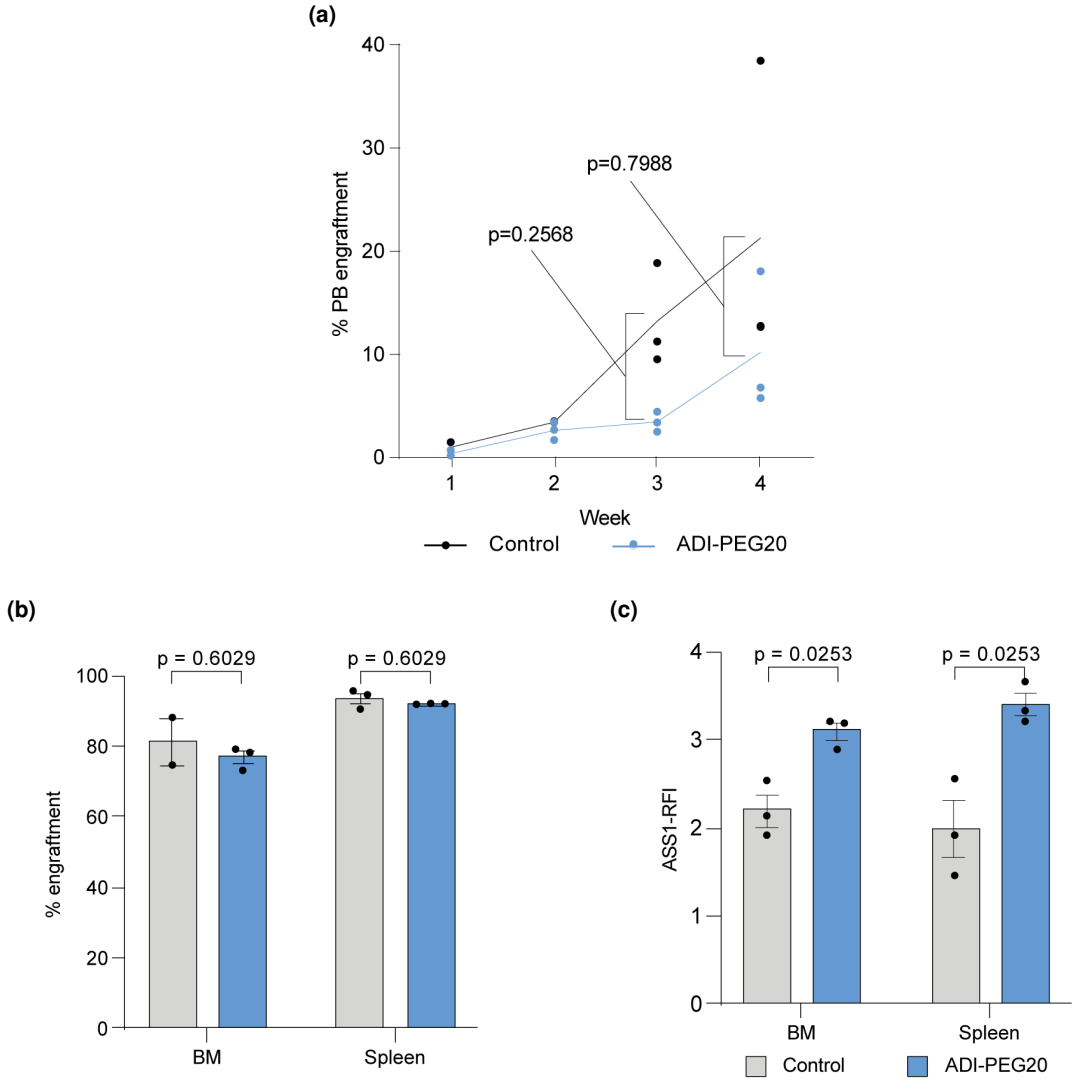

Figure 5.4.4: **ADI-PEG20 is active against *in vivo* models of primary B-ALL**
a) Weekly monitoring of peripheral blood (PB) engraftment measured by FACS in ALL-08 PDX comparing treatment to control. Trend line joins average from analysis of 3 mice per group at each time point, p-values from 2-way ANOVA with treatment and time as factors.
b) Comparison of ALL-08 PDX bone marrow (BM) and spleen engraftment after 4 weeks of treatment with ADI-PEG20. Individual points represent readings per mouse with 3 mice per group except only 2 replicates available for control bone marrow due to technical FACS failure, p-values from t-test per harvested organ, .
c) Comparison of ALL-08 PDX bone marrow (BM) and spleen ASS1 expression measured by FACS after 4 weeks of treatment with ADI-PEG20, p-values from t-test per harvested organ.

measurements from the same leg.

In the ALL-08 model, we did observe a high degree of haematological spread, meaning that we could track disease spillover into peripheral blood via weekly tail vein bleed samples analysed by FACS (figure 5.4.4a). Although not statistically significant by the 2-way ANOVA test, we saw a suggestion of separation in the average peripheral blood disease burden after 2 weeks of ADI-PEG20 treatment with a slower increase of blood disease levels between weeks 2 and 3 in the treated mice. However, after week 3 the rate of peripheral blood increase appeared to accelerate in the treated mice, to match that of the control mice. The mice were then culled within 7 days of the final dose of ADI-PEG20 and we did not see any difference in tumour burden in either the bone marrow or spleen compartments (figure 5.4.4b). We again analysed ASS1 expression by FACS and this time did see a robust increase in expression in both bone marrow and spleen residual tumour cells (figure 5.4.4c).

In the ALL-07 model, there was not enough haematological spillover of tumour cells to perform on-treatment disease monitoring and so the first tumour readout was when the mice were culled, again within 1 week of the final dose of ADI-PEG20 (figure 5.4.5a). In this

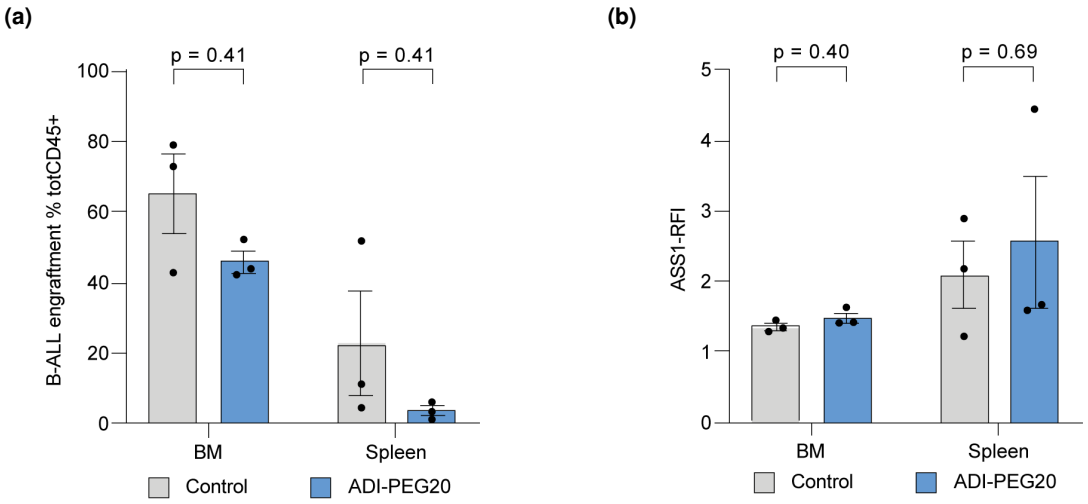

Figure 5.4.5: **ADI-PEG20 is active against *in vivo* models of primary B-ALL**
a) Comparison of ALL-07 PDX bone marrow (BM) and spleen engraftment after 4 weeks of treatment with ADI-PEG20. Individual points represent readings per mouse with 3 mice per group, p-values from Mann-Whitney test per harvested organ.
b) Comparison of ALL-07 PDX bone marrow (BM) and spleen ASS1 expression measured by FACS after 4 weeks of treatment with ADI-PEG20, p-values from t-test (BM) and Mann-Whitney test (spleen).

model we likewise did not observe a significant difference in disease burden between treated and control mice in either the bone marrow or spleen compartments, although there was a trend toward a reduction in tumour cells in the treated mice. Analysing ASS1 by FACS we did not see a statistically significant difference in expression between treated and controls (figure 5.4.5b). This model therefore shares some similarities with that of the ALL-04 PDX, in that *ASS1* was not robustly upregulated and there was a suggestion of some disease responsiveness, although not statistically proven. Given that the baseline *ASS1* expression of ALL-07 was lower than that of ALL-08, this supports the concept, although not robustly, that higher levels of baseline *ASS1* expression allow for a more marked *ASS1* response. Furthermore, it gives an initial, small scale insight into the likely heterogeneity of response across the spread of baseline *ASS1* expression that we have demonstrated across the wider cohort of B-ALL (figure 4.1.1). This is largely in line with the experience of short-term ADI-PEG20 exposure in our panel of cell lines, and is in line with the clinical experience with ADI-PEG20 where only the lowest *ASS1* expressing tumours benefit [98]. The ability to track tumour growth throughout treatment in the ALL-08 model raised the possibility, albeit without robust statistical proof, that ADI-PEG20 had a transient effect on cell proliferation which was ultimately negated, presumably by some tumour adaptation to arginine starvation of which the demonstrated *ASS1* upregulation was likely a feature.

5.5 Contrasting *CEBPB* and *ASS1* co-modulation correlates with survival or death from ADI-PEG20 treatment

We next wanted to ask what, if any, molecular adaptations had been necessary to sustain tumour growth in the ALL-07 and ALL-08 PDX models in the absence of arginine. To answer this, we extracted RNA from sorted bone marrow blasts harvested from the ALL-07 and ALL-08 models immediately after culling the mice and submitted extracts for bulk RNA-sequencing. Using Principal Component Analysis (PCA)-plot dimensional reduction (figure 5.5.1a) we observed that the major transcriptional difference between these samples was dictated by the PDX type (rather than treatment) with the samples separated along the principle component by their PDX origin. Along the 2nd principal component, ALL-07

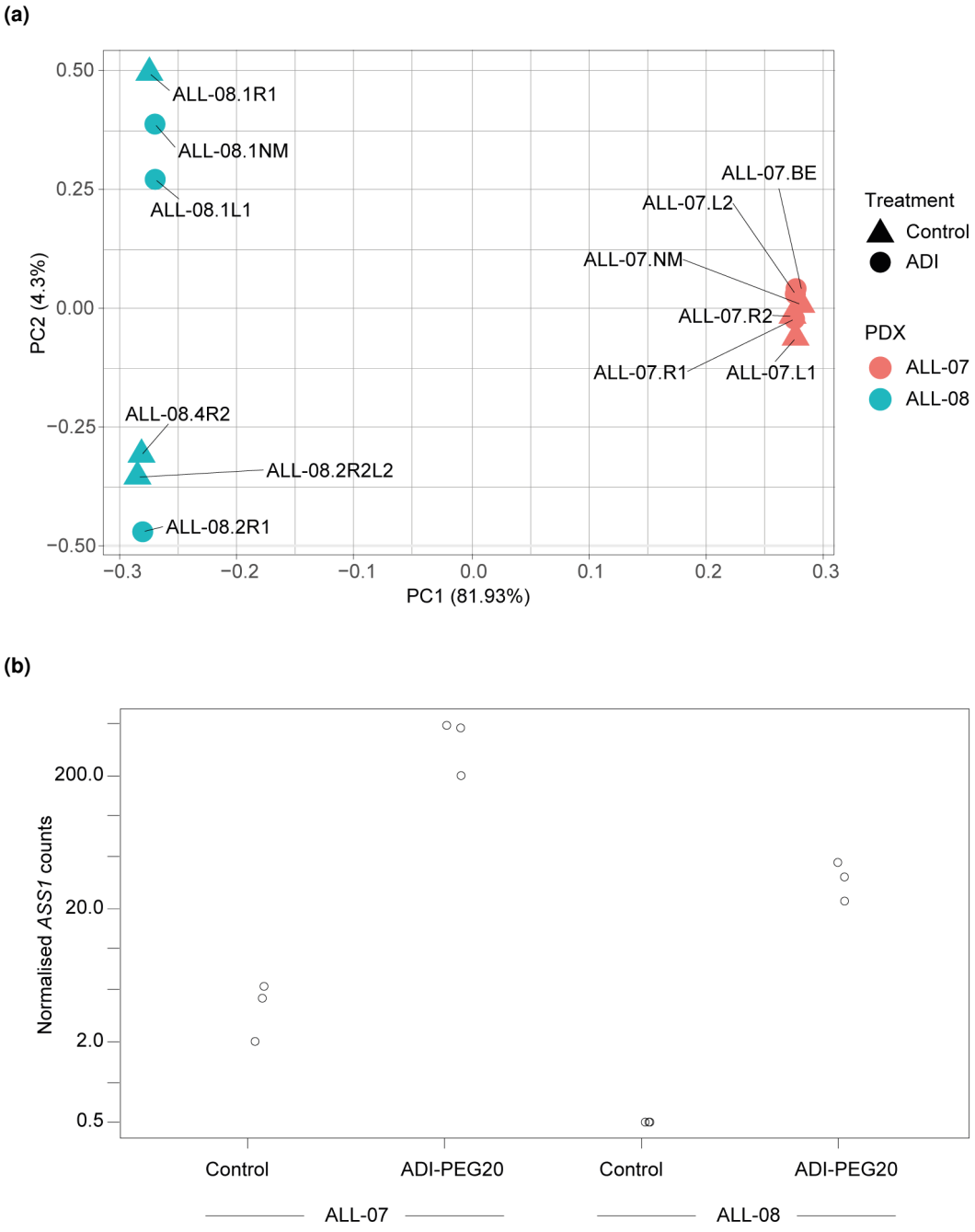

Figure 5.5.1: **Contrasting *CEBPB* and *ASS1* co-modulation correlates with survival or death from ADI-PEG20 treatment**
a) PCA plot depicting dimensionally reduced gene expression profiles for ALL-07 and ALL-08 PDX models comparing ADI-PEG20 (ADI) to control.
b) Quality control comparison of normalised RNA-seq counts for *ASS1* between treatment and control for ALL-07 and ALL-08 PDX models.

showed very little variation regardless of treatment condition, while for the ALL-08 model there was a second axis of variability which seemed to be defined by a cage effect, since mice from cage 1 (upper 3 points) had a treatment-independent difference to those from cages 2 and 4 (bottom 3 points). To confirm that this was not due to transposition of samples ALL-08.1R1 and ALL-08.2R1 we checked *ASS1* expression within the RNA-sequencing data (figure 5.5.1b) and saw that the labels were in-line with the ASS1 modulation by ADI-PEG20 as observed by FACS and qPCR (figure 5.4.4c), *i.e.* all of the treated mice had higher *ASS1* expression than controls.

The lack of treatment-dependent separation in the PCA-plot suggested that this modulation in *ASS1* expression was part of only small scale transcriptional effects. In keeping with this expectation, linear modelling of DEGs using an absolute $\log_2$FC threshold of 1 and adjusted p-value limit of 0.05, revealed only 77 up- and 105 down-regulated genes in the ALL-08 model and similarly only 64 up- and 11 down-regulated genes in the ALL-07 model (figures 5.5.2a and 5.5.2b). In neither model did we discover any enriched pathways by GSEA analysis and we did not choose to "relax" the $\log_2$FC threshold so as to increase the chances of finding sets of modulated genes, since we were limited to 3 replicates per condition per PDX, meaning that small gene perturbations cannot be reliably detected. However, we did discover, by comparing DEGs between the different PDX models that both *ASS1* and *CEBPB* were mutually upregulated by ADI-PEG20 treatment. Since *CEBPB* had been a central gene in our previous TOM-1 RNA-seq experiment (figures 5.3.2 and 5.3.4a) we noted some similarity between the ALL-07 and TOM-1 gene expression data in the form of an overlapping group of ATF4 targets (*CEBPB*, *CHAC1*, *VEGFA*, *TRIB3*; labelled genes, figure 5.5.2b).

CEBPB encodes the transcription factor C/EBPβ that is known to be a stress-responsive, downstream element of the ER-stress pathway and has recently been characterised as a crucial component in the response of cells to arginine starvation, through its co-factor binding with ATF4 to promote transcription of *ASS1* [185]. This suggests that despite apparent successful adaptation to continuous ADI-PEG20 treatment in the ALL-07 and ALL-08 models, as evidenced by the equivalent end-point tumour burdens, they retained an arginine deficit with an ongoing activation of cellular stress response and a requirement

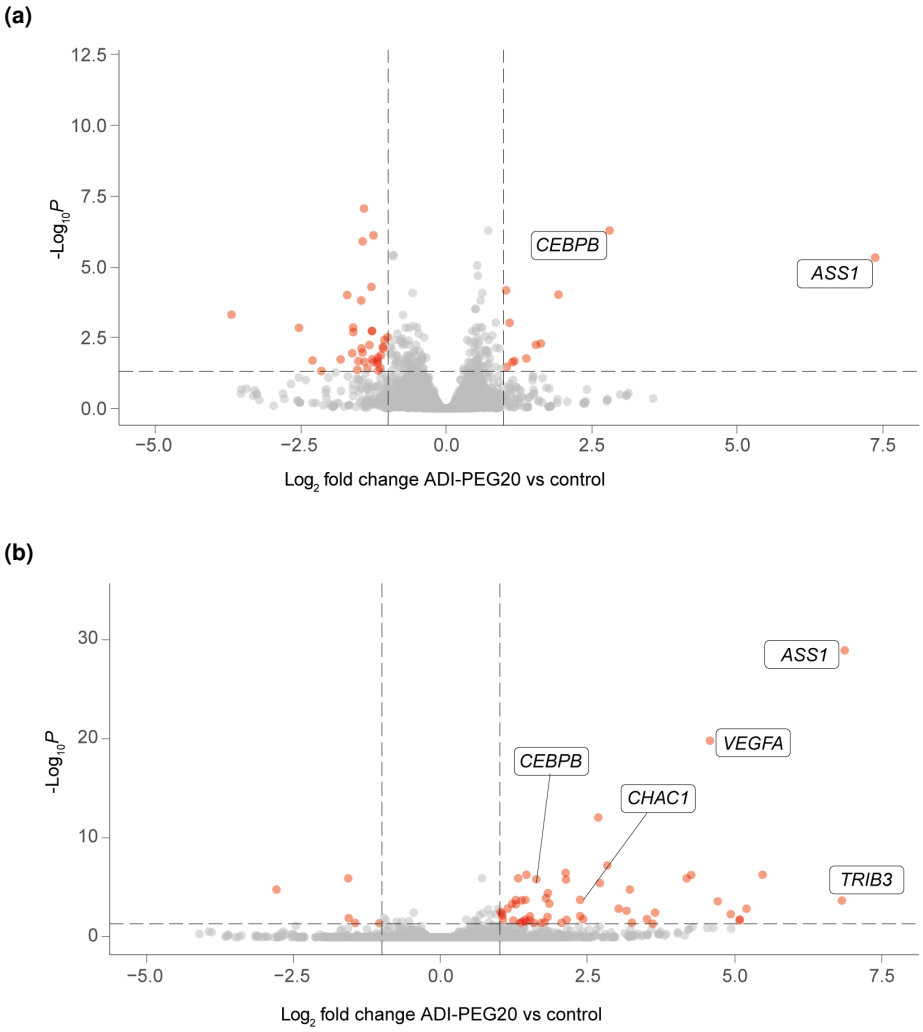

Figure 5.5.2: **Contrasting *CEBPB* and *ASS1* co-modulation correlates with survival or death from ADI-PEG20 treatment**
Volcano plots illustrating DEGs between ADI-PEG20 treated and control from (a) ALL-08 PDX and (b) ALL-07 PDX. Genes labelled according to overlapping DEGs between ALL-07 and ALL-08 models. In (b), extra labels identify ATF4 target genes from TRRUST database [146]. Red points indicate genes with absolute $\log_2$FC > 1 and adjusted $p < 0.05$, grey points are those not meeting same criteria.

for increased transcription of *CEBPB* to drive elevated levels of *ASS1*. The finding of elevated *CEBPB* and *ASS1* expression when measured by RNA-seq *in vivo* fits with our previous data that ADI-PEG20 treatment invokes the ER-stress response. This suggests that, as with the cell line models, the survival of primary ALL is likely dictated by the ability to sufficiently upregulate *ASS1* downstream of *CEBPB* and therefore restore arginine and resolve ER-stress [192].

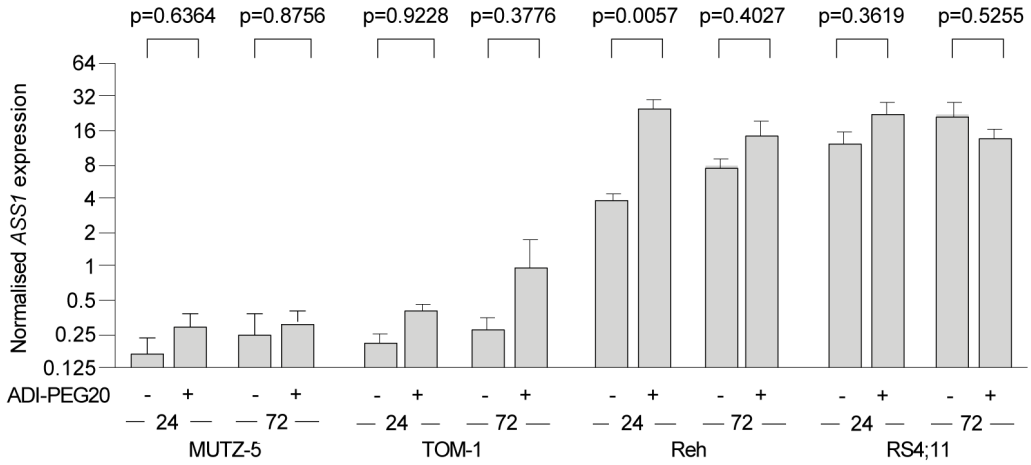

Figure 5.5.3: **Contrasting *CEBPB* and *ASS1* co-modulation correlates with survival or death from ADI-PEG20 treatment**
Normalised *ASS1* expression measured by qPCR in RNA extracts from cell line panel with 24 or 72 hours ADI-PEG20 treatment or control; internal reference is *GAPDH*, baseline reference is all cell line average of 24 hour control expression; Data represent mean and SEM from 3 independent experiments, each performed with technical triplicates, *p*-values from 2-way ANOVA with time and treatment as factors with Šídák's multiple comparisons test.

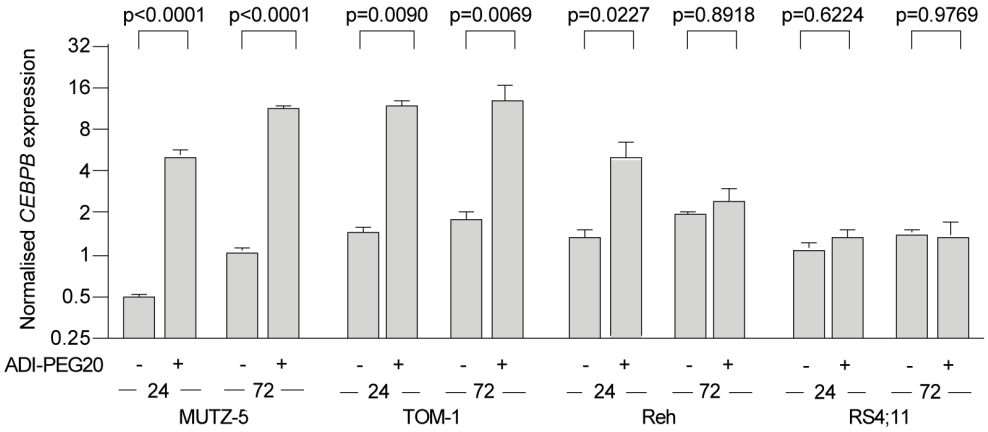

Figure 5.5.4: **Contrasting *CEBPB* and *ASS1* co-modulation correlates with survival or death from ADI-PEG20 treatment**
Normalised *CEBPB* expression measured by QPCR in RNA extracts from cell line panel with 24 or 72 hours ADI-PEG20 treatment or control; internal reference is *GAPDH*, baseline reference is all cell line average of 24 hour control expression; Data represent mean and SEM from 3 independent experiments, each performed with technical triplicates, *p*-values from 2-way ANOVA with time and treatment as factors with Šídák's multiple comparisons test.

Since the upregulation of *CEBPB* appeared to be a common response to ADI-PEG20 treatment in our PDX models, and that this transcription factor is known to promote *ASS1* expression under arginine stress [185], we returned to our cell line panel to characterise the expression of these genes over the course of *in vitro* ADI-PEG20 treatment. We extracted RNA from each of our cell line models after 24 and 72 hours of ADI-PEG20 treatment or control culture conditions and performed qPCR for both *ASS1* (figure 5.5.3) and *CEBPB* (figure 5.5.4). We did not observe a significant *ASS1* upregulation in the *ASS1*-low models MUTZ-5 and TOM-1 with ADI-PEG20 treatment, although there was a trend towards this at both time points. Contrasting this, in the *ASS1*-intermediate cell line Reh, we saw a significant upregulation of *ASS1* at 24 hours of ADI-PEG20 treatment ($p = 0.0057$ from 2-way ANOVA) but that this converged toward the untreated value by 72 hours. In the *ASS1*-high cell line RS4;11, we did not observe any significant change in expression. It is notable that the upregulation of *ASS1* at 24 hours in the intermediate cell line Reh was around a 4-fold change from the Reh baseline value and took the normalised expression into a similar order of magnitude as that for RS4;11, the *ASS1*-high and ADI-PEG20 resistant model. This could suggest that a threshold of *ASS1* expression exists that generates sufficient citrulline metabolising capacity to restore arginine pools and avoid ADI-PEG20 induced cellular death, and this is somewhere between the baseline values of Reh and RS4;11. Furthermore, this theoretical threshold value appears to be 5-7 fold higher than the baseline expression of either MUTZ-5 or TOM-1.

The expression of *CEBPB* was quite clearly modulated in both of the *ASS1*-low cell lines with an approximately 3-4 fold change in expression between treated and control at both time points for MUTZ-5 ($p < 0.0001$ at both time points from 2-way ANOVA) and TOM-1 ($p = 0.0090$ and $p = 0.0069$ at 24 and 72 hours, respectively). This contrasted the pattern in the *ASS1*-intermediate cell line Reh, where there was a significant increase in *CEBPB* expression at 24 hours of ADI-PEG20 treatment ($p = 0.0277$) but this then returned toward the untreated value by 72 hours. As with *ASS1* expression in the *ASS1*-high model RS4;11, we did not see any modulation of *CEBPB*.

The correlation of *CEBPB* relaxation by 72 hours and the avoidance of cell death fits with the concept, originally described by Crump *et al.* [185], of a *competent* stress

response involving *CEBPB* in the Reh cell line, where C/EBPβ promotes upregulation of *ASS1* within 24 hours of arginine starvation, allowing restoration of arginine pools and resolution of stress and hence relaxation of *CEBPB* expression. The resolution of stress is potentially the key feature which allows cell survival, since ER-stress and the resultant unfolded protein response are initially protective mechanisms which switch to instigate cell death processes only after prolonged activation, or non-resolution [192]. Following this, the lack of a *CEBPB* stress signal at either of the tested time points in the *ASS1*-high RS4;11 would suggest either a competent stress response that even more rapidly resolves arginine deficit, or an intrinsically competent degree of *ASS1* expression that allows for normal arginine metabolite flows regardless of ADI-PEG20 treatment. Contrasting this, the association of a persistently upregulated *CEBPB* stress signal and ADI-PEG20 induced cell death in the *ASS1*-low MUTZ-5 and TOM-1 models suggests an *incompetent* stress response that fails to upregulate *ASS1* and therefore cannot restore arginine homeostasis and relax stress responsive transcription.

To understand this process further we next compared the time course expression of the *CEBPB* encoded protein C/EBPβ as well as ASS1 with or without ADI-PEG20 treatment by western blotting (figure 5.5.5). The most striking finding from this analysis was absent expression of ASS1 protein from MUTZ-5 and TOM-1 untreated lysates across both time points and, in keeping with the mRNA expression results, no evidence of significant upregulation by ADI-PEG20 in either model, with only a fractionally appreciable increase in ASS1 expression in 72 hour treated MUTZ-5 lysates. A subtle but more definitive increase in ASS1 expression was observed at the 24 hour time point in ADI-PEG20 treated Reh cells when compared to control and this appeared similar at 72 hours, while there were no clear differences in ASS1 protein expression between treated and control at either time point for RS4;11. This supports the previously introduced notion that a threshold of ASS1 expression is associated with survival during ADI-PEG20 treatment and while this threshold is above the baseline value of Reh, this cell line can competently induce ASS1 expression to restore arginine. As with the previous mRNA analysis, the baseline and treated ASS1 expression of the cell lines MUTZ-5 and TOM-1 appears multiple orders of magnitude lower than that of Reh and RS4;11, and even if a marginal increase in expression is possible this remains

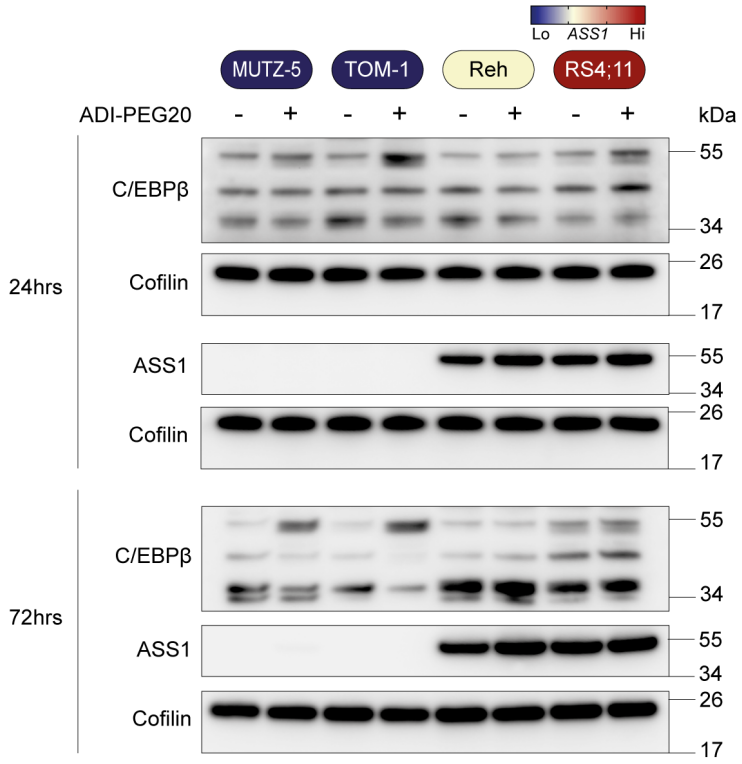

Figure 5.5.5: **ADI-PEG20 leads to growth inhibition via cell cycle arrest and apoptosis in ASS1-low B-ALL**
Western blotting analysis of C/EBPβ and ASS1 expression after 24 or 72 hours of ADI-PEG20 *vs* control.

many times lower than that associated with survival in Reh.

The expression of C/EBPβ appeared more complex. At the 24 hour time point there was a suggestion of an increase in expression of the highest weight isoform of the protein in the TOM-1 and RS4;11 cell lines despite the cell lines not sharing any functional or molecular similarities in previous experiments. What was more clear however, and in-line with the mRNA expression results, was that at 72 hours treatment, there was a marked upregulation of the higher molecular weight isoform by ADI-PEG20 treatment in the MUTZ-5 and TOM-1 cell lines and no such effect in Reh or RS4;11. This effect therefore associates with those cell lines where ADI-PEG20 treatment induces cell cycle arrest and apoptosis at 72 hours and is in keeping with a previous reported role of C/EBPβ in regulating cell death under ER-stress [194]. An alternate view of this, bearing in mind that the protein lysates are generated from cells that remain viable at 72 hours, is that C/EBPβ has a protective role, perhaps by sustaining activation of downstream stress response elements such as

ASS1, something that has also been described in models of ER-stress [195] and would be in keeping with the observed survival of the ALL-07 and ALL-08 PDX models where *CEBPB* was elevated at the end of treatment.

In summary, the investigation of ASS1 and C/EBPβ expression has generated a clear contrast between the previously annotated *ASS1*-low cell lines with the *ASS1*-intermediate and -high cell lines. The former, where we have observed cell cycle arrest and cell death in our functional models, are characterised by a failure of ASS1 upregulation above a putative "survival-threshold" with persistent cell stress, marked by late upregulation of *CEBPB* and its high molecular weight protein isoform. While the similarity of reduced cellular proliferation exists between the *ASS1*-intermediate cell line Reh and the *ASS1*-low models, at the level of ASS1 and C/EBPβ gene and protein expression, this cell line bears more similarity to RS4;11, in that ASS1 levels in treated cells are many orders of magnitude higher than MUTZ-5 and TOM-1, at 72 hours there is no evidence of *CEBPB* induction, and in both of these cell lines this pattern of gene and protein expression is associated with cell survival. We therefore propose that Reh and RS4;11 exist in a functionally defined "*ASS1*-competent" group of cell lines, while MUTZ-5 and TOM-1 are functionally "*ASS1*-incompetent", meaning that they fail to upregulate *ASS1* under arginine stress and so are therefore unable to resolve cellular stress, marked by enhanced C/EBPβ expression.

5.6 *ASS1* promoter hypomethylation associates with enhanced *ASS1*-competency

As already mentioned, the roles of ATF4 and C/EBPβ in promoting ASS1 expression under arginine stress have been unified in the model described by Crump *et al.* [185]. In this model ATF4 and C/EBPβ co-bind to the *ASS1* locus to promote its expression, with arginine availability regulating chromatin accessibility at a key promoter site and hence dictating the ability of cells to respond to arginine stress. Other models of arginine starvation have also suggested epigenetic mechanisms of arginine auxotrophy but have focused on promoter region DNA methylation [94, 196, 197] or on transcription factor networks centred on HIF-1α and c-Myc [198].

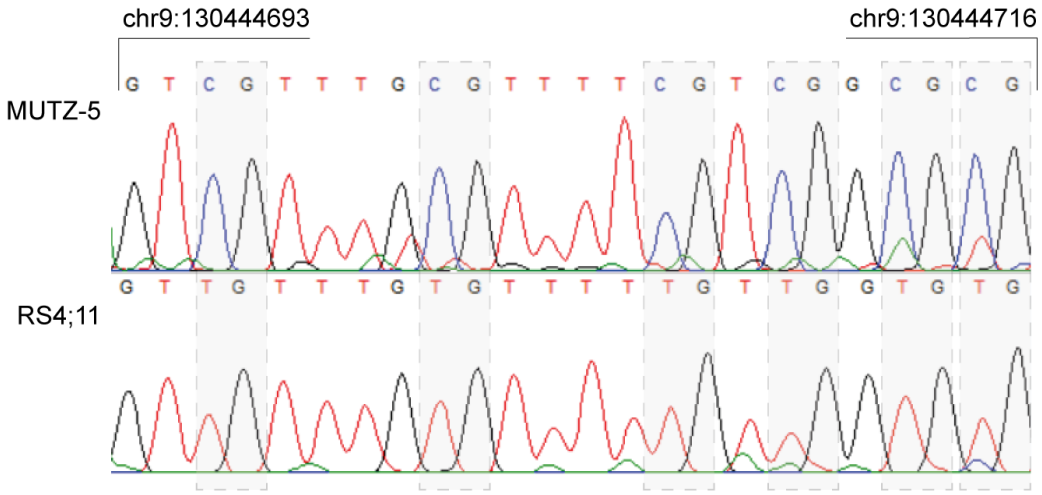

Figure 5.6.1: **ADI-PEG20 leads to growth inhibition via cell cycle arrest and apoptosis in ASS1-low B-ALL**
Representative Sanger-sequence chromatograms illustrating contrasting bisulfite conversion of highly methylated (MUTZ-5) and un-methylated (RS4;11) DNA in *ASS1* promoter region. CpG sites are highlighted in dashed grey boxes.

We have shown that the phenotype of our cell line models under ADI-PEG20 treatment associates with the baseline *ASS1* status and that in the *ASS1*-intermediate model Reh there is a significant degree of *ASS1* upregulation within 24 hours of treatment. While we have shown the ATF4 and C/EBPβ appear to have a role in this process and therefore the Chromatin based model described by Crump *et al.* may be relevant, we first wanted to test whether *ASS1* promoter methylation may correlate with baseline expression.

To test this we performed direct Sanger sequencing of bisulfite converted DNA from a 379 base pair region cited just upstream of the *ASS1* TSS that lies within a known CpG island [199]. The results of this assay revealed a stark difference in DNA methylation between the *ASS1*-high RS4;11 and all other cell lines (example chromatograms from MUTZ-5 and RS4;11, figure 5.6.1) with most pre-guanine cytosines converted to thymine in RS4;11, but preserved as cytosines in the other cell lines. To quantify this effect we utilised the R package *ABSP* [148], but found that we had to relax default quality criteria, by allowing a base call error rate of 1% (default 0.1%) and reducing the threshold of non-mixed positions to 60% (default 75%), to prevent rejection of the Reh sequence replicates (figures 5.6.2 and 5.6.3). We observed that the *ASS1*-high cell line RS4;11 appeared to have a uniquely low degree of methylation in this region when compared to all other cell lines and

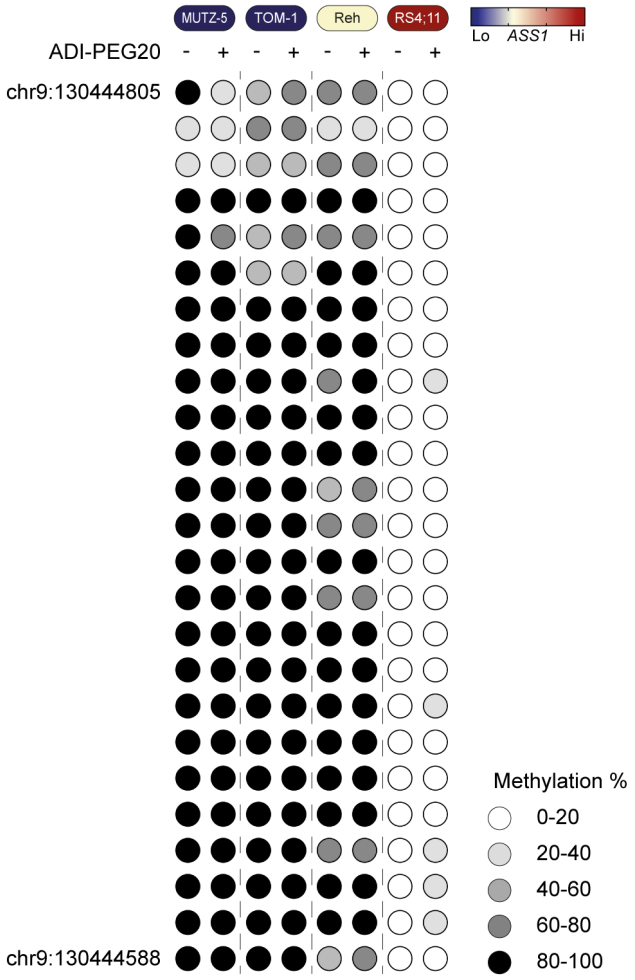

Figure 5.6.2: **ADI-PEG20 leads to growth inhibition via cell cycle arrest and apoptosis in ASS1-low B-ALL**
Lollipop diagram of baseline and ADI-PEG20 treated methylation levels at CpG sites within *ASS1* promoter region (spacing equalised for presentation), cropped to include only those CpG sites with acceptable sequencing quality across all cell lines. Spot shading represents mean methylation over 4-6 replicates per condition, first and last CpG sites are annotated with genomic position of cytosine.

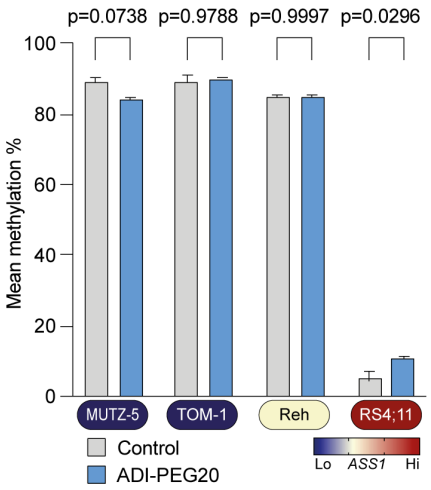

Figure 5.6.3: **ADI-PEG20 leads to growth inhibition via cell cycle arrest and apoptosis in ASS1-low B-ALL**
Average methylation rate across all CpG sites in *ASS1* promoter region. Values represent means of 4-6 replicates per condition, p-values from 2-way ANOVA with cell line and treatment as factors with Šídák's multiple comparisons test.

that upon ADI-PEG20 treatment there was actually an increase in methylation focused at 5 individual CpG sites. Amongst the MUTZ-5, TOM-1 and Reh cell lines we did not see any significant differences between individual cell lines, or between treatment and control conditions within each cell line model.

The hypomethylated DNA pattern in the case of RS4;11 is in keeping with the function of the KMT2Ar fusion protein that is known to result in prominently hypomethylated cytosine bases [133] and in the case of this specific sequence in the *ASS1* promoter region, certainly correlates with the high baseline *ASS1* expression and resistance to ADI-PEG20. Contrasting this, in the other 3 cell lines the DNA methylation profile was similar (figure 5.6.3), despite the clear phenotypic differences between the *ASS1*-incompetent cell lines MUTZ-5 and TOM-1, and the *ASS1*-competent Reh. This suggests that *ASS1* promoter hypomethylation may lead to resistance to ADI-PEG20 and is in agreement with the reported effect of the hypomethylating agent 5-aza-2'-deoxycytidine in generating ADI-PEG20 resistance in lymphoma models [196]. However, the lack of methylation difference amongst MUTZ-5, TOM-1 and Reh suggests that the *ASS1* expression and phenotypic differences between these cell lines is driven by separate factors.

5.7 Summary

In summary, we have shown that arginine starvation with ADI-PEG20 leads to effective cytoreduction in both *in vitro* and *in vivo* models of B-ALL where baseline *ASS1* expression is lowest. The *in vitro* cell line modeling has developed the concept that ADI-PEG20 elicits an ER-stress response involving a network of transcription factors centred around ATF4, C/EBPβ and CHOP. Cell fate then depends on the ability to competently upregulate ASS1 above a threshold that allows resolution of arginine stress and where this survival mechanism is incompetent, B-ALL undergoes cell cycle arrest, likely regulated by the action of p21, and programmed cell death with caspase-3 cleavage.

Perhaps the most important finding of this chapter is the lack of complete tumour clearance *in vivo*, even in the lowest *ASS1* expressing PDX. This fits with the failure of monotherapy in clinical trials [98] and would suggest that for translational benefit ADI-PEG20 needs to be applied as part of a combination therapy. The investigation of this will form the basis of the remainder of this work and is explored in following chapters.

Chapter 6

ADI-PEG20 in combination with pharmacological therapy

Since we saw a significant degree of persistent, residual disease in the ALL-04 PDX (figures 5.4.2b and 5.4.2c) despite very low baseline *ASS1* expression, we wanted to explore the possibility to deepen the effect of ADI-PEG20 by combining with other pharmacological agents. With the goal of complete tumour cell eradication, we set out to explore combination drugs that could either potentiate the effect of ADI-PEG20, independently eradicate persister cells that survive arginine starvation or, taking the alternative perspective, if the addition of ADI-PEG20 could deepen the effect of other drugs with activity in ALL.

6.1 Defining drug combination effectiveness

To screen the combination of ADI-PEG20 with a range of candidate drugs we used a simplified version of the methodology utilised by Jaaks *et al.* [200] for the assessment of drug combinations in cancer therapy. This method, which is based on the Bliss independence model of drug combination effects [201], assesses drug combinations using a defined optimum concentration of a so-called *anchor* drug when combined with a range of partner drug concentrations. This model was therefore appealing for our investigation since we were interested in combining ADI-PEG20 as the *anchor* drug at the defined EC_{max} concentration (where arginine is rapidly depleted from culture media) with other drugs of interest.

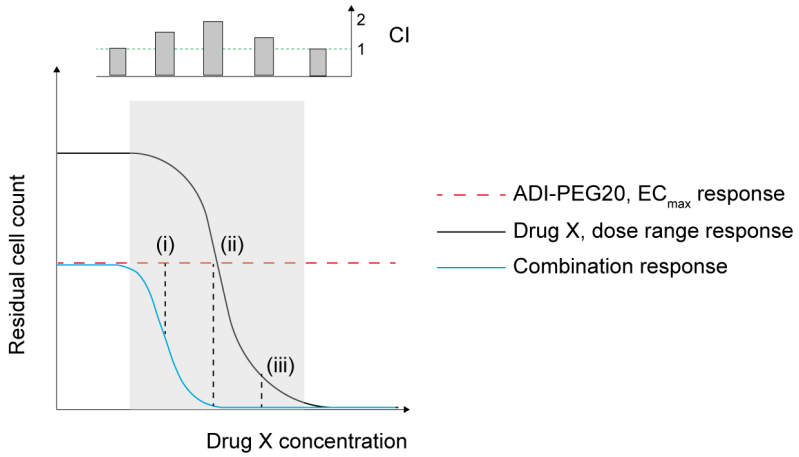

Figure 6.1.1: **Defining drug combination effectiveness**
Following a simplified version of the method of Jaaks *et al.* [200], we compared the cytoreductive effects of (1) the optimised EC_{max} concentration of ADI-PEG20 (red dashed line), (2) a broad dose range of 2nd drug "X" (solid black curve) and (3) the combination of the EC_{max} concentration of ADI-PEG20 with the same range of concentrations of drug "X" (solid blue curve). Using the Highest Single Agent model approach, we defined an effective combination as anywhere the combined effect exceeded that of either individual agent (shaded grey area). Combination indices (CI) are defined as the ratio of the depth of cytoreduction by combined therapy to the highest single agent depth of cytoreduction (depicted by vertical dashed lines, see equation in text) and are displayed by aligned bars in the top annotation, CIs at the indicated points (i), (ii) and (iii) are approximately 1.5, 2 and 1.25, respectively.

In the model proposed by Jaaks *et al.* an effective combination is one where drug synergy exists according to the Bliss independence model, that is, where the observed combination effect is greater than the numerical product of the independent component effects. We chose to simplify the criteria for combination effectiveness using the Highest Single Agent (HSA) (also known as "Gaddum's non-interaction") model of drug combination studies [202] such that the combination of 2 drugs is deemed *effective* when the combined effect is greater than the larger of the 2 individual component effects (figure 6.1.1). The HSA combination effect can be quantified by calculating a combination index (CI) as the ratio of the combination effect (E_{AX}) to the highest of the single agent effects (E_A and E_X):

$$CI = \frac{E_{AX}}{max(E_A, E_X)}$$

Meaning that an effective combination is one where the CI is greater than 1.

In figure 6.1.1, this is demonstrated in the shaded area where the combination effect (blue curve) surpasses the individual effects of both the ADI-PEG20 *anchor* concentration (red dashed line) and the partner drug "X" (black curve), meaning that when combined the drugs have an at least additive effect. In this schematic it can also be seen that at low concentrations of drug X (to the left hand side of the shaded area) the combination effect surpasses that of the partner drug but is no greater than the effect of the fixed concentration of ADI-PEG20. At high concentrations of drug X (to the right hand side of the shaded area) the combination effect is the same as the potent effect of drug X, meaning that the effect of ADI-PEG20 is effectively redundant when combined with these concentrations of X.

The rationale for the use of the less stringent HSA model comes from the conclusion of Jaaks *et al.* themselves, who stated that real synergy is rare and is highly context dependent (*e.g.* confined to tumours with very specific molecular aberrations) [200], and therefore has limited applicability in the real world where intra-tumoral and inter-patient heterogeneity exists. Indeed, the argument has been made using modelling of clinical trial drug effects that real-world benefit of combination regimens is rarely through mechanistically aligned synergy but rather through independent drug action [203, 204], and this therefore favours a more simplistic, less stringent model for pre-clinical development such as HSA.

6.2 ADI-PEG20 as part of drug combination therapy

Pharmacological combinations with conventional ALL chemotherapy

It has been suggested that arginine starvation can enhance DNA-damage caused by the chemotherapy agent cisplatin, through the reliance of DNA-damage repair mechanisms on the presence of arginine [205]. We therefore chose to first screen the conventional DNA damaging drugs that form the backbone of most ALL induction therapy regimens (vincristine, daunorubicin and cytarabine but not cyclophosphamide since this is a prodrug rather than an active compound) as well as the other major backbone drug dexamethasone in combinations with ADI-PEG20, using cell line models representing low, intermediate and high baseline *ASS1* expression. To allow for screening of multiple combinations in multiple

cell lines and over independent replicates we used CellTiter-Glo to measure residual ATP content as a proxy for residual live cell count after 72 hours of treatment.

The combination of ADI-PEG20 and dexamethasone in the *ASS1*-low cell line MUTZ-5 produced a significantly greater effect than either single agent, with a HSA CI of 1.4 at a dexamethasone concentration of 25ng/ml ($p<0.001$ from t-test for difference in mean effect; figure 6.2.1a, left panel). At this dexamethasone dose there was a moderately potent monotherapy cytoreduction to around 40% of untreated cells and the addition of ADI-PEG20 deepened this to a residual cell count of approximately 10%. At the next dose increment of dexamethasone of 500ng/ml, where dexamethasone monotherapy led to almost complete cytoreduction, the addition of ADI-PEG20 still led to a significant increase, albeit subtle, in cytoreduction with CI of 1.004 ($p=0.004$).

The *ASS1*-intermediate cell line Reh is intrinsically resistant to dexamethasone monotherapy and our data confirmed this (figure 6.2.1a, middle panel), with the combination treatment matching that of ADI-PEG20 alone and so giving CI values close to 1 across the dose range. Conversely, the *ASS1*-high cell line RS4;11 is intrinsically resistant to ADI-PEG20 and we observed that the combination treatment response broadly matched that of dexamethasone alone (figure 6.2.1a, right panel), again with CI values close to 1 across the dose range.

For the combination of ADI-PEG20 and vincristine we did not see a significant difference in the combination effect and the highest single agent effect in any cell line at any vincristine concentration with one exception (figure 6.2.1b). This exception was for the highest tested vincristine dose in the *ASS1*-intermediate cell line Reh, where we observed that the single agent effect of vincristine was marginally more potent than the combination effect, with a CI of 0.96 ($p<0.001$). The CI of less than 1 in this case suggests that there may have been an antagonistic effect between ADI-PEG20 and vincristine at this dose, although this fractional relative effect equates to a very small absolute effect because of the high potency at this dose and so the significance is not clear-cut. Another notable point is that the *ASS1*-low cell line MUTZ-5 appeared partially resistant to vincristine, with a maximum cytoreduction to around 40% of untreated cells at high vincristine doses. At these doses the addition of ADI-PEG20 did not enhance the degree of cytoreduction, suggesting a degree

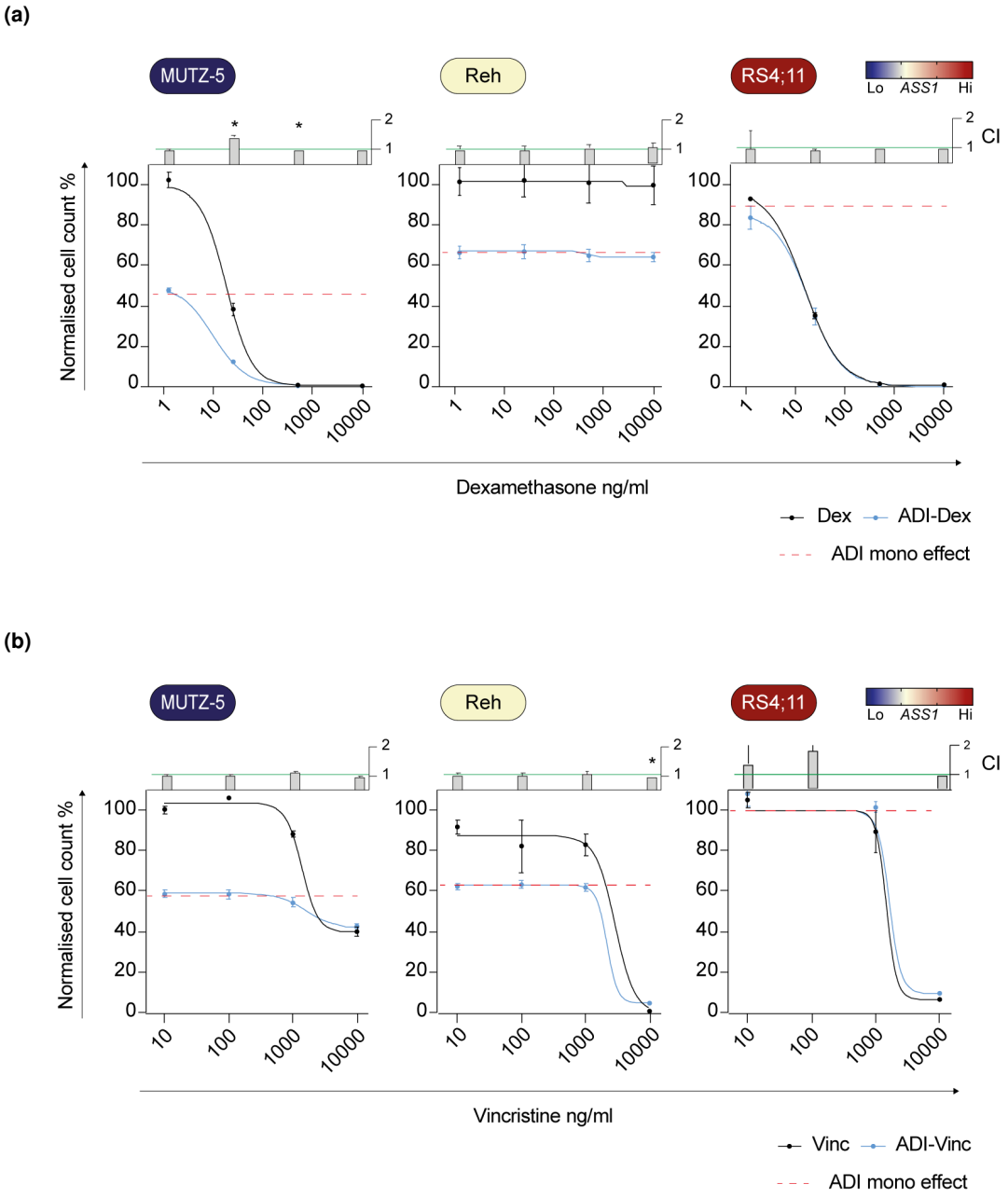

Figure 6.2.1: **ADI-PEG20 as part of drug combination therapy**
Combination screens of 72 hours ADI-PEG20 (ADI) with (a) dexamethasone (Dex) or (b) vincristine (Vinc). Residual cell counts estimated by ATP content. Data from 3 independent microplate runs. Data normalised to untreated wells per plate to account for variable luminescence on individual plate runs. Red dashed lines indicate normalised residual cell count for ADI-PEG20 monotherapy at 1000ng/ml. Black and blue solid lines indicate least-squares non-linear regression fit to residual cell count data generated from individual drugs or combined drug with 1000ng/ml ADI-PEG20, respectively. Bar annotations at top represent CI values from HSA model for each dose level, * $p<0.05$ from t-test for difference in mean response between combination and highest single agent effects, with Šídák's multiple comparisons test; green line represent CI of 1.

of cross-resistance to cell death induction by ADI-PEG20 and vincristine in this cell line, that is, the ability to survive both treatments.

For the combination of ADI-PEG20 and daunorubicin we again did not see a significant difference in the combination effect and the highest single agent effect in any cell line at any daunorubicin concentration with one exception (figure 6.2.2a). In this case the exception was for the *ASS1*-low cell line MUTZ-5 at the highest dose of daunorubicin where we saw a CI of 0.99 ($p = 0.008$), indicating a possible antagonistic relationship between ADI-PEG20 and high concentrations of daunorubicin, although again this equates to a very small absolute effect. For this combination in the Reh cell line model (figure 6.2.2a, middle panel) there was a clear departure of the fitted curves for the combination and single agent data between daunorubicin doses of 2.5 and 10ng/ml which seems an artefact of the low resolution in data points.

For the combination of ADI-PEG20 and cytarabine, we did see an additive effect at the 10ng/ml cytarabine dose for the *ASS1*-low cell line MUTZ-5 (CI=1.13, $p = 0.01$), with an apparent departure of the fitted combination response (blue) curve from the fitted cytarabine single agent response (black) curve and the ADI-PEG20 single dose effect (red dashed line) in this dose region (figure 6.2.2b, left panel). For potent concentrations of cytarabine we saw CI values that were fractionally, but significantly less than 1 in all cell lines, once again suggesting that there may be a marginal antagonistic effect at high doses by the combination with ADI-PEG20. Arguing against this is the fact that we saw significant CI values even for the RS4;11 cell line, which is intrinsically resistant to ADI-PEG20 and therefore there is no biological rationale as to why this might antagonise high doses of cytarabine.

The interpretation of the fitted response curves was somewhat limited by the resolution of dose points and it is unclear how closely the curves would have overlaid or separated if there had been more data points. What does seem clear though is that there is little additional effect to adding ADI-PEG20 to high doses of the traditional DNA-damaging chemotherapy drugs that were tested (vincristine, daunorubicin, cytarabine). Even for the *ASS1*-low cell line MUTZ-5, which is most sensitive to ADI-PEG20 of those tested, we observed that at chemotherapy mono-agent concentrations where the residual cell count was reduced to around 20% or less, the combination response curves overlaid those of the

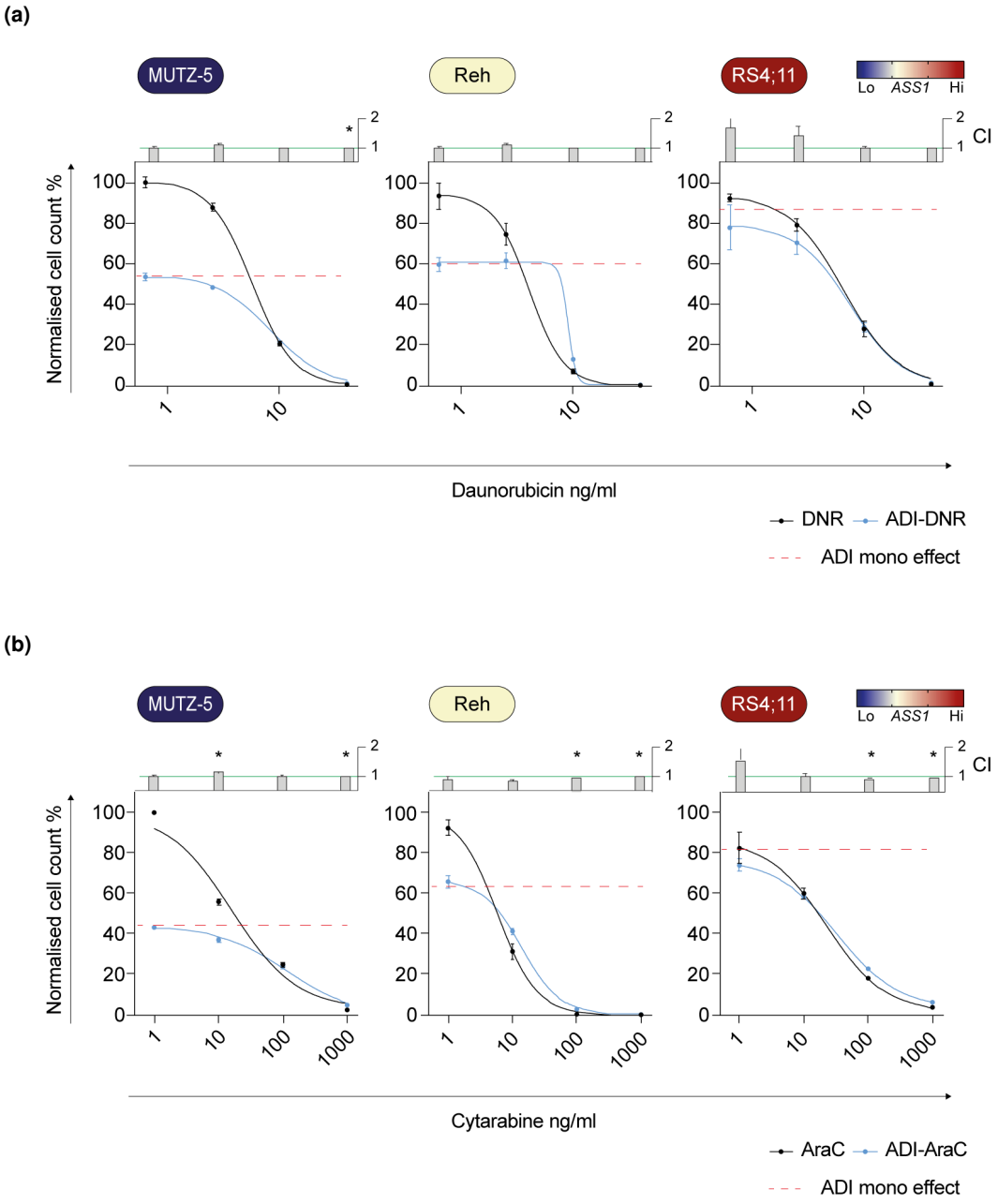

Figure 6.2.2: **ADI-PEG20 as part of drug combination therapy**
Combination screens of 72 hours ADI-PEG20 (ADI) with (a) daunorubicin (DNR) or (b) cytarabine (AraC). Residual cell counts estimated by ATP content. Data from 3 independent microplate runs. Data normalised to untreated wells per plate to account for variable luminescence on individual plate runs. Red dashed lines indicate normalised residual cell count for ADI-PEG20 monotherapy at 1000ng/ml. Black and blue solid lines indicate least-squares non-linear regression fit to residual cell count data generated from individual drugs or combined drug with 1000ng/ml ADI-PEG20, respectively. Bar annotations at top represent CI values from HSA model for each dose level, * $p<0.05$ from t-test for difference in mean response between combination and highest single agent effects, with Šídák's multiple comparisons test; green line represent CI of 1.

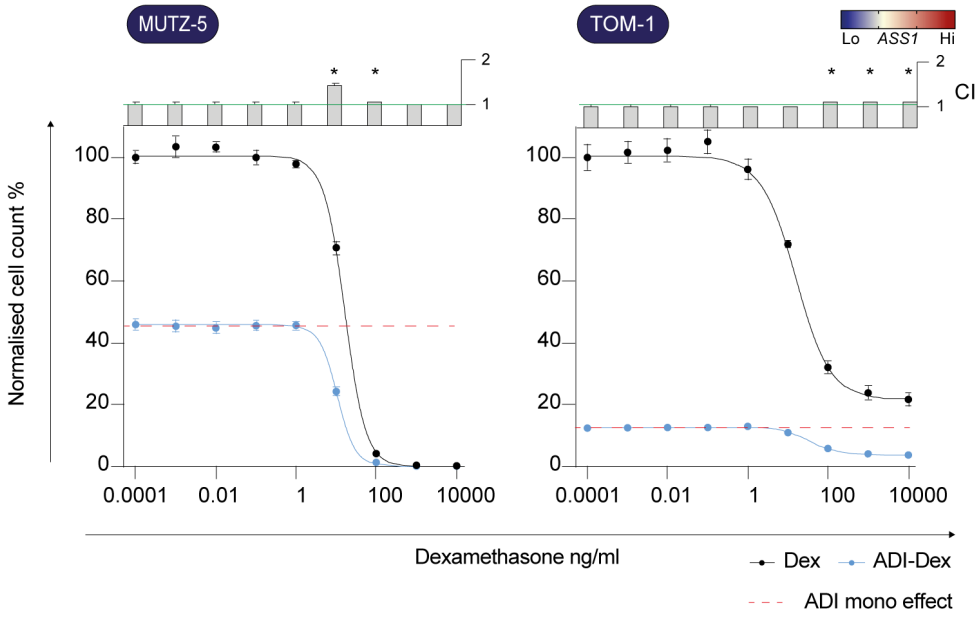

Figure 6.2.3: **ADI-PEG20 as part of drug combination therapy**
Increased resolution combination analysis of ADI-PEG20 (ADI) and dexamethasone (Dex). Cell counts estimated after 72 hours of treatment by ATP content. Data from 3 independent microplate runs, with each run consisting of 3 technical replicates that were normalised to untreated wells for each individual plate prior to aggregation. Red dashed lines indicate estimated cell count for ADI-PEG20 monotherapy at 1000ng/ml. Black and blue solid lines indicate least-squares non-linear regression fit to data generated from dexamethasone or combined dexamethasone and 1000ng/ml ADI-PEG20 treatment, respectively. Bar annotations in top section of each panel represent CI values from HSA model for each tested dose level with * marking those with $p<0.05$ from t-test for difference in mean response between combination and highest single agent effects, with Šídák's multiple comparisons test; green line represent CI of 1. Cell line labels coloured by baseline *ASS1* expression.

single agent chemotherapy curves, signifying that persister cells able to survive the action of the chemotherapy drugs are also able to survive arginine starvation.

The combination effect with dexamethasone, not classically defined as a DNA-damaging chemotherapy agent, was somewhat distinct, in that the addition of ADI-PEG20 could enhance the cytoreductive effect even at moderately potent concentrations of dexamethasone. We therefore chose to investigate this further by combining ADI-PEG20 with a higher resolution dose range of dexamethasone and expanding our screen to also include both *ASS1*-incompetent cell lines, MUTZ-5 and TOM-1 (figure 6.2.3). With an improved range of dexamethasone concentrations we were able to fit more reliable dose response curves to the data and could confirm the findings from the initial screen in the MUTZ-5 cell line

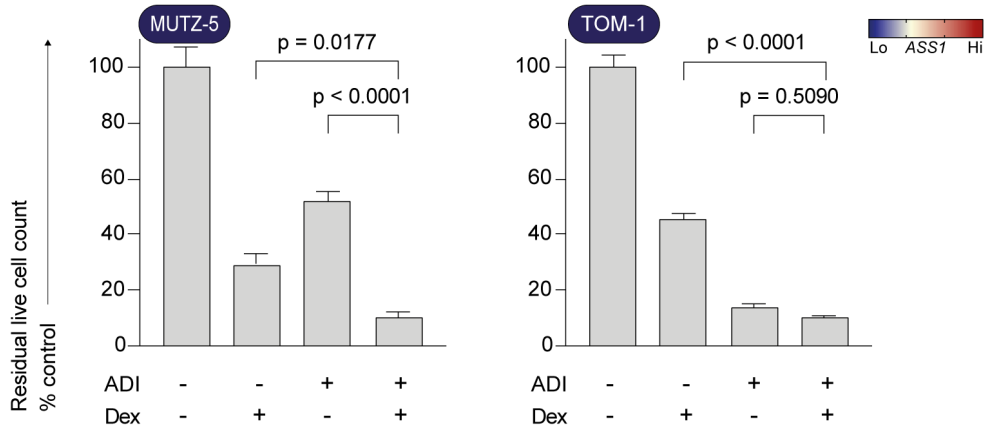

Figure 6.2.4: **ADI-PEG20 as part of drug combination therapy**
Analysis of residual cells after treatment with 1000ng/ml ADI-PEG20, 20ng/ml dexamethasone or combination. Live cells enumerated by FACS as ZombieViolet^{neg}Annexin-V^{neg}. p-values from ANOVA with Šídák's multiple comparisons test; for both cell lines data are from 6 technical replicates aggregated over 2 separate experiments. Cell line labels coloured by baseline *ASS1* expression.

that the combination effect was greater than either single agent effect at close to the IC_{50} concentration of dexamethasone (figure 6.2.3, left panel). Interestingly, we found that the TOM-1 cell line has a partial degree of resistance to dexamethasone at concentrations that were ablative to the MUTZ-5 cultures, but the addition of ADI-PEG20 at these concentrations could deepen the cytoreductive effect (figure 6.2.3, right panel). This finding suggests that there is little cross-resistance in the dexamethasone persister TOM-1 cells to the effects of ADI-PEG20 and this has been suggested as an ideal basis for drug combinations for clinical patient cohorts [203, 204].

Given this finding with the potential for genuine clinical significance, we further interrogated the combination of dexamethasone and ADI-PEG20 in the *ASS1*-incompetent cell lines using FACS analysis of viability and Annexin-V expression, as a more specific measure for non-apoptotic treatment persistent cells (figure 6.2.4). We chose the 20ng/ml concentration of dexamethasone that was expected to kill approximately 50% of cells from both cell line models.

Using this combination of drug concentrations in the MUTZ-5 model we saw that the combination effect of ADI-PEG20-dexamethasone was greater than that for both dexamethasone monotherapy ($p = 0.0177$ from ANOVA) and ADI-PEG20 alone ($p < 0.0001$)

(figure 6.2.4, left panel). In the TOM-1 model we also saw that the combination effect was greater than that for dexamethasone monotherapy ($p < 0.0001$). However, while the final residual cell count after combination therapy was numerically lower than that for ADI-PEG20 monotherapy, this was not statistically significant ($p = 0.5090$, figure 6.2.4, right panel). Since the CI value at 20ng was not significantly greater than 1, this effect is in keeping with the ATP-based assay (figure 6.2.3) and we may have seen a more significant difference had we used a higher concentration of dexamethasone, where we did see CI values that were significantly different to 1. However, this result, at a very small scale, demonstrates the concept that within heterogeneous patient (or tumour cell) populations where response to individual component drugs is variable, drug combinations can lead to effective cytoreduction either by additive effects (as in MUTZ-5) or via the effect of the most potent single agent (ADI-PEG20 in TOM-1 model).

In summary, the combination of ADI-PEG20 with the classical DNA-damaging chemotherapy agents used in ALL induction therapy did not appear to have any additive properties at higher concentrations of the chemotherapy agents, suggesting a degree of cross-resistance to cytoreduction. The combination with dexamethasone was more interesting since ADI-PEG20 could add to the cytoreductive effect of dexamethasone even at higher potency concentrations. Furthermore, in the TOM-1 model where we saw resistance to high dexamethasone concentrations, the addition of ADI-PEG20 appeared to overcome this with a greater combined cytoreduction, although at lower concentrations of dexamethasone the potent effect of ADI-PEG20 dominated.

Combination of ADI-PEG20 with BH3-mimetic agents

As well as testing classical ALL chemotherapy drugs we were interested to test ADI-PEG20 in combination with novel agents and especially those that might be suitable for use in low toxicity, "chemo-free" regimens. We were particularly interested to test the combination of ADI-PEG20 and navitoclax, a clinically relevant inhibitor of Bcl-x_L and Bcl-2, since we had shown that ADI-PEG20 treatment induced the expression of Bcl-x_L (figures 5.2.4 and 5.2.5). To test this, we used the same analytical approach by combining 1000ng/ml ADI-PEG20 with a range of concentrations of navitoclax (figure 6.2.5). We observed an impressive effect

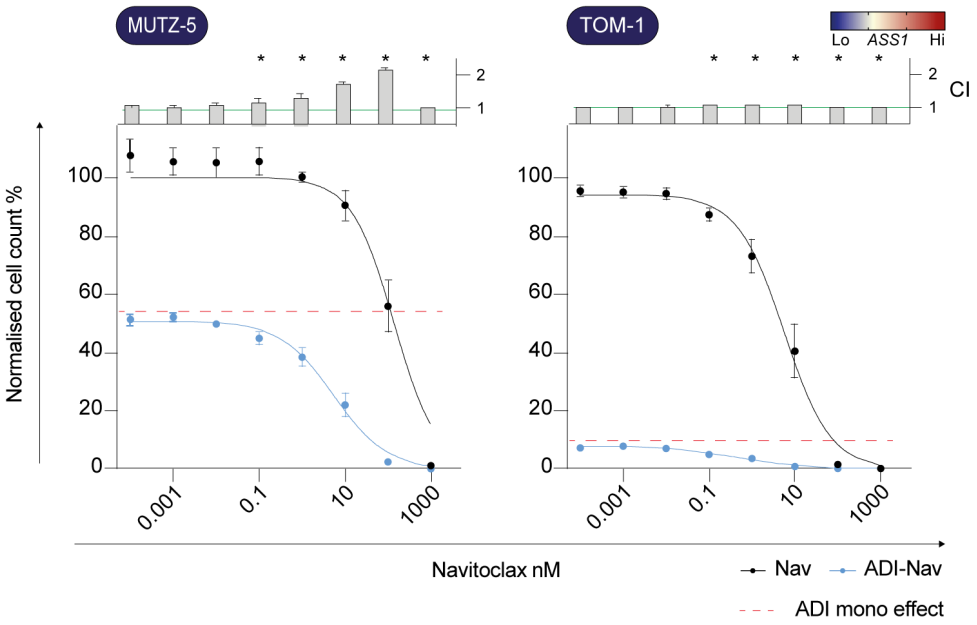

Figure 6.2.5: **ADI-PEG20 as part of drug combination therapy**
Combination analysis of ADI-PEG20 (ADI) and navitoclax (Nav). Cell counts estimated after 72 hours of treatment by ATP content measured by CellTiter-Glo. Data from 3 independent microplate runs, with each run consisting of 3 technical replicates that were normalised to untreated wells for each individual plate prior to aggregation. Red dashed lines indicate normalised residual cell count for ADI-PEG20 monotherapy at 1000ng/ml. Black and blue solid lines indicate least-squares non-linear regression fit to residual cell count data generated from navitoclax or combined navitoclax and 1000ng/ml ADI-PEG20 treatment, respectively. Bar annotations in top section of each panel represent CI values from HSA model for each tested dose level with * marking those with p<0.05 from t-test for difference in mean response between combination and highest single agent effects, with Šídák's multiple comparisons test; green line represent CI of 1. Cell line labels coloured by baseline *ASS1* expression.

for both *ASS1*-incompetent cell lines where the combination of both drugs led to a resultant effect that was markedly greater than for either individual component over a broad range of doses. At 100nM navitoclax the combination lead to an almost complete ablation of the MUTZ-5 cultures, despite each individual component being at an approximate IC_{50}, leading to a HSA CI of 2.13 ($p < 0.001$). In the case of TOM-1, we observed very little residual activity at combinations containing 10nM or greater navitoclax, which was, as with MUTZ-5, about 10 times lower than the concentration required for an equivalent effect with navitoclax alone, with CI values of up to 1.10 (a 10% increase in effect). Although the HSA model does not test for mechanistic synergy, the stark separation of the single agent and combination response curves, especially for MUTZ-5, does suggest a cooperative effect in which the

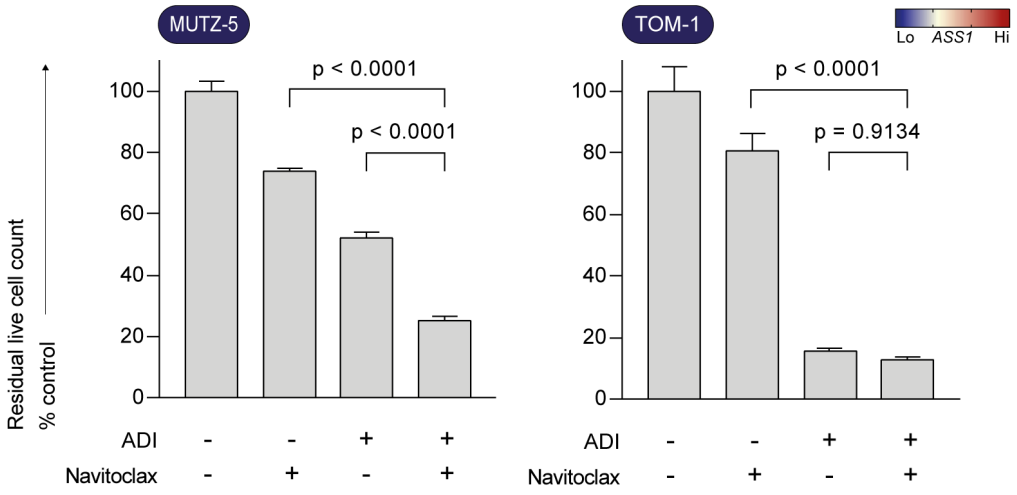

Figure 6.2.6: **ADI-PEG20 as part of drug combination therapy**
Analysis of residual cells after 72 hours treatment with 1000ng/ml ADI-PEG20, 1nM navitoclax or combination. Live cells enumerated by FACS as ZombieViolet^{neg}Annexin-V^{neg}. p-values from ANOVA with Šídák's multiple comparisons test; MUTZ-5 data from 6 technical replicates aggregated over 2 separate experiments and TOM-1 data from 3 technical replicates from a single experiment. Cell line labels coloured by baseline *ASS1* expression.

effect of either drug is potentiated by the presence of the other.

To investigate this apparent cooperative effect further we repeated the combination experiments using ADI-PEG20 combined with 1nM navitoclax. We chose this concentration such that the anticipated single agent effect would result in about a 25-50% cytoreduction, hence allowing us to detect if residual cells would be sensitive to the addition of ADI-PEG20. We enumerated residual live cells with viability and Annexin-V staining followed by FACS acquisition (figure 6.2.6). Once again we saw a remarkable effect in the MUTZ-5 cell line model whereby the combination of ADI-PEG20 and navitoclax reduced residual live cells to 25.29% (95%CI 21.79-28.78%) which was significantly more potent than navitoclax alone ($p < 0.0001$ from ANOVA) or ADI-PEG20 alone ($p < 0.0001$).

In the case of TOM-1 we also saw that the addition of ADI-PEG20 could increase the cytotoxicity of navitoclax at a relatively low potency dose. However, when analysed by FACS using 1nM navitoclax we saw that while the resultant effect was numerically greater than that from ADI-PEG20 alone this was not statistically significant by ANOVA. This echoes the combination of ADI-PEG20 and dexamethasone, where the effect of ADI-PEG20 monotherapy dominated the combination effect, with little benefit to the addition of navitoclax

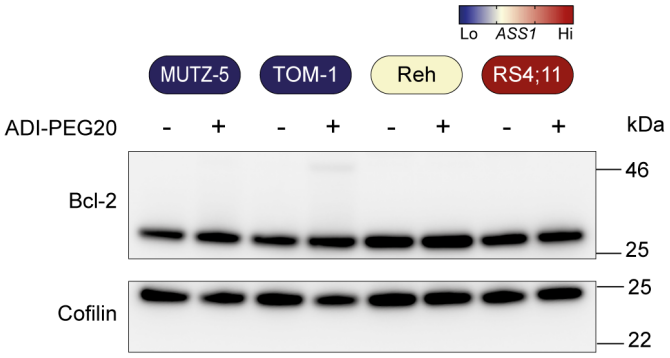

Figure 6.2.7: **ADI-PEG20 as part of drug combination therapy**
Western blotting analysis of Bcl-2 protein expression from whole cell lysates generated after 72 hours 1000ng/ml ADI-PEG20 or control. Cell line labels coloured by baseline *ASS1* expression.

at this low concentration.

We next chose to test the related compound venetoclax, which is a daughter drug of navitoclax, but which inhibits Bcl-2 only without activity against Bcl-x_L. We chose to include this drug as a combination partner for ADI-PEG20 since we had seen an upregulation of Bcl-2 in our previous experiments (figure 5.2.4), although this had been less marked in MUTZ-5 than TOM-1. Furthermore, it is arguably a more clinically relevant drug than navitoclax, having become a component of standard of care treatment for numerous haematological malignancies as well as currently being trialled in combination with ADI-PEG20 for AML [206].

We first retested protein expression of Bcl-2 using western blotting and found at most a subtle change in expression in the *ASS1*-incompetent cell lines MUTZ-5 and TOM-1 after treatment with ADI-PEG20 (figure 6.2.7). We did observe a dimerisation of Bcl-2 in the lysates generated from TOM-1 cells after treatment with ADI-PEG20, although there is no way of telling without further testing if this reflects a genuine mechanistic change in the function of Bcl-2 as a response to ADI-PEG20, or whether it is simply an *in vitro* phenomena associated with *e.g.* the high rate of apoptosis in treated TOM-1 cells.

Again using the ATP based assay, we observed a similar response to that from the ADI-PEG20 and navitoclax combination, with a marked increase in the resultant effect of the combination treatment compared to either individual component effect (figure 6.2.8). Once

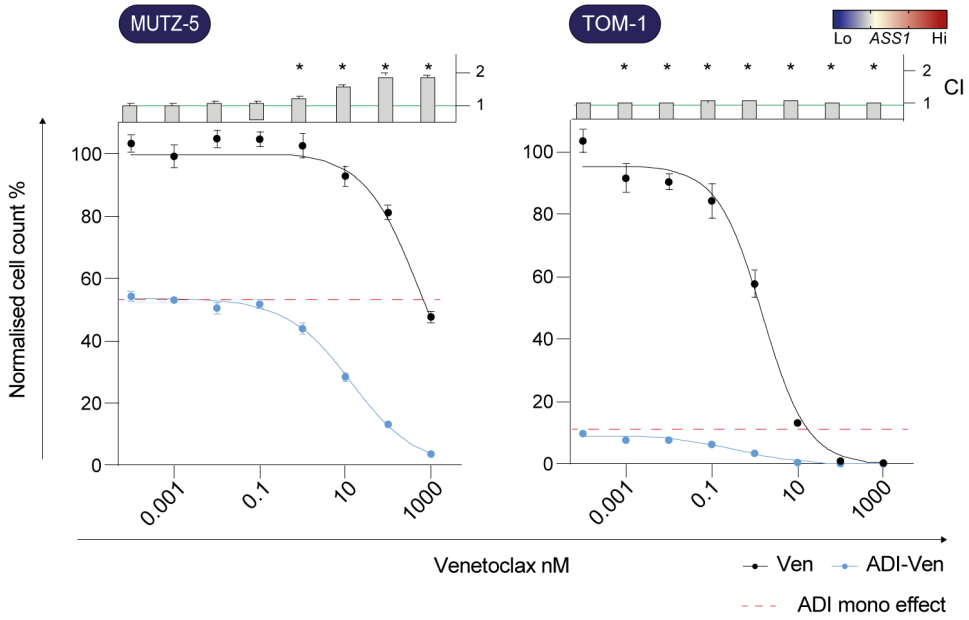

Figure 6.2.8: **ADI-PEG20 as part of drug combination therapy**
Combination analysis of ADI-PEG20 (ADI) and venetoclax (Ven). Cell counts estimated after 72 hours of treatment by ATP content measured by CellTiter-Glo. Data from 3 independent microplate runs, with each run consisting of 3 technical replicates that were normalised to untreated wells for each individual plate prior to aggregation. Red dashed lines indicate normalised residual cell count for ADI-PEG20 monotherapy at 1000ng/ml. Black and blue solid lines indicate least-squares non-linear regression fit to residual cell count data generated from venetoclax or combined venetoclax and 1000ng/ml ADI-PEG20 treatment, respectively. Bar annotations in top section of each panel represent CI values from HSA model for each tested dose level with * marking those with p<0.05 from t-test for difference in mean response between combination and highest single agent effects, with Šídák's multiple comparisons test; green line represent CI of 1. Cell line labels coloured by baseline *ASS1* expression.

again, this effect seemed most marked in the MUTZ-5 cell line which was more resistant to venetoclax monotherapy than TOM-1 with maximum CI of 1.88 ($p < 0.001$) at 100nM venetoclax, where the addition of ADI-PEG20 led to a high degree of cytoreduction even when combined with concentrations of venetoclax that had little single agent effect. The greater sensitivity of TOM-1 to both venetoclax and ADI-PEG20 meant that in this cell line we were able to achieve a highly effective cytoreduction when ADI-PEG20 was combined with low nanomolar concentrations of venetoclax, although the proportional increase was less impressive than that for MUTZ-5, with a maximum CI of 1.12 at 10nM ($p < 0.001$).

We followed the initial ATP based testing with FACS analysis of paired viability and Annexin-V expression (figure 6.2.9). Using this assay in the MUTZ-5 cell line we saw a

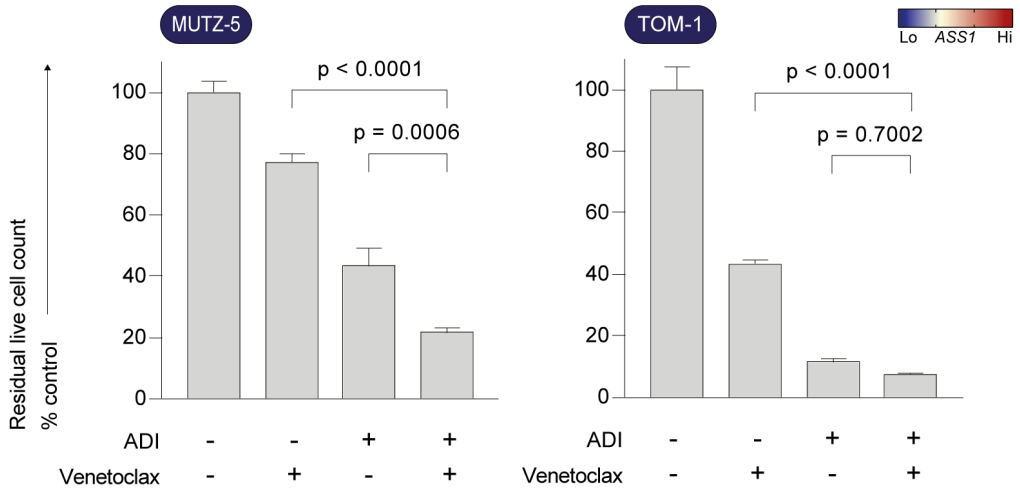

Figure 6.2.9: **ADI-PEG20 as part of drug combination therapy**
Analysis of residual cells after 72 hours treatment with 1000ng/ml ADI-PEG20, 10nM or 1nM venetoclax (MUTZ-5 or TOM-1, respectively) or combination. Live cells enumerated by FACS as ZombieViolet^{neg}Annexin-V^{neg}. p-values from ANOVA with Šídák's multiple comparisons test; for both, data from 9 technical replicates aggregated over 3 separate experiments. Cell line labels coloured by baseline *ASS1* expression.

combined effect with a residual cell count of 21.79% (95%CI 18.40-25.18%) which was significantly lower when compared to that from to venetoclax alone ($p < 0.0001$ from ANOVA) or ADI-PEG20 alone ($p = 0.0006$). In the TOM-1 model we saw a combined effect cytoreduction to a residual cell count of 7.47% (95%CI 6.62-8.33%) which was statistically greater than venetoclax alone ($p < 0.0001$) but not greater than the effect of ADI-PEG20 alone ($p = 0.7002$). Once again demonstrating that in the TOM-1 cell line, where the potency of ADI-PEG20 is high, the addition of low doses of partner drugs has little, if any, additive benefit.

In this section we have demonstrated an exciting potential for a cooperative relationship between ADI-PEG20 and BH3 mimetics, which seemed particularly capable of enhancing the moderate sensitivity of MUTZ-5 to ADI-PEG20 when combined with low potency concentrations of navitoclax or venetoclax. Testing at higher BH3 mimetic concentrations may be useful to see if they can enhance the more potent effect of ADI-PEG20 in the more sensitive cell line TOM-1, but expanding the testing to combine physiologically achievable concentrations of ADI-PEG20 and either venetoclax or navitoclax *in vivo* is arguably a more informative strategy for the purpose of clinical translation.

Targeting Ph+ B-ALL with ADI-PEG20 combination therapy

The final combination drug that we wanted to screen was one specific for treatment of Ph+ ALL, since this subgroup was predicted to have a large proportion of *ASS1*-low patients (figure 4.1.7) and so would be a rational patient group to target with ADI-PEG20. In clinical practice this subgroup is managed distinctly from most other ALL subgroups, with the addition of a TKI to treatment protocols. We therefore wanted to investigate the effect of the addition of ADI-PEG20 to dasatinib, a commonly used TKI in the treatment of Ph+ ALL. Using the same approach to combination analysis we observed that the addition of dasatinib at most tested concentrations to ADI-PEG20 appeared to have a benefit, albeit marginal, in depth of cytoreduction (figure 6.2.10a), with maximum CI of 1.04 at 1000nM dasatinib (p<0.001), indicating a 4% increase in effect. To understand this effect further, we again followed up the ATP based residual cell analysis with FACS analysis of paired viability and Annexin-V staining but chose to analyse the combination of ADI-PEG20 with a fixed combination of dasatinib and dexamethasone (based on recent evidence for the clinical utility of this combination [207], figure 6.2.10b). Contrasting what we had previously seen in drug combination experiments with TOM-1, the combination of ADI-PEG20 with dasatinib-dexamethasone left a residual cell count of 6.98% (95%CI 3.60-10.36%) that was significantly more effective than either ADI-PEG20 alone ($p < 0.0001$ from ANOVA) or dasatinib-dexamethasone ($p = 0.0005$).

To summarise, we found that dexamethasone appeared to have the most potential to form an effective combination with ADI-PEG20 in cell line models and we noted that in the Ph+ cell line TOM-1 resistance to high concentrations of dexamethasone could be at least partially overcome with the addition of ADI-PEG20. We then used a rational approach based on a previously demonstrated ADI-PEG20 induced stimulation of Bcl-x_L (and to a lesser extent Bcl-2) expression to test combinations with both navitoclax and venetoclax and found an apparent cooperative effect. This could be tested further at a mechanistic level and might reveal more about the molecular pathways of cell death instigated by ADI-PEG20.

Encouraged by the ability of ADI-PEG20 to add to the effect of dexamethasone in the Ph+ TOM-1 cell line model, we chose to extend our drug screening further to investigate the addition of ADI-PEG20 to the clinically relevant, Ph+ specific combination of dasatinib-

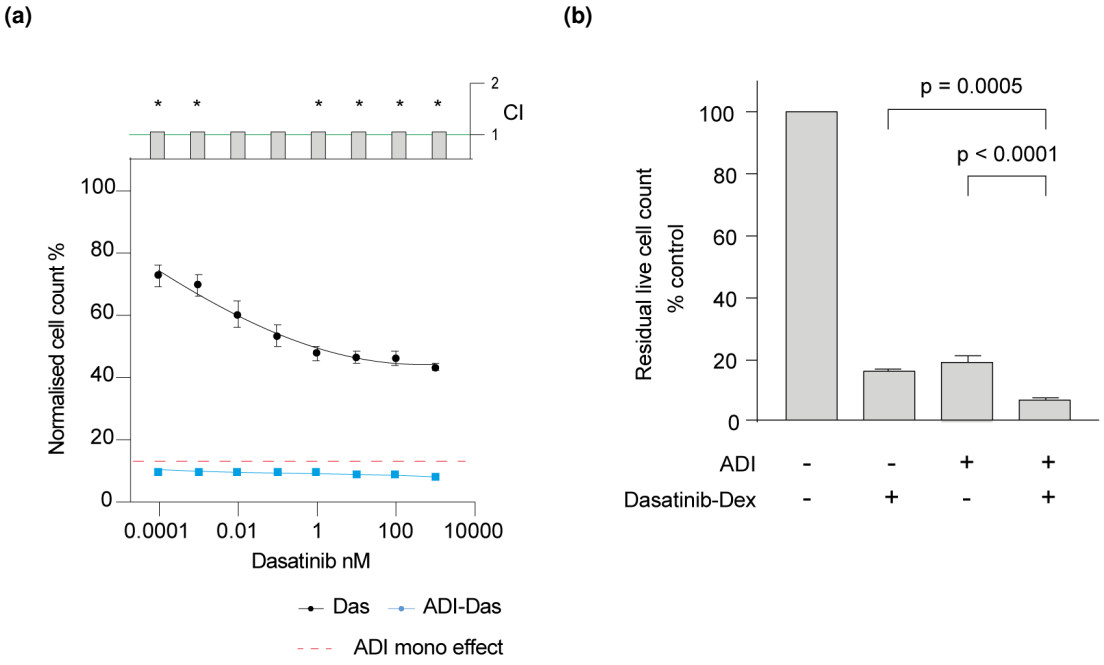

Figure 6.2.10: **Pharmacological combinations with conventional ALL chemotherapy**
a) Combination analysis of 1000ng/ml ADI-PEG20 (ADI) and dasatinib (Das). Cell counts estimated after 72 hours of treatment by ATP content measured by CellTiter-Glo. Data from 3 independent microplate runs, with each run consisting of 3 technical replicates that were normalised to untreated wells for each individual plate prior to aggregation. Red dashed lines indicate normalised residual cell count for ADI-PEG20 monotherapy at 1000ng/ml. Black and blue solid lines indicate least-squares non-linear regression fit to residual cell count data generated from dasatinib or combined dasatinib and 1000ng/ml ADI-PEG20 treatment, respectively. Bar annotations in top section represent CI values from HSA model for each tested dose level with * marking those with p<0.05 from t-test for difference in mean response between combination and highest single agent effects, with Šídák's multiple comparisons test; green line represent CI of 1.
b) Analysis of residual TOM-1 cells after 72 hours treatment with 1000ng/ml ADI-PEG20, combined Dasatinib-Dexamethasone (Dex) (0.1nM and 20ng/ml, respectively) or triplet combination. Live cells enumerated by FACS as ZombieViolet^{neg}Annexin-V^{neg}. p-values from ANOVA with Šídák's multiple comparisons test; data from 3 technical replicates from a single experiment.

dexamethasone. This 3 drug combination produced a cytoreductive effect that exceeded that of both ADI-PEG20 and dasatinib-dexamethasone. The combination of dasatinib-dexamethasone has received attention recently due to the impressive response of Ph+ patients to these drugs (with subsequent blinatumomab consolidation) in the phase 2 GIMEMA LAL2116 D-ALBA (D-ALBA) trial [207]. Despite the excellent outcomes in this trial, it is notable that only 29% of patients achieved a molecular response (defined as undetectable BCR::ABL1 transcripts) during the dasatinib-dexamethasone induction phase. Improving this response rate with the addition of an active, low-toxicity drug such as ADI-PEG20 would be desirable, since 100% of patients who achieved a molecular response by the end of dasatinib-dexamethasone induction survived in a disease-free remission until the end of follow up. We therefore felt that the combination of ADI-PEG20 and dasatinib-dexamethasone presented a particularly exciting combination, especially since we have predicted that a large proportion of Ph+ patients would be sensitive to ADI-PEG20 via low baseline *ASS1* expression.

6.3 Drug resistance modelling

In our *ASS1*-low ALL-04 PDX model we had seen an impressive initial cytoreduction but with subsequent persistent disease, suggesting that some tumour cells are able to tolerate arginine starvation. We therefore wanted to test whether our profiled ADI-PEG20 based combination therapies might be able to eradicate these persister cells prior to further pre-clinical development using *in vivo* models. One of the potential modes of persistence is via *derepression* of *ASS1* and we have seen that greater *ASS1* plasticity associates with survival both *in vitro* and *in vivo*. Another major resistance mode to ADI-PEG20 from clinical trials is the formation of anti-ADI-PEG20 antibodies but, while potentially clinically relevant, this could not be a cause of the cellular persistence in the NSG mouse model. Finally, provision of argininosuccinate by infiltrating macrophages has been shown to support arginine auxotrophic cells under arginine starvation [109] and this may have been at play in the ALL-04 residual tumour cells given that *ASS1* was not significantly upregulated.

Regardless of the mechanism, the final outcome of all resistance modes is normalisation

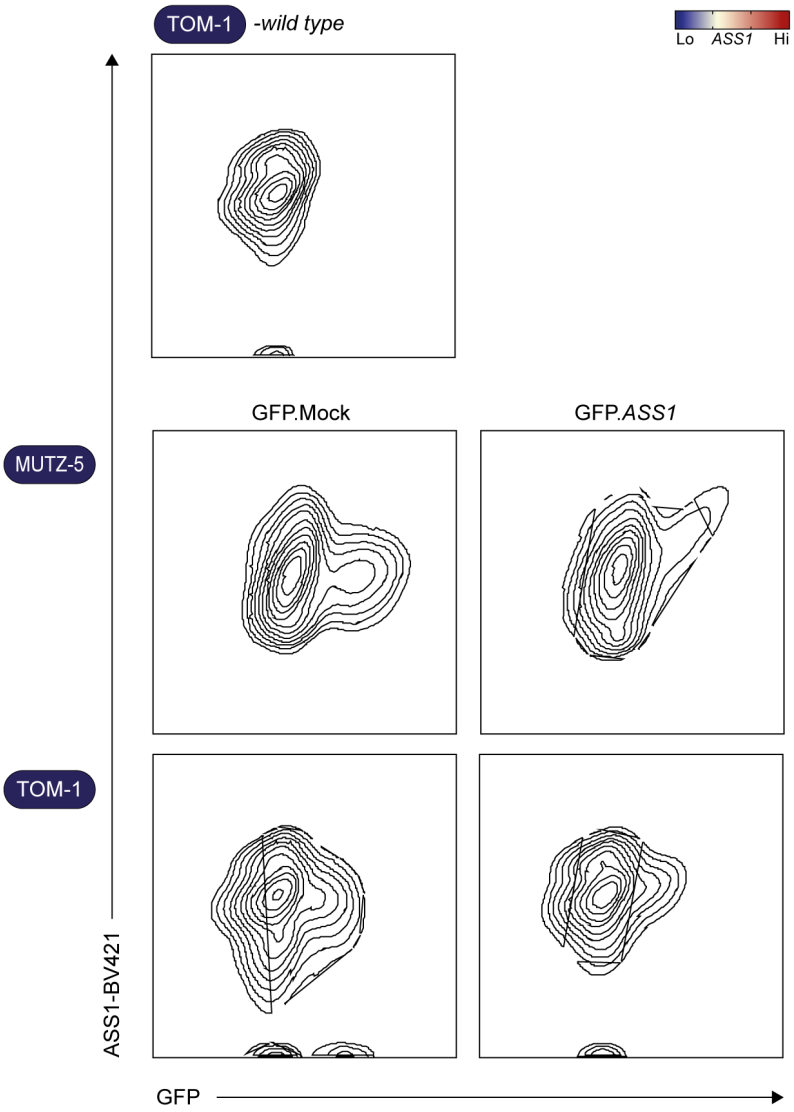

Figure 6.3.1: **Drug resistance modelling**
Representative flow plots comparing ASS1 and GFP expression as measured by FACS in TOM-1 wild type (top-left), MUTZ-5.GFP.Mock (middle-left) and MUTZ-5.GFP.ASS1 (middle-right), TOM-1.GFP.Mock (bottom-left) and TOM-1.GFP.ASS1 (bottom-right). Contour lines represent logarithmic count thresholds. Cell line labels coloured by baseline *ASS1* expression.

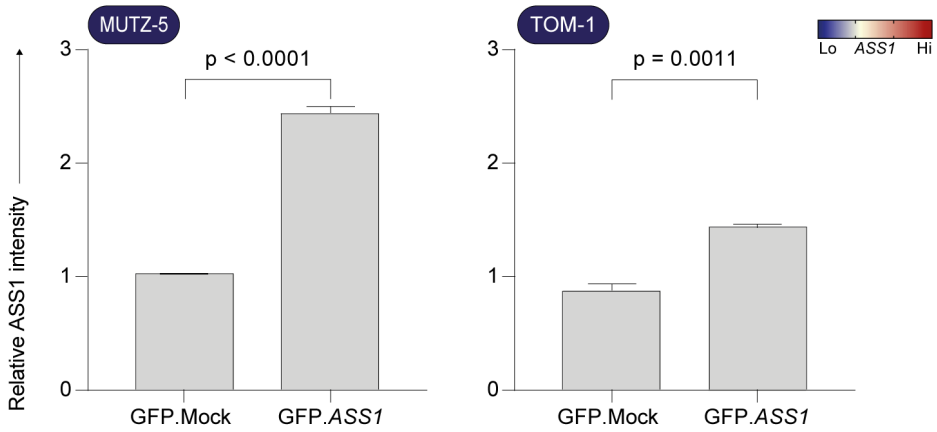

Figure 6.3.2: **Drug resistance modelling**
Ratio of FACS determined ASS1 expression between GFP^{pos} and GFP^{neg} cells from MUTZ-5 and TOM-1 cells after transduction with GFP.Mock or GFP.ASS1 cDNA clones. Relative ASS1 intensity calculated as ratio of GFP^{pos} cells ASS1 intensity to that from same-tube GFP^{neg} wild-type cells. p-values from t-test; data from 3 separate cell line samples in each case.

of arginine availability in tumour cells. We therefore wanted to test the ability of ADI-PEG20 based combination therapy to eradicate persister cells in an *in vitro* model where cells could correct their arginine deficit and to do this we designed a model with enhanced *ASS1* plasticity. In our standard culture models we did not observe a significant degree of *ASS1* upregulation during 72 hours of ADI-PEG20 treatment (the maximum time period in which cells could remain in log-phase growth without media exhaustion, figure 5.5.3) and so to achieve this we constructed an investigative model in which *ASS1* could be derepressed by the outgrowth of a pre-existing *ASS1* overexpressing subclone. We virally transduced both MUTZ-5 and TOM-1 cells with either a GFP tagged *ASS1* cDNA clone or a similarly tagged mock cDNA sequence not corresponding to any known gene. We intentionally used retronectin based transduction, with which we had previously experienced low transduction efficiency in these cell lines, and after transgene insertion did not perform any cell selection such that the resultant GFP^{pos} subclones represented approximately 5% of total cells (figure 6.3.1). Using FACS we then confirmed that the GFP^{pos} subclones from the *ASS1*-transgene models expressed ASS1 at higher levels than the GFP^{neg}, non-transduced bulk cells, but with no effect in the mock-transduced models (figure 6.3.2).

Using this model we wanted to first test if we could recreate the normal cell cycle that we

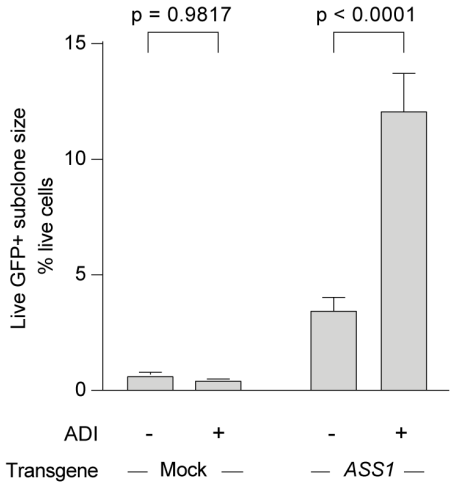

Figure 6.3.3: **Drug resistance modelling**
GFP^{pos} subclone size in mock transduced and ASS1 transduced TOM-1 cells after 72 hours 1000ng/ml ADI-PEG20 treatment compared to control. Subclone % calculated from proportion of GFP^{pos} to total live cells. p-values from 2-way ANOVA with transgene and treatment as factors and Šídák's multiple comparisons test; data from 6 technical replicates aggregated from 2 independent experiments.

had observed in the persister cells of the treatment group from the Ph+ ALL-04 PDX model (figure 5.4.3a) and so treated the transduced Ph+ TOM-1 subclone models with 1000ng/ml ADI-PEG20 for 72 hours before analysis with FACS. In the *ASS1*-transduced model we saw a significant increase in the GFP^{pos} subclone size that did not occur in the mock-transduced model (figure 6.3.3), suggesting that the overexpression of *ASS1* conferred a survival advantage over the wild-type cells during exposure to ADI-PEG20. Analysing the cell cycle of live cells we observed that for both mock- and *ASS1*-transduced models, GFP^{pos} cells were found at all stages of the cell cycle under control conditions, but while ADI-PEG20 treatment caused mock-transduced cells to accumulate in the G0 cell cycle state along with their wild-type counterparts, the *ASS1*-transduced cells remained distributed throughout the cell cycle (figures 6.3.4a, 6.3.4b and 6.3.5). Indeed, the distribution of GFP^{pos} cells across cell cycle states in the *ASS1*-transduced model was indistinguishable between treated and control conditions ($p = 0.5007$ from X^2-test, figure 6.3.5 right panel), while the GFP^{pos} mock-transduced cells matched the significant alteration in cell cycle occupancy as seen previously in wild-type cells between control and treatment, with a marked increase in G0 cells and a reduction in other states ($p < 0.0001$, figure 6.3.5 left panel).

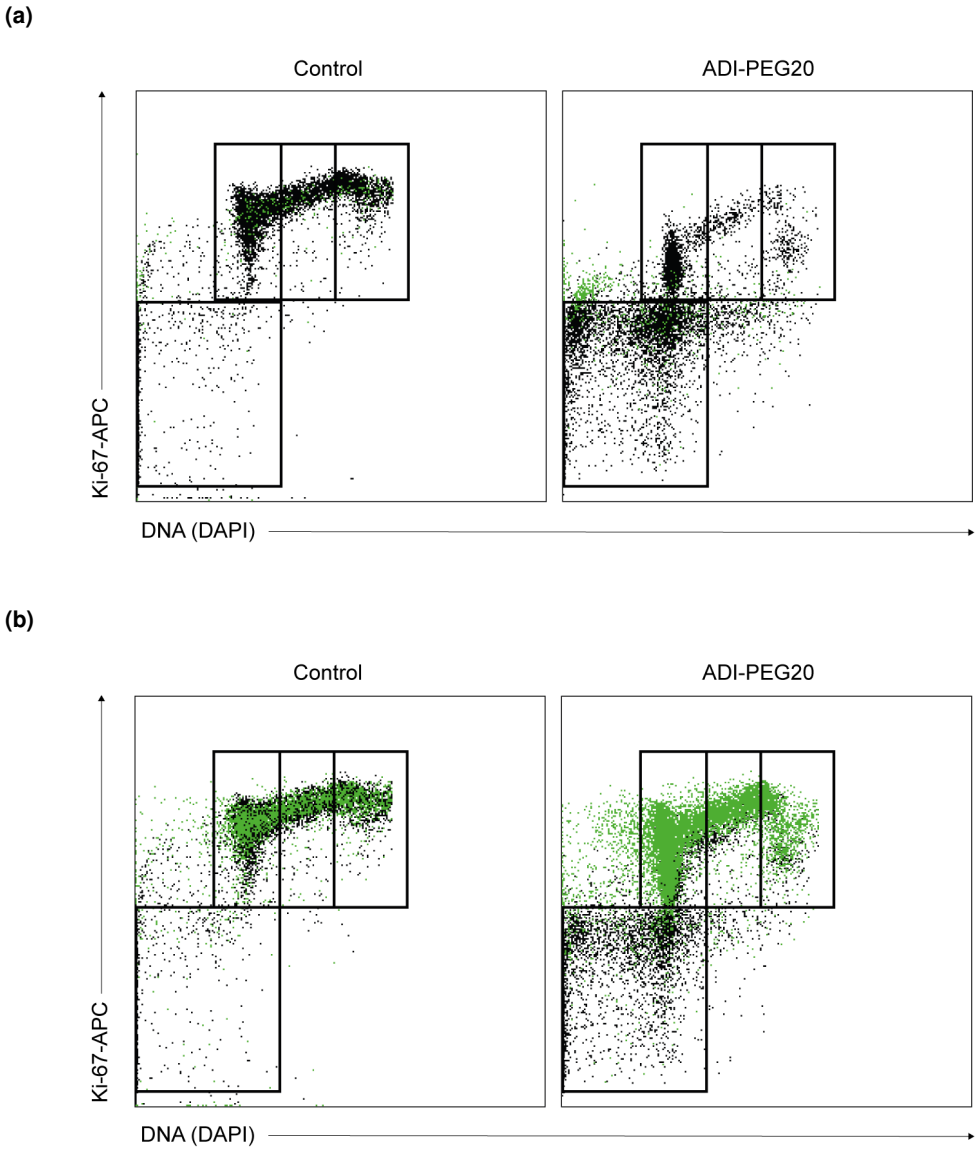

Figure 6.3.4: **Drug resistance modelling**
Representative FACS dot plots showing cell cycle state occupancy for (a) mock transduced or (b) ASS1 transduced TOM-1 cells with or without 72 hours 1000ng/ml ADI-PEG20 treatment. Green dots represent GFP^{pos} cells while black represent GFP^{neg} wild-type cells.

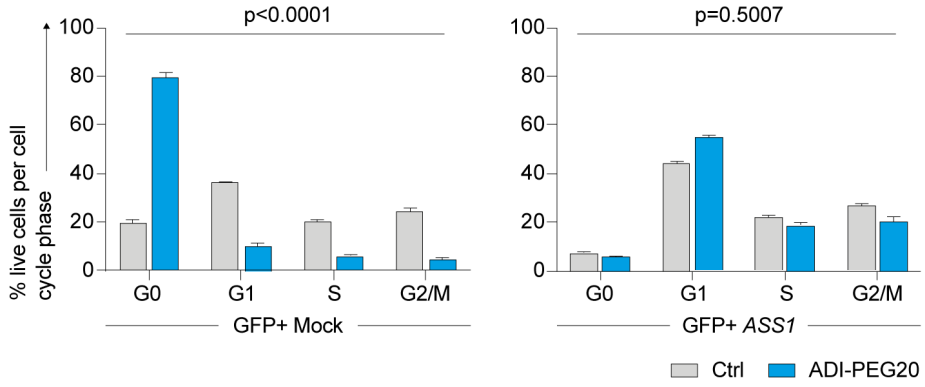

Figure 6.3.5: **Drug resistance modelling**
Cell cycle state occupancy for mock transduced (left panel) or ASS1 transduced (right panel) TOM-1 cells with or without 72 hours 1000ng/ml ADI-PEG20 treatment. p-values from Chi-squared test using average % cell cycle state occupancy from 6 technical replicates aggregated over 2 independent experiments.

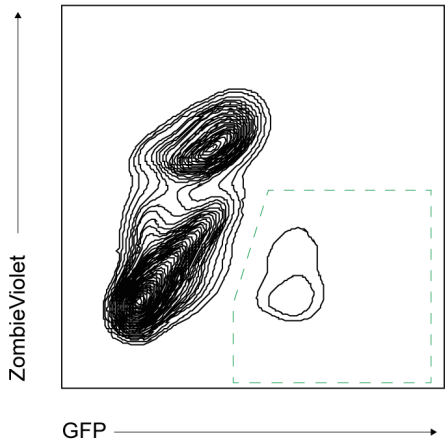

Figure 6.3.6: **Drug resistance modelling**
Representative FACS plot of viability (ZombieViolet) *vs* GFP intensity in transduced TOM-1 cells, used for gating events for drug combination analysis.

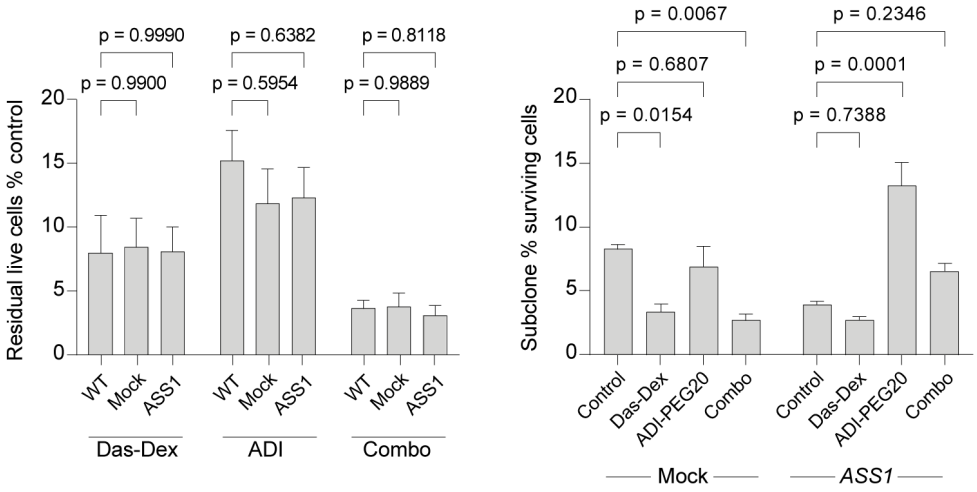

Figure 6.3.7: **Drug resistance modelling**
Left panel - FACS analysis of total (GFP^{pos} and GFP^{neg}) residual live TOM-1 cells after 72 hours dasatinib-dexamethasone (Das-Dex; 0.1nM and 20ng/ml, respectively), ADI-PEG20 (ADI, 1000ng/ml) or triplet combination treatment of wild-type (WT), mock-transduced or ASS1-transduced resistant subclone models. Cells enumerated as $ZombieViolet^{neg}Annexin\text{-}V^{neg}$ and normalised to untreated wells from corresponding wild-type or transduced conditions.
Right panel - Residual subclone size after same treatment, calculated as proportion of $ZombieViolet^{neg}Annexin\text{-}V^{neg}GFP^{pos}$ from total (GFP^{pos} and GFP^{neg}) residual live cells for each wild-type or transduced condition.
For both, p-values from 2-way ANOVA with transgene and treatment as factors and Dunnett's multiple comparisons test; data are averages from 3 independent experiments each consisting of 3 technical repeats.

The expansion of the *ASS1*-overexpressing subclone with a cell cycle that was unaffected by ADI-PEG20 from the Ph+ TOM-1 model therefore resembled the phenotype of the persister cells from the Ph+ ALL-04 PDX and so we chose to use this model to test our Ph+ specific combination of ADI-PEG20 with dasatinib-dexamethasone. To test the effects of the drug treatment on the outgrowth of the *ASS1*-overexpressing subclone cells we again used FACS analysis of paired viability and Annexin-V expression. Of note, we restricted our analysis to live cells, defined as $ZombieViolet^{neg}Annexin\text{-}V^{neg}$ since we expected that in the dead or dying GFP^{pos} cells there would be some modulation of GFP intensity, as well as a possible increase in fluorescence intensity in the blue 530nm/30nm bandpass channel amongst dying or dead GFP^{neg} cells (figure 6.3.6).

After treatment with dasatinib-dexamethasone, ADI-PEG20 or the triplet combination

we did not find any difference in the amount of residual live cells between wild-type, mock-transduced or *ASS1*-transduced when compared to corresponding untreated controls (figure 6.3.7, left panel). This is perhaps not surprising since the subclone sizes were only approximately 5% of the total population. However, what we did see very clearly was that the subclone size of GFP^{pos} cells in the *ASS1*-transduced model expanded upon ADI-PEG20 monotherapy (figure 6.3.7, right panel; $p = 0.0001$ from 2-way ANOVA using untreated clone size as control), but this effect was suppressed by the combination with dasatinib-dexamethasone ($p = 0.2346$ for difference from untreated clone size).

Unexpectedly we saw that the mock-transduction process appeared to render GFP^{pos} cells more sensitive to dasatinib-dexamethasone, evidenced by the decrease in subclone size after dasatinib-dexamethasone treatment ($p = 0.0154$) but we did not see any change in the sensitivity to ADI-PEG20 ($p = 0.6807$). The fact that the *ASS1*-transduction did not change sensitivity to dasatinib-dexamethasone in GFP^{pos} cells ($p = 0.7368$) raises the possibility that the insertion of the *ASS1* transgene somehow counteracted the increase in sensitivity to dasatinib-dexamethasone induced by general viral transduction effects, or possibly that some insertion related phenomena specific to the mock-transgene had an unexpected biological effect.

We next wanted to test whether the apparently cooperative relationship between ADI-PEG20 and venetoclax might also be able to reduce the outgrowth of the *ASS1*-overexpressing subclone in the TOM-1 model. Looking first at the effect on the total cell count we again did not see any difference at the bulk cell level in the response to either ADI-PEG20, venetoclax or the combination (figure 6.3.8, left panel). However, when we analysed the effect of the different treatments on the subclone sizes, we saw that conversely to the dasatinib-dexamethasone effect, the combination of ADI-PEG20 and venetoclax was unable to suppress the outgrowth of the *ASS1*-overexpressing subclone that was again seen with ADI-PEG20 monotherapy (figure 6.3.8, right panel; from 2-way ANOVA comparison to untreated subclone size, $p = 0.0051$ and $p = 0.0015$ for ADI-PEG20-monotherapy and combination therapy, respectively).

We then retested the same combination in the transduced MUTZ-5 models and once again saw that the combination of ADI-PEG20 and venetoclax could not prevent the out-

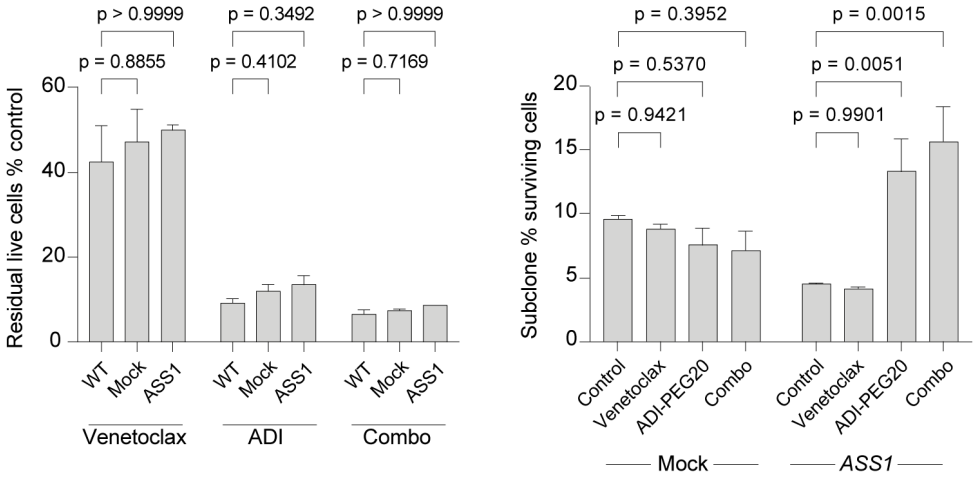

Figure 6.3.8: **Drug resistance modelling**
Left panel - FACS analysis of total (GFP^{pos} and GFP^{neg}) residual live TOM-1 cells after 72 hours venetoclax (Ven, 1nM), ADI-PEG20 (ADI, 1000ng/ml) or triplet combination treatment of wild-type (WT), mock-transduced or ASS1-transduced resistant subclone models. Cells enumerated as $ZombieViolet^{neg}Annexin\text{-}V^{neg}$ and normalised to same from untreated wells for corresponding wild-type or transduced conditions.
Right panel - Residual subclone size after same treatment, calculated as proportion of $ZombieViolet^{neg}Annexin\text{-}V^{neg}GFP^{pos}$ from total (GFP^{pos} and GFP^{neg}) residual live cells for each wild-type or transduced condition.
For both, p-values from 2-way ANOVA with transgene and treatment as factors and Dunnett's multiple comparisons test; data are averages from 3 independent experiments each consisting of 3 technical repeats.

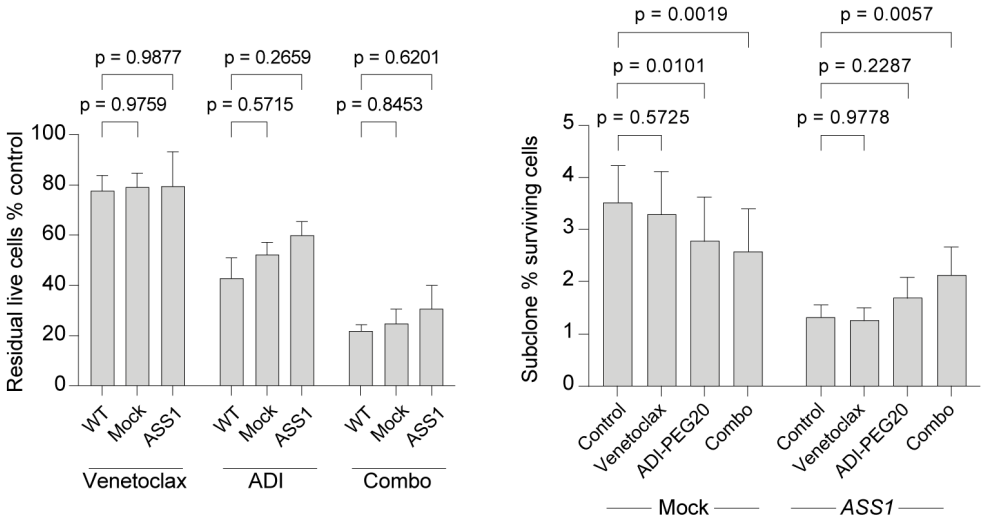

Figure 6.3.9: **Drug resistance modelling**
Left panel - FACS analysis of total (GFP^{pos} and GFP^{neg}) residual live MUTZ-5 cells after 72 hours venetoclax (Ven, 10nM), ADI-PEG20 (ADI, 1000ng/ml) or triplet combination treatment of wild-type (WT), mock-transduced or ASS1-transduced resistant subclone models. Cells enumerated as $ZombieViolet^{neg}Annexin\text{-}V^{neg}$ and normalised to same from untreated wells for corresponding wild-type or transduced conditions.
Right panel - Residual subclone size after same treatment, calculated as proportion of $ZombieViolet^{neg}Annexin\text{-}V^{neg}GFP^{pos}$ from total (GFP^{pos} and GFP^{neg}) residual live cells for each transduced condition.
For both, p-values from 2-way ANOVA with transgene and treatment as factors and Dunnett's multiple comparisons test; data are averages from 3 independent experiments each consisting of 3 technical repeats.

growth of the *ASS1*-overexpressing subclone, although in this model we did not see such a convincing outgrowth of the subclone with ADI-PEG20-monotherapy, potentially because MUTZ-5 is a much slower growing cell line than TOM-1, or possible because the effects of the viral transduction process alone had apparently increased sensitivity to ADI-PEG20, as evidenced by the reduction in clone size of the mock-transduced cells with either ADI-PEG20 or combination therapy (figure 6.3.9).

From this analysis we therefore decided to prioritise the combination of ADI-PEG20 with dasatinib-dexamethasone against Ph+ B-ALL for further pre-clinical development. This combination has the advantage that both the dasatinib-dexamethasone and ADI-PEG20 components were independently effective at the drug concentrations tested in our model system but when combined produced an effect that was statistically greater than either individual component (figure 6.2.10b). Furthermore, this combination appeared to have the

ability to suppress, or at least reduce, the emergence of resistant cells.

6.4 ADI-PEG20 combination therapy *in vivo*

The use of so-called *chemotherapy-free* induction therapy in Ph+ B-ALL, consisting of a TKI combined with steroids or blinatumomab, has recently gained attention given promising response data set against the backdrop of high toxicity and treatment failure rates in traditional treatment regimens [114]. One of the exciting signals from this new approach to treating Ph+ B-ALL is that for patients who achieve a complete molecular response (defined as undetectable BCR::ABL1 transcripts by qPCR) with chemotherapy-free treatment there is an excellent prognosis and the possibility to avoid allogeneic stem cell transplantation [207, 208]. In the study of Foá *et al*., who used dasatinib-dexamethasone as induction followed by blinatumomab consolidation, 29% of patient achieved a complete molecular response with induction alone and this increased to 60% after consolidation [207]. We therefore wondered if our combination of ADI-PEG20 with dasatinib-dexamethasone, which appeared to be more potent that dasatinib-dexamethasone alone (figure 6.2.10b), might be able to increase the rate of response in Ph+ B-ALL.

To test this in a pre-clinical setting we generated PDX bearing NSG mice by re-transplanting leukaemia cells harvested from control mice from the previous *ASS1*-low ALL-04 PDX experiment. After transplantation, engraftment was monitored by fortnightly bone marrow aspiration and mice were enrolled once leukaemic blasts made up at least 10% of all bone marrow $CD45^{pos}$ cells. Enrolled mice were randomised to 3 experimental arms consisting of control, dasatinib-dexamethasone or ADI-PEG20-dasatinib-dexamethasone and were treated with 3 weekly cycles of 5 daily doses of 1mg/kg dexamethasone and 20mg/kg dasatinib by combined intraperitoneal injection with or without a single weekly dose of 5IU ADI-PEG20, or vehicle control injections. At the end of the 3 weeks of treatment a bone marrow aspirate was performed to confirm that treated mice had gone into remission, defined as <5% engraftment by FACS, and then repeated fortnightly to monitor duration of remission and time to relapse, defined as a return of engraftment to >10%. We also defined bone marrow engraftment of $\geq$ 90% as a pre-lethal degree of tumour that would trigger an

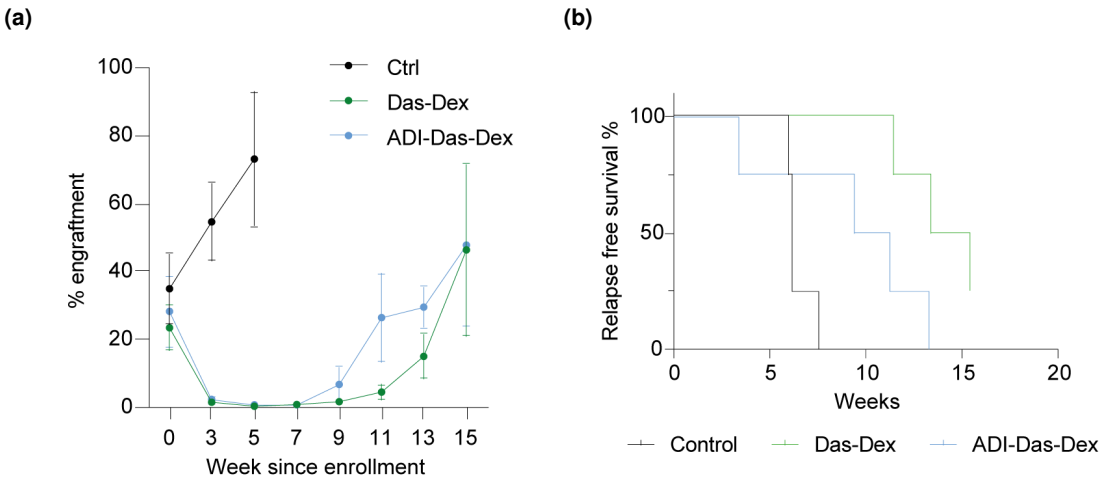

Figure 6.4.1: **ADI-PEG20 combination therapy *in vivo***
a) Serial bone marrow engraftment measurements in respective experimental arms each of 4 mice, measured by FACS with engraftment defined as the proportion of human$CD45^{pos}CD19^{pos}$ from total human and mouse $CD45^{pos}$ cells. No significant differences were detected at any timepoint by repeated measures ANOVA comparing the ADI-PEG20-dasatinib-dexamethasone (ADI-Das-Dex) mice to dasatinib-dexamethasone (Das-Dex) mice.
b) Relapse free survival functions for respective treatment arms, see text for differences between groups.

automatic humane end-point.

Due to an unexpectedly slow engraftment trajectory (given secondary transplanted PDX models usually engraft more rapidly than primograft cells [209]) we were limited to 4 mice per arm. After all mice had been enrolled, there were no differences in the starting degree of engraftment between the 3 experimental arms ($p = 0.6925$ from ANOVA). Immediately after the end of the 3rd week of treatment one of the mice from the ADI-PEG20-dasatinib-dexamethasone arm lost weight and developed a poor clinical phenotype and so was culled. Most mice in both treatment arms lost some weight, as has been reported previously for this combination of drugs in NSG mice [210], but this was the only mouse that developed a phenotype that met our humane end-point threshold. Analysis of harvested bone marrow and spleen cells from this mouse revealed levels of leukaemia consistent with remission and so it was therefore unclear if this toxicity was a result of the addition of ADI-PEG20 or was driven by the known adverse effects of dasatinib-dexamethasone alone.

In the treated mice, the bone marrow aspiration at the end of the final week of therapy

showed that all mice had achieved our pre-defined remission status, while the control mice had progressive degrees of tumour burden (figure 6.4.1a). Over the following 4 weeks, the control mice became unwell or displayed unacceptably high degrees of engraftment and so were culled. In the treated mice, serial bone marrow aspirates showed an initially sustained remission with an eventual rise in engraftment levels (figure 6.4.1a). The average tumour burden after this point was numerically higher in the ADI-PEG20 with dasatinib-dexamethasone group but there were no significant differences at any interval time-point by repeated-measures ANOVA. Using the composite end-point of death or post-remission relapse, pre-defined as an increase in engraftment to >10% in a mouse having previously achieved remission, we saw that the probability of relapse-free survival appeared lower in the ADI-PEG20 plus dasatinib-dexamethasone group when compared to the dasatinib-dexamethasone alone group. However, the only statistically significant comparison was that between the control mice and the dasatinib-dexamethasone mice ($p = 0.0069$ from log-rank test), while the comparisons of control with ADI-PEG20-dasatinib-dexamethasone mice ($p = 0.1067$) and dasatinib-dexamethasone with ADI-PEG20-dasatinib-dexamethasone mice ($p = 0.0424$) did not meet the Bonferroni adjusted α rate of 0.017. These p-values demonstrate the difficulty of analysing survival in very small cohorts, especially if survival functions have crossed, as in the case of the control and ADI-PEG20-dasatinib-dexamethasone mice.

While the repeated measures ANOVA and log-rank tests could not formally reject the null hypotheses that there were no differences in engraftment trajectory or survival, respectively, there is clearly no evidence that ADI-PEG20-dasatinib-dexamethasone was superior. This result was somewhat disappointing given our promising *in vitro* findings. One of the possible factors leading to the apparent lack of benefit to adding ADI-PEG20 to dasatinib-dexamethasone was the high responsiveness to dasatinib-dexamethasone alone meaning that the addition of ADI-PEG20 could at best give very small incremental gains. However, it is unclear if the possible increase in speed of re-engraftment of the ADI-PEG20-dasatinib-dexamethasone treated mice is due purely to random effects which we could not dissect due to low numbers or if there may have been a biological interaction between arginine starvation and dasatinib-dexamethasone meaning that residual disease relapsed more rapidly. Unfortunately, we were unable to analyse this further since no

material was harvested during the "remission" period and this is an important consideration for future experiments.

6.5 Summary

In summary, ADI-PEG20 is active in both *in vitro* and *in vivo* models of *ASS1*-low B-ALL. However, the degree of residual disease left after monotherapy *in vivo* mandates that ADI-PEG20 is combined with other treatment to aim for eradication of disease. We have shown using *in vitro* models that the combination of ADI-PEG20 with both dasatinib-dexamethasone and BH3-mimetic agents venetoclax and navitoclax can deepen response rates. Based on our *in vitro* models we expected that the combination of ADI-PEG20 with a second agent or agents that could kill target cells irrespective of their *ASS1* status or arginine homeostatic state would be beneficial and it appeared as though dasatinib-dexamethasone was a good candidate for these criteria. However, in a single PDX model the combination of ADI-PEG20 and dasatinib-dexamethasone did not provide any pre-clinical benefit. Further studies, incorporating the addition of BH3-mimetics to ADI-PEG20 when combined with other agents, possibly including dasatinib-dexamethasone, are warranted but should be done in conjunction with efforts to understand the altered biology of residual cells after ADI-PEG20 based combination therapy.

Chapter 7

Priming B-ALL for CAR-T immunotherapy with ADI-PEG20

7.1 Rationale for investigation of ADI-PEG20 with CAR-T

During manufacture of CAR-T cells, patients with B-ALL will usually undergo some form of "bridging" therapy, implemented to control disease symptoms and reduce tumour bulk prior to CAR-T infusion (figure 7.1.1). Recent evidence has suggested that, while low disease burden immediately prior to CAR-T infusion improves outcomes and reduces CAR-T related toxicity in B-ALL [115], no particular bridging therapy choice appears to specifically improve outcomes over alternatives [116]. Furthermore, prolonged or more intensive bridging chemotherapy is likely to worsen outcomes by increasing non-CAR related toxicity [115, 116]. Contrasting this, studies of bridging for CAR-T therapy of Diffuse Large B-cell Lymphoma (DLBCL) have found that polatuzumab based bridging appears to reduce likelihood of disease progression and death post CAR-T when compared to alternatives [117] and there is also a suggestion that radiotherapy bridging may be beneficial due to a proposed increase in tumour susceptibility to subsequent CAR-T [211].

With regard to tumour susceptibility, there is a growing interest in the addition of a "priming" therapy immediately prior to, or concomitant with, CAR-T infusion that increases target cell sensitivity to CAR-T either through tumour intrinsic mechanisms or via a more favourable stimulation of CAR-T effector cells (figure 7.1.1). Researchers have reported

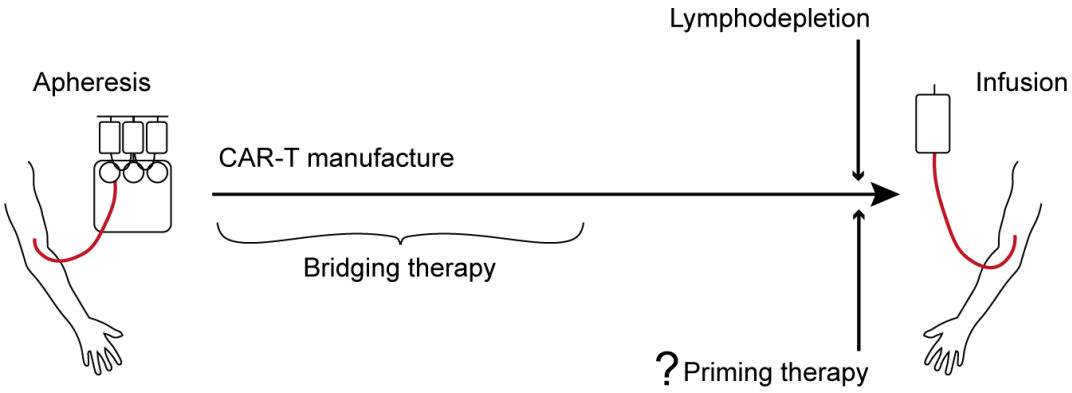

Figure 7.1.1: **Priming B-ALL for CAR-T immunotherapy with ADI-PEG20**
Schematic diagram of interval between apheresis and infusion of CAR-T cells. Lymphodepletion is standard of care prior to infusion while pre-infusion "priming" therapies are currently experimental.

that tumour cell susceptibility can be optimised by a number of strategies; including (a) enhancing sensitivity to death receptor mediated apoptosis by tumour cell upregulation of the TRAIL receptor DR5 [118, 119], (b) using epigenetic reprogramming to optimise immunogenicity via target antigen and co-stimulatory molecule modulation [212–214] or (c) inhibiting tumour cell anti-apoptosis machinery [53, 215]. In a comprehensive analysis, Singh *et al.* [53] employed a genome wide knockout screen combined with pre-infusion tumour transcriptome data to identify that low expression of pro-apoptotic genes of the DR-pathway was associated with clinical CAR-T resistance. Using functional inhibition of the B-ALL DR-pathway in cell line models they discovered that a *decrease* in functionality led to target cell primary resistance to CAR-T that itself led to a reduction in the long-term functionality of effector cells due to chronic exposure to apoptosis resistant target cells. A range of immune-cell derived ligands can instigate DR-pathway mediated apoptosis upon binding to death receptors and multiple reports, including the aforementioned study by Singh *et al.*, have implicated TRAIL as a key death ligand for CAR-T function [53, 118, 119]. Intriguingly, the action of ADI-PEG20 has itself been reported to promote cancer-cell sensitivity to the DR-pathway, through upregulation of TRAIL cell surface receptors DR4 and DR5 [120].

We therefore hypothesised that ADI-PEG20 might have dual benefits when combined with CAR-T. Firstly, as a short-term low-toxicity bridging therapy, based on the pre-clinical

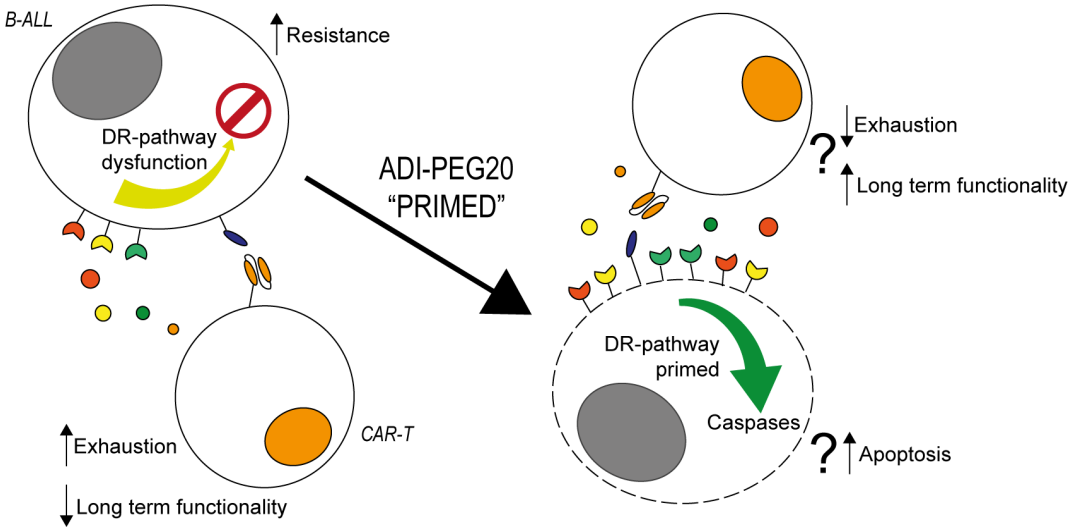

Figure 7.1.2: **Priming B-ALL for CAR-T immunotherapy with ADI-PEG20**
Following the concept developed by Singh *et al.* [53] who showed that dysfunction in the DR-pathway leads to B-ALL resistance and CAR-T exhaustion and reduced functionality long-term (left hand side), we hypothesised that ADI-PEG20 priming would promote DR-pathway functionality with the potential resultant effect of an increase in long-term CAR-T functionality (right hand side).

activity we have demonstrated (figure 5.4.3b). Next, as a priming therapy to *increase* DR-pathway functionality and thus, based on the conclusion of Singh *et al.*, potentially reduce tumour-cell resistance and improve CAR-T functionality through reduction in chronic antigen exposure (figure 7.1.2). We therefore attempted to characterise the interaction of ADI-PEG20 and the DR-pathway of *ASS1*-incompetent B-ALL and if changes to the state of this pathway, driven by ADI-PEG20 "priming" therapy, might have beneficial impacts on both tumour cell sensitivity to CAR-T and on the phenotype and function of CAR-T cells themselves.

We were specifically interested in the use of transient arginine starvation immediately prior to CAR-T to "reset" baseline DR-pathway function, as per the findings of Singh *et al.* [53], and not concomitant arginine starvation, which is accepted to be an immunosuppressive factor in some tumour microenvironments [122] and so would likely be counterproductive if effected during CAR-T.

7.2 ADI-PEG20 priming enhances functionality of TRAIL-DR pathway

ADI-PEG20 induces transcription of DR-pathway genes

In the study by Singh *et al.* [53], the authors defined a 17-gene signature in which enhanced expression predicts reduced resistance to CAR-T therapy in B-ALL. It has been reported elsewhere that ADI-PEG20 enhances expression of some components of this signature in *ASS1*-deficient tumours [120] and we have confirmed in our initial experiments that in *ASS1*-incompetent B-ALL ADI-PEG20 stimulates expression of DR4 and DR5 (figure 5.2.4). We therefore extended our analysis to compare expression of this complete signature after treatment with 72 hours of ADI-PEG20. As controls, we measured untreated, baseline gene expression within the DR-pathway signature as well as the same following treatment with vincristine, a standard-of-care agent in B-ALL management, dose titrated to induce an equivalent degree of viability loss as ADI-PEG20. Using qPCR we found a remarkable ADI-PEG20 tropism for DR-pathway signature gene expression when compared to vincristine or untreated values, with all but 5 members of the signature significantly upregulated by ADI-PEG20 at least 1 of the cell lines when compared to baseline (figure 7.2.1; genes with no significant modulation by ADI-PEG20 *vs* baseline in either cell line were *BID*, *CASP10*, *FADD*, *TNFRSF25*, *TNFRSF9*).

Unexpectedly, we saw little change in gene expression within this signature after vincristine treatment, with only *CASP8* and *TRADD* being significantly modulated, and this in the TOM-1 cell line alone. Conventional cytotoxic chemotherapy agents are classically described as causing cell death via the intrinsic, also known as mitochondrial, apoptosis pathway [216], and so it may not be as much of a surprise that there seemed to be little interaction with the DR- (also known as the extrinsic) apoptosis pathway. Furthermore, since both of these cell lines were isolated at relapse it is almost certain that neither are vincristine-naïve and possibly harbour a degree of vincristine resistance.

In our qPCR data the most striking, concordant gene modulation was that of *TNFRSF10A* and *TNFRSF10B*, which respectively encode DR4 and DR5, the principle pro-apoptotic membrane receptors for TRAIL (figure 7.2.1, both of which were also observed to be

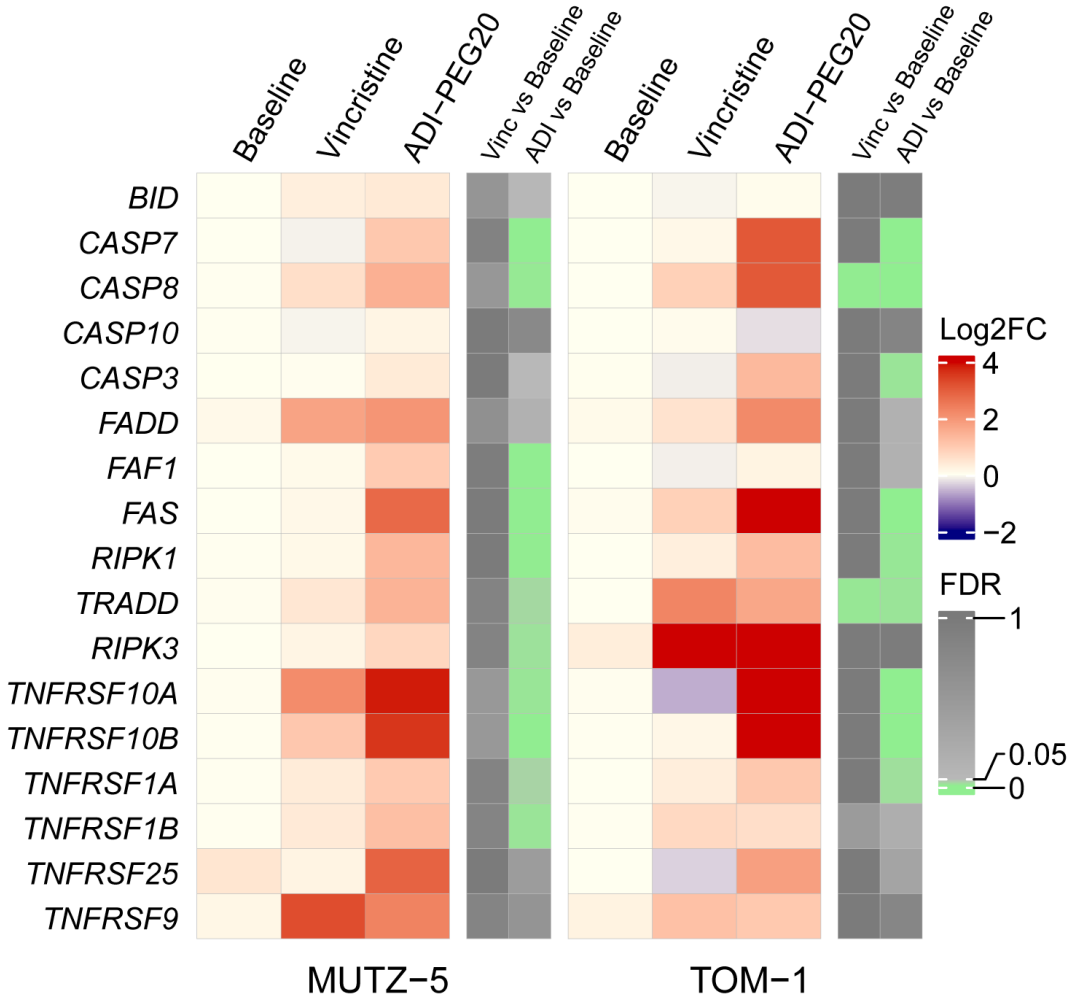

Figure 7.2.1: **ADI-PEG20 priming enhances functionality of TRAIL-DR pathway** qPCR analysis of gene expression within DR-signature defined by Singh *et al.* [53] after 72 hour treatment with vincristine or ADI-PEG20. Data displayed as relative fold expression from cross sample baseline with ΔΔCt method, using *GAPDH* for internal normalisation, generated from 3 independent experiments with each cDNA preparation ran in technical triplicates. Comparison of treatment effect to baseline with ANOVA and Tukey's test, with FDR p-values corrected for multiple comparisons with Benjamini-Hochberg method.

upregulated in our previous immunoblotting array analysis (figure 5.2.4)). Also included in the signature and modulated in at least 1 of the cell lines by ADI-PEG20, are genes encoding the other major death receptors *TNFRSF1A/B* and *Fas* whose ligands are TNFα and FasL, respectively. The biology of these receptor-ligand systems is complex [217, 218], but all can transduce apoptotic signals and have each been implicated in T-cell effected cancer-immunotherapy [219, 220]. The other modulated components of the signature consist of downstream proteins which are involved in the transduction or execution of death receptor triggered apoptotic signalling [221].

A range of concordant studies support the concept that increased expression of DR-pathway genes would be beneficial for CAR-T efficacy. As discussed, Singh *et al.* reported that increased expression amongst the entire signature is associated with reduced resistance to CAR-T [53]. Furthermore, in another comprehensive analysis, Dufva *et al.* showed that *TNFRSF10B* plays a crucial role in sensitivity to CAR-T driven apoptosis [215]. In this latter study, the authors also discovered baseline variations in cell line expression of DR-pathway proteins that correlated with variations in functional dependence of CAR-T sensitivity on these individual DR-proteins. Other studies have also implicated *TNFRSF10B* expression specifically as a crucial component of CAR-T sensitivity [118, 119], suggesting that DR5 may be a key molecule in the wider importance of the DR-pathway for CAR-T effect.

Given this evidence implicating the DR-pathway as a sensitivity factor to CAR-T, we predicted that the demonstrated effect of ADI-PEG20 on the DR-receptor gene expression signature should confer an increased sensitivity to CAR-T if used as a pre-treatment, which we have termed target cell "priming". Moreover, the ADI-PEG20 driven upregulation of gene expression across multiple DR-pathway components conceivably introduces a beneficial redundancy into the system, with the potential to reduce the reliance of sensitivity to CAR-T on individual components of the DR-pathway.

TRAIL-DR pathway functionality is primed by ADI-PEG20

To explore the functional consequences of this ADI-PEG20 induced gene expression pattern, we screened the sensitivity of ADI-PEG20 primed cells to the 3 major death receptor ligands:

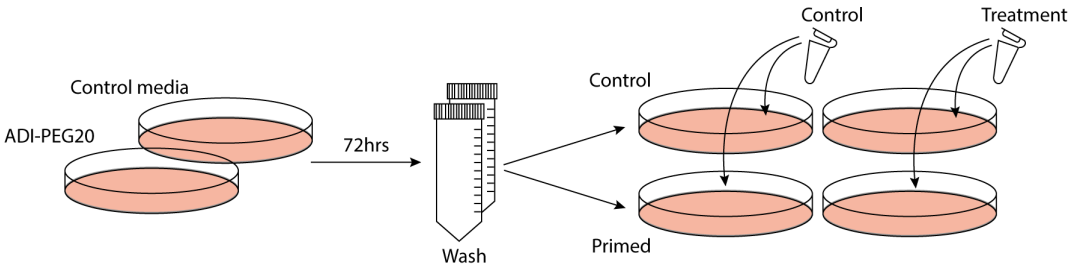

Figure 7.2.2: **ADI-PEG20 priming enhances functionality of TRAIL-DR pathway** Schematic representation of experimental design for ADI-PEG20 priming followed by treatment with death receptor ligands or control.

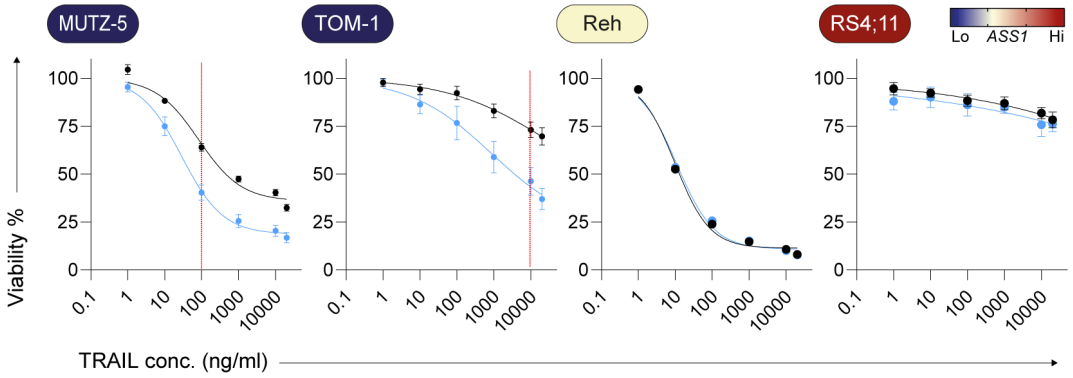

Figure 7.2.3: **ADI-PEG20 priming enhances functionality of TRAIL-DR pathway** Normalised dose response in control (black points/lines) or ADI-PEG20 pre-treated (blue points/lines) to 72 hours recombinant TRAIL exposure in B-ALL cell lines with viability estimated by ATP content. Viability at each dose level was normalised to the viability of corresponding control or pre-treated cultures without TRAIL exposure. Red dotted lines represent dose thresholds above which significant differences in viability exist between conditions, as measured by multiple t-tests with Holm-Šídák correction for multiple comparisons. Points and bars represent mean and SEM of 9 replicates acquired over 3 experiments.

TNFα, FasL and TRAIL. To do this, we exposed cell lines to 72 hours of ADI-PEG20, after which cells were washed, resuspended in complete media at equal live cell concentrations and allowed to equilibrate to standard culture conditions for 8 hours before the addition of recombinant death receptor ligands to the media (figure 7.2.2).

To screen a broad range of ligand concentrations across the entire panel we initially used the CellTiter-Glo luminescent assay of ATP to provide a surrogate measure for residual live cell count post sequential ADI-PEG20 priming then DR-ligand exposure. To control for latent inhibition by ADI-PEG20 pre-treatment, response profiles for each condition are normalised to the corresponding condition (either ADI-PEG20 or control) without subsequent exposure to each DR-ligand.

In the *ASS1*-incompetent cell line models we observed a clear divergence in the TRAIL dose response profiles between ADI-PEG20 primed and un-primed conditions, suggesting a reduction in the TRAIL IC_{50} and increase in inhibition at EC_{max} for the primed cells (figure 7.2.3, MUTZ-5 and TOM-1), strongly suggesting the ADI-PEG20 priming increases sensitivity to TRAIL. Supporting the modulation of TRAIL sensitivity by ADI-PEG20 as a function of *ASS1*-incompetence, we observed no effect in the *ASS1*-competent models (figure 7.2.3, Reh and RS4;11).

Since the TOM-1 and RS4;11 cell lines were relatively insensitive to TRAIL at baseline, we could not practically test TRAIL response over a broad enough concentration range to fully characterise the IC_{50} and depth of response at EC_{max} and so were unable to satisfactorily fit regression models to allow a statistical comparison of these parameters between the conditions. Therefore, to test for statistical differences in the TRAIL response we chose instead to compare each pair of individual dose responses with t-tests, correcting for multiple comparisons with the Holm-Šídák method. In this series of comparisons, we observed a significant decrease in viability for ADI-PEG20 primed MUTZ-5, with adjusted $p < 0.001$ at all TRAIL concentrations of 100ng/ml or higher, and likewise for TOM-1, where the relative reduction in viability was significant with adjusted $p \leq 0.03$ for concentrations at or above 10000ng/ml (red dashed lines indicate thresholds, figure 7.2.3). We observed no such statistical significance in either of the *ASS1*-competent cell line models.

As well as screening TRAIL we also tested FasL and TNFα using the same experimental design. Unexpectedly, given that the genes encoding the corresponding receptors *Fas* and *TNFRSF1A/B*, respectively, were upregulated at the mRNA level, we found no sensitisation effect of ADI-PEG20 priming apart from a small but statistically significant difference in the response to FasL in MUTZ-5 (figure 7.2.4).

To explore the more consistent interaction with ADI-PEG20 priming and TRAIL further, we next measured residual live cell counts after sequential ADI-PEG20 then TRAIL using FACS analysis of paired viability and Annexin-V staining. We used a 72 hour exposure to a fixed TRAIL concentration of 100ng/ml, which was the threshold for a significant difference in the previous MUTZ-5 analysis, and observed that sequential ADI-PEG20 priming then TRAIL led to significantly reduced residual live cell numbers when compared

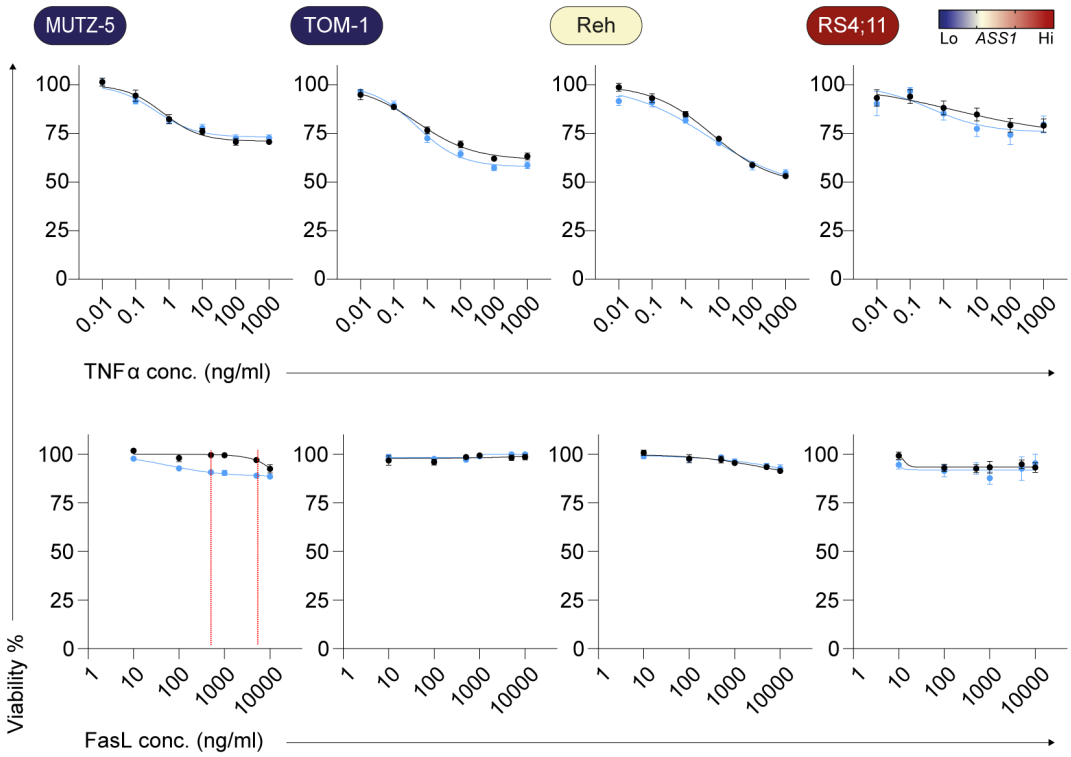

Figure 7.2.4: **ADI-PEG20 priming enhances functionality of TRAIL-DR pathway**
Dose response in control (black points/lines) or ADI-PEG20 pre-treated (blue points/lines) to 72 hours recombinant TNFα (top row) or FasL (bottom row) exposure in B-ALL cell lines with viability estimated by ATP content. Viability at each dose level was normalised to the viability of corresponding control or pre-treated cultures without death ligand exposure. Red dotted lines enclose dose range with significant difference in viability between conditions, as measured by multiple t-tests with Holm-Šídák correction for multiple comparisons. Points and bars represent mean and SEM of 9 replicates acquired over 3 experiments.

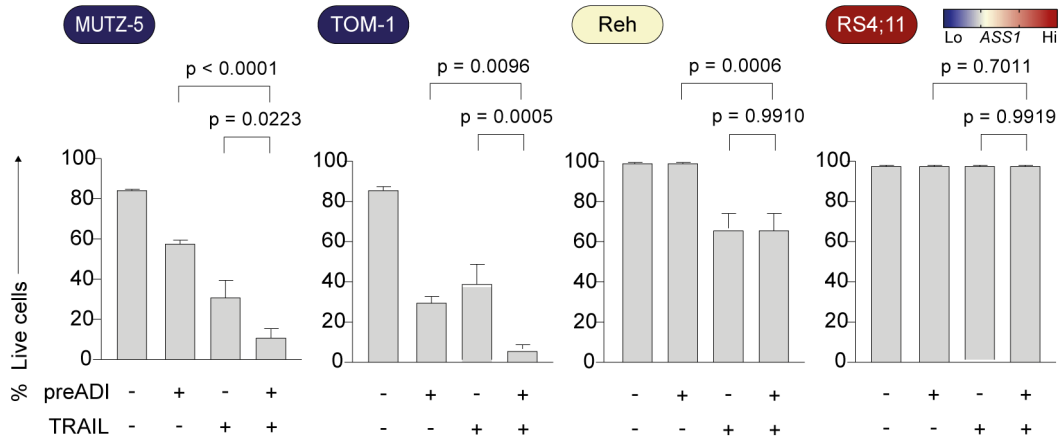

Figure 7.2.5: **ADI-PEG20 priming enhances functionality of TRAIL-DR pathway**
FACS analysis of residual live cells, identified as ZombieViolet^{neg}Annexin-V^{neg}, after ADI-PEG20 priming followed by 72 hours TRAIL or control, as a proportion of total acquired singlet cell events
Bars and errors represent mean and SEM from 9 replicates aggregated from 3 independent experiments. p-values from ANOVA with Šídák's multiple comparisons test.

to priming or TRAIL individually in the *ASS1*-incompetent cell lines MUTZ-5 (from ANOVA, $p < 0.0001$ sequence *vs* priming alone and $p = 0.0233$ sequence *vs* TRAIL alone) and TOM-1 ($p = 0.0096$ sequence *vs* priming alone and $p = 0.0005$ sequence *vs* TRAIL alone) (figure 7.2.5). In keeping with the previous analysis, we did not see the same effect in the *ASS1*-competent cell lines.

Taken together, these complimentary assays suggest that ADI-PEG20 pre-treatment enhances the pro-apoptotic functionality of the TRAIL-DR pathway. This refines the previously proposed concept of general DR-pathway priming to one that is more specific for increased functionality of the TRAIL "arm" of the DR-pathway.

TRAIL sensitisation is correlated with but not dependent on DR5 upregulation

To understand the mechanism leading to specific ADI-PEG20 priming of the TRAIL-DR pathway we next tested protein expression of the principal membrane receptors for each DR-pathway arm (figure 7.2.6a). In keeping with the sensitisation to TRAIL, we observed a clear upregulation of DR5 protein expression after 72 hours of ADI-PEG20 in *ASS1*-incompetent cell lines with no change in *ASS1*-competent controls. The expression of DR4 was most

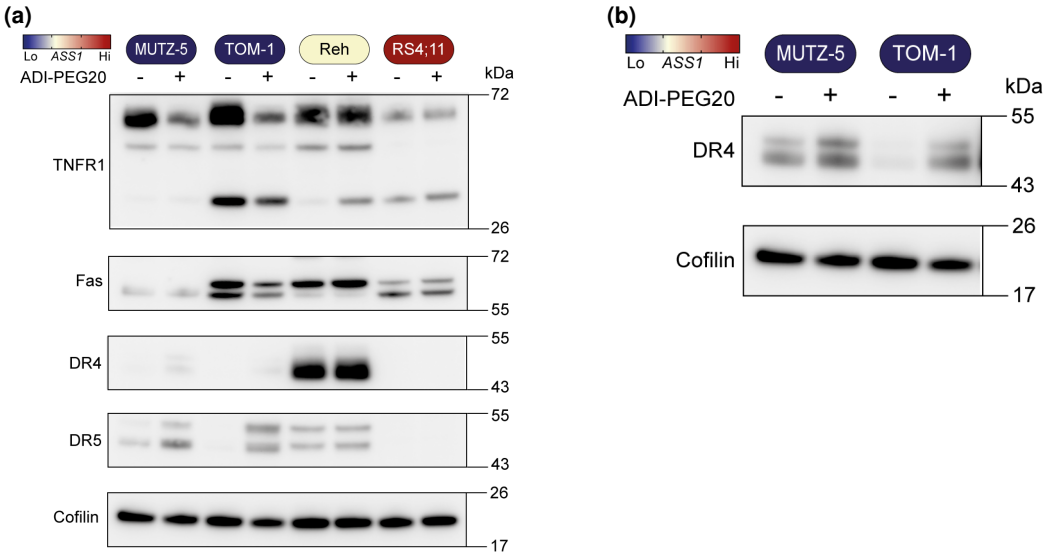

Figure 7.2.6: **ADI-PEG20 priming enhances functionality of TRAIL-DR pathway**
a) Western blotting analysis of death receptor expression after 72 hours ADI-PEG20, with cofilin as loading control.
b) Re-analysis of DR4 membrane from a) with high expressing Reh masked off and 10 times exposure time.

prominent in the Reh cell line, with protein levels apparently many orders of magnitude higher than in other cell lines, but with no discernible change upon ADI-PEG20 treatment. A faintly detectable upregulation of DR4 in the ASS1-incompetent cell lines (figure 7.2.6a) was confirmed by removing the Reh lysate lanes from the membrane and re-developing with a longer exposure time (figure 7.2.6b).

The functional connection between DR4/5 expression level and TRAIL cytotoxicity is also supported by the observed correlation between baseline receptor expression in all cell lines and the effect of TRAIL seen in previous experiments (figure 7.2.3). That is, for the RS4;11 cell line, where we had demonstrated very little effect of TRAIL we did not observe detectable expression of DR4 or -5. Contrasting this, the Reh cell line was most sensitive to TRAIL and had the highest baseline expression of both DR4 and -5. The ASS1-incompetent cell lines had an intermediate baseline sensitivity to TRAIL, with MUTZ-5 more sensitive than TOM-1, and again in keeping with this the baseline expression of both DR4 and -5 was higher in MUTZ-5, but not as high as that for Reh.

With regard to the other tested death ligand-receptor systems we did not see a clear

correlation between receptor expression and ligand effect. In the case of FasL treatment of MUTZ-5 we did see an increase in sensitivity after ADI-PEG20 treatment but this was not matched by a change in Fas expression, suggesting that other ADI-PEG20 modulated pathway components might be at play. For TOM-1 we observed an apparent decrease in Fas expression with ADI-PEG20 but no change in FasL sensitivity, and for Reh and RS4;11 ADI-PEG20 neither changed Fas expression nor FasL sensitivity.

For TNFα, we saw no change to sensitivity in any cell line after ADI-PEG20 treatment. This was despite seeing a downregulation of TNFR1 in both ASS1-incompetent cell lines after ADI-PEG20. Moreover, we observed an upregulation of the 30kDa splice isoform of TNFR1 in Reh. This lower weight isoform is usually described as a soluble form of TNFR1, which could act as a sink for TNFα in culture media, although we did not see any functional change to TNFα response (either apoptotic or proliferative) to correlate with this, so the significance is unclear.

Since DR4 was only expressed at low levels and there was a more prominent modulation of DR5 by ADI-PEG20 priming, we wanted to ask whether the change in expression of DR5 was the major factor in the change in sensitivity to TRAIL exposure. To test this we generated a GFP+ DR5 knockdown model by lentivirally transducing the TOM-1 cell line with shRNA that achieved a significant reduction in the degree of DR5 upregulation after ADI-PEG20 priming (figure 7.2.7a).

To test whether this abrogation of DR5 upregulation would modulate the interaction between ADI-PEG20 and TRAIL we then exposed either mock-transduced or shDR5 transduced TOM-1 cells to recombinant TRAIL with or without pre-treatment with ADI-PEG20 following the same experimental design as previous, with residual live cells enumerated by FACS analysis of paired viability and Annexin-V staining. By using live cell enumeration we avoided potential bias introduced by modulation of GFP fluorescence by cell death, since we cultured unselected/unsorted cell lines harbouring a mixture of GFP^{pos} and GFP^{neg} cells.

We confirmed with this model that ADI-PEG20 priming enhances the clearance of TOM-1 cells by TRAIL in the mock-transduced cells (figure 7.2.7b). However, we unexpectedly observed that, despite the demonstrated abrogation of DR5 upregulation by the DR5 shRNA, there was no difference between the effect of TRAIL after ADI-PEG20 priming between the

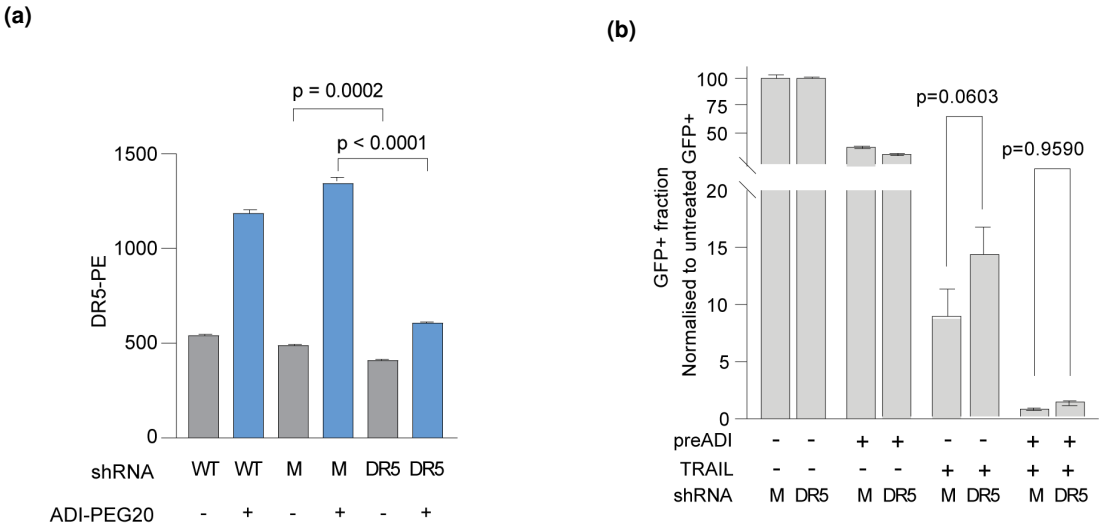

Figure 7.2.7: **ADI-PEG20 priming enhances functionality of TRAIL-DR pathway**
a) FACS analysis of DR5 expression in wild-type (WT), mock-transduced (M) and shDR5-transduced (DR5) TOM-1 cells. Data represent expression from 3 independent sub-cultures of each cell line.
b) FACS analysis of residual live mock- (M) and shDR5- (DR5) transduced cells after ADI-PEG20 priming with or without exposure to TRAIL. Live cells enumerated as $GFP^{pos}ZombieViolet^{neg}Annexin\text{-}V^{neg}$ and normalised to live GFP^{pos} from control condition (*i.e.* no pre-treatment, no TRAIL). Data represents mean and SEM from 3 independent experiments each performed in triplicate.
p-values in both from ANOVA with Šídák's multiple comparison's test.

shDR5 and mock transduced conditions. As well as preventing upregulation, the shDR5 did partially reduce baseline DR5 expression ($p = 0.0002$, figure 7.2.7a) and this corresponded to a suggestion of reduced TRAIL sensitivity, although this was a non-significant and small absolute terms trend, with normalised residual cell counts after TRAIL monotherapy in the mock-transduced cells being 8.88% (95% CI 3.36-14.40%) compared to 14.32% (95% CI 8.71-19.94%) for shDR5 transduced.

Had the shRNA-induced inhibition of DR5 upregulation prevented the sensitising interaction between ADI-PEG20 priming and TRAIL exposure, we would have expected a contrasting residual live cell proportional reduction between the mock- and shDR5-transduced cells. However, we saw in the case of the mock-transduced cells that live cell counts after sequential therapy were 8.59% (propagated 95% CI 5.08-20.46%) of that for TRAIL monotherapy and in the case of shDR5-transduced cells the same metric was 9.75% (propagated 95% CI 6.41-16.00%), with clearly overlapping confidence intervals.

The results of the shRNA analysis suggest that while the partial DR5 knockdown may have a modest effect on baseline sensitivity to TRAIL, abrogating DR5 upregulation does not prevent ADI-PEG20 induced sensitisation to subsequent TRAIL exposure. We chose to focus specifically on DR5 modulation as a potential rate-limiting step in this interaction since unlike DR4 it was markedly upregulated at the protein level. However, given the wide range of DR-pathway genes for which transcription is activated by ADI-PEG20 (figure 7.2.1), this result can be rationalised by the likely amplified signalling downstream from DR5, and in parallel from DR4, that appears to allow redundancy in the degree of DR5 expression change.

Taken together, these data demonstrate that ADI-PEG20 produces a marked upregulation of genes belonging to the DR-pathway, whose expression is known to clinically correlate with reduced resistance to CAR-T [53]. The functional effect on the DR-pathway of this induced gene expression is to sensitise cells to subsequent exposure to TRAIL, and this axis in particular has been reported as important in models of CAR-T therapy [118, 119]. We have also shown that this functional consequence is not solely dependent on the marked upregulation induced in DR5, indicating that the ADI-PEG20 primed DR-pathway may contain some redundancy with respect to dependency on individual proteins although further testing would be required to properly assess redundancy.

7.3 ADI-PEG20 priming of ASS1-incompetent B-ALL increases absolute blast clearance by CAR-T

We next wanted to ask whether this stimulated gene expression signature and associated increase in the function of the TRAIL-DR pathway would, as predicted following the work of Singh *et al.* [53], lead to a reduced resistance to CAR-T therapy. The authors of this study also reported that by *decreasing* tumour cell DR-pathway function by knocking out individual pathway components, they could generate tumour cell resistance leading to chronic exposure of CAR-T cells to apoptosis resistant targets that went on to cause longer-term impairment of CAR-T functionality. We therefore hypothesised that by *increasing* the function of the DR-pathway with ADI-PEG20 priming we may conversely increase the fitness

of CAR-T cells. To begin to test this, we set out to investigate the function and phenotype of CAR-T cells after stimulation by ADI-PEG20 primed *ASS1*-incompetent B-ALL blasts.

To test the interaction between ADI-PEG20 and CAR-T therapy we chose to model the latter using a generic, investigational CAR construct. The construct we chose was a 2nd generation anti-CD19 CAR, with binding domain derived from the FMC63 mouse anti-human CD19 antibody and a CD28 co-stimulatory domain. This was therefore similar in design to that utilised by brexu-cel, the commercial CAR-T product that is currently licensed for adult patients with relapsed B-ALL. Also included in the construct used was a c-Myc epitope tag expressed in the extracellular portion of the CAR to allow easy identification using FACS. Our primary question was how tumour cell biology modulation as a result of arginine starvation would affect treatment dynamics and so we chose to perform all experiments with this single CAR construct to reduce extra sources of variation. However, the known differences in activation dynamics associated with CD28 and 4-1BB co-stimulatory domains may suggest that results are not generalisable across all constructs and expanded future experiments will be necessary.

Priming therapy enhances absolute ALL blast clearance by CAR-T

Our first question was whether or not target cell ADI-PEG20 priming would change the overall killing capacity of CAR-T cells, perhaps by sensitising target cells to cytolysis through the TRAIL-DR pathway. To test this, we co-cultured both *ASS1*-incompetent cell line models with 2nd generation, CD28 co-stimulatory domain anti-CD19 CAR-T cells with a c-Myc epitope tag for cellular identification, with or without ADI-PEG20 priming of target cells. In an attempt to control for *latent* inhibition of *ASS1*-incompetent cell lines by ADI-PEG20 pre-treatment, we used a 2nd control by priming B-ALL with vincristine at a titrated dose to produce the same post-priming target cell viability, knowing that this alternate priming therapy would cause latent inhibition but relatively little interaction with the DR-pathway (figure 7.2.1).

Cell lines were exposed to a sequence of 72 hours ADI-PEG20, vincristine or standard culture conditions as an "un-primed" control, washed and resuspended at equivalent live cell counts and concentrations and then allowed to equilibrate to standard culture conditions

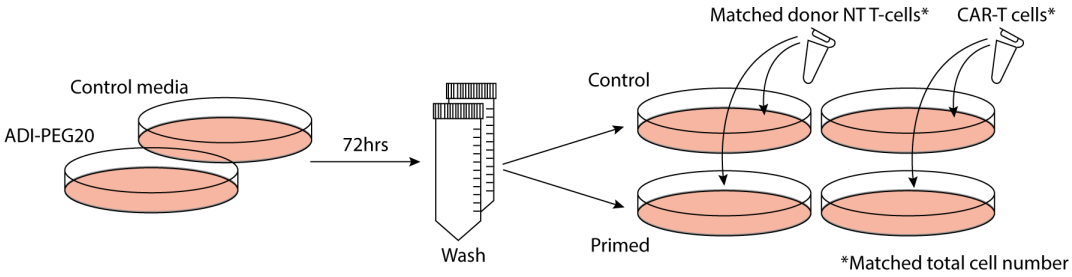

Figure 7.3.1: **Priming therapy enhances absolute ALL blast clearance by CAR-T** Schematic diagram of experimental design of pre-treatment followed by CAR-T or Non-transduced (NT) co-culture.

in complete media for 8 hours. Co-cultures were then initiated by the addition of CAR-T or control, NT T-cells (the latter to control for alloreactivity effects) at identical co-culture ratios (figure 7.3.1). After a further 72 hours of co-culture, residual live B-ALL cells were enumerated by FACS and normalised to that from the un-primed NT T-cell co-culture condition.

Using a panel of CAR-T cells generated from 4-7 different Peripheral blood mononuclear cell (PBMC) donors per experiment, we observed that in *ASS1*-incompetent B-ALL, sequential ADI-PEG20 or vincristine priming followed by CAR-T led to a reduction in residual live B-ALL cells, when compared to the "non-primed" CAR-T monotherapy control (figure 7.3.2). We used the paired t-test to compare the ratios of residual live B-ALL cells between primed CAR-T and un-primed CAR-T from matched PBMC donors and saw a significant reduction in residual live B-ALL after priming therapy with both ADI-PEG20 (MUTZ-5 $p = 0.0238$, TOM-1 $p = 0.0001$) and vincristine (MUTZ-5 $p = 0.0146$, TOM-1 $p = 0.0049$).

By further analysing these same ratios, we saw that for ADI-PEG20 priming, the proportional depth of blast clearance was deeper for TOM-1 (geometric mean 33.1%, 95% CI 23.6-46.5) than MUTZ-5 (64.8%, 95% CI 45.3-92.6), but these proportional differences were even greater for vincristine priming in both TOM-1 (14.5%, 95% CI 6.4-32.9) and MUTZ-5 (27.9%, 95%, CI 12.5-61.8). We had matched the post-priming target cell viability and absolute cell counts between ADI-PEG20 and vincristine treatments, but we observed that the degree of latent inhibition in NT co-cultures (assuming no effect from NT T-cell alloreactivity) by vincristine was much greater than that by ADI-PEG20. It was therefore possible that the enhanced blast clearance by either sequential therapy was actually a

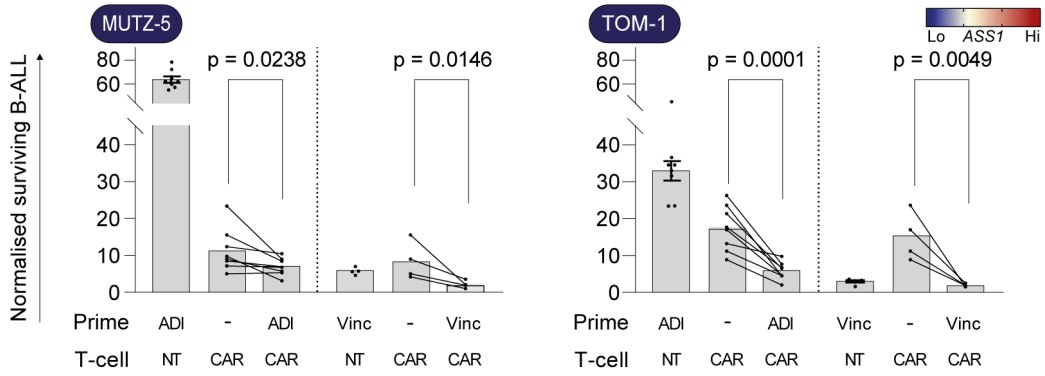

Figure 7.3.2: **Priming therapy enhances absolute ALL blast clearance by CAR-T** FACS analysis of residual live B-ALL cells after priming with ADI-PEG20 (ADI) or vincristine (Vinc) followed by co-culture with CAR-T or NT T-cells. Residual B-ALL cells identified as $CD3^{neg}$c-Myc^{neg} and single or double positive for either CD19 and CD20 and normalised to live B-ALL cell count from un-primed NT T-cell co-cultures. Joined points represent the paired average residual B-ALL counts from experiments using same donor PBMC for CAR-T manufacture, each done in triplicate repeats. p-values from t-test comparing ratios of paired values.

function of the degree of latent inhibition from the priming therapy, rather than any change in interaction between target and effector cell.

However, we also noticed that the increase in blast clearance by CAR-T after vincristine priming was relatively small compared to the potent latent inhibition by vincristine in NT co-cultures when compared to the same after ADI-PEG20 priming. To quantify this, we re-normalised the residual cell counts from each primed CAR-T condition to that from the correspondingly primed NT co-cultures, to try to isolate a "CAR-T specific" effect, separated from the latent effects of either priming drug. By normalising the residual cell counts this way we found that the proportional cell survival actually stayed approximately the same between un-primed and ADI-PEG20 priming, but after vincristine priming the proportional survival appeared greater than un-primed CAR-T alone (figure 7.3.3). This suggests that while the absolute blast clearance was greatest with vincristine priming, the proportional kill by CAR-T cells was lowest, despite the matched Effector:Target (E:T) ratio at the beginning of the co-culture.

One possible contributing factor to this apparent loss of proportional killing by CAR-T after vincristine priming is modulation of CD19 expression, and we observed a significant

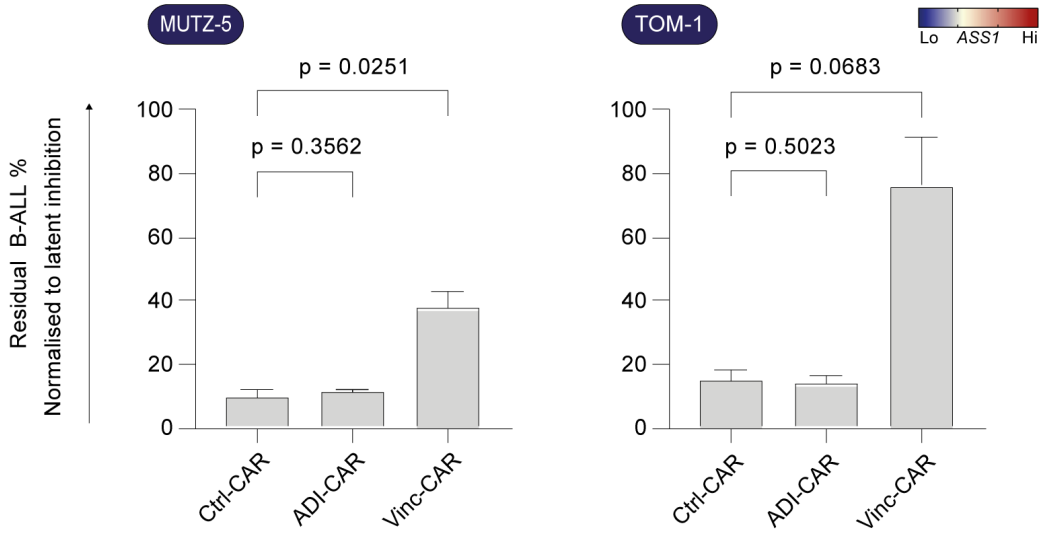

Figure 7.3.3: **Priming therapy enhances absolute ALL blast clearance by CAR-T** Residual live B-ALL counts after CAR-T co-culture from figure 7.3.2 with data re-normalised against surviving B-ALL cell counts from each corresponding priming condition followed by NT T-cell co-cultures, to give an estimate of ongoing survival of B-ALL against CAR-T amongst cells that survive the "latent inhibition" from the priming therapy alone. Ctrl - no priming, ADI - ADI-PEG20 priming, Vinc - vincristine priming. p-values from ANOVA with Dunnett's multiple comparisons test.

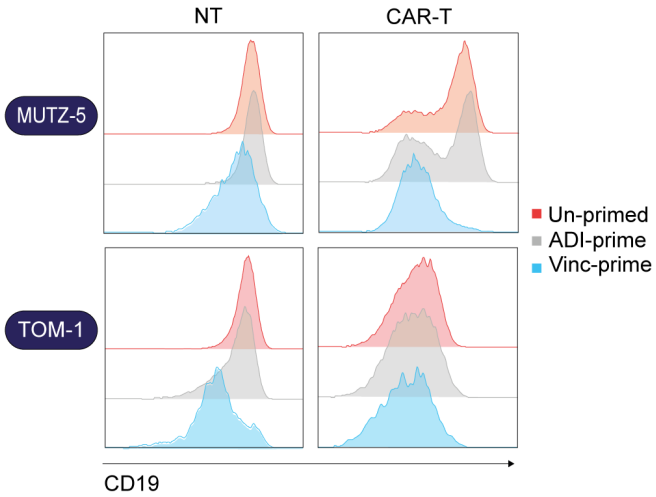

Figure 7.3.4: **Priming therapy enhances absolute ALL blast clearance by CAR-T** Representative CD19 intensity histograms from FACS analysis in figure 7.3.2.

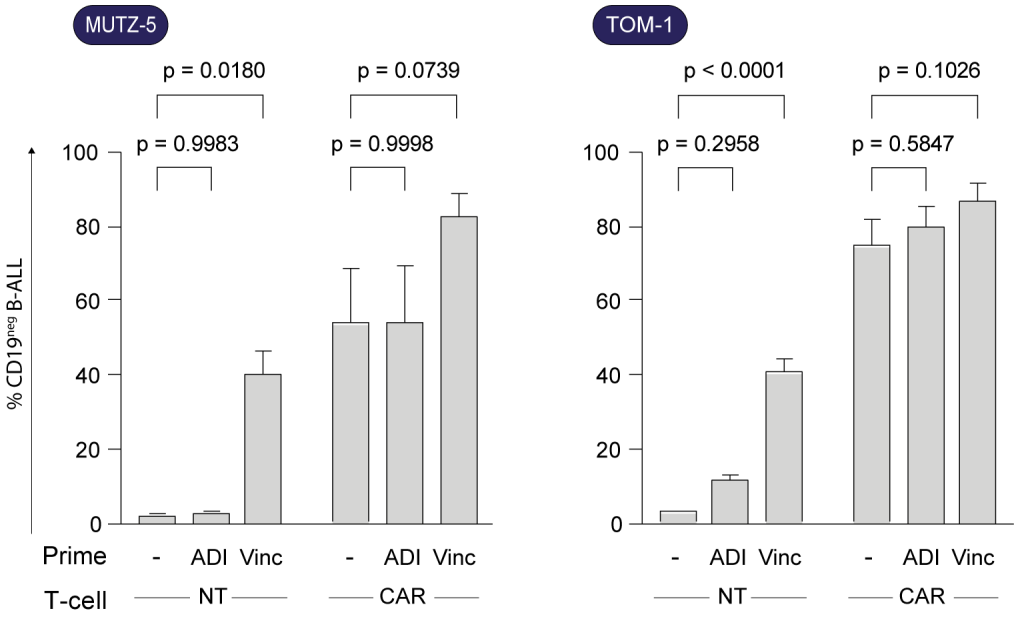

Figure 7.3.5: **Priming therapy enhances absolute ALL blast clearance by CAR-T** Residual live B-ALL with negative expression of CD19 as a proportion of total residual B-ALL cell count after priming and co-culture as in figure 7.3.2. p-values from 2-way ANOVA with priming and NT/CAR-T as separate factors with Dunnett's multiple comparisons test, data aggregated from 3 independent donors, each performed in triplicate.

increase in the proportion of $CD19^{neg}$ B-ALL cells, identified as both $CD3^{neg}$c-Myc^{neg} and $CD20^{pos}CD19^{neg}$, after vincristine priming even without CD19 directed therapy, *i.e.* in NT co-cultures (figure 7.3.4). Furthermore, the proportion of $CD19^{neg}$ B-ALL after vincristine-primed CAR-T tended to increase, while in the ADI-PEG20-primed CAR-T co-cultures the appearance of $CD19^{neg}$ cells occurred at a similar rate as in un-primed CAR-T (figure 7.3.5). This was especially clear in the MUTZ-5 experiments, where the un-primed and ADI-PEG20-primed CAR-T conditions generated a clear bimodal population of $CD19^{pos}$ and $CD19^{neg}$ cells while vincristine priming led to a single $CD19^{neg}$ peak. In the TOM-1 experiments we observed a somewhat intermediate effect, with a clear reduction in CD19 expression after vincristine priming in NT co-cultures compared to un-primed ($p < 0.0001$ from 2-way ANOVA) but with a trend toward the appearance of a $CD19^{neg}$ population after ADI-PEG20 in NT co-cultures and a less marked difference amongst the 3 different CAR-T conditions. The spread of data in CAR-T conditions was highly donor dependent, with some CAR-T cells displaying much more potent CD19 modulatory pressure than others.

The trend toward greater disappearance of $CD19^{pos}$ cells from the vincristine primed CAR-T co-cultures may represent more potent anti-CD19 CAR-T effect, perhaps due to a conventional chemotherapy driven sensitisation of B-ALL to CAR-T as has been reported by others [222], or more simply due to an effectively increased effector:$CD19^{pos}$-target ratio, since more target cells converted to $CD19^{neg}$ from the effect of vincristine alone. However, an increased potency against the $CD19^{pos}$ fraction appears to come at the cost of a more complete emergence of $CD19^{neg}$ cells in this co-culture model.

Combined, these data suggest that, ADI-PEG20 priming of *ASS1*-incompetent B-ALL leads to a greater numerical blast clearance by CAR-T without changing the proportional kill, suggesting that the reduction in residual cells is related to ongoing, latent inhibition by the priming therapy. By comparing ADI-PEG20 priming to vincristine, which induces even more potent latent inhibition but does not target the DR-pathway, we have shown that some forms of priming may come at the cost of greater conversion of target cells to $CD19^{neg}$ and this may reduce the proportional cell kill by subsequent CAR-T.

7.4 Target cell arginine starvation modulates secretory phenotype of CAR-T cells

Since the target cell priming with ADI-PEG20 led to greater overall blast clearance, we next asked whether the activation profile of CAR-T cells by primed target cells would be different to stimulation by un-primed blasts. We used the TOM-1 cell line model as a prototype for this given the more profound priming effect from previous experiments. Again using the work by Singh *et al.* [53] as a basis, we reasoned that since the E:T ratios between conditions were the same at the initiation of the co-culture experiments, the initial CAR-T activation characteristics would be similar, whereas differences in the "post-activation" phenotype may be more marked due to differences in ongoing interactions between activated CAR-T cells and primed target cells, for example, due to enhanced TRAIL susceptibility. We therefore chose to continue using the 72 hour timepoint from our co-culture model to measure CAR-T characteristics.

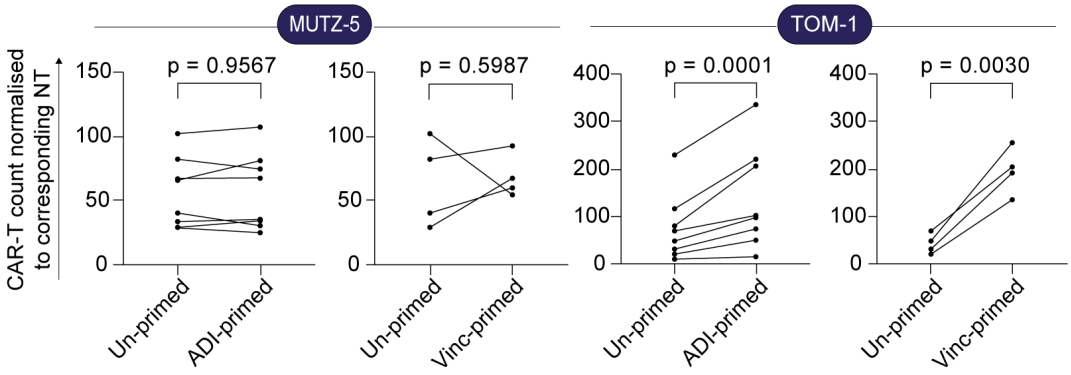

Figure 7.4.1: **Target cell arginine starvation modulates secretory phenotype of CAR-T cells**
FACS analysis of recovered CAR-T cells after co-culture with primed B-ALL. CAR-T cells were identified as $CD3^{dim}$c-Myc^{pos} and are represented as a proportion of total NT T-cells, identified as $CD3^{bright}$c-Myc^{neg}, from the equivalent priming condition to control for variations in the starting total T-cell count between replicates. Joined points represent CAR-T cell numbers from paired experiments using same donor PBMC for CAR-T manufacture. p-values from t-test of ratios between paired values.

TOM-1 priming enhances CAR-T proliferation and reduces post-activation IFN-γ secretion

Having established that ADI-PEG20 priming leads to an increase in the absolute reduction in target cell count by subsequent CAR-T, we next asked if the phenotype of effector cells was in some way modulated by stimulation with arginine starved B-ALL blasts. To begin we measured recovered numbers of CAR-T cells after 72 hours of co-culture with primed or un-primed B-ALL (figure 7.4.1). To do this we used FACS to enumerate CAR-T cells, identified as $CD3^{dim}$c-Myc^{pos}, as the percentage of total NT T-cells in the corresponding priming condition, identified as $CD3^{bright}$c-Myc^{neg}, to account for any CAR independent proliferation due to T-cell intrinsic or alloreactivity factors. In the TOM-1 model, where the increase in absolute blast clearance after both ADI-PEG20- and vincristine-priming was most marked we saw a significant increase in CAR-T counts (figure 7.3.2, from ratio paired t-test, ADI-PEG20-primed $p = 0.0001$, vincristine-primed $p = 0.003$), suggesting that priming generated a more immunogenic stimulus that led to greater CAR-T proliferation and/or longevity. However, this effect was not seen in the MUTZ-5 cell line models with either priming therapy, despite using the same panel of PBMC donors, suggesting that the effect of priming on CAR-T stimulation is cell line dependent.

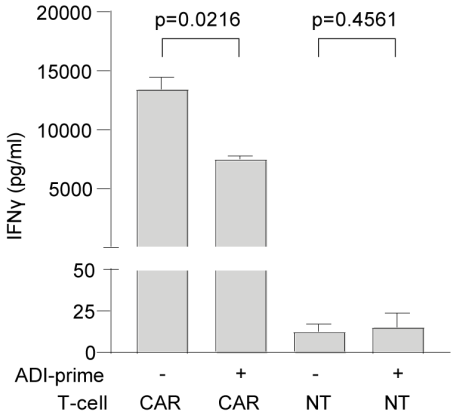

Figure 7.4.2: **Target cell arginine starvation modulates secretory phenotype of CAR-T cells**
IFN-γ concentration in supernatants from ADI-PEG20 (ADI) primed co-culture experiments. p-values from paired t-tests, analysing CAR-T and NT supernatants separately.

Since the 72 hour recovered CAR-T count was increased in the TOM-1 co-cultures after target cell priming with ADI-PEG20 we next asked whether this also translated to a change in effector functions that might account for the absolute increase in blast clearance seen in the previous section. As a basic assay of effector function we therefore measured IFN-γ levels in 72 hour co-culture supernatants with or without ADI-PEG20 priming of target cells, using a panel of 3 different PBMC donors (figure 7.4.2). To our surprise, we saw a significant reduction in co-culture supernatant IFN-γ levels where target cells were ADI-PEG20-primed ($p = 0.0216$ from paired t-test), despite the established increase in blast clearance and increase in CAR-T counts at this time point. There was no difference between supernatant IFN-γ concentration in the NT conditions and these levels were around the lower limit of detection of the assay used (25pg/ml) suggesting that IFN-γ was effectively undetectable in NT T-cell co-cultures and verifying that T-cell activation was exclusively via CAR ligation and not through alloreactivity.

This result was surprising since IFN-γ secretion is a commonly used proxy for CAR-T activation and effector function and thus we had not expected it to be lower, since CAR-T cell numbers were greater and B-ALL killing remained effective (figure 7.3.3). Achieving at least an equivalent degree of target cell killing but with reduced IFN-γ secretion made us hypothesise that CAR-T cells were killing ADI-PEG20-primed blasts more efficiently,

potentially in-keeping with our data that ADI-PEG20-primed TOM-1 was more sensitive to TRAIL and in-line with reports from other researchers that enhancing the interaction of TRAIL and DR5 makes tumour cells more susceptible to CAR-T mediated cytolysis [53, 118, 119, 215].

CAR-T cell cytokine/chemokine signalling is modulated by target cell ADI-PEG20 priming

If CAR-T cells were able to kill ADI-PEG20-primed blasts in a more "cytokine-efficient" manner, we reasoned that this would be reflected in their post-activation transcriptional state and so next chose to compare the phenotype of CAR-T cells between target cell primed and un-primed conditions using bulk RNA-sequencing after 72 hours of co-culture. To achieve this we used FACS to isolate CAR-T cells, identified as $CD3^{dim}$c-Myc^{pos}, from harvested co-cultures with ADI-PEG20-primed or un-primed TOM-1 cells, using a panel of 3 PBMC donors and extracting RNA from duplicated experimental conditions. We had to perform an RNA amplification step as part of the library preparation for sequencing since the recovered RNA was of low quantity.

After data processing, we used principle component analysis to form a basic overview of the sequencing outputs, and observed that in all but 1-pair of samples, the ADI-PEG20-priming separated CAR-T gene expression across the first principal component (figure 7.4.3). In 2 of the samples, identified as T1 and T3 in the PCA plot, there appeared to be the possibility that the priming information had been transposed since their position on the primary PCA axis was inverted compared to the trend from the other samples. Unfortunately, since we only had duplicate samples we could not say whether this was likely or whether it had been caused by biological variability between PBMC donors and therefore analysed the data as depicted in the PCA plot.

Using a linear model with the R package *deseq2* [128] to compare differential gene expression between the priming conditions we found only 38 genes upregulated with an adjusted $p < 0.05$ and only 95 downregulated with the same criteria. This small subset of genes in part reflects the challenge of obtaining robust transcript reads when only low input volume and quality is possible. However, since we had also seen significant inter-donor

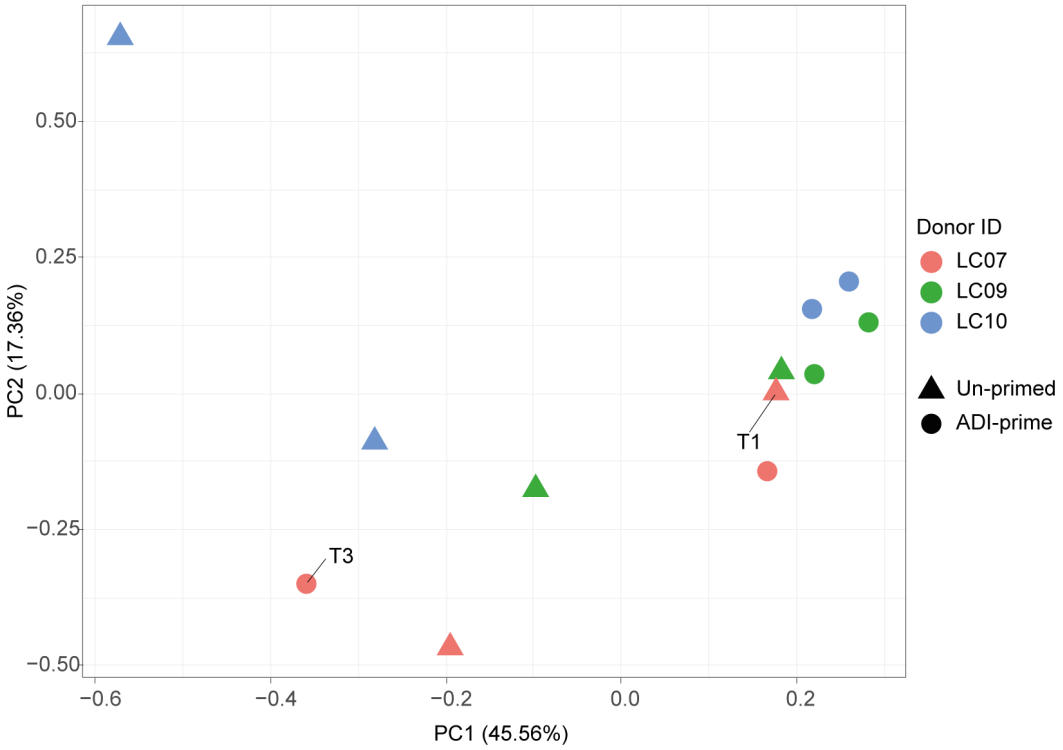

Figure 7.4.3: **Target cell arginine starvation modulates secretory phenotype of CAR-T cells**
PCA plot of bulk RNA-sequencing data from co-culture experiments with or without ADI-PEG20 (ADI) priming. Points T1 and T3 labelled with explanation in text.

variations not dependent on priming condition (including CAR transduction efficiency, post-activation cell counts and blast clearance effect) it was unlikely given the input material came from 3-biologically distinct PBMC donors that we would have seen large scale concordant gene expression changes, and as such this small pool of genes was somewhat reassuring for effective false discovery rate control.

To account for the limited number of replicates, we reduced the data set even further by limiting our analysis to only those DEGs with an absolute Log_2FC of at least 1, giving a set of 19 upregulated and 67 downregulated genes (figures 7.4.4 and 7.4.5). Despite the challenges described in the technical execution of the sequencing experiment, we observed a highly significant, and consistent modulation of genes involved in cytokine and chemokine signalling as well as modulation of the JAK-STAT pathway, which regulates cellular response to cytokine receptor signalling [223].

In agreement with our assay of IFN-γ secretion at the same time-point (figure 7.4.2),

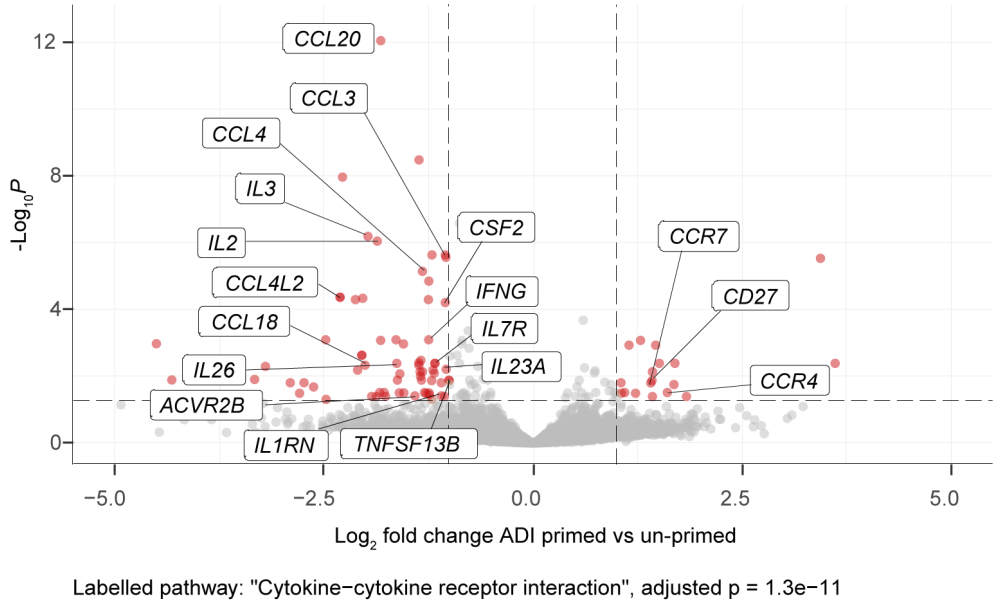

Figure 7.4.4: **Target cell arginine starvation modulates secretory phenotype of CAR-T cells**
Volcano plot of bulk RNA-sequencing from figure 7.4.3. Red points represent genes modulated with FDR adjusted p-value of <0.05 and absolute $\log_2$ fold change from control of >1, genes not meeting these criteria are grey.

we observed a significant downregulation of *IFNG* expression in CAR-T cells that were stimulated by ADI-PEG20-primed blasts. We also saw a reduction in the expression of genes encoding other classically implicated CAR-T effector cytokines including *IL2* and *CSF2* (which encodes GM-CSF) as well as other inflammatory chemokine/cytokine encoding genes including *CCL3*, *CCL4*, *CCL18*, *CCL20* and *IL3*.

The analysis so far of ADI-PEG20-priming before CAR-T cell treatment in *in vitro* co-culture models has therefore suggested that the major effect of the priming therapy is to reduce cytokine secretion, especially that of IFN-γ, by CAR-T cells when measured at a post-activation time-point and this would not classically be considered to be a favourable effect. However, since we assayed the co-culture supernatants and CAR-T gene expression at a time-point where most target cells had been dispatched, and we knew that CAR-T cells had performed at least an equivalent amount of killing in primed co-cultures as in controls, we reasoned that if target cells were killed more rapidly, *e.g.* through enhanced TRAIL

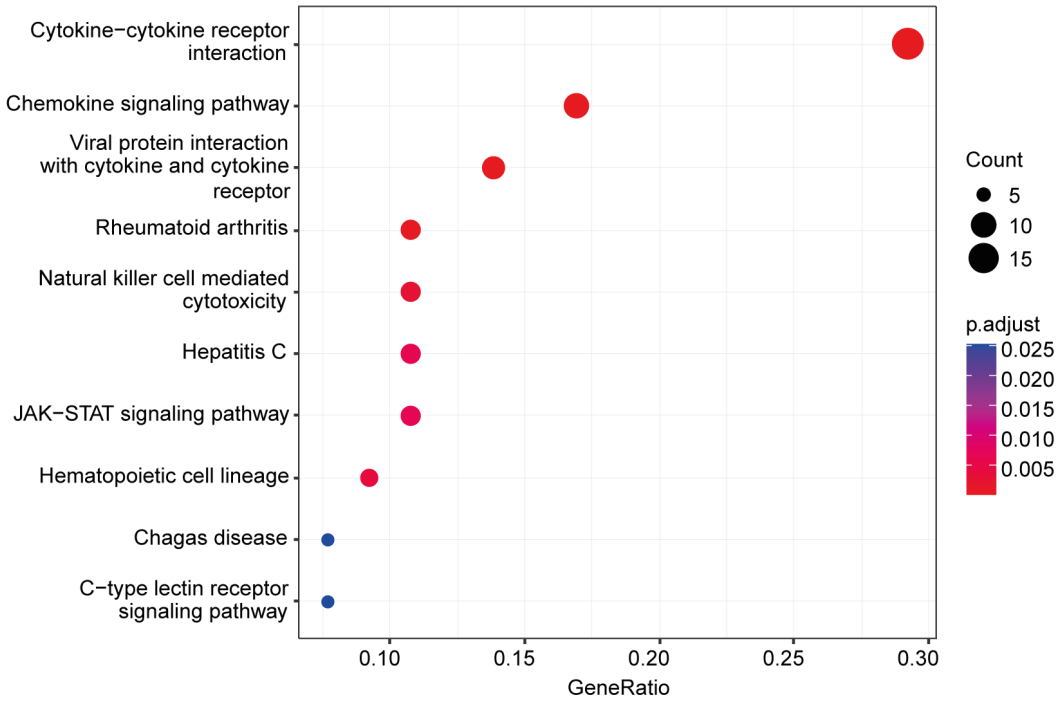

Figure 7.4.5: **Target cell arginine starvation modulates secretory phenotype of CAR-T cells**
Over-representation analysis of differentially expressed genes in figure 7.4.4 using KEGG database for reference.

sensitivity, then each effector cell would have fewer CAR-CD19 ligation interactions with target cells and hence would follow that production of effector cytokines such as IFN-γ might be "switched-off" sooner.

The reduction in CAR-T IFN-γ secretion and reduced expression of genes encoding other cytokines such as GM-CSF, without a reduction in the degree of target cell killing, might have beneficial implications for CAR-T therapy since the incidence and severity of the principal CAR-T specific toxicities of Cytokine Release Syndrome (CRS), Immune effector cell-associated neurotoxicity syndrome (ICANS) and Haemophagocytic lymphohistiocytosis (HLH) all correlate with serum levels of IFN-γ and other inflammatory cytokines that are secreted by CAR-T directly or from immune-bystander cells that are recruited by CAR-T secreted factors [224–226]. Importantly, it has also been shown that blockade of IFN-γ does not reduce the efficacy of CAR-T in haematological malignancy: In a recent study, Larson *et al.* found that IFN-γ receptor signalling was important for CAR-T therapy of solid tumours, but not for haematological tumour models including B-ALL, mantle cell lymphoma

and myeloma, with knockout of the IFN-γ receptor not changing responses either *in vitro* (all 3 aforementioned models) or *in vivo* (B-ALL model) [227]. Yet more intriguingly for the context of our results, Bailey *et al.* showed that genetic deletion of *IFNG* from CAR-T cells reduced immune checkpoint protein expression with no detrimental effect on antitumor efficacy against CD19-positive leukaemia, lymphoma and myeloma models both *in vitro* and *in vivo* [228]. Using models with immune-bystander cells intact, the authors also reported that blockade of IFN-γ could mitigate both CRS and ICANS. Concordant with these findings, a recent case report of the use of emapalumab, an anti-IFN-γ antibody, demonstrated that blocking IFN-γ could salvage a critically ill patient with HLH as a complication of CAR-T, without impairing available disease response metrics [229].

7.5 Single cell analysis of ADI-PEG20 primed CAR-T treatment

Since we had robustly shown reduction in CAR-T IFN-γ at the 72-hour time-point, and found a wider picture of cytokine modulation in the bulk RNA-sequencing data, we next wanted to understand with higher resolution the expression of these molecules in our ADI-PEG20-primed co-culture model and how this might vary amongst subsets of CAR-T cells. We therefore chose to further interrogate the CAR-T phenotype when stimulated by ADI-PEG20-primed TOM-1 using single cell protein expression measured with CyTOF. We curated a panel of protein expression markers based on differentially expressed cytokine and cytokine receptor encoding genes from our bulk RNA-sequencing results, markers to distinguish between CAR-T effector- and memory-subsets [230], markers of T-cell exhaustion and activity, activity of the TRAIL-DR pathway, cell-cycle and B-cell markers to allow for a parallel analysis of target cell effects (table 7.1).

We used the panel to analyse ADI-PEG20-primed and un-primed co-cultures of TOM-1 cells with NT or CAR-T cells from 4 different donors, which were performed in 2 batches. After staining, acquisition and processing, we were able to analyse 1.6×10^6 intact, live cells; of which 1.25×10^5 cells were CAR-T cells.

Group	Target
CAR-T ID	CD3
	c-Myc
B-cell ID	CD10
	CD19
CAR-T	CD4
phenotype	CD8a
	CD25
	CD27
	CD44
	CD45RO
	CD45RA
	CD62L/L-selectin
	CD69
	CD95/Fas
	CD127/IL-7Ra
	CD194/CCR4
	CD197/CCR7
	HLA-DR
CAR-T effector	Perforin
	GranzymeB
	IL-2
	IFNγ
	TNFα
	GM-CSF
CAR-T exhaustion	CD279/PD-1
	TIM-3
TRAIL-DR pathway	TRAIL
	DR5
	Caspase8-cleaved
	Caspase3-cleaved
Cell cycle	IdU
	CyclinB1

Table 7.1: CyTOF target antigens, listed by functional group.

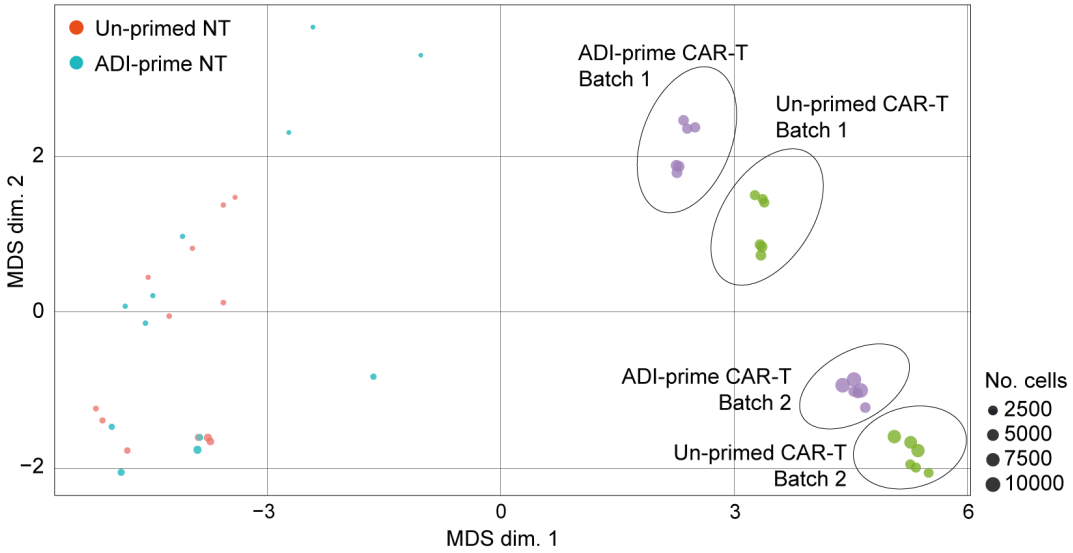

Figure 7.5.1: **Single cell analysis of ADI-PEG20 primed CAR-T treatment** Multidimensional Scaling (MDS) plot of protein expression across full CyTOF panel for CAR-T cells, gated as $CD3^{dim}$c-Myx^{pos}.

Overview comparison to RNA-seq data

We started the analysis of the CyTOF data by restricting the dataset to CAR-T cells only, using the same gating strategy as used for the FACS isolation of CAR-T cells prior to bulk RNA-sequencing. That is, we filtered the dataset to include only CAR-T cells that were identified as $CD3^{dim}$c-Myc^{pos} using FlowJo software and then exported the gated cells for analysis using the *CATALYST* [151, 152] and *diffcyt* [231] packages in R.

We first generated a MDS plot to represent the data in dimensionally reduced space and with this confirmed that very few cells from the non-CAR-T experimental conditions had made it in to the CAR-T gated dataset (figure 7.5.1, red and blue points). These cells must represent B-cells or NT T-cells with aberrant high signal in the c-Myc channel and given their low frequency and distribution away from CAR-T cells in MDS space, we felt that any similar cells included in the gates for the CAR-T containing conditions would not impact significantly on results. With the same MDS plot we observed a clustering of CAR-T cells according to the 2 batches in which the samples were stained and acquired, with the within-batch samples separated by priming condition rather than donor. This strongly suggested a batch effect but given we had also seen inter-donor biological heterogeneity we chose not to batch-correct the data but rather to include the batch and donor as factors

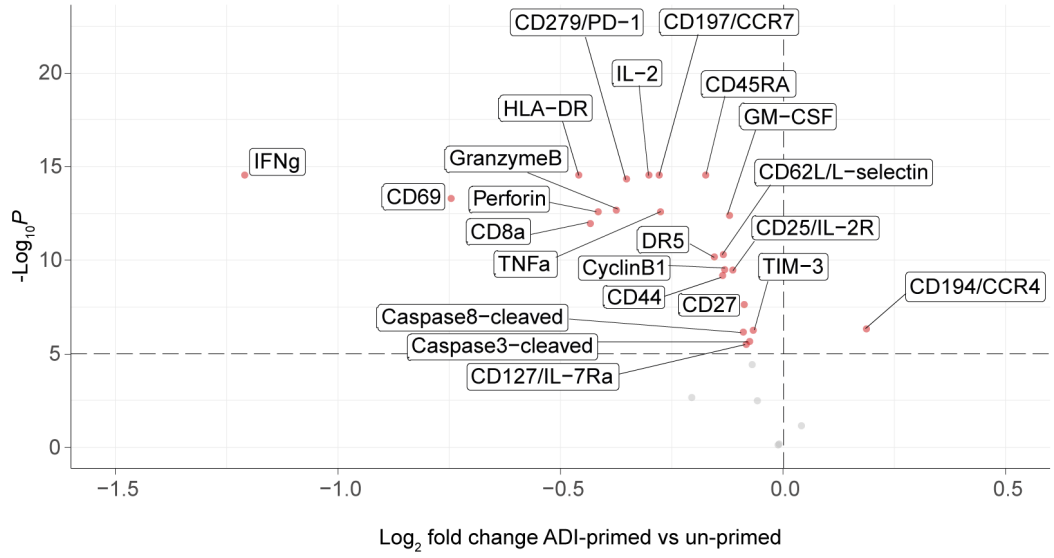

Figure 7.5.2: **Single cell analysis of ADI-PEG20 primed CAR-T treatment**
Volcano plot of protein expression modulation between ADI-PEG20 (ADI) primed CAR-T co-culture and un-primed. Red points represent proteins modulated with FDR adjusted p-value of <0.05, proteins not meeting these criteria are grey.

in the data analysis, such that comparisons were made between priming conditions per-donor-within-batch, to try to mitigate batch differences without artificially removing donor related sources of biological variation.

Using the batch as a fixed effect and the donor ID as a random effect in a linear model we next sought to compare the CyTOF results to the bulk RNA-sequencing, as an initial verification step prior to looking at the data in higher resolution. We found a general agreement in expression differences between ADI-PEG20-primed and un-primed conditions for the protein markers that we had included based on the RNA-sequencing result (figure 7.5.2). For example, IFN-γ was again observed to be significantly downregulated, along with Il-2 and GM-CSF, all in agreement with the RNA-sequencing output (figure 7.4.4). Also in agreement with the RNA-sequencing was the upregulation of CD194/CCR4 but we conversely saw a downregulation of CD27 and CD197/CCR7, that had both been upregulated at the mRNA level. In the wider set of protein markers we saw a consistent downregulation of other effector molecules (TNFα, GranzymeB, Perforin, TRAIL) and of markers of exhaustion (CD279/PD-1, TIM-3).

This overview analysis again supports the concept of a reduction in IFN-γ expression in CAR-T cells stimulated by ADI-PEG20-primed TOM-1, and extends to a downregulation of other effector molecules and exhaustion markers. The downregulation of CD279/PD-1, TIM-3 and DR5 (which acts as a TRAIL responsive, auto-regulatory receptor on CAR-T cells [232]) again is in keeping with the findings of Bailey *et al.* who showed that blockade of IFN-γ was associated with a reduction in CAR-T exhaustion [228].

Boolean gating analysis of CAR-T major characteristics

We next performed a more detailed analysis of protein expression using a conventional Boolean gating strategy to subdivide $CD3^{dim}$c-Myc^{pos} CAR-T cells into CD4 and CD8 subsets. To account for the inter-donor and batch effects we analysed average marker expression in these subsets using a 2-way ANOVA design with both priming and donor ID as factors (since the donor ID also effectively accounts for the batch effect). In agreement with previous analyses, the expression of IFN-γ was reduced in both CD4 and CD8 CAR-T subsets after stimulation by ADI-PEG20-primed TOM-1, ($p < 0.0001$ for both subsets, figure 7.5.3a, left panel) and the same true for CD279/PD-1 expression amongst both CD4 and CD8 CAR-T cells ($p < 0.0001$ for both subsets, figure 7.5.3a, right panel).

Using the same gating strategy we measured the CAR-T CD4:CD8 ratio, which was significantly increased when stimulated by ADI-PEG20-primed TOM-1, but was always below 1 ($p < 0.0001$ from 2-way ANOVA, figure 7.5.3b, left panel). This metric has gained much attention in pre-infusion CAR-T products, and a fixed ratio of 1 is the basis of the commercial CAR-T product lisocabtagene maraleucel, which is manufactured to be infused at a balanced CD4:CD8 ratio, with the rationale being that this leads to a more effective expansion of multiple cooperating CAR-T subsets [233]. We also observed an increase in the proportion of both CD4 and CD8 CAR-T cells in the G0 or G1 cell cycle phases, defined as $IdU^{neg}CyclinB1^{neg}$, after stimulation by ADI-PEG20-primed TOM-1 (from 2-way ANOVA $p = 0.0179$ (CD4) and $p = 0.0008$ (CD8), figure 7.5.3b middle and right panels).

While these data require benchmarking by further functional tests to define their exact significance, the reduction in PD-1 expression would generally be seen as a favourable characteristic of CAR-T. Furthermore, within the context of enhanced blast clearance in the

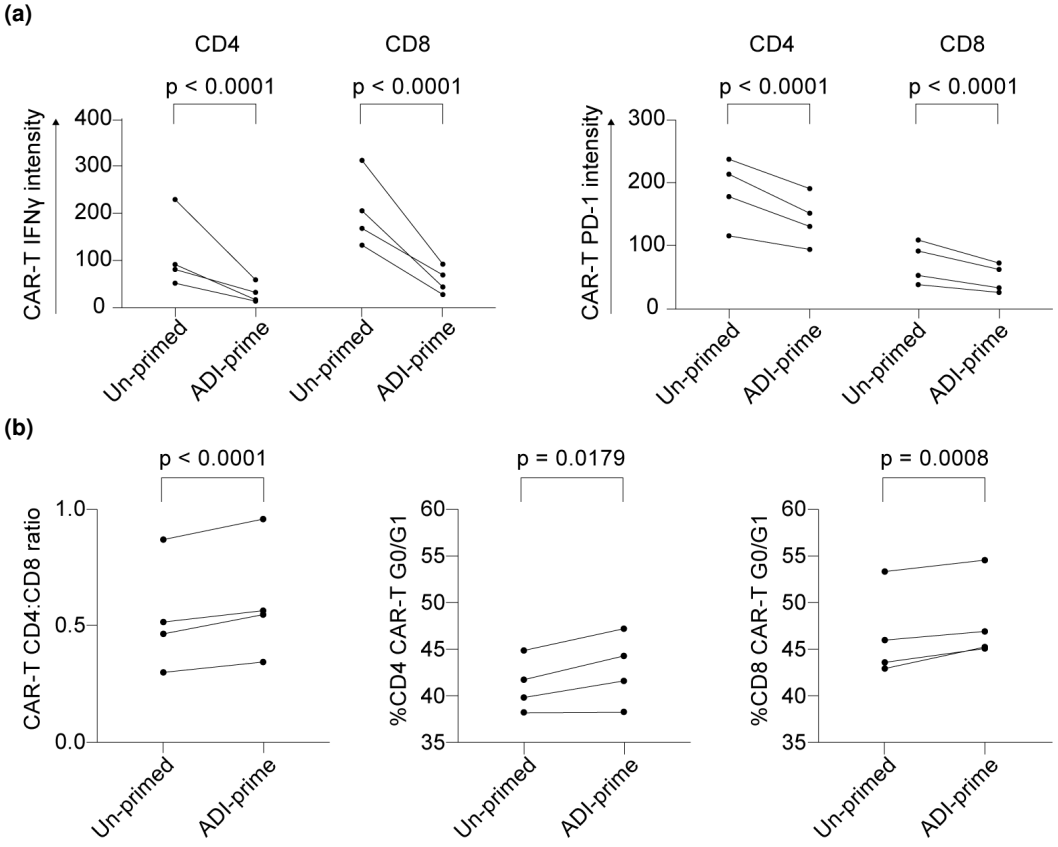

Figure 7.5.3: **Single cell analysis of ADI-PEG20 primed CAR-T treatment**
a) Comparison of IFN-γ and PD-1 expression amongst CD4 and CD8 CAR-T cells between ADI-PEG20 (ADI) primed and un-primed co-cultures.
b) Comparison of CD4:CD8 ratio (left), CD4 CAR-T cell cycle (middle) and CD8 cell cycle (right) between ADI-PEG20 (ADI) primed and un-primed co-cultures.
Data from experiments using 4 separate PBMC donors for CAR-T manufacture, each performed in triplicate. p-values from 2-way ANOVA with donor and priming condition as separate factors.

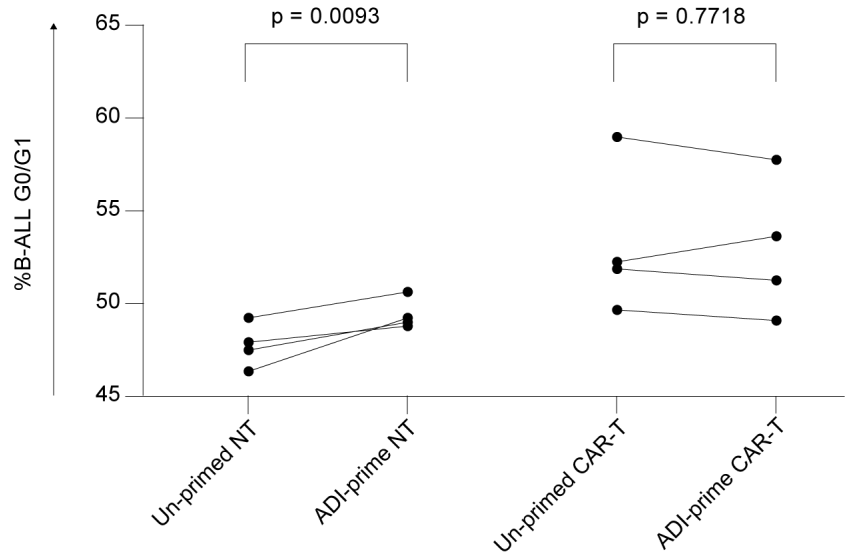

Figure 7.5.4: **Single cell analysis of ADI-PEG20 primed CAR-T treatment**
Comparison of residual B-ALL cell cycle between ADI-PEG20 (ADI) primed and un-primed co-cultures with both NT and CAR-T cells.
Data from experiments using 4 separate PBMC donors for CAR-T manufacture, each performed in triplicate. p-values from 2-way ANOVA with donor and priming condition as separate factors

ADI-PEG20 primed condition, the increase in CAR-T cells within the resting phases of the cell cycle, along with the reduction in IFN-γ (figure 7.3.2), support the previously introduced hypothesis that there is a faster resolution of CAR-T stimulation after ADI-PEG20-priming. The increase in CD4:CD8 ratio is in-line with the general concept that the CAR-T phenotype is modulated by target cell priming and is intriguing, given the known significance of this ratio in pre-infusion CAR-T products. However, the impact of this on CAR-T efficacy and potential for long term disease control is yet to be defined and further analysis of CAR-T subsets follows.

Boolean gating analysis of residual B-ALL

Again using conventional Boolean gating we next assessed the phenotype of residual TOM-1 cells, identified as $CD3^{neg}$c-$Myc^{neg}CD10^{pos}$. In keeping with the known effects of ADI-PEG20 on TOM-1, we observed an increase in the proportion of $IdU^{neg}CyclinB1^{neg}$, G0/G1 cell cycle phase in the NT co-cultures ($p = 0.0093$ from 2-way ANOVA, figure 7.5.4) in keeping with an ongoing, latent cell cycle effect from priming. We did not observe any

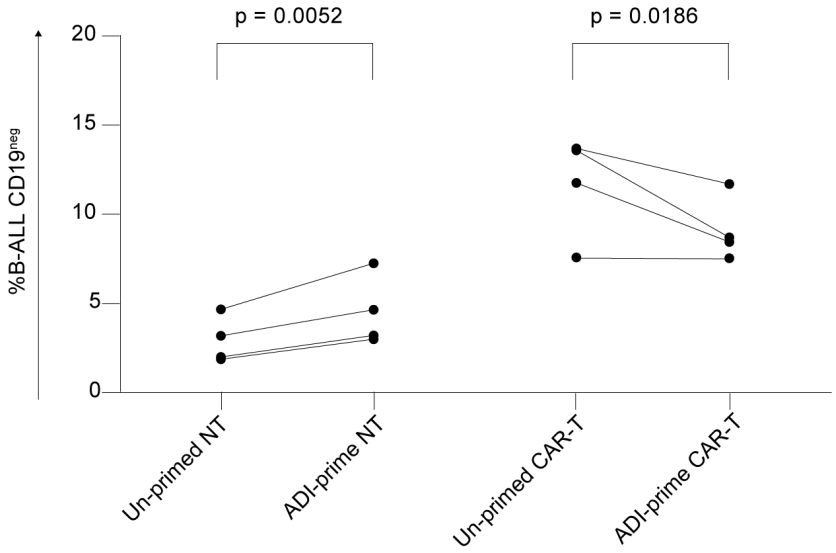

Figure 7.5.5: **Single cell analysis of ADI-PEG20 primed CAR-T treatment**
Comparison of proportion of CD19^{neg} B-ALL between ADI-PEG20 (ADI) primed and un-primed co-cultures with both NT and CAR-T cells.
Data from experiments using 4 separate PBMC donors for CAR-T manufacture, each performed in triplicate. p-values from 2-way ANOVA with donor and priming condition as separate factors

difference between residual B-ALL cell cycle in either CAR-T co-culture condition (figure 7.5.4) but there was a qualitative increase in G0 and G1 cell cycle when compared to NT co-cultures, raising the possibility that surviving target cells were being arrested in the cell cycle, possibly due to a reduction in cooperative paracrine signalling due to a reduced density of B-ALL (we have observed that TOM-1 grows very poorly in monoculture at low density).

We next measured the proportion of residual TOM-1 cells that were CD19^{neg} and observed an increase in this metric in ADI-PEG20-primed B-ALL after NT co-culture ($p = 0.0052$ from 2-way ANOVA) but a decrease in CAR-T co-culture in the primed condition ($p = 0.0186$ figure 7.5.5). These metrics are somewhat different to those seen in our previous FACS analysis of co-cultures, with the most striking difference being the much lower rate of CD19 negativity in CAR-T co-cultures compared to that measured by FACS (figure 7.3.5). We did observe in the initial FACS analysis that the rate of increase in CD19^{neg} B-ALL was highly donor dependent and it is possible that this represents a panel of donors with less effect by this metric. Another possible source of difference which may contribute to this is in methanol fixation step required for the CyTOF workflow which may

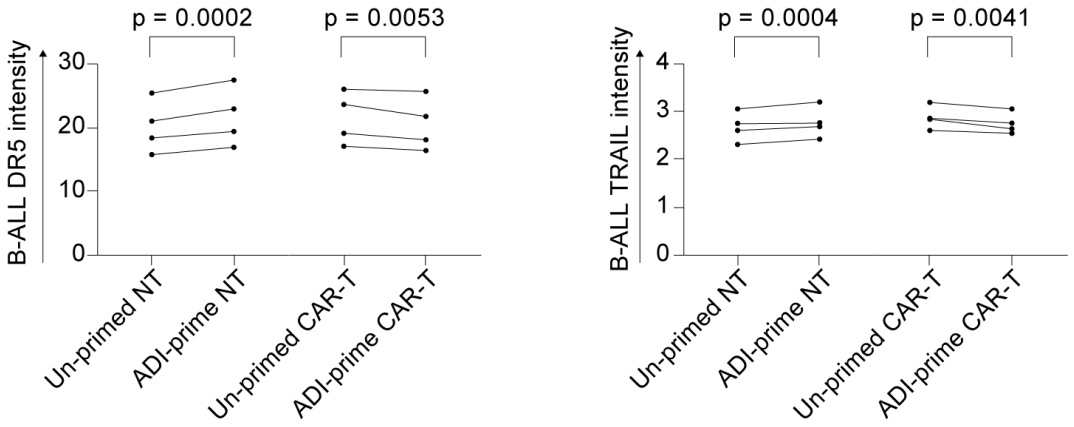

Figure 7.5.6: **Single cell analysis of ADI-PEG20 primed CAR-T treatment**
Comparison of residual B-ALL expression of DR5 (left) and staining for TRAIL (right) between ADI-PEG20 (ADI) primed and un-primed co-cultures with both NT and CAR-T cells.
Data from experiments using 4 separate PBMC donors for CAR-T manufacture, each performed in triplicate. p-values from 2-way ANOVA with donor and priming condition as separate factors

alter the intensity from labelled epitopes even after prior fixation.

Finally, we wanted to ask if we could detect differences in components of the TRAIL-DR pathway. To answer this we analysed the staining amongst residual TOM-1 for DR5, TRAIL and cleaved-caspase-8. In keeping with previous DR5 expression results we noted an increase after ADI-PEG20 priming of NT co-cultures ($p = 0.0002$ from 2-way ANOVA) but a decrease after CAR-T co-culture ($p = 0.0053$, figure 7.5.6, left panel) . A possible explanation for this might be enhanced sensitivity to TRAIL meaning that CAR-T cells preferentially killed target cells with higher DR5 expression. We also compared the B-ALL expression of TRAIL, reasoning that cells that had ligated and internalised TRAIL via the DR system would be tagged by the anti-TRAIL antibody. We found an increase in TRAIL expression after ADI-PEG20 priming of NT co-cultures and the opposite effect in CAR-T co-cultures (figure 7.5.6, right panel). However, it must be noted that the overall expression intensity was low and also very similar between NT and CAR-T co-cultures, suggesting that the anti-TRAIL staining of B-ALL cells was not effective for picking up TRAIL ligation and/or internalisation by TOM-1. Possible explanations for this include a low rate of CAR-T derived TRAIL ligation on TOM-1 cells or perhaps if ligation does occur it is not readily detectable due to receptor-ligand complex formation altering antibody binding. We did not detect any

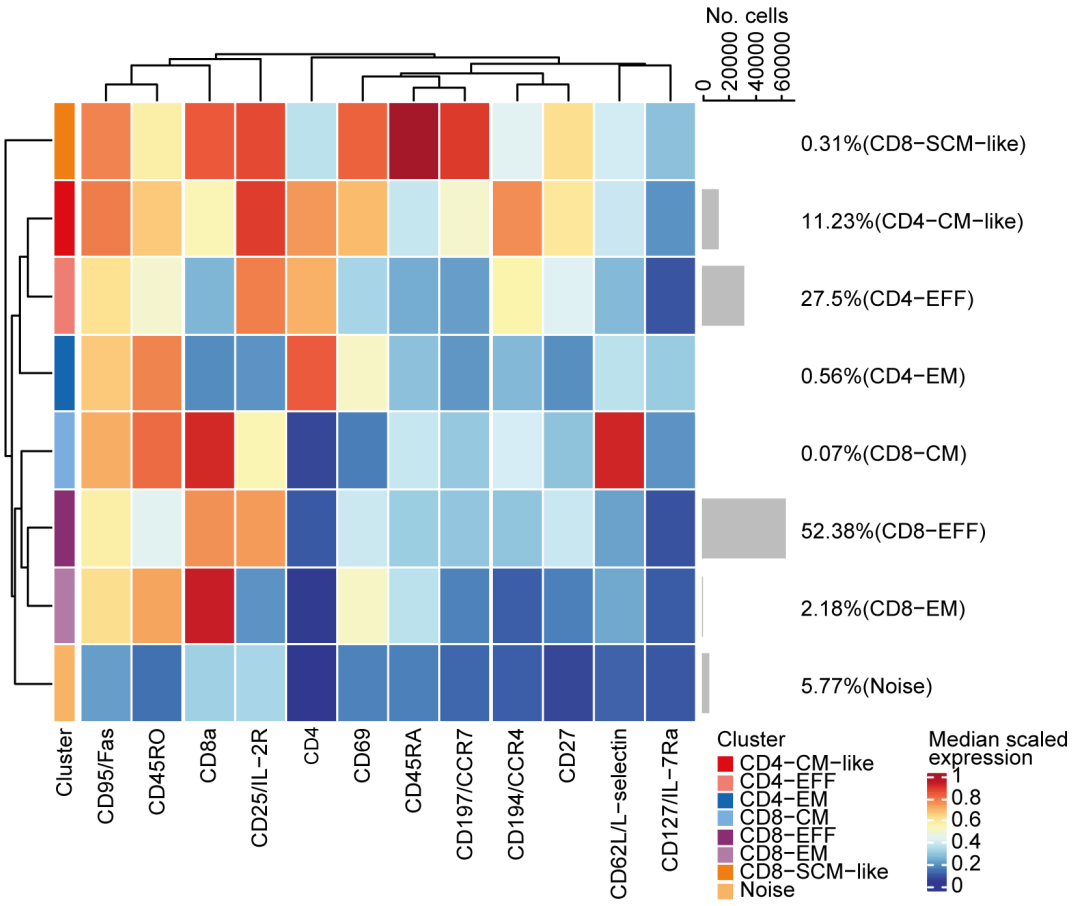

Figure 7.5.7: **Single cell analysis of ADI-PEG20 primed CAR-T treatment**
Heatmap of differential expression of T-cell phenotypic proteins between CAR-T subsets identified by Self-organising Maps clustering method. Each cluster was annotated manually based on expression of core phenotypic proteins CD45RO, CD45RA, CCR7, CD62L, CD95/Fas and CD27 and is labelled with proportion of total CAR-T cell count (n=1.25×10^5).

differences in cleavage of caspase-8 (data not shown).

Single cell analysis of CAR-T characteristics after stimulation by ADI-PEG20 primed B-ALL

Given the CAR-T cell changes driven by ADI-PEG20 priming within CD4 and CD8 subsets of CAR-T, we wanted to extend the analysis to a higher resolution using the full data complexity of the CAR-T gated, single cell data set. We used an unsupervised machine learning approach with Self Organising Maps (SOM) to project the CAR-T gated dataset into 2D space based on the expression of the markers within our panel that defined T-cell phenotype (CD4, CD8a, CD25/IL-2R, CD27, CD45RA, CD45RO, CD62L/L-selectin,

CD69, CD95/Fas, CD127/IL-7Ra, CD194/CCR4, CD197/CCR7), using the *FlowSOM* [234] package in R. The data was initially clustered around a 10x10 grid and then consensus clusters were obtained at lower resolution using the R package *ConsensusClusterPlus* [235]. We manually inspected the lower resolution clusters to arrive at a final set of 8 clusters that related to biologically defined subsets of CAR-T cells based on the expression patterns of CD45RO, CD45RA, CCR7, CD62L, CD95/Fas and CD27; as suggested in the work by Goldberg *et al.* [230] (figure 7.5.7). Within this clustering system, we identified cells corresponding to CD4+ and CD8+ effector (EFF) phenotypes, negative for all of CD45RA, CD45RO, CCR7 and CD62L, which made up the majority of the dataset as 27.5% and 52.38% of cells, respectively. The next most frequent cells, 11.23% of the dataset, bore a similarity to a CD4+ central memory (CM) phenotype with positivity for CD45RO and CCR7, but lacking the expression of CD62L that would typically define this group, and we therefore annotated these as "CD4-CM-like". Following this group, we identified CD8+ effector memory (EM) phenotype cells, positive for CD45RO and double negative for CCR7 and CD62L, constituting 2.18% of the dataset. Beyond this group, remaining subsets were rare and corresponded to CD4+ EM (0.56%) and CD8+ CM (0.07%). We also observed a similarly rare (0.31% of cells) but interesting phenotype of CD8+ CAR-T cells that matched a stem cell memory (SCM) like phenotype, positive for CD45RA, CCR7 and CD95/Fas, although lacking the typical expression of CD62L of this phenotype; hence labelled as CD8-SCM-like. The final cluster we defined had low expression of all the T-cell phenotypic markers and existed at a relatively low frequency of 5.77%, most likely corresponding to the previously described non-CAR-T cells with aberrant high c-Myc expression, which we therefore annotated as "Noise".

Displaying these cell populations in UMAP space (figure 7.5.8), we observed a general separation according to the different CD4+ or CD8+ subsets and only subtle differences in the spread of these groups according to the priming condition. To analyse this proportional spread further we again used a linear model to compare abundances between priming conditions (figure 7.5.9) and found that 3 groups were at significantly different abundances after ADI-PEG20-priming of target cells. We saw a significant increase in the abundance of CD4-EFF cells ($\log_2$FC 0.47, adjusted $p = 0.0013$) and a significant decrease in the

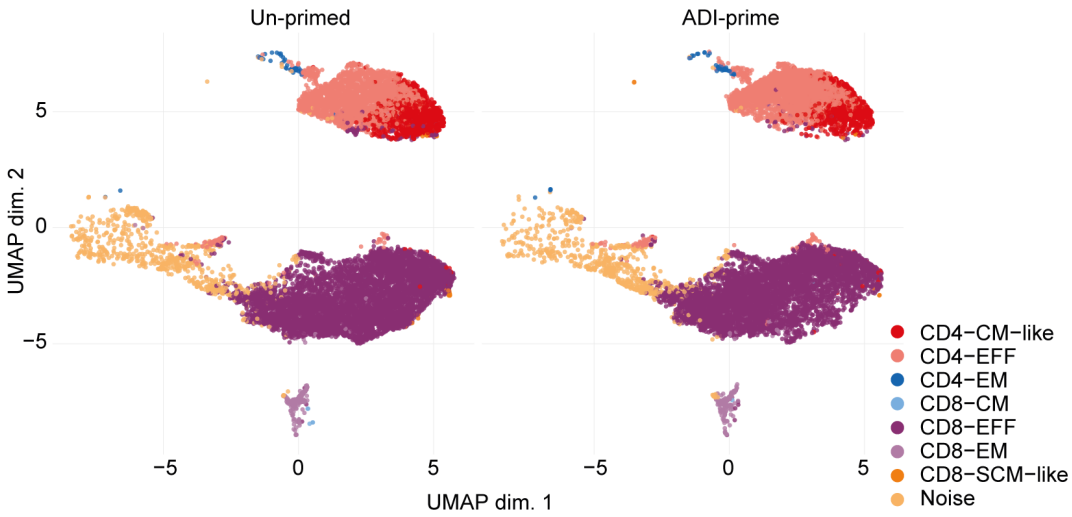

Figure 7.5.8: **Single cell analysis of ADI-PEG20 primed CAR-T treatment**
UMAP plot of CAR-T cell protein expression of T-cell phenotypic markers, comparing distribution between ADI-PEG20 (ADI) and un-primed co-cultures.

proportion of CD8-SCM-like cells ($\log_2$FC -2.48, adjusted $p = 6.63e-30$) and CD4-CM-like cells ($\log_2$FC -0.99, adjusted $p = 1.57e-15$). Given that the number of recovered CAR-T cells is greatest when target cells are primed with ADI-PEG20, the biggest impact here in terms of absolute cell numbers is from the upregulation of CD4-EFF cells and this is in keeping with the increase in the CD4:CD8 we observed via the Boolean gating analysis (figure 7.5.3b). The reduction in the abundance of CD8-SCM-like and CD4-CM phenotype cells may be countered by the increase in the overall cell count. However, these cell types are thought to possess favourable characteristics of persistence and self-renewal for long term disease control in adoptive T-cell therapies [236–238] and so the implication of their proportional reduction needs to be tested in models assaying long term function.

We next used linear model analysis to compare the expression of proteins within CD4+ and CD8+ CAR-T subsets (figures 7.5.10 and 7.5.11, respectively). These heatmaps are ordered such that adjacent column-sets of technical triplicates represent contrasting priming conditions between matched donors, to reflect the paired design of the analysis. The batch effect seen in the MDS plot (figure 7.5.1) is particularly noticeable in the CD8+ subgroup analysis, with a general increase in average protein intensity in donors 12 and 13 which were analysed together in batch 2 (figure 7.5.11). In keeping with the bulk analysis of both gene and protein expression we saw a downregulation of IFN-γ in CD4-EFF and CD8-EFF cells

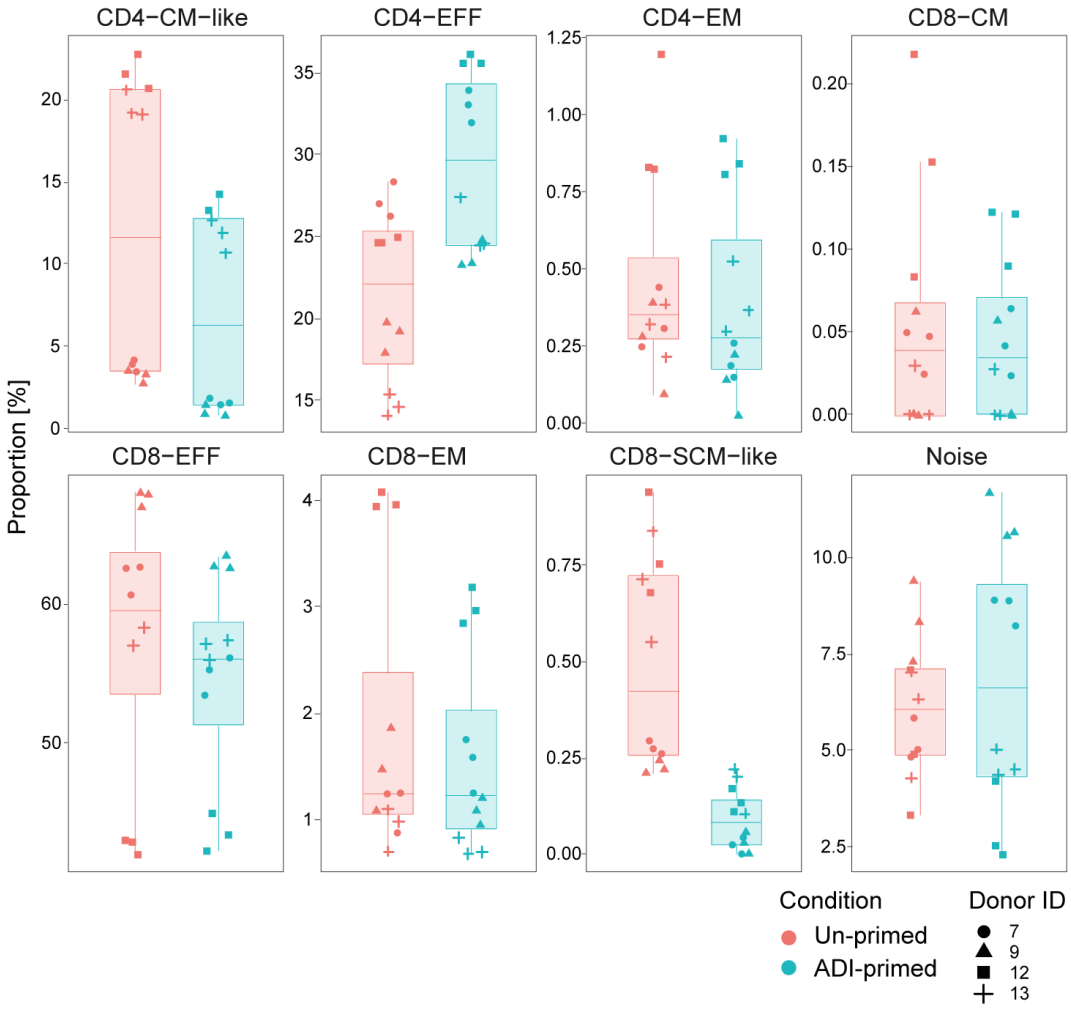

Figure 7.5.9: **Single cell analysis of ADI-PEG20 primed CAR-T treatment** Comparative abundances of cells per CAR-T sub-cluster as defined in figure 7.5.7 between priming conditions.

and since these are the 2 cell types with the highest abundance, this reflects the changes seen at the global level (figures 7.4.4 and 7.5.2). In these same cell subsets there was a general decrease in effector molecule and cytokine expression, including IL-2, GranzymeB and Perforin, and a decrease in exhaustion/checkpoint markers PD-1, TIM-3 and DR5. The differential protein expression in CD4-CM-like cells tracked that of CD4-EFF cells and reflects the overall similarity of the expression of phenotypic protein markers between these subsets, which were only separated by the final dendogram branch of the initial clustering definition (figure 7.5.7).

Of particular interest was the upregulation of TRAIL by CD8-EFF (adjusted $p = 0.0017$

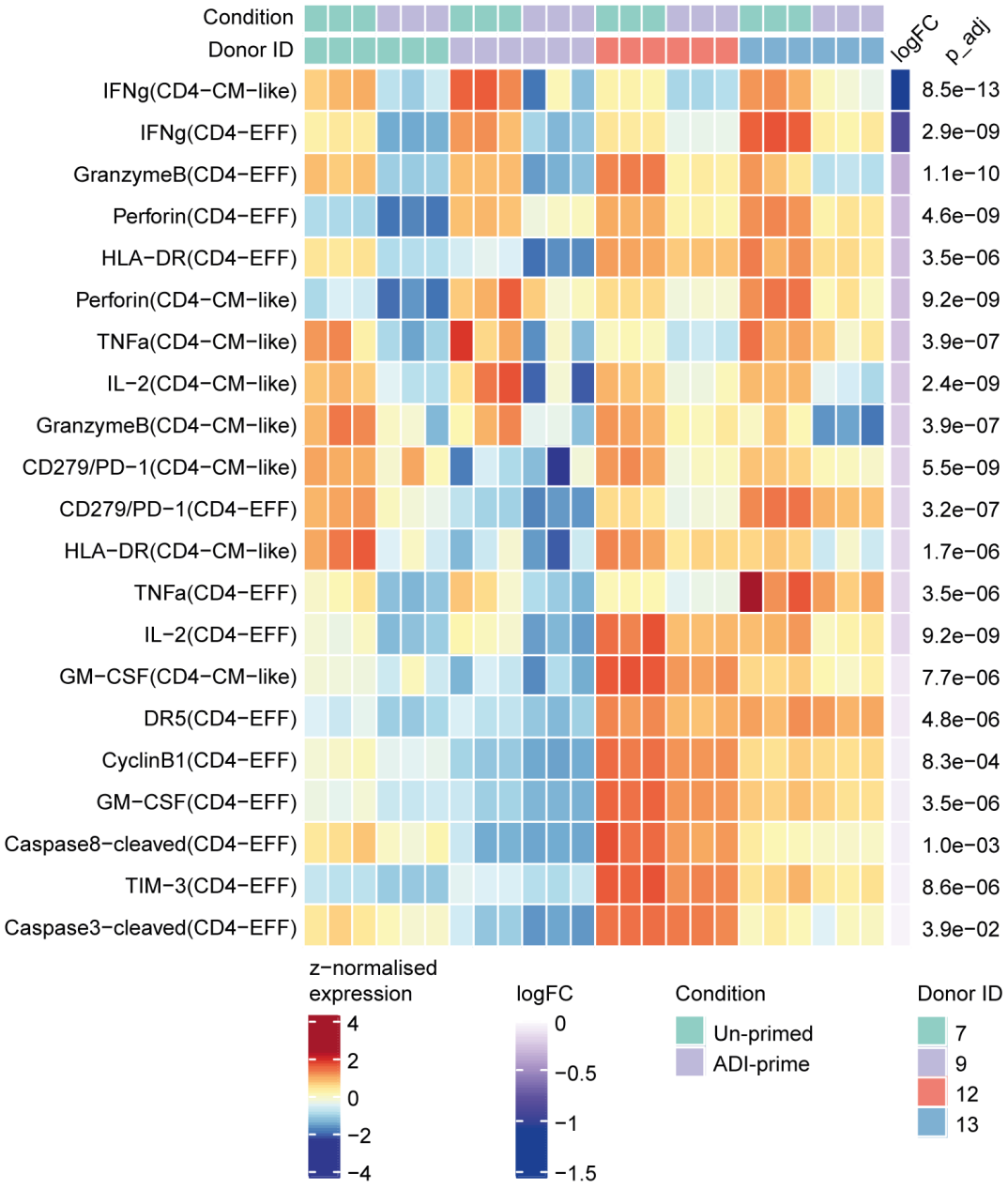

Figure 7.5.10: **Single cell analysis of ADI-PEG20 primed CAR-T treatment** Differentially expressed proteins between ADI-PEG20 (ADI) primed and un-primed co-culture CD4+ CAR-T cells according to CAR-T sub-cluster.

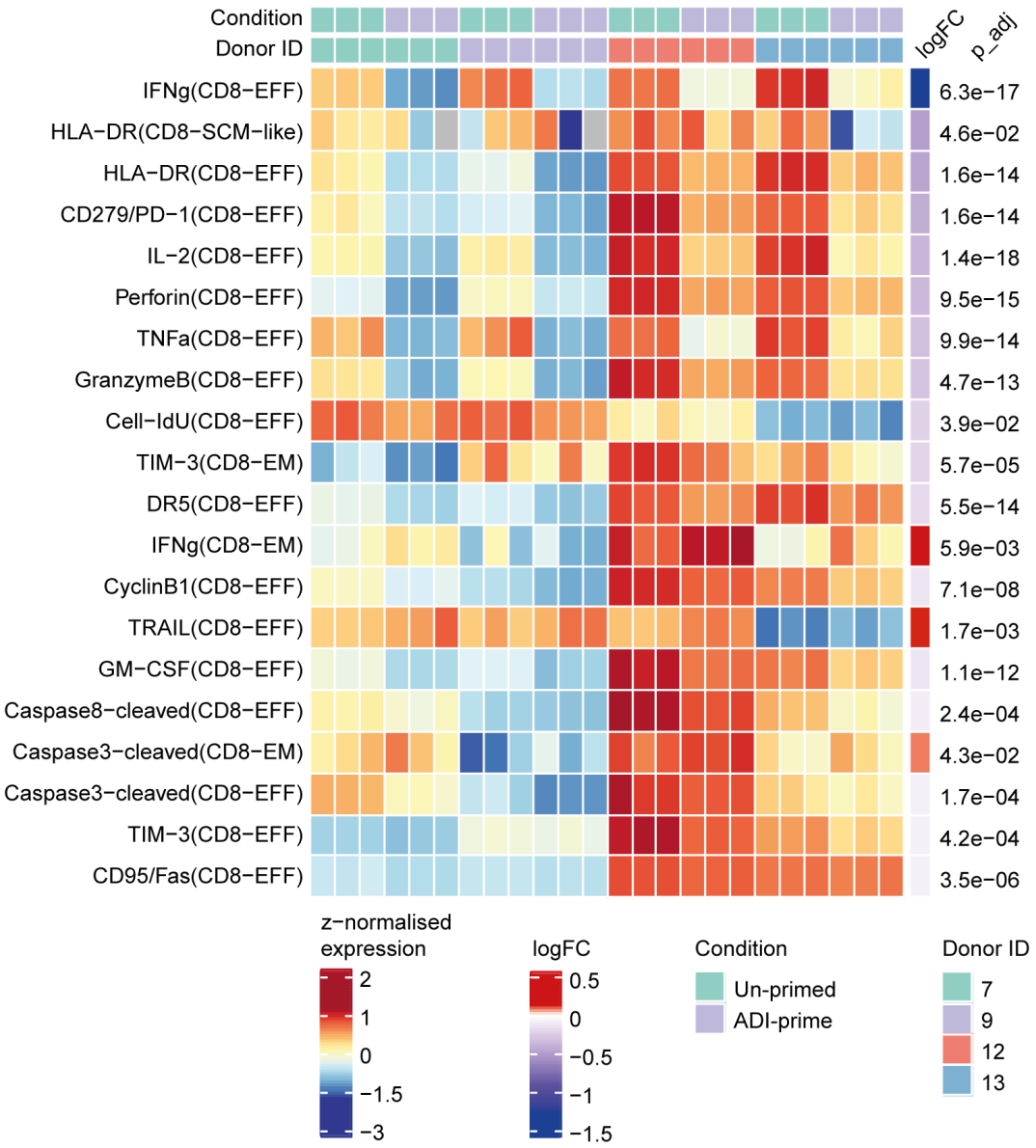

Figure 7.5.11: **Single cell analysis of ADI-PEG20 primed CAR-T treatment** Differentially expressed proteins between ADI-PEG20 (ADI) primed and un-primed co-culture CD8+ CAR-T cells according to CAR-T sub-cluster.

when stimulated by ADI-PEG20-primed blasts, which contrasts the downregulation of other effector molecules. Dissecting the significance of this is complex, since TRAIL also has an autoregulatory role and CAR-T expression of DR5, which transduces autoregulatory signals was downregulated. However, it is intriguing to speculate whether this upregulation may be linked to the TRAIL-DR5 primed state of target cells and further experiments designed to analyse this are needed to throw light on the subject.

Another intriguing cell subset was the CD8-EM group, which contributed 2.18% of CAR-T cells (figure 7.5.7) without a significant difference in abundance between the priming conditions (adjusted $p = 0.61$). Contrasting CD8-EFF cells, this subset expressed upregulated IFN-γ in CAR-T cells stimulated by ADI-PEG20-primed TOM-1 when compared to un-primed stimulation, but had reduced expression of TIM-3, with no change in CD279/PD-1. The classical functional description of CD8-EM cells is of an antigen-experienced cell that can rapidly produce IFN-γ on antigen re-encounter [239]. Given the context, it can be speculated that despite the overall downregulation in IFN-γ, this finding suggests that the CD8-EM subset of CAR-T cells after initial stimulation by ADI-PEG20-primed TOM-1 retain an enhanced capacity to activate effector functions (with IFN-γ as a proxy) when encountering residual tumour cells. However, this would need to be tested and an analysis of CD19-antigen re-challenge would elucidate some of the longer term functional implications of this and other observed changes in CAR-T phenotype when stimulated by ADI-PEG20-primed TOM-1.

7.6 Summary

Taken together these data, first showing that ADI-PEG20 priming enhances sensitivity of *ASS1*-incompetent B-ALL to TRAIL and then that these primed cells stimulate CAR-T such that their IFN-γ expression is robustly downregulated when measured at a post-stimulation time-point of 72 hours, suggest an intriguing functional relationship between the arginine metabolic state of target B-ALL cells and the activation of CAR-T. Added to this, we observed a general reduction in other effector molecules and also exhaustion markers which suggests, given the context of an increase in absolute blast clearance in the primed condition, that priming led to CAR-T effected cytolysis that was more "cytokine-efficient" with potential

translational benefits in terms of reduced systemic toxicity. While we were able to show this effect clearly in our *in vitro* system, the long term effects of this change in phenotype need to be tested before more substantial inferences can be made about potential translational benefits of ADI-PEG20 priming of target B-ALL cells.

Chapter 8

Discussion

8.1 In B-ALL heterogeneous *ASS1* expression is non-random and under-expression is associated with altered gene and metabolic networks

Through re-analysis of a large, publicly available gene expression data set [125], we have shown that *ASS1* expression is heterogeneous in B-ALL and is lowest in a cohort of patients that is enriched for major prevalence subgroups including ETV6::RUNX1, HeH and Ph-L. Pathway enrichment analysis of DEGs between cohorts of *ASS1*-high and -low expressing patients has suggested that *ASS1*-low status is a component of a recurrent metabolic phenotype, supporting low *ASS1* expression as a feature of altered arginine metabolism, rather than simply representing random variation in expression.

We then defined a narrower sub-network of genes based on relationship in function to *ASS1* and showed that within this network *ASS1*-low status appeared to be coordinated with modulation of a core of metabolism related genes and in particular upregulation of *NOS2*, *ACOX1* and *COL5A1*. This gene expression signature was also seen as a recurrent feature amongst numerous other subgroups of B-ALL outside of those that were originally assigned to our *ASS1*-low cohort, including the major prevalence adult subgroup, Ph+.

Together these findings suggest that, rather than being distributed randomly across the entire B-ALL cohort, *ASS1*-low status is part of a coordinated phenotype found in a

significant cohort of patients with B-ALL. As has been seen in other cancer types, loss of *ASS1* expression may confer some form of fitness or survival advantage to tumour cells [89], and the same may be true here. We did not investigate at a functional level how the expression of the extended set of genes might be related to arginine biology and this could form the basis of a useful future study that would increase the understanding of arginine metabolism in ALL, as similar studies have been used to further understand asparagine biology [79]. We also did not extend our study to examine patterns of *ASS1* expression in T-ALL since we had always planned to investigate the role of arginine starvation in anti-CD19 CAR-T therapy. Some evidence does exist to suggest T- as well as B-lineage disease may be responsive to arginine starvation [111] and given the lack of effective options for T-lineage disease that does not respond to conventional agents [113] a detailed examination of its full potential for pre-clinical development remains outstanding.

Prior to our investigation, a single published study [110] had assessed the likely response of primary B-ALL to arginine starvation and reported that 9/14 samples tested *ex vivo* displayed some sensitivity, with the authors also showing that 16/19 tested adults and 5/13 tested children had low or no bone marrow staining for ASS1. While neither series of patient samples were large enough to make any conclusions about the possibility for *ASS1* repression being associated with any specific subgroup of ALL, the proportion of patients described is in keeping with the concept from our study that *ASS1*-low status occurs in a significant cohort of B-ALL patients, although the proportion of paediatric samples with low ASS1 staining in the series of trephine samples is marginally lower than might be expected since ETV6::RUNX1 and HeH subgroups account for around half of children with ALL [240]. Importantly, in their functional arginine starvation models the authors used arginase, as opposed to ADI-PEG20, and this theoretically targets both *ASS1*-low and *OTC*-low tumours, meaning the comparison is not direct in this case.

In our analysis, 4 patient groups were found to be statistically significantly *ASS1*-low when compared to a control group, and 4 patient groups were found to be *ASS1*-high (figure 4.1.2). The inclusion of ETV6::RUNX1 and HeH cytogenetic groups in the *ASS1*-low cohort provides encouragement that arginine starvation is worthy of investigation in paediatric ALL since, as mentioned already, these 2 groups represent around half of paediatric

patients. However, they also represent groups with relatively good prognosis with current chemotherapy protocols and therefore are low priority for exploration of novel therapies. The possible opportunity for arginine starvation in this context would be either in the relapse setting or as a toxicity reduction approach in patients who were intolerant of asparaginase.

However, we decided to focus our interest on the potential application of arginine starvation in adult ALL, where undoubtedly the need for novel therapies is greater. This is especially true of Ph-L ALL which remains a poor prognosis subgroup, with no consensus optimal treatment strategy [241–243]. A specific issue in Ph-L ALL is the failure in many cases of typical induction therapies to elicit even a cytological response and therefore is an area of unmet need. Ph+ ALL, which clustered with *ASS1*-low samples in our UMAP analysis (figure 4.1.5), contrasts Ph-L ALL in that major improvements in survival have been achieved since the addition of TKIs to treatment protocols [244]. However, in some treatment protocols, conventional amino acid starvation with asparaginase is omitted from induction for Ph+ patients owing to a toxic interaction with TKIs and it is feasible that less toxic arginine starvation could be a useful addition where asparaginase is contra-indicated [67]. In addition to this, recent trials have suggested that Ph+ ALL can be effectively managed with "chemo-free" therapy [207] and given its low toxicity, arginine starvation with ADI-PEG20 could be a useful addition in this setting. When we tested *ASS1* expression in our library of PDX samples (table 5.1 and figure 5.4.1) we noted that both Ph+ samples fell in the lowest range of expression. This is in agreement with that seen from our *in silico* analysis but a much larger prospective cohort is needed to validate the findings properly.

Amongst the *ASS1*-high cohort from our analysis the most familiar subgroup is Low Hypodiploid, a very poor prognosis subgroup characterised by mutations in *TP53*. The association of this subgroup and elevated baseline *ASS1* is interesting since it has been reported that *TP53* transactivates *ASS1* [245], although in the case of low hypodiploid ALL the majority of *TP53* mutations are loss-of-function type [246], meaning that enhanced transactivation is less likely. What can be said with a greater degree of confidence is that patients with ALL corresponding to the highest *ASS1*-expressing subgroups (Low hypodiploid, MEF2D, NUTM1 and PAX5 P80R) are least likely to benefit from arginine starvation therapy.

An apparent linkage between molecular subgroups of B-ALL and aberrant *ASS1* expression does correlate with evidence from other tumour types, where it has been shown in pre-clinical and clinical studies that response to arginine starvation can be molecular subgroup specific. For example, in a pre-clinical study of arginine starvation sensitivity in SCLC it has been shown that c-Myc driven subsets of this disease are particularly vulnerable to arginine starvation with ADI-PEG20 due to a distinct metabolic phenotype characterised by an enhanced dependence on arginine regulated pathways [95]. Conversely, mesothelioma with mutated *BAP1*, a frequent occurrence in the epithelioid subgroup, has been shown to over-express *ASS1* with associated resistance to ADI-PEG20 [97]. Furthermore, it has been shown in a *post hoc* analysis of data across clinical trials of ADI-PEG20 in HCC that the subgroup of disease characterised by the *WWOX*-rs13338697-GG genotype had a significant survival benefit when treated by ADI-PEG20 monotherapy [96]. Mechanistically, this genotype was associated with reduced *ASS1* levels due to the effect of WWOX loss enhancing HIF1α (a negative regulator of *ASS1*) expression under hypoxic conditions.

Our GSEA analysis of DEGs between *ASS1*-low and -high cohorts highlighted a loss of expression of c-Myc targets as a broader phenotypic association with *ASS1*-low B-ALL. It has been established the c-Myc positively regulates *ASS1* expression [198, 247, 248] and so it is rational that the *ASS1*-low cohort of patient samples might be characterised by reduced expression across other c-Myc targets. Indeed, in models of melanoma it has been shown that sensitivity to ADI-PEG20 is associated with a lack of activity of the c-Myc transcription factor at the *ASS1* promoter region [247] while resistance, via ADI-PEG20 induced *ASS1* upregulation, can be generated via stabilisation of c-Myc downstream of arginine starvation induced activity in the Ras/PI3K/Akt/ERK pathway [248]. However, the positive regulatory effect of c-Myc on *ASS1* does not correlate with the previously discussed study in which c-Myc driven subsets of SCLC are sensitive to ADI-PEG20 [95]. To reconcile this paradox it can be commented that c-Myc overexpression does not necessarily lead to c-Myc driven positive gene regulation at all c-Myc targets and this is potentially due to epigenetic effects such as chromatin accessibility at individual c-Myc responsive elements, a factor that could feasibly drive a context specific effect of c-Myc on *ASS1* and other amino acid metabolism related genes.

A technical note on the GSEA analysis of DEGs between *ASS1*-low and *ASS1*-high groups is our use of an absolute Log_2FC threshold of 0 with an FDR-q threshold of 0.001 for classification of significant DEGs. It is much more common to see the use of an absolute Log_2FC threshold of 2 in DEGs analysis. However, this higher threshold is more relevant for small sample size experiments, such as 3 *vs* 3 samples, where increased noise requires more robust identification of DEGs. In the current analysis the group sizes ($n = 40$ *vs* $n = 40$) were sufficiently large to mean that we were able to consider as significant any genes even with marginal modulations between groups where the FDR-q value was below the defined threshold [249].

We next investigated the gene expression within a network of *ASS1*-related genes, derived by filtering all DEGs to those known or predicted to interact with *ASS1* using the STRING application [131]. By reducing the dimensionality of this filtered dataset using UMAP we found a distinct cluster (cluster 2) of patient samples that was enriched for *ASS1*-low cohort subgroups 4.1.5. Into this cluster were also assigned numerous samples from other subgroups that were not originally defined as *ASS1*-low, while the overall cluster mean *ASS1* remained lowest. An example of this is the assignment of around 75% of Ph+ samples to cluster 2, implying that the majority, but not all of Ph+ patient samples have a distinct transcriptional signature with regard to *ASS1* and related genes. The fact that most of the remaining Ph+ samples were assigned to cluster 1, the 3rd highest cluster by *ASS1* expression and home to the majority of *ASS1*-high PAX5 P80R samples, likely reflects biological heterogeneity within the Ph+ cohort that can also be seen by the somewhat disparate, bimodal clustering of Ph+ samples in the dimensional reduction analysis performed by the original data set authors [125].

Of note in the UMAP analysis is the apparent discrete clustering of entire subgroups into single, unique clusters. This suggests that within B-ALL, amino acid metabolism and possibly more specifically arginine metabolism is intrinsically linked to the gene programs defined by certain molecular/cytogenetic abnormalities. For example, clusters 5, 6 and 8 are almost exclusively populated by DUX4, KMT2A/KMT2A-like and BCL2/MYC samples, respectively. To our knowledge there are no published studies where comparisons of metabolic phenotypes between different subgroups of B-ALL, except for a study of asparaginase

responsiveness [79], have been reported but further investigation in this area could yield interesting results that may explain the different clinico-biological behaviours of some B-ALL subgroups.

We were then able to further refine the gene set used to create the dimensionally reduced clusters to a set of 19 "marker" genes which were consistently modulated in cluster 2 when compared to all other clusters. The utility of this is that recurrently co-modulated genes support the concept that *ASS1*-low status is part of a coordinated gene/metabolic program, as opposed to simply being randomly distributed. Using these marker genes we were able to show a high degree of concordance in cluster assignment between the Gu *et al.* and Geng *et al.* data sets for both Ph+ and Ph-L. This supports the hypothesis generated from the exploratory analysis that the majority of adult Ph+ and Ph-L ALL samples cluster together with the *ASS1*-low cohort and, while inferences about likely sensitivity to arginine starvation cannot be made without functional models, these subtypes are therefore good candidates for further characterisation as potentially treatable with arginine starvation.

To facilitate this validation step we had reclassified some of the previously unclassified samples from the Geng *et al.* data set as either Ph-L with $k-$means clustering. This is not technically a classification tool but comes with the advantage of using the inbuilt Ph+ patient data as quality control for the newly annotated Ph-L and this also follows the methodology of early clinical systems for classification of Ph-L samples [134]. Then using K-NN classification of expression profiles within the 19-gene marker set we found a similar distribution of B-ALL subtypes from the adult only Geng *et al.* data set across the previously defined clusters from the Gu *et al.* data.

Ultimately, the only known clinically relevant factor from this analysis is the distribution of *ASS1* expression and so the elaboration to include a wider network of genes remains speculative. At the very least, the finding of coordinated modulation of transcription within defined gene sets supports the concept that variation of *ASS1* expression is not simply random but rather associated with contrasting gene expression signatures, which should be an expected finding if arginine auxotrophism is genuinely present within subsets of B-ALL [89]. Our work did not extend to validating the findings of the gene expression analysis, for example by testing expression of our curated marker genes in the cell line models which

did prove to be arginine auxotrophic compared to those with an intact response to arginine starvation. A useful investigation here would be to perform functional genomic analyses of the subset of genes highlighted in the *in silico* analysis (or taking an unbiased approach) and this may elucidate whether correlations in gene expression of *ASS1* and those uncovered by the marker gene analysis are simple byproducts of, necessary adaptation to, or even drivers of an arginine auxotrophic phenotype.

8.2 Functional models of ADI-PEG20 susceptibility in B-ALL

We began our functional experimentation by identifying a panel of cell lines, with the goal of benchmarking functional effects of ADI-PEG20 against baseline *ASS1* expression. We were encouraged that the gene expression of the Ph-L cell line MUTZ-5 matched our prediction for this subgroup of B-ALL but found next that the available data for ETV6::RUNX1 and Ph+ cell lines did not fit, although in a separate data set we were able to profile an *ASS1*-low Ph+ cell line. The fact that the cell line RNA-seq data did not match with that from the large scale analysis of primary sample gene expression was not a concern as the cell line panel was intended to provide functional models representing a range of *ASS1* expression and not to validate the predictions from the previous chapter. Several biological differences exist between these 2 groups of samples, principally from the fact that cell lines have been habituated to growing in non-physiological conditions and also since cell lines usually represent relapse disease with a significant selection bias based on the ability to grow *in vitro*, which is not universal amongst primary samples.

As mentioned we had not set out to investigate the effects of arginine starvation in T-ALL, mainly because we had a planned focus on the use of ADI-PEG20 with anti-CD19 CAR-T therapy. From the cell line RNA-seq data, accepting the caveat from the previous paragraph as a limitation, there does appear to be a broad range of *ASS1* expression amongst T-lineage models (figure 5.1.1) but with a concentration towards the low end of the spectrum. This suggests that amongst T-ALL cell line models at least, there are numerous good candidates for investigation of arginine starvation and given the challenging clinical nature of this disease, especially in relapse [113], an extension project is planned.

We next established a concentration of 1000ng/ml as our optimal concentration for testing of ADI-PEG20. This appeared to be close to the EC_{max} for all cell lines regardless of baseline *ASS1* expression and using LC-MS/MS we demonstrated that at this concentration arginine is rapidly and completely removed from culture media. We did the latter experiment in acellular media and it might have been useful to repeat it with cultured cell supernatants and at different concentrations of ADI-PEG20. However, the number of permutations of experimental conditions that this would have generated would have been cost-prohibitive and so we were satisfied to at least demonstrate that at this concentration arginine is rapidly converted from culture media and this approximates the *in vivo* pharmacodynamics of clinical doses of ADI-PEG20 [174, 175].

Using *in vitro* models we then demonstrated that ADI-PEG20 induces cytostasis and regulated, apoptotic cell death with caspase 3 cleavage and annexin-V expression as well as G0 cell cycle arrest with upregulation of p21 in our cell line models with lowest baseline *ASS1* expression. These basic functional tests bring our results in line with those of Hernandez *et al.* [111], who treated T-ALL cell line models with arginine starvation using arginase, but partially contrasts those of De Santo *et al.* [110], who also found G0/G1 cell cycle arrest in arginase treated B-ALL cells but found necrosis, rather than apoptosis as the induced form of cell death. At this point it would have also been useful to generate an *ASS1* knock-down or knock-out model in, for example, the RS4;11 cell line to validate the dependence of the effect of arginine starvation on expression of the gene.

The comparison with the latter study is intriguing since De Santo *et al.* demonstrated that arginase could induce cell cycle arrest in the Reh cell line which we did not observe with ADI-PEG20. The fundamental difference here is with the use of arginase, which converts arginine to ornithine, as opposed to arginine deiminase (ADI-PEG20), which converts arginine to citrulline. The vulnerability of Reh to arginase but not ADI-PEG20 suggests that Reh can metabolise citrulline to restore arginine homeostasis via ASS1 but is unable to do the same with ornithine, a reaction that requires both Ornithine transcarbamylase (OTC) and ASS1 functionality. It is therefore arguable that arginase based therapeutic enzymes may have wider clinical scope than those based on arginine deiminase such as ADI-PEG20. However, clinical evidence regarding the use of BCT-100, a pegylated version of arginase

(that was used by both Hernandez *et al.* [111] and De Santo *et al.* [110] in their pre-clinical studies) is not as advanced as that for ADI-PEG20 [91] and where tested in other tumour types, OTC expression does not appear to predict responsiveness, while that of ASS1 does [250]. However, it would be useful to compare the response of cell line models to both arginase and arginine deiminase based arginine starvation side-by-side, as this would allow better understanding of the ability of each model to compensate for arginine stress depending on substrate availability; this has now been incorporated into ongoing research and results are awaited.

The functional effects of ADI-PEG20 echo those produced by asparaginase [71] *in vitro* although subtle differences in the mechanisms that produce these effects between arginine and asparagine starvation have been reported [72]. Since asparaginase already has well documented clinical benefit when combined with multi-agent chemotherapy protocols it is logical to ask whether arginine starvation could perform likewise if used in the same context. The answer to this would depend firstly on the difference between the prevalence of metabolic dependence on arginine when compared to asparagine and glutamine (which are both targeted by asparaginase [73, 251]) in ALL, and also whether or not the action of partner chemotherapy drugs differ in the absence of arginine as opposed to the absence of asparagine and glutamine. Given the central nature of asparaginase to modern ALL treatment, investigating blanket substitution with any alternative agent is unlikely to gain any traction, meaning targeted substitution in those areas where asparaginase is too toxic or in subsets of patients where resistance to asparaginase exists is a more viable aim.

In our experiments the functional models that displayed the greatest effect of ADI-PEG20 represented Ph-L and Ph+ subgroups of B-ALL which is in line with predictions from our bioinformatic analysis. However, we only saw a transient effect at most in the Reh cell line which represents the ETV6::RUNX1 subgroup, which had been predicted to be sensitive. The discriminating factor between these models, and including the resistant model RS4;11, with regard to their response to ADI-PEG20 is baseline *ASS1* expression, as is known to be the fundamental predictor of ADI-PEG20 effect. Whether or not Reh has outlying baseline *ASS1* for its subgroup is unknown but the lack of cell death in this cell line does suggest that arginine auxotrophy is not a subgroup defined metabolic feature and patient selection

for use of ADI-PEG20 should therefore take into account *ASS1* expression over cytogenetic subgroup. It would have been useful here to assess expression of our defined set of marker genes to test whether these allowed a better prediction of sensitivity to ADI-PEG20, but time availability did not allow for this.

We then identified ATF4 and CHOP as likely key players in the response to ADI-PEG20, with the latter associated with the induction of apoptosis. We generated these results starting with direct observations from unbiased transcriptome analysis which were then filtered using bioinformatic tools to arrive at the involvement of ATF4 and the centrality of the gene *DDIT3*, which encodes CHOP. There is a clear biological rationale for the involvement of these elements in the response to arginine starvation and the marked degree of protein regulation demonstrated by western blotting confirms this. However, to truly delineate the function of this system with regards to the differing fates of cell survival or death we would need to extend our analysis to studies using direct genetic manipulation, *i.e.* by knock-down or knock-out of these elements, and with the use of downstream modulation of stress induced pathways with inhibitor compounds. With this in mind a full characterisation of ER-stress pathway engagement by ADI-PEG20, usually involving analysis of PERK and EIF2α phosphorylation as well as extending to include ATF6 and IRE1 would be useful to guide functional studies.

In our PDX model with the lowest baseline *ASS1* expression, ALL-04, we were able to show that ADI-PEG20 leads to a significant and maintained tumour cell reduction over 4 weeks of treatment. Despite this cytoreduction, the residual treatment-persistent B-ALL cells had a cell cycle distribution that matched that of controls, contrasting the shorter term effect seen *in vitro* and suggesting that persistent cells had either acquired or intrinsic resistance. Furthermore, the cell cycle distribution might suggest that residual engraftment would have begun to expand at the same rate as controls had the experiment continued. We tested ASS1 expression as a potential acquired resistance factor but did not see a significant difference in treated cells when compared to controls. Alternative modes of resistance have been described, chiefly through metabolic substrate support from local macrophage infiltration [109] or anti-ADI-PEG20 antibody formation [252]. In the NSG mouse model the latter is impossible, but macrophage activity exists and could potentially have supported

persistent B-ALL engraftment in the absence of robust *ASS1* upregulation. The result of any of these modes of tumour cell resistance is normalisation of tumour intracellular arginine and measuring this directly would have been a useful assay to perform in this and future experiments.

In the ALL-07 and ALL-08 PDX models, where baseline *ASS1* was higher we did not see a statistically significant tumour reduction in ADI-PEG20 treated mice, although in the ALL-07 model there was a trend toward this. In the ALL-08 model, where the harvested organs had very closely matched degrees of tumour engraftment there was a clear and robust upregulation of ASS1 after ADI-PEG20 treatment, making gene expression plasticity a highly likely mode of resistance for at least some B-ALL, as has been seen in other tumour types [252, 253]. In the ALL-08 model we had seen a suggestion of a short lived reduction in tumour engraftment based on the week 3 blood results and this raises the possibility that pharmacologically preventing *ASS1* upregulation could lead to more sustained effects even in B-ALL with mid-range baseline expression.

A very clear message from this set of *in vivo* experiments is that group sizes were too small, which is disappointing since there were apparent trends towards tumour response in the ALL-07 PDX as well ASS1 upregulation in ALL-04 that were ultimately not significant and so could not add to our understanding of response to ADI-PEG20 treatment in primary B-ALL. We had not performed power calculations when planning these experiments since we had no prior estimates of effect size in terms of either cytoreduction or *ASS1* expression modulation. Therefore, despite some data not being significant, these experiments have provided useful information for planning future work in this area.

By analysing the transcriptomes of the ADI-PEG20 resistant PDX models we discovered a shared upregulation of both *CEBPB* and *ASS1* that echoed the findings of recently published evidence on the role of C/EBPβ on co-binding with ATF4 to stimulate *ASS1* expression during arginine starvation [185]. We then investigated this finding further using our *in vitro* system and discovered a clear association with cell death fate and a failure of sufficient *ASS1* upregulation coupled with ongoing *CEBPB* expression above baseline. This expression signature suggests that where *ASS1* cannot be induced to restore arginine availability, stress signalling through ATF4 and C/EBPβ persist and this drives cell death,

likely through the known pro-apoptotic activity of CHOP. If the expression of CEBP/β is therefore a likely surrogate for arginine deficit then the RNA-seq data also suggests that despite resistance to tumour cytoreduction in the ALL-07 and ALL-08 mouse models, there remained an ongoing arginine deficit in which the tumour cells were able to maintain proliferation. To properly elucidate the roles of a network involving ATF4, C/EBPβ, CHOP and ASS1 in ADI-PEG20 treatment of B-ALL it would have been useful to have also tested their expression in the ALL-04 model. Furthermore, more in depth work using genetic manipulation as well as chromatin occupancy studies are necessary to properly investigate this and could provide useful understanding on mechanisms of ADI-PEG20 resistance.

Others have proposed models of responsiveness to arginine starvation based on *ASS1* repression and plasticity of *ASS1* as functions of DNA hypermethylation [196] or chromatin modifications [185]. To understand the relevance of these proposed models we chose to test the methylation state of a segment of DNA from a CpG island situated in the promoter region of the *ASS1* gene and compare this to baseline gene expression in our cell line panel. While we did find a stark pattern of hypomethylation in the *ASS1*-high RS4;11 cell line there were no clear differences in the other cell lines despite the contrast in ADI-PEG20 response between Reh and the *ASS1*-incompetent cell lines MUTZ-5 and TOM-1. Indeed, within the segment of DNA that was bisulfite converted for direct sequencing the consensus motifs for both ATF4 and C/EBPβ binding are not found, which may explain why the lack of contrast in methylation between 3 of the 4 cell lines did not correlate with ADI-PEG20 response. If this were the case then it is feasible that the RS4;11 cell hypomethylated pattern in this DNA region is coincidental, likely as part of a globally hypomethylated genome known to be associated with the KMT2Ar subgroup [133], and not functionally related to the overexpression of *ASS1*. Since we had already generated evidence to suggest ATF4 and C/EBPβ were involved in regulating ASS1 expression it would have been a better approach to investigate binding of these transcription factors to the *ASS1* locus. Moreover, we may have found more interesting results by designing our experiments using the data published by Szlosarek *et al.* [107], who showed in clinical trial mesothelioma tissue samples that low ASS1 expression actually correlated with DNA hypomethylation at a single site within the *ASS1* gene body, with no difference found in the promoter region.

Taking the work from this chapter together, we have built evidence to show that in B-ALL the response to ADI-PEG20 correlates with baseline *ASS1* expression and where this gene is lowly expressed and not responsive to upregulatory cues during arginine stress, tumour cells are cell cycle arrested and undergo programmed cell death. Our *in vivo* findings strongly support further pre-clinical development but highlight the need to position ADI-PEG20 within therapy combinations that can eradicate arginine starvation persistent cells, even where *ASS1* is lowest.

8.3 ADI-PEG20 in combination with pharmacological therapy

ALL, like most cancers, is a heterogeneous disease both across patient cohorts and also within individual patients, due to variations in both tumour cell intrinsic factors as well as the microenvironment in which tumour cells reside [254, 255] and this leads to heterogeneous responses to treatment. To counter this, most cancer therapy is based on multi-agent drug combinations that increase the probability of response by targeting cancer cells with multiple independent mechanisms [203].

More recently, novel cancer therapies have been investigated with the goal of designing rational drug combinations for optimised, synergistic drug partnerships that maximise anti-cancer effect. Drug combination synergy is defined as an observed combination effect that exceeds the total expected effect from each component applied individually. However, there is no universally agreed definition for how the total expected effect is estimated and there are numerous ways in which the observed and estimated effects can be compared [256]. Furthermore, rational combinations that result from synergy investigations are generally defined using isogenic cell line models which are then extended into small scale PDX experiments, leaving a high risk that synergy mechanisms may not be borne out in larger, more heterogeneous, clinical cohorts of patients [203].

Our initial experiments with typical ALL induction agents highlighted dexamethasone as the most likely partner drug to form an effective combination with ADI-PEG20 in the *ASS1*-incompetent cell lines MUTZ-5 and TOM-1, including when also combined with dasatinib. Perhaps the most interesting facet of this was the ability of ADI-PEG20 to deepen the

response to dexamethasone of the TOM-1 cell line, which displayed a degree of resistance to high single agent dexamethasone concentrations. The potential clinical significance of this relates to the fact that glucocorticoid resistance is a key feature of relapsed or refractory ALL [257] and so drugs that are effective against tumour cells that can survive glucocorticoids are desirable in this setting. The ability of ADI-PEG20 to also deepen the response of the more steroid sensitive MUTZ-5 model at approximately the IC_{50} dexamethasone concentration also supports the concept that the addition of ADI-PEG20 to dexamethasone in a range of patients with varying steroid responsiveness could improve tumour control at a cohort level.

When we retested the ADI-PEG20-dexamethasone effect by FACS at a dexamethasone concentration where we had seen a significant HSA CI in MUTZ-5 we could confirm that the combination was more effective than either component alone. We used the same dexamethasone concentration for FACS analysis in the TOM-1 cell line and found that the combined effect was not significantly greater than ADI-PEG20 monotherapy and this matched the non-significant CI from the ATP-based assay at this dexamethasone concentration, highlighting that combination effects are dependent on the concentration of the individual drugs. An improved design would have been to also combine ADI-PEG20 with dexamethasone where we had seen a CI >1 for the TOM-1 cell line. It might have also been useful to test a model of *ASS1*-incompetent B-ALL that had a greater degree of resistance to dexamethasone as this, if demonstrative of an effective combination, would also support the rationale for the utility of adding ADI-PEG20, for example, to relapse therapy where steroid unresponsiveness is common.

We also found an exciting combination effect when partnering ADI-PEG20 with the BH3-mimetic agents navitoclax or venetoclax. Venetoclax in particular has emerged as a paradigm changing treatment for numerous haematological malignancies but especially AML and Chronic Lymphocytic Leukaemia (CLL) where it is now standard-of-care in some settings. In ALL, the use of combined navitoclax and venetoclax with low-intensity chemotherapy has gained some traction based on the encouraging results of a recently reported phase 1 study [177] and therefore the potential combination of ADI-PEG20 with either or both of these agents already has clinical intrigue. Another potentially interesting aspect of the combination of ADI-PEG20 with BH3-mimetic agents is a biological rationale for a potentiating effect

between these agents since both Bcl-2 and Bcl-x_L play a role in regulating ER-stress driven apoptosis [258, 259]. It is therefore logical that disruption of these molecules' function could exacerbate arginine stress elicited by ADI-PEG20 and this should form the basis of a deeper mechanistic investigation into the combination.

When we tested ADI-PEG20 with conventional, cytotoxic chemotherapy drugs we found that the combination effect was dominated by the chemotherapy mono-effect at high concentrations and by ADI-PEG20 mono-effect at lower concentrations. Of note was the combination of ADI-PEG20 and vincristine in the MUTZ-5 cell line, where despite sensitivity to ADI-PEG20, the combination was unable to overcome resistance to vincristine, suggesting a degree of cross-resistance. Of note, we did not test cyclophosphamide, which is another frequently used agent for ALL induction therapy, since this is a pro-drug which requires hepatic conversion into its active form, and so therefore is not functional *in vitro*.

One of the clear drawbacks in the practical use of the CellTiter-Glo ATP assay was imprecise results, and this was manifested especially in the control wells which were used to normalise treated values, meaning that especially at high cell viability we got inconsistent results. To try to counter this we increased the number of control wells from which the normalisation denominator was generated and doing this we noticed that edge effects appeared to be a factor in imprecision. The definitive way to deal with this was demonstrated by Jaaks *et al.* [200], who utilised a robotic liquid handling platform to randomise well positions and then computer software to deconvolute luminescence readings. Unfortunately this was not possible in our experiments, but CellTiter-Glo remains a useful assay for this type of analysis and so well distribution is an important consideration for future work.

We next built an ADI-PEG20 resistance model based on an outgrowth effect of an *ASS1*-overexpressing subclone. This is not necessarily the mechanism that had supported surviving leukaemia cells in the ALL-04 PDX but does model the final effect of any of the major modes of resistance, which is normalisation of arginine provision and/or its downstream metabolic flows. Using our model we were able to phenocopy the residual tumour cell cycle from the ALL-04 PDX and also showed that the *ASS1*-overexpressing subclone could indeed grow out under arginine stress. With this model we then showed that the combination of ADI-PEG20 with dasatinib-dexamethasone could suppress the

outgrowth of this resistant subclone, while the ADI-PEG20-venetoclax combination could not. A likely reason for this contrast is the postulated effect of venetoclax in amplifying the apoptotic consequences of arginine starvation in *ASS1*-incompetent cells whereas in the *ASS1*-overexpressing subclone, the cells are able to prevent an arginine deficit by converting citrulline to arginine and so there is less apoptotic effect to amplify. Conversely, dasatinib-dexamethasone appeared to be independently potent and can therefore kill cells regardless of their arginine homeostatic state.

To generate this model we used an intentionally low-transduction efficiency gene transfer technique, such that the resultant *ASS1*-overexpressing subclone represented only a small portion of the total cells. A better design for the generation of this model would have been to transduce cells with *ASS1* cDNA and then select them by FACS or with puromycin such that a fixed proportion subclone model could then be generated by mixing transduced and wild-type cells. This would have overcome a difficulty we found in that the subclone size drifted over time (especially for mock-transduced) and was not equal between mock-transduced and *ASS1*-transduced. However, we found that both MUTZ-5 and TOM-1 the cells did not tolerate puromycin or FACS selection well and failed to grow out in subsequent cultures.

When we tested the promising ADI-PEG20-dasatinib-dexamethasone combination in the ALL-04 PDX model we found a slightly disappointing result in that the combination was no better than dasatinib-dexamethasone alone. Given the potency of ADI-PEG20 in our previous experiments with this model, this was surprising but is likely explained by the high sensitivity of the PDX to dasatinib-dexamethasone alone, meaning that incremental benefits from additional agents are difficult to achieve. We had originally planned larger group sizes for this experiment but due to time pressures and a slower-than-expected degree of engraftment we were unable to include all mice. This again highlights the previously demonstrated importance of group size in mouse models and greater numbers would have helped to clarify the cause of the early death in the triplet combination arm and whether or not the speed of re-engraftment was different between the treatment arms. Furthermore, with greater numbers we could have afforded to sacrifice a sub-cohort of mice for analysis of tumour cells during the remission period to try to understand what, if any, differences arginine starvation had imprinted in the tumour cells.

8.4 Priming B-ALL for CAR-T immunotherapy with ADI-PEG20

The finding of a specific interaction between ADI-PEG20 and the TRAIL arm of the DR-pathway, as has been found in other tumour types [120], was intriguing given the reported importance of this for the effect of CAR-T cell therapy [53, 118, 215]. When we measured gene expression in response to vincristine there was apparently very little interaction with the DR-pathway and it would have been useful to test whether vincristine altered sensitivity to TRAIL, as this could have strengthened evidence for a link between ADI-PEG20 driven transcriptional modulation and functional TRAIL susceptibility.

Our finding of potent ADI-PEG20 stimulation of DR5, and to a lesser extent DR4, expression is in keeping with our previously introduced concept of the involvement of ER-stress signalling via CHOP in the *ASS1*-incompetent cell lines. CHOP has been characterised as acting downstream of ER-stress to upregulate DR5 expression [186] and at a mechanistic level it would have increased understanding had we confirmed this link using functional experiments. We did attempt to generate a CHOP shRNA knock-down model in both the MUTZ-5 and TOM-1 using lentivirus but the transduced cells failed to remain viable in culture, which was surprising given the reported pro-apoptotic role of CHOP.

We did investigate the centrality of the modulation of DR5 to the functional effect of ADI-PEG20 on TRAIL sensitivity. Using lentivirally transduced shRNA we were able to block the upregulation of DR5 (as well as making a fractional reduction in baseline expression) but this did not change the enhancement of TRAIL sensitivity. A plausible explanation for this is that the wider stimulation of gene expression amongst other pro-apoptotic components of the DR-pathway introduces redundancy into the system, to reduce dependence on a single molecule. To test this more completely it would have been useful to take a knock-out approach, for example with CRISPR-Cas9, and it would be possible to design an experiment with a library of CRISPR guides to individually ablate the entire DR-pathway so as to allow determination of the molecular dependence of the increased TRAIL sensitivity after ADI-PEG20 treatment. However, there does exist the possibility that enhanced TRAIL sensitivity is independent of the modulation of DR-pathway expression and one alternative explanation

is the reported preference of TRAIL activity in cell cycle arrested cells [260]. Since we also showed a potent ADI-PEG20 induction of cell cycle arrest, further controls with cells in synchronised phases of the cell cycle would help answer this question.

Based on the sensitisation of *ASS1*-incompetent B-ALL to TRAIL after ADI-PEG20 exposure we next tested if ADI-PEG20, given as a priming treatment, could modulate the effect of CAR-T. To test this we were faced with the challenge of isolating the target cell intrinsic effects of ADI-PEG20 from the basic effect of an increased E:T ratio given that exposure to ADI-PEG20 would also kill some of the target cells. We therefore developed a model where primed or unprimed target cells were washed and then resuspended in complete media at identical cell count and concentration, such that co-cultures could be started with matched E:T ratios. We chose a "stressed" E:T ratio of 1:40 (based on initial titration experiments) such that residual B-ALL counts after co-culture would be around 25% of NT co-cultures. This E:T ratio is arguably more representative of the *in vivo* dynamic between effector and target cells and also modelled a "resistance" scenario, albeit based on a simple numerical disadvantage rather than target cell intrinsic factors, such that we could test for differences in residual target cell counts depending on the priming condition.

At the most simplistic level we found that the combination of ADI-PEG20 priming followed by CAR-T led to a reduced number of surviving blast cells after a co-culture period of 72 hours when compared to no priming. This was also seen for vincristine and in the case of the comparison between ADI-PEG20 and control we observed that the proportion of cells killed specifically by CAR-T (*i.e.* when normalising against the ADI-PEG20-primed NT condition) was the same as for unprimed co-cultures, suggesting that the increased clearance was a function of the latent effect of priming rather than a change in sensitivity to CAR-T.

This observation goes against the hypothesis that ADI-PEG20 priming would increase B-ALL sensitivity to CAR-T. However, the net reduction in final blasts cells due to the effect of a pre-treatment drug which reduces target cell proliferation and/or has an ongoing cytoreductive effect during the co-culture period has a strong rationale for translation to the clinic since current standard of care drugs for CAR-T bridging come with numerous drawbacks, not least because most patients will have been exposed to them already and

therefore are likely to be in part resistant. Furthermore, most patients in this clinical context will have acquired multiple treatment and disease related morbidities and therefore ADI-PEG20, with a good safety record [82, 98], may have advantages over more intensive drugs that evidence suggests do harm in the bridging period [115, 116]. A parallel here based on existing clinical data is the finding of favourable outcomes for polatuzumab bridging therapy for patients with DLBCL [117], which may be at least in part be due to the fact that most patients in the studied cohort would not have been treated with the drug in prior lines of therapy.

Our next finding of an enhanced proliferation of CAR-T cells in the TOM-1 co-culture models with a seemingly paradoxical reduction in IFN-γ prompted us to hypothesise that a major effect of ADI-PEG20 priming was to alter the phenotype of CAR-T, presumably by a difference in the dynamics of stimulation. To measure differential stimulation of effector cells between primed and un-primed conditions we followed the methodology that had recently been described by Michelozzi *et al.* for the analysis of resultant CAR-T phenotypes using single cell proteomics by CyTOF [149, 261], the first step of which was to perform bulk RNA-seq on CAR-T cells sorted after co-culture experiments to help curate a panel of target proteins. Although we had shown a reduction in IFN-γ secretion into supernatants from CAR-T stimulated by ADI-PEG20 primed TOM-1, we approached these results with genuine curiosity about the possibility for transcriptional modulation and so were excited by results that firstly confirmed a corresponding reduction in *IFNG* expression and next robustly implicated altered cytokine expression and signalling in those effector cells that were stimulated by primed blasts. Generating this RNA-seq data was challenging since we only recovered limited amounts of cells by FACS purification and so starting RNA quantity and quality was limited. To overcome this we submitted RNA for more sophisticated library preparation and this comes with limitations in terms of amplification of noise. To avert this problem we could have employed a dedicated kit for RNA extraction from low input cell numbers which performs cell lysis and stabilisation of RNA directly from the FACS analyser, such as the QIAGEN QIAseq FX Single Cell RNA Library Kit.

Our CyTOF data elaborated on the concept that effector cells in general expressed lower levels of IFN-γ and other effector cytokines. Given this change in cytokine expression was

already functionally benchmarked to an effective tumour cell eradication we interpreted this as representing a more "cytokine efficient" target killing, *i.e.* target cells were killed without the need for persistent and prolonged cytokine secretion. The significance of this could be important in a translational sense since the major toxicities of CAR-T therapy are associated with cytokines such as IFN-γ and if priming therapy can allow for equivalent killing with less cytokine secretion then this could reap major clinical benefits [228].

The power of CyTOF, as a single cell assay, is to use the full complexity of acquired data to generate highly granular descriptions of groups of cells based on clusters of phenotypic similarity. We used self-organising maps to partition the data based on a core set of T-cell phenotypic markers [230] and found that our data generated plausible clusters of cells that closely matched classical immune-cell subset descriptions. Using this granularity of data we were able to see that the major difference in CAR-T phenotype in the ADI-PEG20 primed target cell conditions was an increase in the proportion of CD4-Effector cells, as well as a reduction in the secretion of effector proteins.

The significance of these changes with regard to a potential clinical benefit is unclear beyond the association with a net reduction in residual blast cells in an *in vitro* co-culture system that has so far only used one cell line model. However, the fact that a robust alteration in CAR-T phenotype, which has theoretical benefits in terms of clinical efficacy and toxicity [228], has been generated suggests that the metabolic state of target cells has a significant influence on effector cell behaviour and potentially important understanding of the interaction between CAR-T cells and tumour cells can be learned by interrogating this interaction further.

One of the most important questions to ask is what the ongoing capacity of CAR-T cells for tumour surveillance and control is when their initial stimulation is by arginine starved blasts. The main *in vitro* methodology for asking this question is with repeated antigen rechallenge experiments [262] and this can answer questions such as what the longer-term significance of the reduction in exhaustion markers is and whether or not the presence of downregulated IFN-γ expression in all but CD8-EM cells allows for ongoing disease control with fewer cytokine related toxicities. A long-lived, persistent pool of CAR-T cells has emerged as clinically important for prevention of relapse and recent reports have unearthed

a specific transcriptional signature that associates with this in clinical patient samples [263]. The convergence or divergence of CAR-T to or from this phenotype when stimulated by arginine starved blasts is therefore a key question and testing this could provide a strong rationale for further clinical development.

The demonstration of this effect and its further characterisation *in vivo* is now a key priority and mouse models can be used to answer various important questions. The long term effect on CAR-T activity is perhaps more instructive *in vivo* than using *in vitro* rechallenge experiments since a genuine test of surveillance and activity against low levels of residual disease can be modelled in this way. Testing *in vivo* also gives the opportunity to test longer term characteristics of tumour cells as well as serial measurements of CAR-T phenotype and an elegant strategy that could be used as a basis for this testing was recently published by Rodriguez-Marquez *et al.* using the NSG mouse model [264]. Another important question that can only really be answered with *in vivo* models is the feasibility of delivering a transient period of arginine starvation that resolves prior to CAR-T infusion as was the case for our *in vitro* models and if the tumour cell priming effect persists despite normalisation of arginine. Furthermore, it is also key to ask whether a residual arginine deficit, if not completely resolved by the time of infusion, may be tolerated by effector cells [88]. Using mouse models would also allow the assessment of the potential benefit of direct tumour cell reduction by ADI-PEG20, as well as a priming effect, in the bridging period, and this could be tested against standard-of-care bridging agents such as dexamethasone. Regardless of a postulated priming effect, the basic ability to cytoreduce B-ALL in a patient that has developed resistance to conventional drugs by incorporating a novel agent such as ADI-PEG20 should not be overlooked, since alone this could be highly beneficial for patients in which disease control is otherwise impossible in the bridging period.

At a mechanistic level we attempted to ask whether or not the change in dynamics was due to an alteration in the state of the tumour cell DR-pathway. We were able to show that ADI-PEG20 does have a significant priming effect on cell sensitivity to TRAIL but whether this translated to being the driver of the change in CAR-T phenotype was not proven. Others have had success in interrogating this relationship and a TRAIL-null CAR-T cell, as demonstrated by DeSelm *et al.* [118], could be an ideal model for testing this.

Mechanistic testing with alternative CAR constructs is another key consideration given the predominance of 4-1BB costimulatory CAR-T in paediatric B-ALL management. Finally, it would also be important to ask whether the other effects of ADI-PEG20, such as its profound cell cycle effect, may be at play in the change in CAR-T phenotype and synchronised cell cycle target cells may be a valuable control in future experiments.

Chapter 9

Conclusion

In this work we set out to perform a wide ranging analysis of the potential of arginine starvation with ADI-PEG20 in B-ALL with regard to the scope of applicability, the basic functional effects and whether or not this approach could be used in conjunction with conventional and/or CAR-T therapy.

Possibly the most significant finding has been the non-random range of *ASS1* expression in B-ALL that appears to be part of wider metabolic signature. This, combined with the sensitivity of our *ASS1*-incompetent cell line models, strongly suggests that there is genuine clinical scope to incorporate ADI-PEG20 into management of B-ALL as long as patient selection is well planned.

In our functional modelling of ADI-PEG20 treatment we found the effects of potent cell cycle arrest and apoptosis with a core network of response elements centered on ATF4, C/EBPβ, ASS1 and CHOP and introduced the concept of survival or death based on the competence of the cellular ability to upregulate ASS1 and alleviate arginine stress. Furthermore, we saw in our *ASS1*-low PDX model that ADI-PEG20 could elicit a significant cytoreduction as monotherapy, that gives strong motivation for further pre-clinical development.

To counter disease persistence in our ADI-PEG20 monotherapy PDX model we investigated drug combinations with conventional agents as well as BH3-mimetics. When combined with dexamethasone and dasatinib we saw a potent *in vitro* effect, including the ability to suppress our resistance model, but this was unfortunately not borne out in *in*

vivo testing. Although the *in vitro* combinations with navitoclax and venetoclax were less effective against our resistance model, the impressive combination effects against wild type *ASS1*-incompetent cell lines, along with the clinical relevance of these drugs in ALL, has prompted plans for further development in this area.

Our investigation into the potential for ADI-PEG20 pre-treatment to modulate the effect of CAR-T started with the demonstration that ADI-PEG20 functionally enhances sensitivity to TRAIL. When using the same pre-treatment system to "prime" B-ALL for CAR-T we did not find a clear indication that this TRAIL effect had changed the sensitivity of target cells to CAR-T but we did see a robust change in the cytokine secretory phenotype of effector cells after stimulation by arginine starved blasts. Further investigation is needed into the longer term consequences of this modulation, as well as the feasibility of applying transient arginine starvation clinically, but the observation of increased "cytokine-efficiency" warrants further development given the plausible clinical benefits that this may bring.

Appendix A

FMC63-28ζ amino acid sequence

MALPVTALLLPLALLLHAARPDIQMTQTTSSLSASLGDRVTISCRASQDISKYLNWYQQK
PDGTVKLLIYHTSRLHSGVPSRFSGSGSGTDYSLTISNLEQEDIATYFCQQGNTLPYTFG
GGTKLEITGGGGSGGGGSGGGGSEVKLQESGPGLVAPSQSLSVTCTVSGVSLPDYGV
SWIRQPPRKGLEWLGVIWGSETTYYNSALKSRLTIIKDNSKSQVFLKMNSLQTDDTAIYY
CAKHYYYGGSYAMDYWGQGTSVTVSSAAAIEVEQKLISEEDLLDNEKSNGTIIHVKGKHL
CPSPLFPGPSKPFWVLVVVGGVLACYSLLVTVAFIIFWVRSKRSRLLHSDYMNMTPRRP
GPTRKHYQPYAPPRDFAAYRSRVKFSRSADAPAYQQGQNQLYNELNLGRREEYDVLD
KRRGRDPEMGGKPRRKNPQEGLYNELQKDKMAEAYSEIGMKGERRRGKGHDGLYQG
LSTATKDTYDALHMQALPPR

Bibliography

1. Acute lymphoblastic leukaemia (ALL) incidence statistics | Cancer Research UK. https://www.cancerresearchuk.org/health-professional/cancer-statistics/statistics-by-cancer-type/leukaemia-all/incidence#heading-Zero.
2. Malard, F. & Mohty, M. Acute lymphoblastic leukaemia. *The Lancet* **395,** 1146–1162. ISSN: 01406736 (10230 Apr. 2020).
3. Roman, E. *et al.* Cohort Profile Update: The Haematological Malignancy Research Network (HMRN) UK population-based cohorts. *International Journal of Epidemiology* **51.** ISSN: 14643685 (3 2022).
4. Haematological Malignancy Research Network. hmrn.org.
5. Górecki, M. *et al.* Updates in KMT2A Gene Rearrangement in Pediatric Acute Lymphoblastic Leukemia. *Biomedicines* **11.** ISSN: 22279059 (3 2023).
6. Greaves, M. Infection, immune responses and the aetiology of childhood leukaemia. *Nature Reviews Cancer* **6,** 193–203. ISSN: 1474175X. https://pubmed.ncbi.nlm.nih.gov/16467884/ (3 Mar. 2006).
7. Alaggio, R. *et al.* The 5th edition of the World Health Organization Classification of Haematolymphoid Tumours: Lymphoid Neoplasms. *Leukemia* **36.** ISSN: 14765551 (7 2022).
8. Vlierberghe, P. V. & Ferrando, A. The molecular basis of T cell acute lymphoblastic leukemia. *Journal of Clinical Investigation* **122.** ISSN: 00219738 (10 2012).

9. Wrench, B. P. *et al.* Final Results from UKALL60+ (NCT01616238), a UK National Cancer Research Institute Trial for Older People with De Novo Acute Lymphoblastic Leukaemia. *Blood* **140.** ISSN: 0006-4971 (Supplement 1 2022).

10. Miller, D. R. A tribute to Sidney Farber - The father of modern chemotherapy. *British Journal of Haematology* **134.** ISSN: 00071048 (1 2006).

11. Pui, C. H. & Evans, W. E. A 50-year journey to cure childhood acute lymphoblastic leukemia. *Seminars in Hematology* **50.** ISSN: 00371963 (3 2013).

12. Bartram, J., Veys, P. & Vora, A. Improvements in outcome of childhood acute lymphoblastic leukaemia (ALL) in the UK – a success story of modern medicine through successive UKALL trials and international collaboration. *British Journal of Haematology* **191.** ISSN: 13652141 (4 2020).

13. Maury, S. *et al.* Rituximab in B-Lineage Adult Acute Lymphoblastic Leukemia. *https://doi.org/10.1056/NEJMoa1605085* **375,** 1044–1053. https://www.nejm.org/doi/full/10.1056/NEJMoa1605085 (11 Sept. 2016).

14. M, B. & M, K. Minimal residual disease in adult ALL: technical aspects and implications for correct clinical interpretation. *Blood advances* **1,** 2456–2466. ISSN: 2473-9529. https://pubmed.ncbi.nlm.nih.gov/29296895/ (25 Nov. 2017).

15. Bartram, J. *et al.* High-throughput sequencing of peripheral blood for minimal residual disease monitoring in childhood precursor B-cell acute lymphoblastic leukemia: A prospective feasibility study. *Pediatric Blood and Cancer* **69.** ISSN: 15455017 (3 2022).

16. Ribera, J. M. Allogeneic stem cell transplantation for adult acute lymphoblastic leukemia: When and how. *Haematologica* **96.** ISSN: 03906078 (8 2011).

17. Dhédin, N. *et al.* Role of allogeneic stem cell transplantation in adult patients with Ph-negative acute lymphoblastic leukemia. *Blood* **125.** ISSN: 15280020 (16 2015).

18. Kantarjian, H. *et al.* Blinatumomab versus Chemotherapy for Advanced Acute Lymphoblastic Leukemia. *http://dx.doi.org/10.1056/NEJMoa1609783* **376,** 836–847. https://www.nejm.org/doi/full/10.1056/NEJMoa1609783 (9 Mar. 2017).

19. Gökbuget, N. *et al.* Blinatumomab for minimal residual disease in adults with B-cell precursor acute lymphoblastic leukemia. *Blood* **131,** 1522–1531. ISSN: 0006-4971. http://ashpublications.org/blood/article-pdf/131/14/1522/1727202/blood798322.pdf (14 Apr. 2018).

20. Gökbuget, N. *et al.* Curative outcomes following blinatumomab in adults with minimal residual disease B-cell precursor acute lymphoblastic leukemia. *Leukemia and Lymphoma* **61.** ISSN: 10292403 (11 2020).

21. Van der Sluis, I. M. *et al.* Blinatumomab Added to Chemotherapy in Infant Lymphoblastic Leukemia. *New England Journal of Medicine* **388.** ISSN: 0028-4793 (17 2023).

22. Litzow, M. R. *et al.* Consolidation Therapy with Blinatumomab Improves Overall Survival in Newly Diagnosed Adult Patients with B-Lineage Acute Lymphoblastic Leukemia in Measurable Residual Disease Negative Remission: Results from the ECOG-ACRIN E1910 Randomized Phase III National Cooperative Clinical Trials Network Trial. *Blood* **140.** ISSN: 0006-4971 (Supplement 2 2022).

23. Kantarjian, H. M. *et al.* Inotuzumab Ozogamicin versus Standard Therapy for Acute Lymphoblastic Leukemia. *https://doi.org/10.1056/NEJMoa1509277* **375,** 740–753. https://www.nejm.org/doi/full/10.1056/nejmoa1509277 (8 June 2016).

24. HM, K. *et al.* Inotuzumab ozogamicin versus standard of care in relapsed or refractory acute lymphoblastic leukemia: Final report and long-term survival follow-up from the randomized, phase 3 INO-VATE study. *Cancer* **125,** 2474–2487. ISSN: 1097-0142. https://pubmed.ncbi.nlm.nih.gov/30920645/ (14 July 2019).

25. SL, B. *et al.* Phase II study of nelarabine (compound 506U78) in children and young adults with refractory T-cell malignancies: a report from the Children's Oncology Group. *Journal of clinical oncology : official journal of the American Society of Clinical Oncology* **23,** 3376–3382. ISSN: 0732-183X. https://pubmed.ncbi.nlm.nih.gov/15908649/ (15 2005).

26. DJ, D. *et al.* Nelarabine induces complete remissions in adults with relapsed or refractory T-lineage acute lymphoblastic leukemia or lymphoblastic lymphoma: Can-

cer and Leukemia Group B study 19801. *Blood* **109,** 5136–5142. ISSN: 0006-4971. https://pubmed.ncbi.nlm.nih.gov/17344466/ (12 June 2007).

27. Shimony, S. *et al.* Nelarabine combination therapy for relapsed or refractory T-cell acute lymphoblastic lymphoma/leukemia. *Blood Advances* **7.** ISSN: 24739537 (7 2023).

28. Hogan, L. E. *et al.* Efficacy and safety of daratumumab (DARA) in pediatric and young adult patients (pts) with relapsed/refractory T-cell acute lymphoblastic leukemia (ALL) or lymphoblastic lymphoma (LL): Results from the phase 2 DELPHINUS study. *Journal of Clinical Oncology* **40.** ISSN: 0732-183X (16 suppl 2022).

29. Emily Whitehead Foundation. https://emilywhiteheadfoundation.org/.

30. Guedan, S., Calderon, H., Posey, A. D. & Maus, M. V. Engineering and Design of Chimeric Antigen Receptors. *Molecular Therapy - Methods and Clinical Development* **12.** ISSN: 23290501 (2019).

31. Shah, N. N. *et al.* CD4/CD8 T-cell selection affects chimeric antigen receptor (CAR) T-cell potency and toxicity: Updated results from a phase I anti-CD22 CAR T-cell trial. *Journal of Clinical Oncology* **38.** ISSN: 15277755 (17 2020).

32. Myers, R. M. *et al.* Humanized CD19-Targeted Chimeric Antigen Receptor (CAR) T Cells in CAR-Naive and CAR-Exposed Children and Young Adults With Relapsed or Refractory Acute Lymphoblastic Leukemia. *Journal of Clinical Oncology* **39.** ISSN: 15277755 (27 2021).

33. Mitra, A. *et al.* From bench to bedside: the history and progress of CAR T cell therapy. *Frontiers in Immunology* **14.** ISSN: 16643224 (2023).

34. Kawalekar, O. U. *et al.* Distinct Signaling of Coreceptors Regulates Specific Metabolism Pathways and Impacts Memory Development in CAR T Cells. *Immunity* **44.** ISSN: 10974180 (2 2016).

35. Maude, S. L. *et al.* Tisagenlecleucel in children and young adults with B-cell lymphoblastic leukemia. *New England Journal of Medicine* **378,** 439–448. ISSN: 15334406. https://pubmed.ncbi.nlm.nih.gov/29385370/ (5 Feb. 2018).

36. Laetsch, T. W. *et al.* Three-Year Update of Tisagenlecleucel in Pediatric and Young Adult Patients with Relapsed/Refractory Acute Lymphoblastic Leukemia in the ELIANA Trial. *Journal of Clinical Oncology* **41.** ISSN: 15277755 (9 2023).

37. Shah, B. D. *et al.* KTE-X19 for relapsed or refractory adult B-cell acute lymphoblastic leukaemia: phase 2 results of the single-arm, open-label, multicentre ZUMA-3 study. *The Lancet* **398.** ISSN: 1474547X (10299 2021).

38. Shah, B. D. *et al.* Two-year follow-up of KTE-X19 in patients with relapsed or refractory adult B-cell acute lymphoblastic leukemia in ZUMA-3 and its contextualization with SCHOLAR-3, an external historical control study. *Journal of Hematology and Oncology* **15.** ISSN: 17568722 (1 2022).

39. Santomasso, B. D. *et al.* Management of Immune-Related Adverse Events in Patients Treated with Chimeric Antigen Receptor T-Cell Therapy: ASCO Guideline. *Journal of Clinical Oncology* **39.** ISSN: 15277755 (35 2021).

40. Jain, M. D., Smith, M. & Shah, N. N. How I treat refractory CRS and ICANS after CAR T-cell therapy. *Blood* **141.** ISSN: 15280020 (20 2023).

41. Jain, T., Olson, T. S. & Locke, F. L. How I treat cytopenias after CAR T-cell therapy. *Blood* **141.** ISSN: 15280020 (20 2023).

42. Gutierrez, C., Neilan, T. G. & Grover, N. S. How I approach optimization of patients at risk of cardiac and pulmonary complications after CAR T-cell therapy. *Blood* **141.** ISSN: 15280020 (20 2023).

43. Santomasso, B. D., Gust, J. & Perna, F. How I treat unique and difficult-to-manage cases of CAR T-cell therapy–associated neurotoxicity. *Blood* **141.** ISSN: 15280020 (20 2023).

44. Shah, N. N. & Fry, T. J. Mechanisms of resistance to CAR T cell therapy. *Nature Reviews Clinical Oncology* **16.** ISSN: 17594782 (6 2019).

45. Rabilloud, T. *et al.* Single-cell profiling identifies pre-existing CD19-negative subclones in a B-ALL patient with CD19-negative relapse after CAR-T therapy. *Nature Communications* **12.** ISSN: 20411723 (1 2021).

46. Fischer, J. *et al.* CD19 isoforms enabling resistance to CART-19 immunotherapy are expressed in B-ALL patients at initial diagnosis. *Journal of Immunotherapy* **40.** ISSN: 15374513 (5 2017).

47. Bueno, C. *et al.* CD34+CD19-CD22+ B-cell progenitors may underlie phenotypic escape in patients treated with CD19-directed therapies. *Blood* **140.** ISSN: 15280020 (1 2022).

48. Fry, T. J. *et al.* CD22-targeted CAR T cells induce remission in B-ALL that is naive or resistant to CD19-targeted CAR immunotherapy. *Nature Medicine* **24.** ISSN: 1546170X (1 2018).

49. Kokalaki, E. K. *et al.* A High Sensitivity aCD22 CAR Combined with aCD19 CAR to Generate Dual Targeting CAR T Cells for the Treatment of r/r B-ALL. *Blood* **138,** 1710–1710. ISSN: 0006-4971 (Supplement 1 Nov. 2021).

50. Spiegel, J. Y. *et al.* CAR T cells with dual targeting of CD19 and CD22 in adult patients with recurrent or refractory B cell malignancies: a phase 1 trial. *Nature Medicine* **27.** ISSN: 1546170X (8 2021).

51. Park, J. H. *et al.* Long-Term Follow-up of CD19 CAR Therapy in Acute Lymphoblastic Leukemia. *New England Journal of Medicine* **378,** 449–459. ISSN: 0028-4793. http://www.nejm.org/doi/10.1056/NEJMoa1709919 (5 Feb. 2018).

52. Gardner, R. A. *et al.* Intent-to-treat leukemia remission by CD19 CAR T cells of defined formulation and dose in children and young adults. *Blood* **129.** ISSN: 0006-4971 (25 2017).

53. Singh, N. *et al.* Impaired death receptor signaling in leukemia causes antigen-independent resistance by inducing CAR T-cell dysfunction. *Cancer Discovery* **10,** 552–567. ISSN: 21598290. https://cancerdiscovery.aacrjournals.org/content/10/4/552%20https://cancerdiscovery.aacrjournals.org/content/10/4/552.abstract (Apr. 2020).

54. Singh, N., Perazzelli, J., Grupp, S. A. & Barrett, D. M. Early memory phenotypes drive T cell proliferation in patients with pediatric malignancies. *Science Translational Medicine* **8.** ISSN: 19466242 (320 2016).

55. Bai, Z. *et al.* Single-cell antigen-specific landscape of CAR T infusion product identifies determinants of CD19-positive relapse in patients with ALL. *Science Advances* **8.** ISSN: 23752548 (23 2022).

56. Long, A. H. *et al.* 4-1BB costimulation ameliorates T cell exhaustion induced by tonic signaling of chimeric antigen receptors. *Nature Medicine* **21,** 581–590. ISSN: 1546170X. /pmc/articles/PMC4458184/%20/pmc/articles/PMC4458184/?report=abstract%20https://www.ncbi.nlm.nih.gov/pmc/articles/PMC4458184/ (6 June 2015).

57. Khan, A. N. *et al. Immunogenicity of CAR-T Cell Therapeutics: Evidence, Mechanism and Mitigation* 2022.

58. Ghorashian, S. *et al.* Enhanced CAR T cell expansion and prolonged persistence in pediatric patients with ALL treated with a low-affinity CD19 CAR. *Nature Medicine* **25,** 1408–1414. ISSN: 1546170X. https://www.nature.com/articles/s41591-019-0549-5 (9 Sept. 2019).

59. Roddie, C. *et al.* Safety and efficacy of obecabtagene autoleucel (obe-cel, AUTO1), a fast-off rate CD19 CAR, in relapsed/refractory adult B-cell acute lymphoblastic leukemia (r/r B-ALL): Top line results of the pivotal FELIX study. *Journal of Clinical Oncology* **41,** 7000–7000. ISSN: 0732-183X (16 suppl June 2023).

60. Watanabe, N., Mo, F. & McKenna, M. K. Impact of Manufacturing Procedures on CAR T Cell Functionality. *Frontiers in Immunology* **13.** ISSN: 16643224 (2022).

61. Egler, R. A., Ahuja, S. P. & Matloub, Y. L-asparaginase in the treatment of patients with acute lymphoblastic leukemia. *Journal of Pharmacology and Pharmacotherapeutics* **7.** ISSN: 09765018 (2 2016).

62. Wetzler, M. *et al.* Effective asparagine depletion with pegylated asparaginase results in improved outcomes in adult acute lymphoblastic leukemia: Cancer and Leukemia Group B study 9511. *Blood* **109.** ISSN: 00064971 (10 2007).

63. Storring, J. M. *et al.* Treatment of adults with BCR-ABL negative acute lymphoblastic leukaemia with a modified paediatric regimen. *British Journal of Haematology* **146.** ISSN: 00071048 (1 2009).

64. Stock, W. *et al.* A pediatric regimen for older adolescents and young adults with acute lymphoblastic leukemia: Results of CALGB 10403. *Blood* **133.** ISSN: 15280020 (14 2019).

65. Gupta, S. *et al.* Impact of asparaginase discontinuation on outcome in childhood acute lymphoblastic leukemia: A report from the children's oncology group. *Journal of Clinical Oncology* **38,** 1897–1905. ISSN: 15277755. https://pubmed.ncbi.nlm.nih.gov/32275469/ (17 Apr. 2020).

66. Aldoss, I. *et al.* The impact of early PEG-asparaginase discontinuation in young adults with ALL: a post hoc analysis of the CALGB 10403 study. *Blood Advances* **7.** ISSN: 24739537 (2 2023).

67. Patel, B. *et al.* Pegylated-asparaginase during induction therapy for adult acute lymphoblastic leukaemia: Toxicity data from the UKALL14 trial. *Leukemia* **31,** 58–64. ISSN: 14765551. https://pubmed.ncbi.nlm.nih.gov/27480385/ (1 Jan. 2017).

68. Kidd, J. G. REGRESSION OF TRANSPLANTED LYMPHOMAS INDUCED IN VIVO BY MEANS OF NORMAL GUINEA PIG SERUM. *Journal of Experimental Medicine* **98.** ISSN: 0022-1007 (6 1953).

69. BROOME, J. D. Evidence that the L-asparaginase of guinea pig serum is responsible for its antilymphoma effects. I. Properties of the L-asparaginase of guinea pig serum in relation to those of the antilymphoma substance. *The Journal of experimental medicine* **118.** ISSN: 00221007 (1963).

70. Akagi, T. *et al.* Methylation analysis of asparagine synthetase gene in acute lymphoblastic leukemia cells. *Leukemia* **20.** ISSN: 14765551 (7 2006).

71. Ueno, T. *et al.* Cell cycle arrest and apoptosis of leukemia cells induced by L-asparaginase. *Leukemia* **11.** ISSN: 08876924 (11 1997).

72. Métayer, L. E., Brown, R. D., Carlebur, S., Burke, G. A. & Brown, G. C. Mechanisms of cell death induced by arginase and asparaginase in precursor B-cell lymphoblasts. *Apoptosis* **24,** 145–156. ISSN: 1573675X (1-2 Feb. 2019).

73. Chan, W. K. *et al.* Glutaminase activity of L-asparaginase contributes to durable preclinical activity against acute lymphoblastic leukemia. *Molecular Cancer Therapeutics* **18.** ISSN: 15388514 (9 2019).

74. Liu, C. *et al.* Clinical utility and implications of asparaginase antibodies in acute lymphoblastic leukemia. *Leukemia* **26.** ISSN: 08876924 (11 2012).

75. Tong, W. H. *et al.* A prospective study on drug monitoring of PEGasparaginase and Erwinia asparaginase and asparaginase antibodies in pediatric acute lymphoblastic leukemia. *Blood* **123.** ISSN: 15280020 (13 2014).

76. Laranjeira, A. B. *et al.* IGFBP7 participates in the reciprocal interaction between acute lymphoblastic leukemia and BM stromal cells and in leukemia resistance to asparaginase. *Leukemia* **26.** ISSN: 14765551 (5 2012).

77. Ehsanipour, E. A. *et al.* Adipocytes Cause Leukemia Cell Resistance to L-Asparaginase via Release of Glutamine. *Cancer research* **73,** 2998. ISSN: 00085472. /pmc/articles/PMC3684066/%20/pmc/articles/PMC3684066/?report=abstract%20https://www.ncbi.nlm.nih.gov/pmc/articles/PMC3684066/ (10 May 2013).

78. Chiu, M. *et al.* ALL blasts drive primary mesenchymal stromal cells to increase asparagine availability during asparaginase treatment. *Blood Advances* **5.** ISSN: 24739537 (2021).

79. Ferguson, D. C. *et al.* Amino acid stress response genes promote L-asparaginase resistance in pediatric acute lymphoblastic leukemia. *Blood Advances* **6.** ISSN: 24739537 (11 2022).

80. Lynggaard, L. S. *et al.* Asparaginase encapsulated in erythrocytes as second-line treatment in hypersensitive patients with acute lymphoblastic leukaemia. *British Journal of Haematology* **197.** ISSN: 13652141 (6 2022).

81. Sandley, M. & Angus, J. Asparaginase therapy in patients with acute lymphoblastic leukemia: expert opinion on use and toxicity management. *Leukemia and Lymphoma* **64.** ISSN: 10292403 (4 2023).

82. Szlosarek, P. W. *et al.* Abstract CT007: Phase 2-3 trial of pegargiminase plus chemotherapy versus placebo plus chemotherapy in patients with non-epithelioid pleural mesothelioma. *Cancer Research* **83** (8 Supplement 2023).

83. Grzywa, T. M. *et al.* Myeloid Cell-Derived Arginase in Cancer Immune Response. *Frontiers in Immunology* **11,** 938. ISSN: 16643224. www.frontiersin.org (May 2020).

84. Rodriguez, P. C., Zea, A. H., Culotta, K. S., Zabaleta, J. & Ochoa, J. B. O. A. C. Regulation of T cell receptor CD3ζ chain expression by L-arginine. *Journal of Biological Chemistry* **277.** ISSN: 00219258 (24 2002).

85. Wu, G. & Morris, S. M. Arginine metabolism : nitric oxide and beyond. *Biochem. J* **336,** 1–17 (1998).

86. Wu, G. *et al.* Arginine metabolism and nutrition in growth, health and disease. *Amino Acids* **37,** 153–168. ISSN: 09394451. /pmc/articles/PMC2677116/?report=abstract%20https://www.ncbi.nlm.nih.gov/pmc/articles/PMC2677116/ (1 May 2009).

87. Chantranupong, L. *et al.* The CASTOR Proteins Are Arginine Sensors for the mTORC1 Pathway. *Cell* **165.** ISSN: 10974172 (1 2016).

88. Werner, A. *et al.* Reconstitution of T cell proliferation under arginine limitation: Activated human T cells take up citrulline via L-Type amino acid transporter 1 and use it to regenerate arginine after induction of argininosuccinate synthase expression. *Frontiers in Immunology* **8.** ISSN: 16643224. /pmc/articles/PMC5523021/?report=abstract%20https://www.ncbi.nlm.nih.gov/pmc/articles/PMC5523021/ (JUL July 2017).

89. Rabinovich, S. *et al.* Diversion of aspartate in ASS1-deficient tumours fosters de novo pyrimidine synthesis. *Nature* **527,** 379–383. ISSN: 14764687. https://www.nature.com/articles/nature15529 (Nov. 2015).

90. Feun, L. & Savaraj, N. Pegylated arginine deiminase: A novel anticancer enzyme agent. *Expert Opinion on Investigational Drugs* **15.** ISSN: 13543784 (7 2006).

91. Mussai, F. *et al.* A randomised evaluation of low-dose Ara-C plus pegylated recombinant arginase BCT-100 versus low dose Ara-C in older unfit patients with acute myeloid leukaemia: Results from the LI-1 trial. *British Journal of Haematology* **200.** ISSN: 13652141 (5 2023).

92. Riess, C. *et al.* Arginine-Depleting Enzymes – An Increasingly Recognized Treatment Strategy for Therapy-Refractory Malignancies. *Cellular Physiology and Biochemistry* **51,** 854–870. ISSN: 1015-8987 (2 2018).

93. Szlosarek, P. W. *et al.* In vivo loss of expression of argininosuccinate synthetase in malignant pleural mesothelioma is a biomarker for susceptibility to arginine depletion. *Clinical Cancer Research* **12,** 7126–7131. ISSN: 10780432. www.aacrjournals.org (23 Dec. 2006).

94. Miraki-Moud, F. *et al.* Arginine deprivation using pegylated arginine deiminase has activity against primary acute myeloid leukemia cells in vivo. *Blood* **125,** 4060–4068. ISSN: 15280020 (26 June 2015).

95. Chalishazar, M. D. *et al.* MYC-Driven Small-Cell Lung Cancer is Metabolically Distinct and Vulnerable to Arginine Depletion. *Clinical Cancer Research* **25,** 5107–5121. ISSN: 1078-0432. https://clincancerres.aacrjournals.org/content/25/16/5107%20https://clincancerres.aacrjournals.org/content/25/16/5107.abstract (Aug. 2019).

96. Chu, Y. D., Liu, H. F., Chen, Y. C., Chou, C. H. & Yeh, C. T. WWOX-rs13338697 genotype predicts therapeutic efficacy of ADI-PEG 20 for patients with advanced hepatocellular carcinoma. *Frontiers in Oncology* **12,** 6737. ISSN: 2234943X (Dec. 2022).

97. Barnett, S. E. *et al.* BAP1 Loss Is Associated with Higher ASS1 Expression in Epithelioid Mesothelioma: Implications for Therapeutic Stratification. *Molecular Cancer Research.* http://www.meso (2023).

98. Abou-Alfa, G. K. *et al.* Phase III randomized study of second line ADI-PEG 20 plus best supportive care versus placebo plus best supportive care in patients with advanced hepatocellular carcinoma. *Annals of Oncology* **29,** 1402–1408. ISSN: 0923-

7534. https://academic.oup.com/annonc/article/29/6/1402/4961397 (June 2018).

99. Ott, P. A. *et al.* Phase I/II study of pegylated arginine deiminase (ADI-PEG 20) in patients with advanced melanoma. *Investigational New Drugs* **31.** ISSN: 01676997 (2 2013).

100. Hall, P. E. *et al.* Phase II Study of Arginine Deprivation Therapy With Pegargiminase in Patients With Relapsed Sensitive or Refractory Small-cell Lung Cancer. *Clinical Lung Cancer* **21.** ISSN: 19380690 (6 2020).

101. Tomlinson, B. K. *et al.* Phase i trial of arginine deprivation therapy with ADI-PEG 20 plus docetaxel in patients with advanced malignant solid tumors. *Clinical Cancer Research* **21.** ISSN: 15573265 (11 2015).

102. Lowery, M. A. *et al.* A phase 1/1B trial of ADI-PEG 20 plus nab-paclitaxel and gemcitabine in patients with advanced pancreatic adenocarcinoma. *Cancer* **123.** ISSN: 10970142 (23 2017).

103. Hall, P. E. *et al.* A phase I study of pegylated arginine deiminase (Pegargiminase), cisplatin, and pemetrexed in argininosuccinate synthetase 1-deficient recurrent high-grade glioma. *Clinical Cancer Research* **25.** ISSN: 15573265 (9 2019).

104. Chan, P. Y. *et al.* A Phase 1 study of ADI-PEG20 (pegargiminase) combined with cisplatin and pemetrexed in ASS1-negative metastatic uveal melanoma. *Pigment Cell and Melanoma Research* **35.** ISSN: 1755148X (4 2022).

105. Tsai, H. J. *et al.* A Phase II Study of Arginine Deiminase (ADI-PEG20) in Relapsed/Refractory or Poor-Risk Acute Myeloid Leukemia Patients. *Scientific Reports* **7,** 1–10. ISSN: 20452322. www.nature.com/scientificreports/ (Dec. 2017).

106. Tsai, H. J. *et al.* Phase I study of ADI-PEG20 plus low-dose cytarabine for the treatment of acute myeloid leukemia. *Cancer Medicine* **10,** 2946–2955. ISSN: 20457634. https://onlinelibrary.wiley.com/doi/full/10.1002/cam4.3871%20https://onlinelibrary.wiley.com/doi/abs/10.1002/cam4.3871%20https://onlinelibrary.wiley.com/doi/10.1002/cam4.3871 (May 2021).

107. Szlosarek, P. W. *et al.* Arginine Deprivation With Pegylated Arginine Deiminase in Patients With Argininosuccinate Synthetase 1-Deficient Malignant Pleural Mesothelioma: A Randomized Clinical Trial. *JAMA oncology* **3,** 58–66. ISSN: 2374-2445. https://pubmed.ncbi.nlm.nih.gov/27584578/ (1 Jan. 2017).

108. Locke, M. *et al.* Inhibition of the Polyamine Synthesis Pathway Is Synthetically Lethal with Loss of Argininosuccinate Synthase 1. *Cell reports* **16,** 1604–1613. ISSN: 2211-1247. http://www.ncbi.nlm.nih.gov/pubmed/27452468%20http://www.pubmedcentral.nih.gov/articlerender.fcgi?artid=PMC4978703 (6 2016).

109. Phillips, M. M. *et al.* A role for macrophages under cytokine control in mediating resistance to ADI-PEG20 (pegargiminase) in ASS1-deficient mesothelioma. *Pharmacological Reports* **75.** ISSN: 22995684 (3 2023).

110. De Santo, C. *et al.* The arginine metabolome in acute lymphoblastic leukemia can be targeted by the pegylated-recombinant arginase I BCT-100. *International Journal of Cancer* **142,** 1490–1502. ISSN: 10970215 (Apr. 2018).

111. Hernandez, C. P. *et al.* Pegylated arginase I: A potential therapeutic approach in T-ALL. *Blood* **115,** 5214–5221. ISSN: 00064971 (25 June 2010).

112. Gong, H., Zölzer, F., Recklinghausen, G. V., Havers, W. & Schweigerer, L. Arginine deiminase inhibits proliferation of human leukemia cells more potently than asparaginase by inducing cell cycle arrest and apoptosis. *Leukemia* **14.** ISSN: 08876924 (5 2000).

113. Samra, B. *et al.* Outcome of adults with relapsed/refractory T-cell acute lymphoblastic leukemia or lymphoblastic lymphoma. *American Journal of Hematology* **95.** ISSN: 10968652 (9 2020).

114. Jabbour, E., Haddad, F. G., Short, N. J. & Kantarjian, H. Treatment of Adults With Philadelphia Chromosome-Positive Acute Lymphoblastic Leukemia - From Intensive Chemotherapy Combinations to Chemotherapy-Free Regimens: A Review. *JAMA Oncology* **8.** ISSN: 23742445 (9 2022).

115. Perica, K. *et al.* Impact of bridging chemotherapy on clinical outcome of CD19 CAR T therapy in adult acute lymphoblastic leukemia. *Leukemia* **35.** ISSN: 14765551 (11 2021).

116. Shahid, S. *et al.* Impact of Bridging Chemotherapy on Clinical Outcomes of CD19-Specific CAR T Cell Therapy in Children/Young Adults with Relapsed/Refractory B Cell Acute Lymphoblastic Leukemia. *Transplantation and Cellular Therapy* **28.** ISSN: 26666367 (2 2022).

117. Roddie, C. *et al.* Effective bridging therapy can improve CD19 CAR-T outcomes while maintaining safety in patients with large B-cell lymphoma. *Blood advances.* ISSN: 2473-9537. https://pubmed.ncbi.nlm.nih.gov/36724512/ (Feb. 2023).

118. DeSelm, C. *et al.* Low-Dose Radiation Conditioning Enables CAR T Cells to Mitigate Antigen Escape. *Molecular Therapy* **26,** 2542–2552. ISSN: 15250024. /pmc/articles/PMC6225039/?report=abstract%20https://www.ncbi.nlm.nih.gov/pmc/articles/PMC6225039/ (Nov. 2018).

119. Aboelella, N. S. *et al.* Indomethacin-induced oxidative stress enhances death receptor 5 signaling and sensitizes tumor cells to adoptive T-cell therapy. *Journal for ImmunoTherapy of Cancer* **10.** ISSN: 20511426 (7 2022).

120. You, M. *et al.* The combination of ADI-PEG20 and TRAIL effectively increases cell death in melanoma cell lines. *Biochemical and Biophysical Research Communications* **394.** ISSN: 0006291X (3 2010).

121. Zea, A. H. *et al.* L-Arginine modulates CD3ζ expression and T cell function in activated human T lymphocytes. *Cellular Immunology* **232,** 21–31. ISSN: 00088749 (1-2 Nov. 2004).

122. Mussai, F. *et al.* Targeting the arginine metabolic brake enhances immunotherapy for leukaemia. *International journal of cancer* **145,** 2201–2208. ISSN: 1097-0215. http://www.ncbi.nlm.nih.gov/pubmed/30485425 (8 Oct. 2019).

123. Fultang, L. *et al.* Metabolic engineering against the arginine microenvironment enhances CAR-T cell proliferation and therapeutic activity. *Blood* **136,** 1155–1160. ISSN:

15280020. http://ashpublications.org/blood/article-pdf/136/10/1155/1756922/bloodbld2019004500.pdf (10 Sept. 2020).

124. Mussai, F. *et al.* Neuroblastoma arginase activity creates an immunosuppressive microenvironment that impairs autologous and engineered immunity. *Cancer Research* **75,** 3043–3053. ISSN: 15387445. https://pubmed.ncbi.nlm.nih.gov/26054597/ (15 Aug. 2015).

125. Z, G. *et al.* PAX5-driven subtypes of B-progenitor acute lymphoblastic leukemia. *Nature genetics* **51,** 296–307. ISSN: 1546-1718. https://pubmed.ncbi.nlm.nih.gov/30643249/ (Feb. 2019).

126. Anders, S., Pyl, P. T. & Huber, W. HTSeq-A Python framework to work with high-throughput sequencing data. *Bioinformatics* **31.** ISSN: 14602059 (2 2015).

127. R Core Team. *R: A Language and Environment for Statistical Computing* R Foundation for Statistical Computing (Vienna, Austria, 2022). https://www.R-project.org/.

128. Love, M. I., Huber, W. & Anders, S. Moderated estimation of fold change and dispersion for RNA-seq data with DESeq2. *Genome Biology* **15.** ISSN: 1474760X (12 2014).

129. Ritchie, M. E. *et al.* Limma powers differential expression analyses for RNA-sequencing and microarray studies. *Nucleic Acids Research* **43.** ISSN: 13624962 (7 2015).

130. Li, Y., Ge, X., Peng, F., Li, W. & Li, J. J. Exaggerated false positives by popular differential expression methods when analyzing human population samples. *Genome Biology* **23,** 1–13. ISSN: 1474760X. https://genomebiology.biomedcentral.com/articles/10.1186/s13059-022-02648-4 (Dec. 2022).

131. Szklarczyk, D. *et al.* The STRING database in 2021: Customizable protein-protein networks, and functional characterization of user-uploaded gene/measurement sets. *Nucleic Acids Research* **49.** ISSN: 13624962 (2021).

132. Lun, A. T., McCarthy, D. J. & Marioni, J. C. A step-by-step workflow for low-level analysis of single-cell RNA-seq data with Bioconductor. *F1000Research* **5.** ISSN: 1759796X (2016).

133. Geng, H. *et al.* Integrative epigenomic analysis identifies biomarkers and therapeutic targets in adult B-acute lymphoblastic leukemia. *Cancer Discovery* **2,** 1006–1024. ISSN: 21598274 (Nov. 2012).

134. Harvey, R. C. *et al.* Development and Validation Of a Highly Sensitive and Specific Gene Expression Classifier To Prospectively Screen and Identify B-Precursor Acute Lymphoblastic Leukemia (ALL) Patients With a Philadelphia Chromosome-Like ("Ph-like" or "BCR-ABL1-Like") Signature For Therapeutic Targeting and Clinical Intervention. *Blood* **122,** 826–826. ISSN: 0006-4971 (21 Nov. 2013).

135. Ye, J. *et al.* Primer-BLAST: a tool to design target-specific primers for polymerase chain reaction. *BMC bioinformatics* **13.** ISSN: 14712105 (2012).

136. Schmittgen, T. D. & Livak, K. J. Analysis of relative gene expression data using real-time quantitative PCR and the 2(-Delta Delta C(T)) Method. *Methods* **25.** ISSN: 1046-2023 (4 2001).

137. Schneider, V. A. *et al.* Evaluation of GRCh38 and de novo haploid genome assemblies demonstrates the enduring quality of the reference assembly. *Genome Research* **27.** ISSN: 15495469 (5 2017).

138. Dobin, A. *et al.* STAR: Ultrafast universal RNA-seq aligner. *Bioinformatics* **29.** ISSN: 13674803 (1 2013).

139. Li, H. *et al.* The Sequence Alignment/Map format and SAMtools. *Bioinformatics* **25.** ISSN: 13674803 (16 2009).

140. Liao, Y., Smyth, G. K. & Shi, W. The R package Rsubread is easier, faster, cheaper and better for alignment and quantification of RNA sequencing reads. *Nucleic Acids Research* **47.** ISSN: 13624962 (8 2019).

141. K, B., S, R. & M, L. Publication-ready volcano plots with enhanced colouring and labeling. *Bioconductor* (2022).

142. Gu, Z., Eils, R. & Schlesner, M. Complex heatmaps reveal patterns and correlations in multidimensional genomic data. *Bioinformatics* **32.** ISSN: 14602059 (18 2016).

143. Kolde, R. Package 'pheatmap'. *Bioconductor* (2012).

144. Yu, G., Wang, L. G., Han, Y. & He, Q. Y. ClusterProfiler: An R package for comparing biological themes among gene clusters. *OMICS A Journal of Integrative Biology* **16.** ISSN: 15362310 (5 2012).

145. Wu, T. *et al.* clusterProfiler 4.0: A universal enrichment tool for interpreting omics data. *Innovation* **2.** ISSN: 26666758 (3 2021).

146. Han, H. *et al.* TRRUST: A reference database of human transcriptional regulatory interactions. *Scientific Reports* **5.** ISSN: 20452322 (2015).

147. Kuleshov, M. V. *et al.* Enrichr: a comprehensive gene set enrichment analysis web server 2016 update. *Nucleic Acids Research* **44.** ISSN: 13624962 (1 2016).

148. Denoulet, M. *et al.* ABSP: an automated R tool to efficiently analyze region-specific CpG methylation from bisulfite sequencing PCR. *Bioinformatics* **39** (1 2023).

149. Michelozzi, I. M. *et al.* High-dimensional functional phenotyping of preclinical human CAR T cells using mass cytometry. *STAR Protocols* **3.** ISSN: 26661667 (1 Mar. 2022).

150. Nowicka, M. *et al.* CyTOF workflow: differential discovery in high-throughput high-dimensional cytometry datasets. *F1000Research* **6** (2019).

151. Crowell, H., Zanotelli, V. R. T., Chevrier, S., Robinson, M. D. & Bodenmiller, B. CATALYST: Cytometry dATa anALYSis Tools. *Bioconductor version: Release (3.11)* **10** (2020).

152. Crowell, H. L. *et al.* An R-based reproducible and user-friendly preprocessing pipeline for CyTOF data. *F1000Research* **9.** ISSN: 1759796X (2022).

153. Rybakowska, P. *et al.* Data processing workflow for large-scale immune monitoring studies by mass cytometry. *Computational and Structural Biotechnology Journal* **19.** ISSN: 20010370 (2021).

154. McInnes, L., Healy, J., Saul, N. & Großberger, L. UMAP: Uniform Manifold Approximation and Projection. *Journal of Open Source Software* **3** (29 2018).

155. Hahsler, M., Piekenbrock, M. & Doran, D. Dbscan: Fast density-based clustering with R. *Journal of Statistical Software* **91.** ISSN: 15487660 (2019).

156. Amezquita, R. A. *et al.* Orchestrating single-cell analysis with Bioconductor. *Nature Methods* **17.** ISSN: 15487105 (2 2020).

157. Rowe, J. M. *et al.* Induction therapy for adults with acute lymphoblastic leukemia: Results of more than 1500 patients from the international ALL trial: MRC UKALL XII/ECOG E2993. *Blood* **106.** ISSN: 00064971 (12 2005).

158. Roberts, K. G. *et al.* High Frequency and Poor Outcome of Philadelphia Chromosome-Like Acute Lymphoblastic Leukemia in Adults. *Journal of clinical oncology : official journal of the American Society of Clinical Oncology* **35.** ISSN: 15277755 (4 2017).

159. Jain, N. *et al.* Ph-like acute lymphoblastic leukemia: A high-risk subtype in adults. *Blood* **129,** 572–581. ISSN: 15280020. https://ashpublications.org/blood/article-pdf/129/5/572/1401263/blood726588.pdf (5 Feb. 2017).

160. Barretina, J. *et al.* The Cancer Cell Line Encyclopedia enables predictive modelling of anticancer drug sensitivity. *Nature* **483.** ISSN: 00280836 (7391 2012).

161. Meyer, C. *et al.* Establishment of the B cell precursor acute lymphoblastic leukemia cell line MUTZ-5 carrying a (12;13) translocation. *Leukemia 2001 15:9* **15,** 1471–1474. ISSN: 1476-5551. https://www.nature.com/articles/2402212 (Sept. 2001).

162. Meyer, L. K. *et al.* CRLF2 rearrangement in Ph-like acute lymphoblastic leukemia predicts relative glucocorticoid resistance that is overcome with MEK or Akt inhibition. *PLoS ONE* **14.** ISSN: 19326203. /pmc/articles/PMC6638974/%20/pmc/articles/PMC6638974/?report=abstract%20https://www.ncbi.nlm.nih.gov/pmc/articles/PMC6638974/ (June 2019).

163. Greil, J. *et al.* The acute lymphoblastic leukaemia cell line SEM with t(4;11) chromosomal rearrangement is biphenotypic and responsive to interleukin-7. *British Journal of Haematology* **86.** ISSN: 00071048 (2 1994).

164. Arber, D. A. *et al.* The 2016 revision to the World Health Organization classification of myeloid neoplasms and acute leukemia. *Blood* **127,** 2391–2405. ISSN: 15280020. http://ashpublications.org/blood/article-pdf/127/20/2391/1393154/2391.pdf (20 May 2016).

165. Tirtakusuma, R. *et al.* Epigenetic regulator genes direct lineage switching in MLL/AF4 leukemia. *Blood* **140.** ISSN: 15280020 (17 2022).

166. Stong, R. C., Korsmeyer, S. J., Parkin, J. L., Arthur, D. C. & Kersey, J. H. Human Acute Leukemia Cell Line With the t(4; 11) Chromosomal Rearrangement Exhibits B Lineage and Monocytic Characteristics. *Blood* **65,** 21–31. ISSN: 0006-4971 (Jan. 1985).

167. Ragusa, D. *et al.* The RS4;11 cell line as a model for leukaemia with t(4;11)(q21;q23): Revised characterisation of cytogenetic features. *Cancer reports (Hoboken, N.J.)* **2.** ISSN: 2573-8348. https://pubmed.ncbi.nlm.nih.gov/32721124/ (Oct. 2019).

168. Rosenfeld, C. *et al.* An effect human leukaemic cell line: Reh. *European journal of cancer* **13,** 377–379. ISSN: 0014-2964. https://pubmed.ncbi.nlm.nih.gov/194778/ (1977).

169. Aburawi, H. E., Biloglav, A., Johansson, B. & Paulsson, K. Cytogenetic and molecular genetic characterization of the 'high hyperdiploid' B-cell precursor acute lymphoblastic leukaemia cell line MHH-CALL-2 reveals a near-haploid origin. *British Journal of Haematology* **154.** ISSN: 00071048 (2 2011).

170. Naumovski, L. *et al.* Philadelphia chromosome-positive acute lymphoblastic leukemia cell lines without classical breakpoint cluster region rearrangement. *Cancer Research* **48.** ISSN: 0008-5472 (10 1988).

171. Okabe, M. *et al.* Establishment and characterization of a cell line, TOM-1, derived from a patient with Philadelphia chromosome-positive acute lymphocytic leukemia. *Blood* **69.** ISSN: 0006-4971 (4 1987).

172. Duy, C. *et al.* BCL6 enables Ph+ acute lymphoblastic leukaemia cells to survive BCR-ABL1 kinase inhibition. *Nature* **473.** ISSN: 00280836 (7347 2011).

173. Brin, E. *et al.* PEGylated arginine deiminase can modulate tumor immune microenvironment by affecting immune checkpoint expression, decreasing regulatory T cell accumulation and inducing tumor T cell infiltration. *Oncotarget* **8,** 58948–58963. ISSN: 19492553 (35 2017).

174. Izzo, F. *et al.* Pegylated arginine deiminase treatment of patients with unresectable hepatocellular carcinoma: results from phase I/II studies. *Journal of clinical oncology : official journal of the American Society of Clinical Oncology* **22,** 1815–1822. ISSN: 0732-183X. https://pubmed.ncbi.nlm.nih.gov/15143074/ (10 2004).

175. Ascierto, P. A. *et al.* Pegylated arginine deiminase treatment of patients with metastatic melanoma: results from phase I and II studies. *Journal of clinical oncology : official journal of the American Society of Clinical Oncology* **23,** 7660–7668. ISSN: 0732-183X. https://pubmed.ncbi.nlm.nih.gov/16234528/ (30 2005).

176. Zhang, M., Zheng, J., Nussinov, R. & Ma, B. Release of Cytochrome C from Bax Pores at the Mitochondrial Membrane. *Scientific Reports* **7** (1 2017).

177. Pullarkat, V. A. *et al.* Venetoclax and navitoclax in combination with chemotherapy in patients with relapsed or refractory acute lymphoblastic leukemia and lymphoblastic lymphoma. *Cancer Discovery* **11.** ISSN: 21598290 (6 2021).

178. Braun, F., Bertin-Ciftci, J., Gallouet, A. S., Millour, J. & Juin, P. Serum-nutrient starvation induces cell death mediated by bax and puma that is counteracted by p21 and unmasked by Bcl-x L inhibition. *PLoS ONE* **6.** ISSN: 19326203 (8 2011).

179. Manu, K. A., Cao, P. H. A., Chai, T. F., Casey, P. J. & Wang, M. p21cip1/waf1 coordinate autophagy, proliferation and apoptosis in response to metabolic stress. *Cancers* **11.** ISSN: 20726694 (8 2019).

180. Jung, P., Menssen, A., Mayr, D. & Hermeking, H. AP4 encodes a c-MYC-inducible repressor of p21. *Proceedings of the National Academy of Sciences of the United States of America* **105.** ISSN: 00278424 (39 2008).

181. Long, Y. *et al.* Arginine deiminase resistance in melanoma cells is associated with metabolic reprogramming, glucose dependence, and glutamine addiction. *Molecular cancer therapeutics* **12,** 2581–90. ISSN: 1538-8514. http://www.ncbi.nlm.nih.gov/pubmed/23979920%20http://www.pubmedcentral.nih.gov/articlerender.fcgi?artid=PMC3839414 (11 Nov. 2013).

182. Brashears, C. B. *et al.* Systems level profiling of arginine starvation reveals MYC and ERK adaptive metabolic reprogramming. *Cell Death and Disease* **11,** 1–15. ISSN: 20414889. https://doi.org/10.1038/s41419-020-02899-8 (8 Aug. 2020).

183. Takahashi, H. *et al.* Autophagy is required for cell survival under L-asparaginase-induced metabolic stress in acute lymphoblastic leukemia cells. *Oncogene* **36.** ISSN: 14765594 (30 2017).

184. Cheng, C. T. *et al.* Arginine starvation kills tumor cells through aspartate exhaustion and mitochondrial dysfunction. *Communications Biology* **1.** ISSN: 23993642 (1 2018).

185. Crump, N. T. *et al.* Chromatin accessibility governs the differential response of cancer and T cells to arginine starvation. *Cell Reports* **35,** 109101. ISSN: 2211-1247 (6 May 2021).

186. Yamaguchi, H. & Wang, H. G. CHOP is involved in endoplasmic reticulum stress-induced apoptosis by enhancing DR5 expression in human carcinoma cells. *Journal of Biological Chemistry* **279.** ISSN: 00219258 (44 2004).

187. Harding, H. P. *et al.* An integrated stress response regulates amino acid metabolism and resistance to oxidative stress. *Molecular Cell* **11.** ISSN: 10972765 (3 2003).

188. Dey, S. *et al.* Both transcriptional regulation and translational control of ATF4 are central to the integrated stress response. *Journal of Biological Chemistry* **285.** ISSN: 00219258 (43 2010).

189. Jeong, H., Mason, S. P., Barabási, A. L. & Oltvai, Z. N. Lethality and centrality in protein networks. *Nature* **411.** ISSN: 00280836 (6833 2001).

190. Chin, C. H. *et al.* cytoHubba: Identifying hub objects and sub-networks from complex interactome. *BMC Systems Biology* **8.** ISSN: 17520509 (4 2014).

191. Hu, H., Tian, M., Ding, C. & Yu, S. The C/EBP homologous protein (CHOP) transcription factor functions in endoplasmic reticulum stress-induced apoptosis and microbial infection. *Frontiers in Immunology* **10.** ISSN: 16643224 (JAN 2019).

192. Lu, M. *et al.* Opposing unfolded-protein-response signals converge on death receptor 5 to control apoptosis. *Science (New York, N.Y.)* **345,** 98–101. ISSN: 1095-9203. https://pubmed.ncbi.nlm.nih.gov/24994655/ (6192 2014).

193. Ensor, C. M., Holtsberg, F. W., Bomalaski, J. S. & Clark, M. A. Pegylated arginine deiminase (ADI-SS PEG20,000 mw) inhibits human melanomas and hepatocellular carcinomas in vitro and in vivo. *Cancer research* **62,** 5443–50. ISSN: 0008-5472. http://www.ncbi.nlm.nih.gov/pubmed/12359751 (19 Oct. 2002).

194. Meir, O., Dvash, E., Werman, A. & Rubinstein, M. C/EBP-β regulates endoplasmic reticulum stress-triggered cell death in mouse and human models. *PLoS ONE* **5.** ISSN: 19326203 (3 2010).

195. Marchildon, F., Fu, D., Lala-Tabbert, N. & Wiper-Bergeron, N. CCAAT/enhancer binding protein beta protects muscle satellite cells from apoptosis after injury and in cancer cachexia. *Cell Death and Disease* **7.** ISSN: 20414889 (2 2016).

196. Delage, B. *et al.* Promoter methylation of argininosuccinate synthetase-1 sensitises lymphomas to arginine deiminase treatment, autophagy and caspase-dependent apoptosis. *Cell death & disease* **3,** e342. ISSN: 2041-4889. http://www.ncbi.nlm.nih.gov/pubmed/22764101%20http://www.pubmedcentral.nih.gov/articlerender.fcgi?artid=PMC3406582 (July 2012).

197. Nicholson, L. J. *et al.* Epigenetic silencing of argininosuccinate synthetase confers resistance to platinum-induced cell death but collateral sensitivity to arginine auxotrophy in ovarian cancer. *International Journal of Cancer* **125,** 1454–1463. ISSN: 00207136. http://doi.wiley.com/10.1002/ijc.24546 (6 Sept. 2009).

198. Long, Y. *et al.* Cisplatin-induced synthetic lethality to arginine-starvation therapy by transcriptional suppression of ASS1 is regulated by DEC1, HIF-1α, and c-Myc transcription network and is independent of ASS1 promoter DNA methylation. *Oncotarget* **7,** 82658–82670. ISSN: 1949-2553. http://www.ncbi.nlm.nih.gov/pubmed/27765932%20http://www.pubmedcentral.nih.gov/articlerender.fcgi?artid=PMC5347722 (50 Dec. 2016).

199. Kent, W. J. *et al.* The Human Genome Browser at UCSC. *Genome Research* **12.** ISSN: 1088-9051 (6 2002).

200. Jaaks, P. *et al.* Effective drug combinations in breast, colon and pancreatic cancer cells. *Nature 2022 603:7899* **603,** 166–173. ISSN: 1476-4687. https://www.nature.com/articles/s41586-022-04437-2 (7899 Feb. 2022).

201. Bliss, C. I. THE TOXICITY OF POISONS APPLIED JOINTLY. *Annals of Applied Biology* **26.** ISSN: 17447348 (3 1939).

202. Berenbaum, M. C. What is synergy? *Pharmacological Reviews* **41.** ISSN: 00316997 (2 1989).

203. Palmer, A. C. & Sorger, P. K. Combination Cancer Therapy Can Confer Benefit via Patient-to-Patient Variability without Drug Additivity or Synergy. *Cell* **171.** ISSN: 10974172 (7 2017).

204. Plana, D., Palmer, A. C. & Sorger, P. K. Independent Drug Action in Combination Therapy: Implications for Precision Oncology. *Cancer Discovery* **12.** ISSN: 21598290 (3 2022).

205. Savaraj, N. *et al.* Targeting argininosuccinate synthetase negative melanomas using combination of arginine degrading enzyme and cisplatin. *Oncotarget* **6,** 6295–309. ISSN: 1949-2553. http://www.ncbi.nlm.nih.gov/pubmed/25749046%20http://www.pubmedcentral.nih.gov/articlerender.fcgi?artid=PMC4467438 (8 Mar. 2015).

206. NCT05001828: Study of ADI-PEG 20, Venetoclax and Azacitidine in Acute Myeloid Leukemia. https://clinicaltrials.gov/study/NCT05001828 (2023).

207. Foà, R. *et al.* Dasatinib–Blinatumomab for Ph-Positive Acute Lymphoblastic Leukemia in Adults. *New England Journal of Medicine* **383,** 1613–1623. ISSN: 0028-4793. https://www.nejm.org/doi/full/10.1056/NEJMoa2016272 (Oct. 2020).

208. Jabbour, E. *et al.* Ponatinib and blinatumomab for Philadelphia chromosome-positive acute lymphoblastic leukaemia: a US, single-centre, single-arm, phase 2 trial. *The Lancet Haematology* **10.** ISSN: 23523026 (1 2023).

209. Wang, K. *et al.* Patient-derived xenotransplants can recapitulate the genetic driver landscape of acute leukemias. *Leukemia* **31.** ISSN: 14765551 (1 2017).

210. Shi, Y. *et al.* Phase II-like murine trial identifies synergy between dexamethasone and dasatinib in T-cell acute lymphoblastic leukemia. *Haematologica* **106.** ISSN: 15928721 (4 2021).

211. Fan, J. *et al.* Potential synergy between radiotherapy and CAR T-cells - a multicentric analysis of the role of radiotherapy in the combination of CAR T cell therapy. *Radiotherapy and Oncology* **183.** ISSN: 18790887 (June 2023).

212. Xu, N. *et al.* Priming Leukemia with 5-Azacytidine Enhances CAR T Cell Therapy. *ImmunoTargets and Therapy* **Volume 10,** 123–140. ISSN: 2253-1556. https://www.dovepress.com/priming-leukemia-with-5-azacytidine-enhances-car-t-cell-therapy-peer-reviewed-fulltext-article-ITT (Apr. 2021).

213. Khawanky, N. E. *et al.* Demethylating therapy increases anti-CD123 CAR T cell cytotoxicity against acute myeloid leukemia. *Nature Communications 2021 12:1* **12,** 1–20. ISSN: 2041-1723. https://www.nature.com/articles/s41467-021-26683-0 (1 Nov. 2021).

214. Qu, C. *et al.* Decitabine-primed tandem CD19/CD22 CAR-T therapy in relapsed/refractory diffuse large B-cell lymphoma patients. *Frontiers in Immunology* **13.** ISSN: 16643224 (2022).

215. Dufva, O. *et al.* Integrated drug profiling and CRISPR screening identify essential pathways for CAR T-cell cytotoxicity. *Blood* **135,** 597–609. ISSN: 15280020. /pmc/articles/PMC7098811/?report=abstract%20https://www.ncbi.nlm.nih.gov/pmc/articles/PMC7098811/ (Feb. 2020).

216. Sarosiek, K. A., Chonghaile, T. N. & Letai, A. Mitochondria: Gatekeepers of response to chemotherapy. *Trends in Cell Biology* **23.** ISSN: 09628924 (12 2013).

217. Annibaldi, A. & Walczak, H. Death receptors and their ligands in inflammatory disease and cancer. *Cold Spring Harbor Perspectives in Biology* **12.** ISSN: 19430264 (9 2020).

218. Cabal-Hierro, L. & Lazo, P. S. Signal transduction by tumor necrosis factor receptors. *Cellular Signalling* **24.** ISSN: 08986568 (6 2012).

219. Upadhyay, R. *et al.* A critical role for fas-mediated off-target tumor killing in t-cell immunotherapy. *Cancer Discovery* **11,** 599–613. ISSN: 21598290. https://pubmed.ncbi.nlm.nih.gov/33334730/ (3 Mar. 2021).

220. Vredevoogd, D. W. *et al.* Augmenting Immunotherapy Impact by Lowering Tumor TNF Cytotoxicity Threshold. *Cell.* ISSN: 10974172 (2019).

221. Green, D. R. & Llambi, F. Cell Death Signaling. *Cold Spring Harbor Perspectives in Biology* **7.** http://cshperspectives.cshlp.org/ (2020).

222. Wahba, J. *et al.* Chemotherapy-induced apoptosis, autophagy and cell cycle arrest are key drivers of synergy in chemo-immunotherapy of epithelial ovarian cancer. *Cancer Immunology, Immunotherapy* **67,** 1753–1765. ISSN: 14320851. /pmc/articles/PMC6208825/?report=abstract%20https://www.ncbi.nlm.nih.gov/pmc/articles/PMC6208825/ (11 Nov. 2018).

223. Morris, R., Kershaw, N. J. & Babon, J. J. The molecular details of cytokine signaling via the JAK/STAT pathway. *Protein Science* **27.** ISSN: 1469896X (12 2018).

224. Teachey, D. T. *et al.* Identification of predictive biomarkers for cytokine release syndrome after chimeric antigen receptor T-cell therapy for acute lymphoblastic leukemia. *Cancer Discovery* **6.** ISSN: 21598290 (6 2016).

225. Giavridis, T. *et al.* CAR T cell-induced cytokine release syndrome is mediated by macrophages and abated by IL-1 blockade letter. *Nature Medicine* **24.** ISSN: 1546170X (6 2018).

226. Lichtenstein, D. A. *et al.* Characterization of HLH-like manifestations as a CRS variant in patients receiving CD22 CAR T cells. *Blood* **138.** ISSN: 15280020 (24 2021).

227. Larson, R. C. *et al.* CAR T cell killing requires the IFNγR pathway in solid but not liquid tumours. *Nature* **604.** ISSN: 14764687 (7906 2022).

228. Bailey, S. R. *et al.* Blockade or Deletion of IFNγ Reduces Macrophage Activation without Compromising CAR T-cell Function in Hematologic Malignancies. *Blood Cancer Discovery* **3.** ISSN: 2643-3230 (2 2022).

229. Rainone, M. *et al.* Interferon-γ blockade in CAR T-cell therapy-associated macrophage activation syndrome/hemophagocytic lymphohistiocytosis. *Blood Advances* **7.** ISSN: 24739537 (4 2023).

230. Goldberg, L. *et al.* Single-cell analysis by mass cytometry reveals CD19 CAR T cell spatiotemporal plasticity in patients. *OncoImmunology* **11.** ISSN: 2162402X (1 2022).

231. Weber, L. M., Nowicka, M., Soneson, C. & Robinson, M. D. diffcyt: Differential discovery in high-dimensional cytometry via high-resolution clustering. *Communications Biology* **2.** ISSN: 23993642 (1 2019).

232. Tschumi, B. O. *et al.* CART cells are prone to Fas- and DR5-mediated cell death. *Journal for immunotherapy of cancer* **6.** ISSN: 2051-1426. `https://pubmed.ncbi.nlm.nih.gov/30005714/` (1 July 2018).

233. Turtle, C. J. *et al.* CD19 CAR-T cells of defined CD4+:CD8+ composition in adult B cell ALL patients. *Journal of Clinical Investigation* **126.** ISSN: 15588238 (6 2016).

234. Gassen, S. V. *et al.* FlowSOM: Using self-organizing maps for visualization and interpretation of cytometry data. *Cytometry Part A* **87.** ISSN: 15524930 (7 2015).

235. Wilkerson, M. D. & Hayes, D. N. ConsensusClusterPlus: A class discovery tool with confidence assessments and item tracking. *Bioinformatics* **26.** ISSN: 13674803 (12 2010).

236. Golubovskaya, V. & Wu, L. Different subsets of T cells, memory, effector functions, and CAR-T immunotherapy. *Cancers* **8.** ISSN: 20726694 (3 2016).

237. Biasco, L. *et al.* In vivo tracking of T cells in humans unveils decade-long survival and activity of genetically modified T memory stem cells. *Science Translational Medicine* **7.** ISSN: 19466242 (273 2015).

238. Sommermeyer, D. *et al.* Chimeric antigen receptor-modified T cells derived from defined CD8+ and CD4+ subsets confer superior antitumor reactivity in vivo. *Leukemia* **30.** ISSN: 14765551 (2 2016).

239. Tussey, L., Speller, S., Gallimore, A. & Vessey, R. Functionally distinct CD8+ memory T cell subsets in persistent EBV infection are differentiated by migratory receptor expression. *European Journal of Immunology* **30.** ISSN: 00142980 (7 2000).

240. Piette, C. *et al. Differential impact of drugs on the outcome of ETV6-RUNX1 positive childhood B-cell precursor acute lymphoblastic leukaemia: Results of the EORTC CLG 58881 and 58951 trials* 2018.

241. Tasian, S. K., Loh, M. L. & Hunger, S. P. Philadelphia chromosome–like acute lymphoblastic leukemia. *Blood* **130,** 2064–2072. ISSN: 0006-4971. eprint: https://ashpublications.org/blood/article-pdf/130/19/2064/1403168/blood743252.pdf. https://doi.org/10.1182/blood-2017-06-743252 (Nov. 2017).

242. Chiaretti, S. *et al.* Philadelphia-like acute lymphoblastic leukemia is associated with minimal residual disease persistence and poor outcome. First report of the minimal residual disease-oriented GIMEMA LAL1913. *Haematologica* **106.** ISSN: 15928721 (6 2021).

243. Ribera, J. M. Philadelphia chromosome-like acute lymphoblastic leukemia. Still a pending matter. *Haematologica* **106.** ISSN: 15928721 (6 2021).

244. Igwe, I. J. *et al.* The presence of Philadelphia chromosome does not confer poor prognosis in adult pre-B acute lymphoblastic leukaemia in the tyrosine kinase inhibitor era – a surveillance, epidemiology, and end results database analysis. *British Journal of Haematology* **179.** ISSN: 13652141 (4 2017).

245. Miyamoto, T. *et al.* Argininosuccinate synthase 1 is an intrinsic Akt repressor transactivated by p53. *Science advances* **3,** e1603204. ISSN: 2375-2548. http://www.ncbi.nlm.nih.gov/pubmed/28560349%20http://www.pubmedcentral.nih.gov/articlerender.fcgi?artid=PMC5438217 (5 May 2017).

246. Safavi, S. & Paulsson, K. *Near-haploid and low-hypodiploid acute lymphoblastic leukemia: Two distinct subtypes with consistently poor prognosis* 2017.

247. Tsai, W. B. *et al.* Resistance to arginine deiminase treatment in melanoma cells is associated with induced argininosuccinate synthetase expression involving c-Myc/HIF-1α/Sp4. *Molecular Cancer Therapeutics* **8.** ISSN: 15357163 (12 2009).

248. Tsai, W. B. *et al.* Activation of Ras/PI3K/ERK pathway induces c-Myc stabilization to upregulate argininosuccinate synthetase, leading to arginine deiminase resistance in melanoma cells. *Cancer Research* **72.** ISSN: 00085472 (10 2012).

249. Schurch, N. J. *et al.* How many biological replicates are needed in an RNA-seq experiment and which differential expression tool should you use? *RNA* **22.** ISSN: 14699001 (6 2016).

250. Chan, S. L. *et al.* A phase II clinical study on the efficacy and predictive biomarker of pegylated recombinant arginase on hepatocellular carcinoma. *Investigational New Drugs* **39.** ISSN: 15730646 (5 2021).

251. Sugimoto, K. *et al.* A clinically attainable dose of L-asparaginase targets glutamine addiction in lymphoid cell lines. *Cancer Science* **106.** ISSN: 13497006 (11 2015).

252. Szlosarek, P. W. *et al.* Phase 1, pharmacogenomic, dose-expansion study of pegargiminase plus pemetrexed and cisplatin in patients with ASS1-deficient non-squamous non-small cell lung cancer. *Cancer Medicine* **00,** cam4.4196. ISSN: 2045-7634 (Aug. 2021).

253. Feun, L. G. *et al.* Negative argininosuccinate synthetase expression in melanoma tumours may predict clinical benefit from arginine-depleting therapy with pegylated arginine deiminase. *British journal of cancer* **106,** 1481–1485. ISSN: 1532-1827. https://pubmed.ncbi.nlm.nih.gov/22472884/ (9 Apr. 2012).

254. Delahaye, M. C., Salem, K. I., Pelletier, J., Aurrand-Lions, M. & Mancini, S. J. Toward Therapeutic Targeting of Bone Marrow Leukemic Niche Protective Signals in B-Cell Acute Lymphoblastic Leukemia. *Frontiers in Oncology* **10.** ISSN: 2234943X (2021).

255. Heydt, Q. *et al.* Adipocytes disrupt the translational programme of acute lymphoblastic leukaemia to favour tumour survival and persistence. *Nature Communications 2021 12:1* **12,** 1–18. ISSN: 2041-1723. https://www.nature.com/articles/s41467-021-25540-4 (1 Sept. 2021).

256. Duarte, D. & Vale, N. Evaluation of synergism in drug combinations and reference models for future orientations in oncology. *Current Research in Pharmacology and Drug Discovery* **3.** ISSN: 25902571 (2022).

257. Inaba, H. & Pui, C. H. Glucocorticoid use in acute lymphoblastic leukaemia. *The Lancet Oncology* **11.** ISSN: 14702045 (11 2010).

258. Rong, Y. & Distelhorst, C. W. Bcl-2 protein family members: Versatile regulators of calcium signaling in cell survival and apoptosis. *Annual Review of Physiology.* ISSN: 00664278 (2008).

259. Pihán, P., Carreras-Sureda, A. & Hetz, C. BCL-2 family: Integrating stress responses at the ER to control cell demise. *Cell Death and Differentiation* **24.** ISSN: 14765403 (9 2017).

260. Ehrhardt, H., Wachter, F., Grunert, M. & Jeremias, I. Cell cycle-arrested tumor cells exhibit increased sensitivity towards TRAIL-induced apoptosis. *Cell Death and Disease* **4.** ISSN: 20414889 (6 2013).

261. Michelozzi, I. M. *et al.* Activation priming and cytokine polyfunctionality modulate the enhanced functionality of low-affinity CD19 CAR T cells. *Blood Advances* **7.** ISSN: 2473-9529 (9 2023).

262. Wang, D. *et al.* In vitro tumor cell rechallenge for predictive evaluation of chimeric antigen receptor t cell antitumor function. *Journal of Visualized Experiments* **2019.** ISSN: 1940087X (144 2019).

263. Anderson, N. D. *et al.* Transcriptional signatures associated with persisting CD19 CAR-T cells in children with leukemia. *Nature medicine.* ISSN: 1546-170X (2023).

264. Rodriguez-Marquez, P. *et al.* CAR density influences antitumoral efficacy of BCMA CAR T cells and correlates with clinical outcome. *Science Advances* **8.** ISSN: 23752548 (39 2022).